Hydro-mechanical behavior of deep tunnels in anisotropic poroelastic medium

Nam Hung Tran

UNIVERSITÉ D'ORLÉANS

ÉCOLE DOCTORALE
ENERGIE, MATERIAUX, SCIENCES DE LA TERRE ET DE L'UNIVERS

LABORATOIRE PRISME

THÈSE présentée par :

Nam Hung TRAN

Soutenue le : **15 Décembre 2016**

pour obtenir le grade de : **Docteur de l'Université d'Orléans**

Discipline : Génie Civil

Hydro-mechanical behavior of deep tunnels in anisotropic poroelastic medium

THÈSE dirigée par :

Dashnor HOXHA	Professeur, Université d'Orléans

RAPPORTEURS :

Richard GIOT	Professeur, Université de Poitiers
Frédéric COLLIN	Professeur, Université de Liège, Belgique

JURY:

Richard GIOT	Professeur, Université de Poitiers
Frédéric COLLIN	Professeur, Université de Liège, Belgique
Dashnor HOXHA	Professeur, Université d'Orléans
Duc Phi DO	Maître de Conférences, Université d'Orléans
Darius SEYEDI	Examinateur, ANDRA
Balazs VASARHELYI	Professeur, Université de Budapest, Hongrie

ACKNOWLEDGEMENTS

I would first of all like to thank Mr. Richard GIOT and Mr. Frédéric COLLIN who accepted to become reviewers of my thesis. Their very detailed reports as well as their very interesting remarks and questions promoted me in opening other perspectives to my work. I would also like to thank one more time Mr. Richard GIOT for your agreement to preside the committee of thesis examination.

I sincerely thank Mr. Darius SEYEDI and Mr. Balazs VASARHELYI who have kindly to be members of my doctoral examination committee. Their suggestions and discussions will be very useful for me in future works.

I wish to express my deep gratitude to my thesis supervisor, Mr. Dashnor HOXHA, who gave me a very interesting topic of thesis and followed me during three years of thesis. Many thanks for his encouragement for my initiatives and his scientific advices. I would also like to thank Mr. Duc-Phi DO for his availability and for the relevance of his advices to me on scientific work and daily life. I am very much appreciative of the support he provided during my dissertation work.

I also wish to express my friendship to all my colleagues of the team of Civil Engineering at the PRISME Laboratory who helped me a lot during my thesis and with whom I had very good times.

Finally, these last words are addressed to my family, my wife and my daughters, for their support and permanent encouragement. I am thankful to my parents, for their encouragement, support and patience.

CONTENTS

LIST OF FIGURES

ABSTRACT

Deep tunnels are often built in the sedimentary and metamorphic foliated rocks which exhibit usually the anisotropic properties due to the presence of the discontinuities. The analysis of rock and liner stresses due to tunnel construction with the assumption of homogeneous and isotropic rock would be incorrect. The present thesis aims to deal with the deep tunnel in anisotropic rock with a particular emphasis on the effects of hydraulic phenomenon on the mechanical responses or reciprocal effects of hydraulic and mechanical phenomena by combining analytical and numerical approach. On that point of view, a closed-formed solution for tunnel excavated in saturated anisotropic ground is developed taking into account the hydro-mechanical behavior in steady-state. Based on the analytical solution obtained, parametric studies are conducted to evaluate the effects of different parameters of the anisotropic material on the tunnel behavior. The thesis considers also to extend the analytical solution with a time-dependent behavior which takes into account the impact of the pore pressure distribution on mechanical response over time, i.e., one way coupling modeling. In addition, some numerical analysis based on fully-coupled modeling, i.e., two ways coupling, are conducted which are considered as the complete solution for the analytical solution. An application of the closed-form solution on convergence-confinement method is as well referred which can take into account the influence of the tunnel face on the work of the support as well as the massif.

The obtained solution could be used as a quick tool to calibrate tunnels in porous media by combining with design approaches such as convergence-confinement method.

Keywords: *deep tunnels, hydro-mechanical behaviour, elastic anisotropic rock, analytical solution, numerical solution, calibrate tunnels.*

RESUME

Les tunnels profonds sont souvent construits dans les roches sédimentaires et métamorphiques stratifiées qui présentent habituellement des propriétés anisotropes en raison de leur structure et des propriétés des constituants. Le présent travail vise à étudier les tunnels profonds dans un massif rocheux anisotrope élastique en portant une attention particulière sur les effets des couplages hydromécaniques par des approches analytiques et numériques. Une solution analytique pour un tunnel creusé dans un massif rocheux anisotrope saturé est développée en tenant compte du couplage hydro-mécanique dans le régime permanent. Cette solution analytique est utilisée pour réaliser une série d'études paramétriques afin d'évaluer les effets des différents paramètres du matériau anisotrope sur le comportement du tunnel.

Dans un deuxième temps la solution analytique est élargie pour décrire le comportement du tunnel pendant la phase transitoire hydraulique. Afin de compléter ces études analytiques qui prennent en compte seulement un couplage unilatéral (dans le sens que seul le comportement hydraulique influence le comportement mécanique et pas l'inverse) de l'analyse numérique avec un couplage complet, ont été réalisés. Une application de la solution analytique sur la méthode de convergence-confinement est aussi bien abordée qui peut prendre en compte l'influence du front de taille du tunnel sur le travail du soutènement ainsi que sur le massif.

La solution obtenue peut servir comme un outil de dimensionnement rapide des tunnels en milieux poreux en le combinant avec des approches de dimensionnement comme celle de convergence-confinement.

Mots clés: *tunnels profonds, comportement hydro-mécanique, roche anisotrope élastique, solution analytique, solution numérique, dimensionnement des tunnels.*

GENERAL INTRODUCTION

Deep tunnels are widely used in practice such as in the mining industry, petroleum industry, underground transport, nuclear waste storage, etc. A tunnel is called deep if its diameter (or equivalent diameter if the cross section is not circular) is small compared to the depth of its axis, i.e., if H/D>10 where H is the depth of the tunnel axis and D its diameter. This means that the vertical initial stress variation between the upper and lower parts of the tunnel section (before excavation) is negligible compared to the initial vertical stress due to the weight of the ground to the average depth of the tunnel.

Nowadays, with the development of techniques and technologies in the deep storage, especially in the nuclear waste storage, more and more, deep underground constructions are built. A problem often encountered in the construction the tunnels is that they are usually placed in sedimentary and metamorphic foliated rocks where the presence of the discontinuities makes them anisotropic.

The analysis of the tunnels is often made with the assumption of homogeneous and isotropic rock. However, several research results indicate that, stresses and deformations in the rock as well as in the liner of the tunnel in elastic medium differ from those obtained in assuming isotropic properties of materials and strongly depend on the orientation of bedding or foliation with the tunnel axis (Hefny and Lo, 1999; Tonon and Amadei, 2002). This shows the importance of taking into account the anisotropic behavior of the medium.

The rock is a porous medium whose behavior is governed by reciprocal influence of mechanical and hydraulic phenomena. The first theory of poroelasticity which considers the coupled diffusion-deformation phenomenon was proposed by Biot (Biot, 1941). Since then, Biot's isotropic theory has been extended for general anisotropic materials (Biot, 1955; Thompson and Willis, 1991). Several authors have made important contributions in identifying and relating the associated material constants to well-known engineering constants (Amadei, 1983; Cheng, 1997; Abousleiman and Cui, 2000). Thereafter, a number of fundamental analytical solutions were developed which solved the problems of an excavation in anisotropic poroelasticity taking into account coupled behavior of the material (Abousleiman and Ekbote, 2005; Abousleiman and Cui, 1998; Bobet, 2011).

As a continuity of the aforementioned works, the present work devotes to study the behavior of tunnels excavated in saturated, mechanically and hydraulically transversely anisotropic rock mass accounting for hydro-mechanical coupling. Based on complex variable method and on the technique of conformal mapping, closed-form hydro-mechanical solutions for stresses and displacements around the deep tunnels are developed. The Lekhnitskii complex potential approach of anisotropic elasticity is used to include the hydraulic effect. It should be noted that, this solution is based on an one-way-coupling model, i.e., the only effect of hydraulic phenomena on the mechanical response are considered. Therefore, in parallel, numerical analysis also are conducted to evaluate the complete the effects of full-coupled behavior on the tunnel response. This numerical solution is considered as a complete solution for the analytical solution.

The study objectives of the dissertation are to study the work of a lined deep tunnel with circular cross-section in a saturated poroelastic anisotropic medium. Concretely, there are four objectives defined for this thesis and will be presented in chapters 2, 3 and 4:

1. Develop an analytical solution in condition of steady state of groundwater flow. Thus, the solution is based on a behavior model of one way coupling by taking into account the effect of pore pressure distribution on the mechanical responses.

2. Develop a transient analytical solution based also on the behavior model of one-way-coupling which considers the evolution of the pore pressure with time and its effect on the mechanical responses.

3. Evaluate the pertinence of one-way-coupling models by comparison with full coupled analyses. For that, several numerical analyses are performed and compared with analytical one-way-coupling results. Furthermore, the numerical solution also considers the effect of very low permeability of the rock mass on its hydro-mechanical responses.

4. For the purpose of application in tunnel design, an extension of the closed-form solution on convergence-confinement method is referred, which can take into account the influence of the tunnel face on the work of the support as well as the massif. The obtained solution could be used as a quick tool to calibrate tunnels in porous media based on the approach of convergence-confinement method

This dissertation is organized as follows:

Chapter 1 devotes to present the motivation, the basic theoretical concepts of the poroelastic medium and the fundamental assumptions. Constitutive equations for poroelastic that will be used later, are presented. The anisotropic inherence of rock is discussed in the next part that highlights the importance of taking into account anisotropic behavior of the rock being analyzed. Finally, the works that relate to the subject of the thesis are outlined for an overview on study topic and the determination of the objectives of the thesis.

Chapter 2 develops an analytical solution for a lined deep tunnel in saturated anisotropic rock. The analytical solution is developed on the basis of a complex variable method, a powerful method for solving two dimensional elasticity problem. The Lekhnitskii complex potential approach of anisotropic elasticity is used to include the hydraulic effect, i.e., the solution takes into account the effect of pore pressure distribution on the mechanical response. The solution is based on the one way coupling model when the fluid flow attempts a steady state. The closed-form solution also accounts for the liner-rock mass interaction and two drainage conditions of the fluid flow at the liner-rock mass interface: no drainage and full drainage. After that, employing the analytical solution, a series of parametric investigations are carried out to elucidate effects of different parameters on the tunnel response. The closed-form solution is thought to be a useful tool to quickly evaluate the stresses and displacements of the tunnel for design purposes.

Chapter 3 consists of two parts. The first one is devoted to develop an analytical solution for hydro-mechanical problem in transient state on the basis of the one way coupling model. The transient solution can be considered as successive steady-state snapshots using a time dependent influence radius, and therefore, the complex potential approach used in chapter 2 could be applied to each instant of the computational processes. It should be noted that, the one way coupling model cannot fully reflex the hydro-mechanical coupling behavior; however, it could help to observe the impact of the pore pressure distribution on the mechanical response over time. Consequently, the second part of this chapter is devoted for numerical simulations of the tunnels in saturated anisotropic rock based on a fully-coupled hydro-mechanical model. The numerical analyses are performed with the FEM code – ASTER. The parametric estimations are also carried out to evaluate completely the reciprocal effects between mechanical and hydraulic phenomena.

Chapter 4 extends the solution obtained in chapter 2 based on the approach of the convergence-confinement method to study the interaction between the rock mass and the support/liner for a deep tunnel in anisotropic poro-elastic medium. This solution can take into account the distance from the section of support installation to the tunnel face that depends on the instant of support installation, i.e., influence of the tunnel face on the work of the support as well as the massif.

Finally, the general conclusions of the thesis point out the achievements as well as the further perspectives of this work.

INTRODUCTION GENERALE

Les tunnels profonds sont largement utilisés dans la pratique comme dans l'industrie minière, l'industrie pétrolière, le transport souterrain ou le stockage des déchets nucléaires, etc. Un tunnel est estimé profond si son diamètre (ou son diamètre équivalent, au cas où la section transversale n'est pas circulaire) est significativement plus petit que la profondeur de son axe, c'est-à-dire, si H/D>10 avec H la profondeur de l'axe du tunnel et D son diamètre. Cela signifie que la variation de la contrainte entre les bords supérieur et inférieur de la section transversale du tunnel (avant de l'excavation) est négligée par rapport la contrainte initiale verticale (généralement conséquence du poids de sol) à la profondeur moyenne du tunnel.

De nos jours, en accompagnement le développement des techniques et technologies dans le domaine de stockage profond notamment dans le contexte de stockage des déchets radioactifs, les constructions souterraines profondes sont un sujet d'actualité. Un problème souvent rencontré dans la construction de tels tunnels est leur placement dans des milieux poreux sédimentaires stratifiés qui manifestent un comportement mécanique et hydrique plus ou moins anisotrope.

L'analyse des tunnels et leur dimensionnement sont souvent effectués avec l'hypothèse que la roche est homogène et isotrope. Cependant, plusieurs résultats dans la littérature indiquent que le champ de contraintes et de déformations autour d'un tunnel dans un milieu anisotrope ainsi que ces champs dans le revêtement du tunnel diffèrent significativement de ceux obtenus sous l'hypothèse des propriétés isotropes et fortement dépendants de l'orientation de la stratification par rapport l'axe du tunnel (Hefny et Lo, 1999; Tonon et Amadei, 2002). Cela souligne l'importance de la prise en compte du comportement anisotrope du massif dans l'analyse les tunnels.

Une roche est un milieu poreux dont le comportement est régi par une influence réciproque entre les phénomènes mécaniques et hydrauliques. La première théorie du poro-élasticité qui traite du phénomène de diffusion-déformation couplé a été proposée par Biot (Biot, 1941). Depuis lors, la théorie isotrope de Biot a été élargie pour les matériaux anisotropes (Biot, 1955; Thompson et Willis, 1991). Plusieurs auteurs ont également eu des contributions importantes dans l'identification et la mise en rapport des constantes poroélastiques des matériaux avec des constantes d'ingénierie connues (Amadei, 1983; Cheng, 1997; Abousleiman et Cui, 2000). Par la suite, certaines solutions analytiques fondamentales ont été développées. Elles ont résolu les problèmes d'une excavation dans milieu poro-élasticité anisotrope en prenant en compte le comportement couplé des matériaux (Abousleiman et Ekbote, 2005; Abousleiman et Cui, 1998; Bobet, 2011).

En continuité des travaux cités ci-dessus, le présent travail est consacré à l'étude du comportement des tunnels profonds creusés dans les massifs d'anisotropie transverse, saturés en tenant compte du couplage hydro-mécanique. Basée sur la méthode des variables complexes et sur la technique de « conformal mapping », des solutions analytiques des contraintes et des déplacements autour des tunnels profonds sont développées. L’approche du potentiel complexe de Lekhnitskii pour l’élasticité anisotrope est utilisée afin d’inclure l'effet hydraulique. Notons, que ces solutions sont fondées sur un modèle de couplage unilatéral (one-way-coupling), c’est-à-dire, le seul effet des phénomènes hydrauliques sur la réponse mécanique est considéré, et pas l’inverse. Par conséquent, des analyses numériques sont réalisées en parallèle pour évaluer complètement les effets du comportement entièrement couplé sur la réponse du tunnel. Ces analyses numériques complèteront la solution analytique.

Ce travail vise à étudier le comportement d'un tunnel profond de section transversale circulaire dans un milieu poro-élastique anisotrope saturé. Concrètement, il y a quatre objectifs définis pour cette thèse, ils seront présentés dans les chapitres 2, 3 et 4:

1. Développer une solution analytique en régime permanent de l'écoulement interstitiel. De par le choix de la stratégie de l’approche analytique, la solution est obtenue par un modèle de couplage unilatéral, (one-way-coupling), en prenant en compte l'effet de la répartition de la pression des pores sur les réponses mécaniques.

2. Elargir la solution analytique, pour le cas de la transitoire hydraulique en utilisant le même schéma unilatéral de couplage se limitant à l’impact de l'évolution de la pression interstitielle en fonction du temps sur les réponses mécaniques.

3. Évaluer la pertinence des modèles à couplage unilatéral en comparaison avec des analyses réalisées avec un couplage complète. Pour ce faire, plusieurs analyses numériques sont effectuées et comparées avec les résultats obtenus par le couplage à sens unique. Evaluer les solutions proposées dans la situation de dimensionnement des tunnels.

4. Pour des applications dans la conception des tunnels, une extension de la solution analytique sur la méthode convergence-confinement est aussi bien abordée. Avec cette méthode on peut prendre en compte l'influence du front de taille du tunnel sur le travail du soutènement ainsi que sur le massif. La solution obtenue pourrait être utilisée comme un outil rapide pour dimensionnement des tunnels en milieu poreux sur la base de l'approche de la méthode de convergence-confinement.

Ce travail de recherche est organisé comme suit :

Le chapitre 1 est dédié à présenter la motivation, les concepts théoriques de base du milieu poro-élastique et les hypothèses fondamentales. Des équations constitutives pour le milieu poro-élastique utilisées plus tard seront présentées. L’anisotrope inhérente des roches sera examinée en mettant en évidence l'importance de sa prise en compte dans l’analyse des tunnels. Les principaux travaux de recherche issus de la bibliographie en rapport avec les thèmes les objectifs de la thèse sont analysés et résumés.

Le chapitre 2 développe une solution analytique pour un tunnel profond soutenu dans un massif rocheux saturé anisotrope. La solution analytique est développée en se basant sur la méthode des variables complexes, méthode efficace pour résoudre les problèmes de l'élasticité plane. L’approche du potentiel complexe de Lekhnitskii est utilisé pour résoudre le problème élastique anisotrope en prenant compte une distribution stationnaire de pressions de pores. La solution est basée sur un couplage à sens unique et pour un état hydraulique stationnaire. La solution analytique obtenue, décrit également l’interaction entre le massif et le revêtement en deux conditions extrêmes de drainage à l'interface massif-revêtement: non drainé et drainé stationnaire. Ensuite, la solution analytique est utilisée pour réaliser une série d'études paramétriques pour élucider les effets de différents paramètres sur la réponse du tunnel. La solution analytique est considérée comme un outil rapide à évaluer les contraintes et les déplacements autour des tunnels.

Le chapitre 3 se compose de deux parties. La première est consacrée à développer une solution analytique pour le problème hydro-mécanique en régime transitoire basée sur le un couplage unilatéral. La solution transitoire hydraulique peut être considérée comme un ensemble d’états d’équilibre successifs en utilisant un rayon de l’influence en fonction du temps. L'approche du potentiel complexe utilisé dans le chapitre 2 pourrait donc être appliquée à chaque instant du processus de calcul. Notons que le modèle de couplage à sens unique ne peut pas décrire le comportement hydro-mécanique complétement couplé; néanmoins, il pourrait aider à observer l'impact de la répartition de la pression interstitielle sur la réponse mécanique en fonction du temps. Par conséquent, la deuxième partie de ce chapitre est consacrée aux simulations numériques des tunnels dans massifs rocheux saturés anisotropes réalisées avec un couplage hydro-mécanique complet. Les analyses numériques sont réalisées avec le code aux éléments finis Code-ASTER. Les estimations paramétriques seront également réalisées afin d'évaluer complètement les effets réciproques entre les phénomènes mécaniques et hydrauliques.

Le chapitre 4 élargie la solution obtenue au chapitre 2 en s'appuyant sur l'approche de la méthode convergence-confinement pour étudier l'interaction entre le massif rocheux et le soutènement/revêtement pour un tunnel profond en milieu poro-élastique anisotrope. Cette solution peut prendre en compte l'influence de la distance de la section d’installation du soutènement au front de taille du tunnel sur le travail du soutènement ainsi que sur le massif, c'est-à-dire, considérer l’instant d’installer le soutènement.

Enfin, la conclusion générale de la thèse soulignera les résultats acquis ainsi que les perspectives de recherche.

CHAPTER 1: BIBLIOGRAPHIC STUDY ON HYDRO –MECHANICAL BEHAVIOR OF ANISOTROPIC POROUS MEDIA

1.1 Introduction

The determination of stresses and displacements around a deep tunnel is a primary topic in the design and evaluation of stability and safety of underground openings. The engineering practice on this topic is mainly based on the known solutions of deep tunnels on elastic isotropic medium. When the anisotropic behavior of rock masses is considered many of existing works in the literature are limited on the anisotropy of mechanical behavior while the anisotropic poromechanic behavior is often judge quite complex.

This complexity explains why almost always the analyses of stresses and displacements in the liner as well as in the rock surrounding a deep tunnel, are based on simplified assumptions of homogeneous and isotropic rock or/and isotropic initial stresses. The solutions obtained on these assumptions become much simpler. Following that, the responses of the rock and the liner are the same in all directions; moreover, the liner is not bended. However results obtained after these assumptions could be somewhat qualitative for estimation of the stability of tunnels in anisotropic media.

Many analytical solutions for analysis of shallow or deep lined tunnels, which are based on the isotropic assumptions, can be listed here such as: in dry ground or below the water table (Bobet, 2001, 2003, 2007; Bobet et al., 2006, 2007; Carranza-Torres and Zhao, 2009), for elastic problems (Verruijt and Booker 1996; Verruijt 1997, 1998; Exadaktylos and Stavropoulou 2002), for poroelastic problems (Carter and Booker, 1984; Wang, 1996, 2000; Abousleiman, 1997; Chen and Yu, 2015), for plastic problems (Carranza-Torres and Fairhurst 2000, 2004), and poro-plastic rock (Hoxha et al., 2004; Bobet, 2009a).

The tunnels, however, are often built in heterogeneous and anisotropic medium due to the inherent anisotropy of sedimentary rock masses and their stratified structure. Duncan and Goodman (1968), Amadei and Goodman (1981a, 1981b), Wittke (2014) have indicated that, the existence of a stratified structure of rock leads to an anisotropic response of the rock masses under loading and unloading. It is also the case for the response of rock masses traversed by oriented discontinuities even if the intact rock (without discontinuities) is isotropic. In both cases modeling of rock mass as isotropic, could be considered as an approximation more or less accurate depending on the degree of anisotropy of rock masses.

A type of rock encountered usually in tunnel construction, the sedimentary rocks, has stratified structure with directional properties due to the depositional medium. These rocks could be described as transversely isotropic one with the axe of symmetry coinciding with the direction of deposition. Rahn (1984) indicated that, if measured normally and parallel to the bedding plane, the Young modulus of a foliated rock varies by about 50%. Chenevert (1964) measured four different types of stratified rocks and showed that the degrees of anisotropy varied from 1.02 to 1.5. Recently, in constructing the underground rock laboratory (URL) in the context of the underground storage of nuclear waste, one measured the degree of anisotropy of Callovo-Oxfordian clay, Opalinus clay and Boom clay stones in the range of 1.2-2.5 (Armand, 2013; Millard et al., 2013; Charlier et al., 2013). Lama and Vutukuri (1978) presented data records showing the relative frequency of anisotropy in sedimentary rocks as illustrated in Fig. (1.1). It is observed that, the degree of anisotropy for most sedimentary rock estimated is in range of 1.0-1.5.

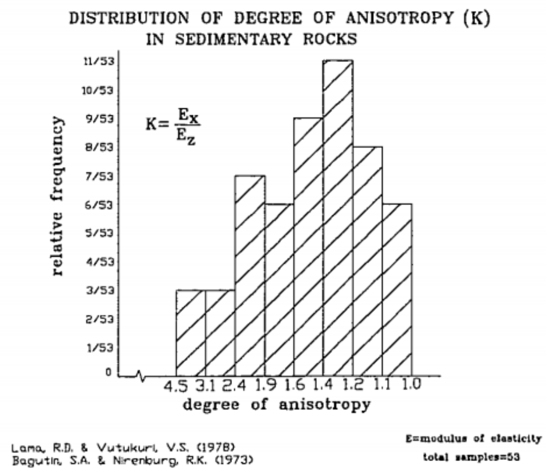

Fig. 1-1: Distribution of degree of anisotropy in sedimentary rocks according to Lama and Vutukuri, 1978

In-situ records and characterization of EDZ in URL in Bure (Fig. 1.2) show that the convergence on the wall of an observation tunnel, which is oriented in the direction of major principle stress, is almost 2 times greater in the horizontal direction than in vertical one while the EDZ extensions in the horizontal direction is almost 8 times greater (Armand et al., 2013, 2014; Carrillo et al., 2015). These manifest clearly an anisotropic response of rock masses since the cross section stress in situ is nearly isotropic. However the role of mechanical and hydraulical anisotropies is not clear.

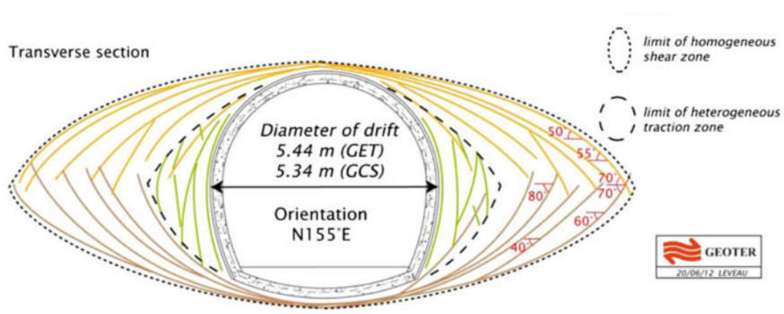

Fig. 1-2: EDZ in GCS (Galerie de conception souple), Bure URL, France (Armand et al., 2014)

For the past two decades, several authors considered the behavior of deep tunnels in elastic anisotropic rocks. For example, Hefny and Lo (1999), Bobet (2011) mentioned the tunnel in dry rock or under the water table; Vu et al. took into account a nonlinear elastic behavior of the material; Tran et al. (2015a) and Zhang and Sun (2011) focused on the tunnel with the arbitrary cross section in dry rock.

Relatively few works deal with behavior of deep tunnels when anisotropic hydro-mechanical coupling is considered. For example, Abousleiman and Cui (1998) investigated the behavior of a borehole in a transversely poroelastic media but they only considered the case that the cross section of the borehole is parallel to the isotropic plane of media whose compatibility equation and fluid diffusion of transversely isotropy are the same as that of isotropy case.

In a recent contribution of Bobet (Bobet and Yu 2015), the authors determine the stress field near the crack tip in the poroelastic transversely isotropic saturated rock. In order to deduce the analytical solution for this problem, Bobet (2015) use the well-known complex potential approach firstly presented by Lekhnitskii (Lekhnitskii 1963) and later adopted and applied for many rock engineering problems by Amadei (1983) in the context of the anisotropic poroelastic medium.

At our best knowledge, a complete study about the behavior of a deep lined tunnel taking into account the hydro-mechanical behavior model is not still well documented, and constitutes in the same time a challenge and an interesting topic research whose application would be interesting in many fields of human activity. A desire to clarify the mechanisms governing the behavior of a lined deep tunnel in saturated anisotropic porous medium as well as the effect of hydro-mechanical parameters on the responses of the tunnel have largely promoted the present work.

This dissertation is oriented towards the development of an analytical solution for the considered problem and it may be used on design of tunnels. As we know, however, the inherent complexity in developing a complete analytical solution taking into account the reciprocal impact mechanism of hydro-mechanical coupling, further numerical analyses are performed to validate and then to complete this analytical solution.

It is envisaged that the hydro-mechanical solution for the deep tunnel in anisotropic rock in the present dissertation will provide an initial view, a quick analysis tool for design and evaluation of the stability of the tunnels. In addition, this could also give the recommendations as basis to orient next studies in the same subject.

1.2 Poroelastic theory

1.2.1 Introduction

Poroelasticity can be sweepingly described as a science, a branch of physics, whose study object is a porous medium subjected to internal and/or external forces. The porous medium consists of a solid matrix and a simply connected pore space which is filled by one or more freely moving fluids or gases (Detounay and Cheng, 1993; Coussy, 1995).

Due to the existence of the mixture filling the pores, the behavior of porous medium is always characterized by a coupling between the deformation of the solid matrix and the diffusion of the interstitial pore fluid pressure. The poromechanical and physical characteristics of the porous medium and the fluid decide the nature of the deformation, rate of diffusion and intensity of the coupling. The coupled response is a result of at least two actions which occur concurrently and influence each other. On the one hand, the applied stress induces a change in pore volume, thereby, influences the fluid pressure or fluid mass. This phenomenon may be considered as the solid-to-fluid coupling. On the other hands, the change in the fluid pressure or fluid mass also produces a change in the volume of the porous material which is referred to as the fluid-to-solid coupling (Wang, 2000). According to Rice and Cleary (1976), and Cleary (1977), the porosity of the medium, the compressibility of the matrix and pores, and the pore fluid affect the intensity of the coupling. The change of the pore pressure field produces a hydraulic gradient which could lead to a diffusive fluid mass transport. This fluid diffusion also progressively influences the deformation which results in a time-dependent response (Detournay and Cheng, 1993; Coussy, 1995). There is a great deal of factors which can influence the poromechanical behavior of geomaterials. Regarding to the stress-deformation relation, many porous material models are proposed such as, the linear elastic, non-linear elastic, viscoelastic and/or plastic models (Coussy, 1995). In addition, the porous medium is considered as either fully or partially saturated and the pore fluids can be modeled as Newtonian or non-Newtonian fluids.

The earliest theory taking into account the influence of pore fluid on the quasi-static deformation of soils was proposed by Terzaghi (1923) who developed a model of one-dimensional consolidation. This theory nowadays is still widely used in soils mechanics. After that, the theory was generalized to three-dimension problem by Rendulic (1936). However, Biot is the pioneer who developed a linear theory of poroelasticity that is fit for the two basic phenomena, i.e., solid-to-fluid coupling and fluid-to-solid coupling as mentioned above (Biot, 1935, 1941). In an attempt to generalize consolidation theory, the theory of anisotropic poroelasticity was formulated by Biot (1955). Rice and Cleary (1976) reformulated Biot theory by expressing the linear elastic behavior law based on other parameters that are well-known in soil mechanics and rock mechanics such as the coefficient of Skempton and undrained Poisson ratio. This theory developed initially for linear elastic behavior of an isotropic material was later generalized to anisotropic poroelastic media and viscosity behavior. Recently, Coussy (2004) proposed a general theory of poroelastoplasticity for saturated porous materials by introducing the concepts of plastic effective stress and plastic porosity.

1.2.2 Description of the porous medium

In porous medium, one distinguishes the closed pores which do not share with their neighbors and connected pores in which exchanges are numerous.

A physical quantity of porous medium used in study is its porosity which is defined as the ratio of the volume of the connected porous space to the total volume (Coussy, 1995, 2004). Henceforth, the porosity is referred to the entire connected porosity. The connected porous space is either fully or partially filled with a number of fluids which are optionally present in several phases (liquid, gas or vapor). It has been shown by several authors that this porosity may have a primarily effect on some rock properties such as permeability (Murky and Zinszner 1985), compressibility (Walsh and Grosenbaugh 1979; Walsh and Brace, 1984). The matrix component is, therefore, assumed to constitute of a solid part and a possible closed porous one, whether saturated or not, but through which no permeation occurs. The solid phase of rock can vary significantly from a rock to another one by its mineralogical composition and structure. It consists of an assembly of grains, often polycrystalline, whose contacts are more or less coherent after sedimentation by forming a cement of various origins. This solid phase is characterized by a strong cohesion in comparison with the soil. The solid phase can be characterized by its mineralogical composition and by its elastic properties which can be measured or estimated on the basis of elastic constants of its components (Brace 1965).

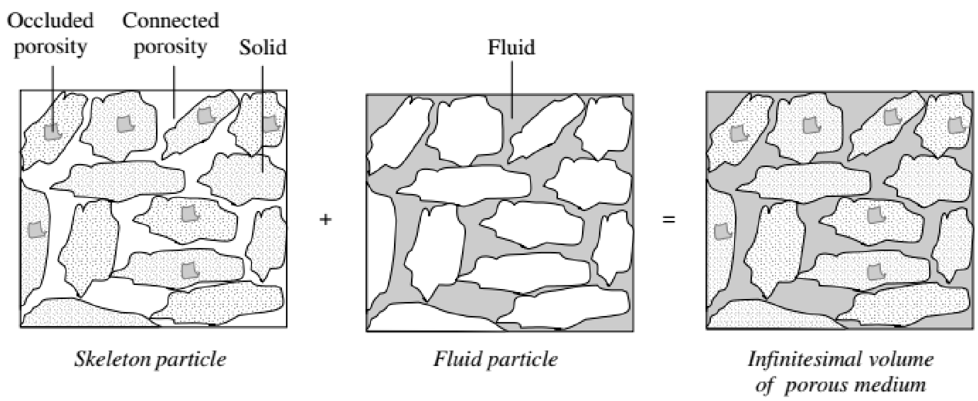

Fig. 1-3: A schematic of the porous media idealization (Coussy 2004)

1.2.3 Assumptions

In the following we present several common assumptions adopted and may be considered as the basic framework for development of the poroelastic models.

- The porous media is considered as a continuous and homogeneous solid-fluid mixture which consists of the matrix and the porous space fully or partially filled by fluids and the fluids can freely move through the connected pores.
- The strain-displacement relations obey the small deformation theory
- The constitutive relations rely on the linear, elastic and reversible Hooke law
- The anisotropy of the medium is a consequence of the structural arrangement of the grains or pores
- The interstitial fluid flow is assumed to be laminar and can be described using Darcy's law
- The sign convention used in mechanics, i.e., the tension is taken as positive and compression as negative

1.2.4 Deformation Restrictions

1.2.4.1 Strain-Displacement Relations:

Under applied loading, the elastic body will change the shape or deform. If we know the displacement field within the elastic body, we can quantify these deformations based on the continuum mechanics approach. The finite strain of the body can be expressed as follows (Sadd, 2009):

$$\varepsilon_{ij} = \frac{1}{2}\left(u_{i,j} + u_{j,i} + u_{k,i}u_{k,j}\right) \tag{1.1}$$

Where ε_{ij} is the strain tensor and u_i is the displacement vector. In Eq. (1.1), the Einstein index convention has been used where a repeated index denotes summation while a comma followed by an index indicates differentiation. According to small deformation theory, the higher order term $u_{k,i}u_{k,j}$ can be eliminated, and thus, one has the simplified strain-displacement relation as:

$$\varepsilon_{ij} = \frac{1}{2}\left(u_{i,j} + u_{j,i}\right) \tag{1.2}$$

It should be noted that the strain is a symmetric second-order tensor, i.e.

$$\varepsilon_{ij} = \varepsilon_{ji} \tag{1.3}$$

1.2.4.2 Strain Compatibility:

With the assumption of continuum porous medium and that the medium is bounded by simply connected region, one has some additional relations necessary to ensure continuous, single-valued displacement field solutions. This means that each element of the medium has been exhaustively deformed; taking into consideration neighboring elements so that the system fits together thus yielding continuous, single-valued displacements. Under the assumption of small displacements and by eliminating the displacements from the strain-displacement relations in Eq. (1.1) one obtains the following relations:

$$\varepsilon_{ij,kl} + \varepsilon_{kl,ji} - \varepsilon_{ik,jl} - \varepsilon_{jl,ik} = 0 \tag{1.4}$$

These relations are referred as the Saint-Venant compatibility equations.

1.2.5 Conduction Laws:

In the porous medium, if there is a difference in potentials, it will induce a flow from higher potential position to lower potential one. For example, a difference in the hydraulic potential causes a fluid flow in the porous medium. This phenomenon also occurrs with the thermal conductivity. The resulting flux is explained by the phenomenological coefficients theory of Onsager which is expressed as follows (De Groot, 1952):

$$J_i = L_{ij} X_{,j} \tag{1.5}$$

In which J_i is the flux, X is potential gradient and L_{ij} are phenomenological coefficients. These coefficients are permeability or heat conductivity, etc. One characteristic of the phenomenological coefficients L_{ij} is symmetric property, i.e., $L_{ij} = L_{ji}$.

Darcy's Laws:

The flow of a fluid through a porous medium can be described by the well-known Darcy's law. The law was proposed in 1856 by Henry Darcy based on the results of experiments on the water flow through sand layers. Darcy's law also can be derived from Navier-Stokes equations by dropping the inertial terms. Darcy's law is defined by the relation between the fluid flux and the pressure gradient in fluid saturated porous material. Therefore, one can replace the matrix of phenomenological coefficients L_{ij} in E.q (1.5) by the anisotropic permeability matrix. The general expression of Darcy's with eliminating the body forces is given in following form (Cheng, 2016):

$$q_i^f = -\kappa_{ij} p_{,j} \tag{1.6}$$

where q_i^f is the specific discharge vector, κ_{ij} is the anisotropic permeability coefficient tensor and $p_{,j}$ denotes the pore pressure gradient. The permeability coefficient tensor is related to the anisotropic intrinsic permeability tensor, k_{ij} by $\kappa_{ij} = k_{ij} / \mu$, where μ is the fluid viscosity. In general, the intrinsic permeability k_{ij} is dependent on pore geometry. In particular, it is strongly dependent on the porosity ϕ of the porous material. For instant, the Carman-Kozeny law indicates a power relation as: $k_{ij} \sim \phi^3 / (1-\phi)^2$ (Detoumay and Cheng, 1993). For an isotropic case, E.q. (1.6) reduces to:

$$q_i^f = \kappa p_{,i} \tag{1.7}$$

In which κ is the isotropic permeability coefficient.

1.2.6 Conservation Laws

1.2.6.1 Mass Conservation

The conservation principle of mass is valid for any system. For the solid, since small movements were observed, it can be considered that the density of the solid is constant. However, for fluids, these equations are very important. The expression of mass balance of fluid in a saturated medium considering input/output mass amounts across an element is given by (Bear, 1972):

$$\frac{\partial \chi}{\partial t}+q_{i,i}=0 \tag{1.8}$$

Where χ is the change in fluid content and q_i is the relative flux.

1.2.6.2 Momentum conservation – mechanical equilibrium

The mechanical balance is satisfied in static or quasi-static state by the nullity of the sum of the forces applied to the system, i.e., volume forces and surface forces:

$$\sigma_{ij,j}+f_i=0 \tag{1.9}$$

where σ_{ij} is stress tensor and f_i is body force vector.

1.2.7 Constitutive Equations:

Under the impact of perturbations, there are changes in dynamic and kinematic quantities of the porous medium. The material constants and constitutive relations of each poromechanics model will determine the changes in these dynamic and kinematic variables of the porous medium. In a porous system, the stresses, pore pressure and temperature are the dynamic variables whereas the strain and the variation of the fluid content are the kinematic variables.

The constitutive equations express the relations between the dynamic variables (stress, pore pressure, temperature) with the kinematic variables (strain, variation of fluid content) through the material coefficients.

In the following part, we will present the constitutive equation for hydro-mechanical model commonly used in studying the porous medium.

1.2.7.1 Concept of effective stress

The role of fluid is usually considered by using the concept of effective stress which is developed by Karl Terzaghi in 1923 (Terzaghi, 1943) in the context of the classical theory of one-dimensional consolidation of saturated soils. The effective stress is defined as the only constraint variable that governs the response of stress and deformation of a porous material, independently on the value of the pore pressure. Although the effective stress model of Terzaghi is based initially on the one-dimensional consolidation problem, it is still valid in three-dimensional one. This concept is expressed by the following relation:

$$\sigma'_{ij}=\sigma_{ij}+p\delta_{ij} \tag{1.10}$$

where σ'_{ij} is the effective stress tensor, σ_{ij} is the total stress tensor, p is pore pressure and δ_{ij} is the Kronecker product tensor. This concept of effective stress is based on the following assumptions: the medium is saturated with a single fluid; the grains constituting the solid matrix and the saturated fluid are incompressible; the fluid flow through the pores is laminar and obeys the Darcy's law.

Later on, Biot proposed the model of poroelasticity which accounts for the coupled diffusion-deformation phenomenon (Biot, 1935, 1941). Therefore, the relation between the effective stress and the pore pressure is adjusted as follows:

$$\sigma'_{ij} = \sigma_{ij} + \alpha_{ij} p \tag{1.11}$$

where α_{ij} is the Biot's effective stress coefficient tensor. Thus, it is seen that, the Terzaghi effective stress model is one special case of the Biot's effective stress model when the Biot's effective stress coefficients are equal to 1.

As presented previously, the Biot's poroelasticity theory is concerned as fundamental framework of soil and rock mechanics and used widely in the study.

1.2.7.2 Constitutive equations of Poroelasticity

Taking into account the relation between the effective stress and the strain through material parameters, i.e., Hooke's law, the general expressions of constitutive equations of the poroelastic medium are given as (Thompson and Willis, 1991; Abousleiman and Cui, 1998):

$$\begin{aligned} \sigma_{ij} &= M_{ijkl}\varepsilon_{kl} - \alpha_{ij} p, \\ p &= M(\chi - \alpha_{ij}\varepsilon_{ij}) \end{aligned} \tag{1.12}$$

where ε_{ij} is the strain tensor, χ indicates the change of fluid volume (per unit volume of porous material), M_{ijkl} is the drained elastic modulus tensor, and M is Biot's modulus.

It is noted that, Eq. (1.12_1) expresses the stress-strain relation, i.e., the relation of the generalized Hooke law, whereas E.q (1.12_2) indicates the relation between the pore pressure, the change of fluid volume and the volumetric strain of the medium $\alpha_{ij}\varepsilon_{ij}$. The Biot's coefficients α_{ij} in E.q (1.12) is the coupling term. The material constants include the drained elastic modulus tensor M_{ijkl} , the Biot's effective stress tensor α_{ij} and the Biot's modulus M .

1.3 Inherent Anisotropy in Rocks

The main difference between anisotropic elasticity and isotropic elasticity is that deformation depends on orientations. In other words, the stress-strain response of a material in one direction is different compared to the others. The rock in which we construct tunnels are usually not isotropic: perfect isotropy of a rock is rarely encountered because of the orientation of minerals and discontinuities. Common examples on underground construction include sedimentary and metamorphic foliated rocks (Amadei, 1983; Cheng, 1997). Therefore, in order to study the work of the tunnels in anisotropic medium, we firstly study the basic physical properties of anisotropic materials. In this part, we mention generally the nature of anisotropic material regarding the (hydro)-mechanical aspect. Several special cases of anisotropic material will be discussed in this section. It should be noted that, we limit the object of this section in the elastic anisotropic material.

1.3.1 Material Symmetry

For the general anisotropic case (also called as triclinic material), one has 21 needed independent elastic constants for characterization of the material response (Lekhnitskii, 1963; Saad, 2009). The drained elastic modulus tensor is given by:

$$M = \begin{pmatrix} M_{11} & M_{12} & M_{13} & M_{14} & M_{15} & M_{16} \\ M_{12} & M_{22} & M_{23} & M_{24} & M_{25} & M_{26} \\ M_{13} & M_{23} & M_{33} & M_{34} & M_{35} & M_{36} \\ M_{14} & M_{24} & M_{34} & M_{44} & M_{45} & M_{46} \\ M_{15} & M_{25} & M_{35} & M_{45} & M_{55} & M_{56} \\ M_{16} & M_{26} & M_{36} & M_{46} & M_{56} & M_{66} \end{pmatrix} \tag{1.13}$$

where M_{ij} are components of the drained elastic modulus tensor.

Many real materials, however, have some types of symmetry, which could reduce further the required number of independent elastic constants (Lekhnitskii, 1963; Saad, 2009).

1.3.1.1 Monoclinic Material

If through each point within a body there is an across plane of symmetry which divides the medium into sides equivalent to each other regarding the elastic properties, this is referred to as a plane of elastic symmetry of the material. As shown in Figure 1-4, the plane of symmetry is *x-y* plane, the direction (*z*-axis) normal to the plane of symmetry is called the principal direction of elasticity. This material is commonly called as a monoclinic material.

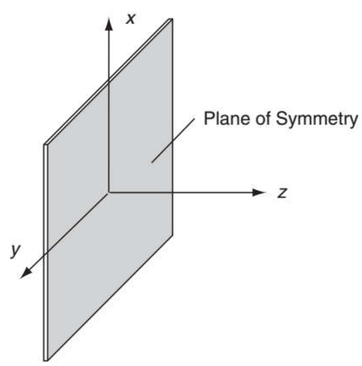

Fig. 1-4: Plane of symmetry for a monoclinic material

The drained elastic modulus is tensor given as follows (Lekhnitskii, 1963; Saad, 2009):

$$M = \begin{pmatrix} M_{11} & M_{12} & M_{13} & 0 & 0 & M_{16} \\ M_{12} & M_{22} & M_{23} & 0 & 0 & M_{26} \\ M_{13} & M_{23} & M_{33} & 0 & 0 & M_{36} \\ M_{14} & 0 & 0 & M_{44} & M_{45} & 0 \\ M_{15} & 0 & 0 & M_{45} & M_{55} & 0 \\ M_{16} & 0 & 0 & 0 & 0 & M_{66} \end{pmatrix} \tag{1.14}$$

Therefore, it can be observed that, for characterization of the monoclinic materials, one must have 13 independent drained elastic moduli.

1.3.1.2 Orthotropy

If through each point in the medium one has three mutually perpendicular planes of symmetry, thereby, the material properties are independent of direction within each plane. The material is referred to as orthotropic material. (see Figure 1-5).

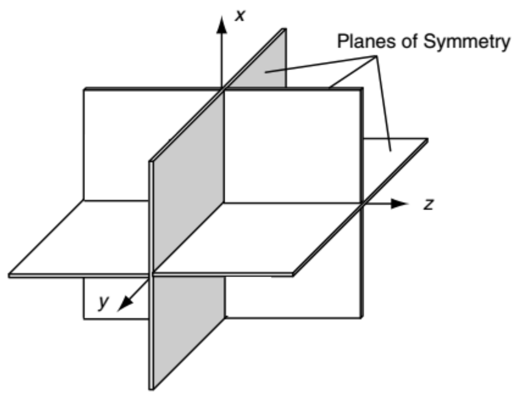

Fig. 1-5: Three planes of symmetry for an orthotropic material.

The drained elastic modulus tensor is given by (Amadei, 1983; Cui, 1995; and Cheng, 1997):

$$M = \begin{pmatrix} M_{11} & M_{12} & M_{13} & 0 & 0 & 0 \\ M_{12} & M_{22} & M_{23} & 0 & 0 & 0 \\ M_{13} & M_{23} & M_{33} & 0 & 0 & 0 \\ 0 & 0 & 0 & M_{44} & 0 & 0 \\ 0 & 0 & 0 & 0 & M_{55} & 0 \\ 0 & 0 & 0 & 0 & 0 & M_{66} \end{pmatrix} \tag{1.15}$$

It is seen from Eq. (1.15) that, to describe an orthotropic material behavior; the number of independent elastic constants is reduced to 9. Let us consider $E_i (i = 1,2,3)$ which are the drained Young's moduli in directions i, and $G_{ij} (i, j = 1,2,3)$ which are the shear moduli for planes parallel to the coordinate planes $i - j$ and ν_{ij} which are the drained Poisson's ratio. These ratios are characterized by the compressive strain in j - direction induced by a tensile stress in the i-direction. For the anisotropic material, the following relations between the moduli and the Poisson ratios must be satisfied to the compatibility of the material parameters (Lekhnitski, 1963; Amadei, 1983):

$$E_1 \nu_{21} = E_2 \nu_{12}; \quad E_2 \nu_{32} = E_3 \nu_{23}; \quad E_3 \nu_{13} = E_1 \nu_{31} \tag{1.16}$$

One can find the expressions of the components of the drained elastic modulus tensor for the orthotropic material in Lekhnitskii (1963), Amadei (1983), or Abousleiman et al. (1996a):

$$M_{11}=\frac{E_1(\nu_{23}\nu_{12}-1)}{\nu_d};\quad M_{12}=-\frac{E_2(\nu_{13}\nu_{32}+\nu_{12})}{\nu_d};$$
$$M_{13}=-\frac{E_3(\nu_{12}\nu_{23}+\nu_{13})}{\nu_d};\quad M_{22}=\frac{E_2(\nu_{13}\nu_{31}-1)}{\nu_d};$$
$$M_{23}=-\frac{E_1(\nu_{13}\nu_{21}+\nu_{23})}{\nu_d};\quad M_{33}=\frac{E_3(\nu_{12}\nu_{21}-1)}{\nu_d};$$
$$M_{44}=G_{12};\quad M_{55}=G_{23};\quad M_{66}=G_{13} \tag{1.17}$$

where ν_d is defined as follows:

$$\nu_d=\nu_{21}\nu_{12}+\nu_{31}\nu_{13}+\nu_{23}\nu_{32}+\nu_{12}\nu_{23}\nu_{31}+\nu_{13}\nu_{32}\nu_{21}-1 \tag{1.18}$$

As we know, the compliance tensor is in inverse to the drained elastic modulus tensor. Thus, based on the drained elastic modulus tensor with the components given above, one deduces the compliance tensor C_{ijkl} in the following:

$$C_{ijkl}=\begin{pmatrix} C_{11} & C_{12} & C_{13} & 0 & 0 & 0 \\ C_{12} & C_{22} & C_{23} & 0 & 0 & 0 \\ C_{13} & C_{23} & C_{33} & 0 & 0 & 0 \\ 0 & 0 & 0 & C_{44} & 0 & 0 \\ 0 & 0 & 0 & 0 & C_{55} & 0 \\ 0 & 0 & 0 & 0 & 0 & C_{66} \end{pmatrix} \tag{1.19}$$

in which:

$$C_{11}=\frac{1}{E_1};C_{22}=\frac{1}{E_2};C_{33}=\frac{1}{E_3};$$
$$C_{12}=-\frac{\nu_{21}}{E_2}=-\frac{\nu_{12}}{E_1};C_{13}=-\frac{\nu_{31}}{E_3}=-\frac{\nu_{13}}{E_1}; \tag{1.20}$$
$$C_{23}=-\frac{\nu_{32}}{E_3}=-\frac{\nu_{23}}{E_2}$$

As mentioned previously, the Biot law is commonly used in poromechanics. For orthotropic porous medium, the Biot's effective stress coefficients are given in three principle directions. Thus, the Biot's effective stress coefficients tensor takes the form (Thompson and Willis, 1991; Abousleiman and Cheng, 1993):

$$[\alpha]=[\alpha_1 \quad \alpha_2 \quad \alpha_3 \quad 0 \quad 0 \quad 0]^T \tag{1.21}$$

With the same form, one has the Skempton's pore pressure coefficient tensor as follows (Thompson and Willis, 1991; Abousleiman and Cheng, 1993):

$$[B]=[B_1 \quad B_2 \quad B_3 \quad 0 \quad 0 \quad 0]^T \tag{1.22}$$

Abousleiman (1996) indicated that, it is difficult to measure the anisotropic coefficients $\alpha_i (i = 1,2,3)$. However, one enables to determine them under a special assumption of micro-isotropy and micro-homogeneity. Concretely, the solid grains are individually homogeneous and isotropic, and the macroscopic anisotropy is a consequence of the structural arrangement of the grains or pores. The components of Biot's effective stress coefficient tensor are related to the components of the drained elastic moduli in the following (Cheng, 1996; Abousleiman, 1996):

$$\begin{aligned} \alpha_1 &= 1 - \frac{M_{11} + M_{12} + M_{13}}{3K_s}; \\ \alpha_2 &= 1 - \frac{M_{12} + M_{22} + M_{23}}{3K_s}; \\ \alpha_3 &= 1 - \frac{M_{13} + M_{23} + M_{33}}{3K_s} \end{aligned} \tag{1.23}$$

where K_s is the solid grain bulk modulus. Therefore, the Biot's effective stress coefficients can be evaluated through one measurement of K_s and with the knowledge of the drained elastic moduli. In the hydrogeology literature, one can determine the Biot's modulus (Biot & Willis, 1957) M as the inverse of the storage coefficient (Green and Wang, 1990), and can be presented as follows (Abousleiman, 1996):

$$M = \frac{K_s^2}{K_s\left[1 + \phi(K_s / K_f - 1)\right] - \bar{M}/9} \tag{1.24}$$

where ϕ is the porosity, K_f is the pore fluid compressibility and $\bar{M}$ is determined by:

$$\bar{M} = M_{11} + M_{22} + M_{33} + 2(M_{12} + M_{23} + M_{13}) \tag{1.25}$$

The other important parameters in poromechanics, Skempton's pore pressure coefficient tensor, are given in the similar form (Cheng, 1997):

$$\begin{aligned} B_1 &= \frac{3K_s(C_{11} + C_{21} + C_{31}) - 1}{K_s\bar{C} + \phi K_s / K_f - (1-\phi)}; \\ B_2 &= \frac{3K_s(C_{12} + C_{22} + C_{32}) - 1}{K_s\bar{C} + \phi K_s / K_f - (1-\phi)}; \\ B_3 &= \frac{3K_s(C_{13} + C_{23} + C_{33}) - 1}{K_s\bar{C} + \phi K_s / K_f - (1-\phi)} \end{aligned} \tag{1.26}$$

in which $\bar{C}$ is determined by:

$$\bar{C} = C_{11} + C_{22} + C_{33} + 2\left(C_{12} + C_{23} + C_{13}\right) \tag{1.27}$$

1.3.1.3 Transverse Isotropy

In fact, one encounters many materials that have the same properties in one plane (e.g. the *x-y* plane, also known as the isotropic plane) whereas they have different properties in the direction normal to this plane, and so, they are named as transversely isotropic materials. These materials have an axis of rotational elastic symmetry. The drained elastic modulus tensor is given by Eq. (1.17) of orthotropic materials with

$$M_{22} = M_{11}; \quad M_{23} = M_{13}; \quad M_{66} = M_{55} \tag{1.28}$$

Therefore, only 5 independent elastic constants are required to describe material behavior, instead of 9 for fully orthotropy. They are denoted by: E, E', ν, ν' and G' where E is the Young's modulus in the isotropic plane, E' is the Young's modulus in the transverse direction, ν is the Poisson's ratio which characterizes the transverse strain reduction in the isotropic plane due to a tensile stress in the same plane, ν' is the Poisson's ratio which gives the transverse strain reduction due to a tensile stress in the direction normal to the isotropic plane, and the shear modulus of a plane normal to the isotropic plane G'. Under the drained condition, the components of the elastic modulus tensor are given by (Cheng, 1997):

$$\begin{gathered} M_{11} = \frac{E(E' - E\nu'^2)}{(1+\nu)(E' - E'\nu - 2E\nu'^2)}; \quad M_{12} = \frac{E(E'\nu + E\nu'^2)}{(1+\nu)(E' - E'\nu - 2E\nu'^2)}; \\ M_{13} = \frac{EE'\nu'}{(E' - E'\nu - 2E\nu'^2)}; \quad M_{33} = \frac{E'^2(1-\nu)}{(E' - E'\nu - 2E\nu'^2)}; \\ M_{44} = G = \frac{E}{2(1+\nu)}; \quad M_{55} = G' \end{gathered} \tag{1.29}$$

The compliance tensor C_{ijki} is given by Eq. (1.20) of orthotropic material with $C_{22} = C_{11}; C_{23} = C_{12}; C_{66} = C_{55}$ for transverse isotropic materials. The components of compliance tensor relate to the elastic constants as follows (Cheng, 1997):

$$\begin{gathered} C_{11} = \frac{1}{E}; \quad C_{12} = -\frac{\nu}{E}; \quad C_{13} = -\frac{\nu'}{E'}; \\ C_{33} = \frac{1}{E'}; \quad C_{44} = \frac{1}{G}; \quad C_{55} = \frac{1}{G'} \end{gathered} \tag{1.30}$$

The elements of Biot's effective stress coefficient tensor (1.23) are given by (Cheng, 1997):

$$\begin{aligned} &\alpha_1 = \alpha_2 = \alpha = 1 - \frac{M_{11} + M_{12} + M_{13}}{3K_s}; \\ &\alpha_3 = \alpha' = 1 - \frac{2M_{13} + M_{33}}{3K_s}; \\ &\alpha_4 = \alpha_5 = \alpha_6 = 0 \end{aligned} \tag{1.31}$$

and Skempton's coefficients:

$$B_1 = B_2 = B = \frac{3K_s[(1-\nu)/E - \nu'/E] - 1}{K_s\bar{C} + \phi K_s / K_f - (1-\phi)};$$
$$B_3 = B' = \frac{3K_s[1/E - 2\nu'/E] - 1}{K_s\bar{C} + \phi K_s / K_f - (1-\phi)}; \tag{1.32}$$
$$B_4 = B_5 = B_6 = 0$$

where

$$\bar{C} = 2C_{11} + C_{33} + 2C_{12} + 4C_{13} \tag{1.33}$$

1.3.1.4 Isotropy

The isotropic material has the property being invariant under translation and rotation. Thus, only 2 elastic constants are required to characterize this material. The drained elastic parameters for the isotropic material are given as:

$$M_{11} = M_{22} = M_{33} = \frac{E(1-\nu)}{(1+\nu)(1-2\nu)};$$
$$M_{12} = M_{13} = M_{21} = M_{23} = M_{32} = M_{31} = \frac{E\nu}{(1+\nu)(1-2\nu)}; \tag{1.34}$$
$$M_{44} = M_{55} = M_{66} = G = \frac{E}{2(1+\nu)}$$

and the elements of the compliance matrix are:

$$C_{11} = C_{22} = C_{33} = \frac{1}{E};$$
$$C_{12} = C_{13} = C_{21} = C_{23} = C_{32} = C_{31} = -\frac{\nu}{E}; \tag{1.35}$$
$$C_{44} = C_{55} = C_{66} = \frac{1}{G} = \frac{2(1+\nu)}{E}$$

The Biot’s effective stress coefficients and the Skempton’s coefficients given as:

$$\alpha_1 = \alpha_2 = \alpha_3 = \alpha = 1 - \frac{K}{K_s};$$
$$\alpha_4 = \alpha_5 = \alpha_6 = 0 \tag{1.36}$$

$$B_1 = B_2 = B_3 = B = \frac{K_s / K - 1}{K_s / K + \phi K_s / K_f - (1-\phi)};$$
$$B_4 = B_5 = B_6 = 0 \tag{1.37}$$

1.3.2 Joint Rock

In rock mechanics, the term “discontinuity” is used as a common term for all planes of weakness where the coherence of intact rock is interrupted. It seems that, one more often uses the term discontinuity instead of the term “fracture” (Wittke, 2014).

In order to classify discontinuities of rock mass, one can estimate the magnitude of shear displacement that the surfaces of the discontinuity have suffered. Furthermore, the term "joints" is used to name the discontinuities whose shear displacement is zero or too small to be visible. In contrary, the "faults" are discontinuities on which larger shear displacements have taken place (Wittke, 2014).

In the geological structure, the joints are by far the most common type. They usually occur in sets that are more or less parallel and regularly spaced. However, there are also several sets which orient in different directions, and thus, the rock mass is broken up into a blocky structure. Therefore, the joints divide a rock mass into different parts, and sliding can occur along the joint surfaces. This explains why studies on joints play an important role in rock mechanics. Moreover, the fluids can flow through the rock mass by the paths that these joints provide (Jaeger et al., 2007).

In general, the joints intersect primary surfaces such as bedding, cleavage and schistosity. In geology, a joint set is defined as a series of parallel joints; a joint system includes two or more intersecting sets; two sets of joints approximately at right angles to one another are called to be orthogonal (Duncan, 1999).

In fact, a structural model of a rock mass is usually obtained by a superposition of models of the grain structure of the intact rock and the discontinuity system. In a certain scope, based on combinations of the grain structure of the intact rock and the discontinuity system, one can know the structural models, and thereby, estimate whether the deformability of a rock mass is isotropic or anisotropic (Wittke, 2014).

Joint rocks are the rock masses which contains one or several sets of discontinuities. The existence of these discontinuities produces anisotropic response of the rock mass to loading and unloading. In comparison to intact rock, the joint rock shows a decreased shear strength, and thereby, an increased deformity along the plane of discontinuity as well as a negligible tensile strength in direction normal to these plane (Amadei and Savage, 1993).

Amadei and Savage also recommended that it be necessary to take into account the presence of discontinuity when modeling rock mass responses to loading and unloading.

For engineering purposes, a comfortable way to model joint rock response is to consider the rock mass as an equivalent anisotropic continuum. Duncan and Goodman (1968) introduced the concept of equivalent anisotropy continuum which was then adopted by Amadei and Goodman (1981a) and Amadei and Goodman (1981b). Following this concept, the joint rock is modeled as an equivalent anisotropic rock which possesses the characteristic reflecting the properties of the intact rock, the directional deformities as well as the shear properties and those of jointed sets, i.e., orientations, normal, shear stiffness, and spacing.

Let us consider a rock mass specimen produced by three mutually perpendicular joint sets, each one is parallel to a symmetry axis. Each joint set i $(i = 1, 2, 3)$ is characterized by its spacing, S_i and its normal stiffness, k_{ni} and shear stiffness, k_{si}. Generally, the intact rock between the joints is assumed to be linearly elastic and orthotropic with respect to the direction defined by coordinate *x, y, z*. In this system, Amadei and Goodman (1981a) indicated that the regularly jointed rock can be replaced by an equivalent orthotropic continuum whose constitutive relation is defined by Hooke law as follows:

$$\varepsilon_{ij} = C_{ijkl}\sigma'_{kl} \tag{1.38}$$

in which C_{ijkl} is determined by Eqs. (1.19) and (1.20) with

$$\frac{1}{E_i^*} = \frac{1}{E_i} + \frac{1}{k_{ni}S_i}; \qquad \frac{1}{G_{ij}^*} = \frac{1}{G_{ij}} + \frac{1}{k_{si}S_i} + \frac{1}{k_{sj}S_j} \tag{1.39}$$

where $i, j = 1,2,3$ respectively (no summation in intended for Eq. (1.39)). The non-zero off diagonal terms in Eq. (1.19) takes the following values (Amadei and Goodman 1981a; Stephen, 1995):

$$C_{12} = C_{21} = -\frac{\nu_{12}^*}{E_1^*}; \qquad C_{23} = C_{32} = -\frac{\nu_{23}^*}{E_2^*}; \qquad C_{31} = C_{13} = -\frac{\nu_{31}^*}{E_3^*}; \tag{1.40}$$

One can decompose instructively the compliance matrix $[C]$ of equivalent anisotropic continuum into two sub-matrixes as follows:

$$[C] = [C_1] + [C_2] \tag{1.41}$$

with

$$[C_1] = \begin{pmatrix} C_{11}^1 & C_{12}^1 & C_{13}^1 & 0 & 0 & 0 \\ C_{21}^1 & C_{22}^1 & C_{23}^1 & 0 & 0 & 0 \\ C_{31}^1 & C_{32}^1 & C_{33}^1 & 0 & 0 & 0 \\ 0 & 0 & 0 & C_{44}^1 & 0 & 0 \\ 0 & 0 & 0 & 0 & C_{55}^1 & 0 \\ 0 & 0 & 0 & 0 & 0 & C_{66}^1 \end{pmatrix} \tag{1.42}$$

in which

$$\begin{gathered} C_{11}^1 = \frac{1}{E_1}; C_{22}^1 = \frac{1}{E_2}; C_{33}^1 = \frac{1}{E_3}; C_{44}^1 = \frac{1}{G_{23}}; C_{55}^1 = \frac{1}{G_{13}}; C_{66}^1 = \frac{1}{G_{12}}; \\ C_{12}^1 = C_{21}^1 = -\frac{\nu_{21}}{E_2}; C_{13}^1 = C_{31}^1 = -\frac{\nu_{31}}{E_3}; C_{23}^1 = C_{32}^1 = -\frac{\nu_{32}}{E_3} \end{gathered} \tag{1.43}$$

and

$$[C_2] = \begin{pmatrix} C_{11}^2 & 0 & 0 & 0 & 0 & 0 \\ 0 & C_{22}^2 & 0 & 0 & 0 & 0 \\ 0 & 0 & C_{33}^2 & 0 & 0 & 0 \\ 0 & 0 & 0 & C_{44}^2 & 0 & 0 \\ 0 & 0 & 0 & 0 & C_{55}^2 & 0 \\ 0 & 0 & 0 & 0 & 0 & C_{66}^2 \end{pmatrix} \tag{1.44}$$

with

$$C_{11}^{2}=\frac{1}{k_{n1}S_{1}};C_{22}^{2}=\frac{1}{k_{n2}S_{2}};C_{33}^{2}=\frac{1}{k_{n3}S_{3}};$$
$$C_{44}^{2}=\frac{1}{k_{s2}S_{2}}+\frac{1}{k_{s3}S_{3}};C_{55}^{2}=\frac{1}{k_{s1}S_{1}}+\frac{1}{k_{s3}S_{3}};C_{66}^{2}=\frac{1}{k_{s1}S_{1}}+\frac{1}{k_{s2}S_{2}} \tag{1.45}$$

According to Amadei and Goodman (1981a), the stiffness k_{ni} and k_{si} can vary with the normal stress acting on each joint set. Therefore, in two compliance matrix above, $\left[C_{1}\right]$ is a constant matrix and represents the contribution of the intact rock in deformation of the rock mass, whereas $\left[C_{2}\right]$ is not constant and represents the contribution of the joint sets. The dependency of stiffness on the normal stress renders the problem a nonlinear one and the application of a linear stress analysis provides only an approximation.

Assuming constant stiffness values and applying the linear theory of elasticity of an anisotropic body, Amadei and Goodman (1981b) studied displacements and stresses around a drilled hole.

One considers now a rock mass specimen cut by a single joint set of spacing S, the normal and shear stiffness k_{n} and k_{s} are perpendicular to the 1-direction. The spacing and stiffness of joint sets 2 and 3 in this case can be taken the infinity value in Eq. (1.39). Thus, the elements of equivalent compliance matrix (Eq. (1.41)) take the form:

$$C_{11}=\frac{1}{E_{1}}+\frac{1}{k_{n}S};C_{22}=\frac{1}{E_{2}};C_{33}=\frac{1}{E_{3}};C_{44}=\frac{1}{G_{23}};C_{55}=\frac{1}{G_{13}}+\frac{1}{k_{s}S};C_{66}=\frac{1}{G_{12}}+\frac{1}{k_{s}S};$$
$$C_{12}=C_{21}=-\frac{\nu_{21}}{E_{2}};C_{13}=C_{31}=-\frac{\nu_{31}}{E_{3}};C_{23}=C_{32}=-\frac{\nu_{32}}{E_{3}} \tag{1.46}$$

In the case of assumption including negligible thickness of the joint in comparison with the spacing, S, the joint does not make any Poisson’s effect. In other words, the joint and the intact rock were assumed to undergo equal strains in the plane parallel to the contact planes. Moreover, the intact rock is also isotropic. It is seen that, in this particular case, the rock mass is transversely isotropic in planes parallel to joint set 1 with the components given as below:

$$C_{11}=\frac{1}{E}+\frac{1}{k_{n}S};C_{22}=\frac{1}{E};C_{33}=\frac{1}{E};C_{44}=\frac{1}{G};C_{55}=\frac{1}{G}+\frac{1}{k_{s}S};C_{66}=\frac{1}{G}+\frac{1}{k_{s}S};$$
$$C_{12}=C_{21}=C_{13}=C_{31}=C_{23}=C_{32}=-\frac{\nu}{E}; \tag{1.47}$$

We have presented above in brief several basic concepts of discontinuity and joint rock in the view point of rock mechanics. This aims to support the standpoint which highlights the importance of taking into account the anisotropic behavior of rock mass in tunnel analysis. Indeed, the presence of discontinuity in almost of rocks makes them become not isotropic even if the intact rock shows the isotropic property, i.e., it is the discontinuities which cause the anisotropy of the rock mass.

1.4 Tunnels in anisotropic media : A literature review

1.4.1 Introduction

In literature, a number of works have been presented on deep tunnels in rocks. In general, these contributions can be classified in two approaches: the first approach is based on the analytical solution whereas the second approach uses the solution obtained from the numerical simulation. Using computer codes, the latter approach allows providing more realistic results thanks to its ability to account for different conditions in the simulation. On the contrary, the analytical solution, usually based on the different simplified hypothesis, is only available in some simple cases and, hence, its application is more limited. However, this approach has always received the attention of the scientific community owing to different reasons below. It provides a quick solution which is very useful, for example in the parametric study; it can be used as the first step in design or as the referenced solution to validate the numerical simulation; it elucidates the nature of the solution and, hence, could help the design engineer to assess the correctness of the numerical analysis.

One of the first analytical solutions is the celebrated Kirsch's solution (Kirsch 1898) which was developed in the framework of a circular tunnel excavated in an isotropic rock. Since then, different contributions have been presented taking into account some extensions. We summarize some study directions below.

Works have been devoted to analyzing more realistic cross-section of the tunnel such as Exadaktylos and Stavropoulou (2002), Zhang and Sun (2011), and Tran et al. (2015a). According to these studies, the shape of the cross section of the tunnel may be semi-circular, double-arch or rectangular. The obtained solutions are based on the complex potential functions and conformal mapping representation. Following that, the realistic cross-sections are transformed into unit circle section in transformation plane by conformal mapping technique. Exadaktylos and Stavropoulou (2002) developed the solutions for an isotropic medium while Zhang and Sun (2011) and Tran et al. (2015a) accounted for the anisotropic behavior of medium. Zhang and Sun (2011) analyzed the tunnel with the axis perpendicular to the isotropic plane whereas Tran et al. (2015a) considered the axis of the tunnel parallel to the isotropic plane.

Concerning the hydro-mechanical coupling in which the reciprocal influence between the hydraulic phenomenon and the mechanical phenomenon are included, one has the solutions of Bobet (2003, 2010), Carranza-Torres and Zhao (2009), and Wang and Wang (2013) for steady state of groundwater flow; Carter and Booker (1982, 1984), Detournay and Cheng (1988), Abousleiman and Cui (1998), and Chen and Yu (2015) for transient one. In the steady state condition of fluid flow, only the influence of pore pressure on the mechanical response is taken into account, i.e., one way coupling, while in the transient state condition, the pore pressure influences on mechanical response and, in turn, the mechanics impacts on the pore pressure, i.e., two ways coupling. The latter accounts for progressive behavior over time whereas this is not the case with steady state condition. With regard to the transient state, one uses the Laplace transform to eliminate the time variable in the Laplace's space. The problem is solved in this transformed space, and hence, the final solution of the problem is derived by inverse transform. Almost all aforementioned contributions focus on the tunnels in isotropic rock; except for Abousleiman and Cui (1998) who considered the opening in transversely isotropic rock where the axis of the opening is normal to the isotropic plane, thus, the problem is addressed as the isotropic one. Even though all these studies are limited in the isotropic cases, it showed, however, the essential role of the hydro-mechanical coupling on the tunnel behavior where the distribution of stresses and displacements can be significantly different from ones obtained in the case of purely mechanical response.

The other ones account for the anisotropic characteristic of the surrounding medium behavior. For example, the trend of taking into account the anisotropic effect has been extensively considered in the last two decades but limited primarily to the mechanical response of the tunnel. Hefny and Lo (1999) used the complex variable method that was reduced by Green and Zerna (1968) to determine the stresses and displacements of unlined circular tunnels excavated in an elastic transversely isotropic medium. Based also on the approach of Green and Zerna (1968), Vu et al. (2013) developed a semi-analytical solution for a circular tunnel excavated in a transversely isotropic formation with non-linear elastic behavior. Kolymbas et al. (2012) back analyzed the material constants of rock by an approximate solution for the displacements and stresses adjacent to the cavity wall for a cavity expansion in transversely isotropic rock. Based on the Lekhnitskii formalism, Bobet (2011) developed a closed-form solution for lined circular tunnels in dry rock or under the water table. Bobet (2011) considered also the work of the tunnel below the water table subjected to the seismic loading that was approximated by a quasi-static one.

It should be also noted that, two sources of anisotropic response of tunnels are distinguished: the first one is due to the origin of rock (orientation of minerals and discontinuities like bedding, foliation in the media) and the second one presents the difference of the principal initial stresses (Hefny and Lo, 1999; Chen and Yu, 2015). By decomposing the anisotropic load into mean stress and deviatory stress, Chen and Yu use the approach of Carter and Booker (1984) to resolve the problem as an isotropic one. It was highlighted that each anisotropic source could affect significantly the tunnel behavior where stresses and deformations in the surrounding rock mass differ from those obtained in assuming the isotropic properties of materials or initial stresses. Indeed, the works based on assumption of anisotropic rock or/and anisotropic initial stresses indicated that, stresses and displacements in rock as well as the loads transferring into the liner are strongly dependent on the orientation of bedding or foliation with the tunnel axis (Hefny and Lo 1999; and Tonon and Amadei 2002). This is not the case of assumption of isotropic properties.

Beside the analytical solution, some numerical analysis codes based on the finite element method, discrete element method or finite-difference methods were developed and used to expand the analysis of the tunnels in anisotropic medium. With the benefits of numerical methods, one can consider the problem in many different complex boundary conditions and behavior model of material. Among them, typical studies may be included Tonon and Amadei (2002), Millard (2013), Wang and Huang (2013), Lisjak et al. (2012), Tran et al. (2015b), Pardoen et al. (2015).

Tonon and Amadei (2002) used the finite element method (FEM) and boundary element method (BEM) to evaluate the effect of elastic anisotropy (transverse isotropy) on the convergence behind a tunnel face by a series of parametric studies. The authors considered two cases of isotropy plane that is parallel to the tunnel axis or not. As a results, the displacement of the rock, and thus, the stresses in the rock around the tunnel strongly depend on the direction of the isotropic plane with respect to the tunnel axis.

Lisjak et al (2013) have developed a numerical code to analyze a tunnel in the anisotropic rock mass based on a combination of FEM and DEM (discrete element method) – FEM/DEM. Following this approach, the rock mass is composed of the solid matrix and the joints/cracks, whereby the elastic deformation of the rock mass is described using continuum mechanics principles while DEM technique and non-linear fracture mechanics theory are used to take into account fracture mechanisms. The presence of joints/cracks makes the rock anisotropic, thus, by modeling the joints/cracks in the rock, the authors can account for the anisotropy of the rock. The results obtained by FEM/DEM approach are employed to evaluate the EDZ around the tunnel. The authors also indicated that, the proposed approach is capable to capture both the deformation and strength anisotropy which are typical of joint rock mass.

Meanwhile, Wang and Huang (2013) and Tran et al. (2015b) use the finite difference method (FDM) code (FLAC3D) to model a tunnel in an anisotropic rock. The authors propose a new anisotropic time-dependent model which includes weak planes of specific orientation and the intact rock with a visco-plastic behavior (Figure 1-6). Following this approach, the rock mass is also considered as a combination of two components, the solid matrix and the joints. The anisotropy of rock is due to the presence of joints. The solid matrix is considered by an isotropic visco-elasto-plastic model (Burger model), whereas the joints is modeled by ubiquitous joints with elasto-plastic behavior under Morh-Colomb criterion. It should be noted that, the "ubiquitous joint" means that the joints could be present at any point in the rock mass. Employing this approach, the authors can back-analyze the anisotropic closure of the tunnel. It is noted also that, the time-dependent behavior of solid matrix in Tran et al. (2015b) is explicitly described while it is taken into account by degrading the strength of rock with time in Wang (2013).

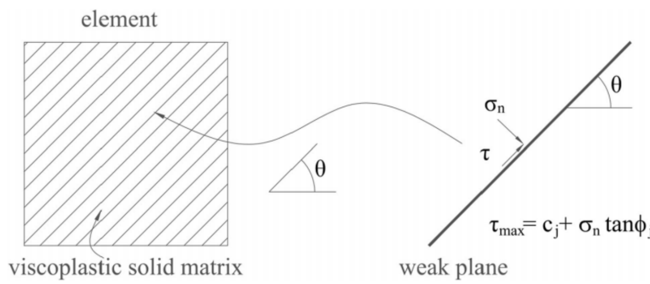

Fig. 1-6: Ubiquitous joint modeling a viscoplastic matrix

The aforementioned works consider the rock mass with the (visco) elasto-plastic behavior while Millard et al. (2013) devotes the particular attention to the hydro-mechanical behavior of anisotropic rock in unsaturated state. Employing FEM code, the authors evaluated the effect of in-situ stress, permeability and mechanical anisotropy on the hydro-mechanical responses of the tunnel. The results obtained are compared to the in-situ measurements such as pore water pressure, relative displacements, etc. Millard et al. (2013) showed that the anisotropy of permeability, in-situ stress and mechanical parameters influence the pore pressure and displacement non-axisymmetric distribution around the tunnel. The authors highlighted also that these hydro-mechanical couplings have important role in describing the experimental observation, and should be taken into account in further investigation.

Pardoen et al. (2015) studied the behavior of excavation fractured zone (EDZ), which develops around a gallery, based on a cross-anisotropic model including anisotropy of the elastic and plastic behaviors. With respect to the plastic part of the model, the anisotropy of a strength parameter is introduced with a microstructure fabric tensor. Then, the fractures are modelled with finite element methods by considering the development of shear strain localisation bands and an enriched model is used to properly reproduce the shear banding. The influence of cross-anisotropy on the shear strain localisation was investigated in this work by numerical simulations. The authors indicated that, the material strength varies with the loading direction and the development and the shape of the EDZ are strongly influenced by the material anisotropy.

We will introduce hereafter several analytical approaches that are commonly used to solve the problems of elastic anisotropy. They are regarded as the canon solutions based on which many analytical solutions are developed and extended to various engineering problems. These approaches are based on the complex variable method which is very useful and powerful in solving the problems of elasticity.

Due to the complexity of analytical solutions to three-dimensional problems, many solutions are developed for reduced problems that typically include plane stress and plane strain ones. Once one considers a 2-D problem, the complex variable method proves very useful and powerful to resolve it. The method is based on the reduction of the elasticity boundary value problem to a formulation in the complex domain. This method is used firstly by Kolosov (1909), and then it was expanded and further developed by Muskhelisvili (1953) to resolve several boundary value problems. Employing this method can also be found in Milne-Thomson (1960), Stroh (1962), Lekhnitskii (1963, 1968), Green and Zerna (1968).

Between the approaches aforementioned, those of Stroh, Lekhnitskii and Green and Zerna are well-known and commonly used to develop many solutions for engineering problems in anisotropic elastic. All three approaches are for the analysis of two-dimensional deformation of an anisotropic linear elastic. While Lekhnitskii (1963) and Green and Zerna (1968) consider the two-dimensional stresses as the unknowns, Stroh (1962) (Hwu, 2010) begins with the two-dimensional displacements. Owing to the convenience in utilizing, the approaches of Leknitskii and Green and Zerna are more employed in practice.

We will present below the Lekhnitskii (1963) and Green and Zerna (1968) approaches. Particularly, we will present the Lekhnitskii formalism in more detail for the purpose of employing in the next chapters where the analytical solutions will be developed based on this formalism.

1.4.2 Lekhnitskii approach

1.4.2.1 Assumptions and geometry of the problem

Let us consider a two-dimensional problem of a linear elastic, continuous and homogeneous anisotropic body bounded by a finite or infinite cylindrical surface. The region of the cross section may be simply connected or multiply connected; the length of the body can be finite or infinite. The body shows rectilinear anisotropy nature, subjected to body forces and tractions distributed along the lateral surface. For the satisfaction of conditions of plane problem, the body forces and surface tractions are assumed to act in planes normal to the generator of the cylindrical surface and do not vary along the generator. Let the body in the Cartesian coordinate system *x, y, z* in which the *z*-axis is parallel to the generators and the *xy*-plane be perpendicular to the generators.

The projections of the forces distributed over the cylindrical surface per unit area are X_n, Y_n in which n denotes the normal to the cylindrical surface and the components of the body forces per unit volume acting within the body are f_x, f_y.

The problem is to determine the distribution of stresses, strains and displacements within the body that are induced by the surface and body forces. One often knows this problem as the first fundamental problem of the statics of an elastic body that is presented in Muskhelishvili (1953).

In the case of a body of finite length and finite cross section, the stresses are assumed to reduce to an equivalent axial force and moment which act on the ends of the body.

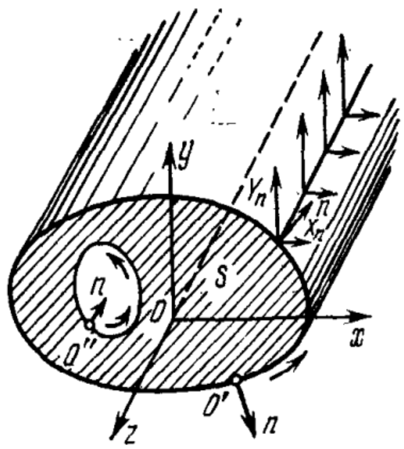

Fig. 1-7: Geometry of the problem described by Lekhnitskii (1963)

1.4.2.2 General formulas

a. Governing differential equations

The solution of any elasticity problem must satisfy the following conditions: equilibrium equations for static loading conditions, the strain–displacement relations for small deformations, as well as constitutive model (and boundary conditions).

Equilibrium equations for the elasticity body with body forces:

$$\frac{\partial \sigma_x}{\partial x}+\frac{\partial \tau_{xy}}{\partial y}-\frac{\partial \overline{U}}{\partial x}=0, \quad \frac{\partial \tau_{xy}}{\partial x}+\frac{\partial \sigma_y}{\partial y}-\frac{\partial \overline{U}}{\partial y}=0, \quad \frac{\partial \tau_{xz}}{\partial x}+\frac{\partial \sigma_{yz}}{\partial y}=0, \tag{1.48}$$

where $\bar{U}$ is the potential of the body forces f_x, f_y, i.e.,

$$f_x=\frac{\partial \overline{U}}{\partial x}, f_y=\frac{\partial \overline{U}}{\partial y}. \tag{1.49}$$

The relation of strain - displacement:

$$\begin{aligned} &\varepsilon_x=\frac{\partial u}{\partial x}, \quad \varepsilon_y=\frac{\partial v}{\partial y}, \quad \varepsilon_z=\frac{\partial w}{\partial z}, \\ &\gamma_{yz}=\frac{\partial w}{\partial y}+\frac{\partial v}{\partial z}, \quad \gamma_{xz}=\frac{\partial w}{\partial x}+\frac{\partial u}{\partial z}, \quad \gamma_{xy}=\frac{\partial v}{\partial x}+\frac{\partial u}{\partial y}. \end{aligned} \tag{1.50}$$

The constitutive equations:

$$\begin{aligned} \varepsilon_x &= a_{11}\sigma_x + a_{12}\sigma_y + a_{13}\sigma_z + a_{14}\tau_{yz} + a_{15}\tau_{zx} + a_{16}\tau_{xy}, \\ \varepsilon_y &= a_{12}\sigma_x + a_{22}\sigma_y + a_{23}\sigma_z + a_{24}\tau_{yz} + a_{25}\tau_{zx} + a_{26}\tau_{xy}, \\ \varepsilon_z &= a_{13}\sigma_x + a_{23}\sigma_y + a_{33}\sigma_z + a_{34}\tau_{yz} + a_{35}\tau_{zx} + a_{36}\tau_{xy}, \\ \gamma_{yz} &= a_{14}\sigma_x + a_{24}\sigma_y + a_{34}\sigma_z + a_{44}\tau_{yz} + a_{45}\tau_{zx} + a_{46}\tau_{xy}, \\ \gamma_{xz} &= a_{15}\sigma_x + a_{25}\sigma_y + a_{35}\sigma_z + a_{45}\tau_{yz} + a_{55}\tau_{zx} + a_{56}\tau_{xy}, \\ \gamma_{xy} &= a_{16}\sigma_x + a_{26}\sigma_y + a_{36}\sigma_z + a_{46}\tau_{yz} + a_{56}\tau_{zx} + a_{66}\tau_{xy}. \end{aligned} \tag{1.51}$$

In which a_{ij} are the compliance coefficients of elastic rigid-body.

Lekhnitskii (1963) introduces the notation:

$$D(x,y)=a_{13}\sigma_x+a_{23}\sigma_y+a_{33}\sigma_z+a_{34}\tau_{yz}+a_{35}\tau_{zx}+a_{36}\tau_{xy}, \tag{1.52}$$

From (1.52) one obtains:

$$\sigma_z=\frac{D}{a_{33}}-\frac{1}{a_{33}}(a_{13}\sigma_x+a_{23}\sigma_y+a_{34}\tau_{yz}+a_{35}\tau_{zx}+a_{36}\tau_{xy}) \tag{1.53}$$

With the relations given in the third, fourth, and fifth equations of (1.50), integrating the third, fourth, and fifth equations of (1.51) with respect to *z* variable one obtains the following relations:

$$\begin{aligned}
&w=zD(x,y)+W_0(x,y),\\
&v=-\frac{z^2}{2}\frac{\partial D}{\partial y}+z(a_{14}\sigma_x+a_{24}\sigma_y+a_{34}\sigma_z+a_{44}\tau_{yz}+a_{45}\tau_{xz}+a_{46}\tau_{xy}-\frac{\partial W_0(x,y)}{\partial y})+V_0(x,y),\\
&u=-\frac{z^2}{2}\frac{\partial D}{\partial x}+z(a_{15}\sigma_x+a_{25}\sigma_y+a_{35}\sigma_z+a_{45}\tau_{yz}+a_{55}\tau_{xz}+a_{56}\tau_{xy}-\frac{\partial W_0(x,y)}{\partial x})+U_0(x,y).
\end{aligned} \tag{1.54}$$

in which U_0, V_0, W_0 are arbitrary functions of *x* and *y* coordinate which occur as a result of integration with respect to *z*.

Substituting the Eq. (1.54) into the first, second, and sixth equations of Eq. (1.50) and then into the (1.51), and equating the coefficients of z^2, z terms on the left-hand sides and right-hand sides, one obtains three equations for D and two systems of equations for W_0 and U_0, V_0 as follows:

$$\frac{\partial^2 D}{\partial x^2}=0, \quad \frac{\partial^2 D}{\partial y^2}=0, \quad \frac{\partial^2 D}{\partial x\partial y}=0. \tag{1.55}$$

and

$$\begin{aligned}
&\frac{\partial}{\partial x}(a_{15}\sigma_x+a_{25}\sigma_y+a_{35}\sigma_z+a_{45}\tau_{yz}+a_{55}\tau_{xz}+a_{56}\tau_{xy}-\frac{\partial W_0}{\partial x})=0,\\
&\frac{\partial}{\partial y}(a_{14}\sigma_x+a_{24}\sigma_y+a_{34}\sigma_z+a_{44}\tau_{yz}+a_{45}\tau_{xz}+a_{46}\tau_{xy}-\frac{\partial W_0}{\partial y})=0,\\
&\frac{\partial}{\partial y}(a_{15}\sigma_x+a_{25}\sigma_y+a_{35}\sigma_z+a_{45}\tau_{yz}+a_{55}\tau_{xz}+a_{56}\tau_{xy}-\frac{\partial W_0}{\partial x})+\\
&\frac{\partial}{\partial x}(a_{14}\sigma_x+a_{24}\sigma_y+a_{34}\sigma_z+a_{44}\tau_{yz}+a_{45}\tau_{xz}+a_{46}\tau_{xy}-\frac{\partial W_0}{\partial y})=0;
\end{aligned} \tag{1.56}$$

and

$$\frac{\partial U_0}{\partial x} = (a_{11}\sigma_x + a_{12}\sigma_y + a_{13}\sigma_z + a_{14}\tau_{yz} + a_{15}\tau_{xz} + a_{16}\tau_{xy}),$$
$$\frac{\partial V_0}{\partial y} = (a_{12}\sigma_x + a_{22}\sigma_y + a_{23}\sigma_z + a_{24}\tau_{yz} + a_{25}\tau_{xz} + a_{26}\tau_{xy}), \tag{1.57}$$
$$\frac{\partial U_0}{\partial y} + \frac{\partial V_0}{\partial x} = (a_{16}\sigma_x + a_{26}\sigma_y + a_{36}\sigma_z + a_{46}\tau_{yz} + a_{56}\tau_{xz} + a_{66}\tau_{xy}).$$

It follows from (1.55) that D is a linear function of x and y and it takes the form as:

$$D = a_{33}(Ax + By + C), \tag{1.58}$$

where A, B, and C are the arbitrary constants. Hence, the normal stress at cross section, deduced from (1.53), is:

$$\sigma_z = (Ax + By + C) - \frac{1}{a_{33}}(a_{13}\sigma_x + a_{23}\sigma_y + a_{34}\tau_{yz} + a_{35}\tau_{xz} + a_{36}\tau_{xy}) \tag{1.59}$$

Integrating the first two equations of (1.56) and substituting into the third one we obtain the equations for W_0:

$$a_{15}\sigma_x + a_{25}\sigma_y + a_{35}\sigma_z + a_{45}\tau_{yz} + a_{55}\tau_{xz} + a_{56}\tau_{xy} - \frac{\partial W_0}{\partial x} = -\alpha y + \omega_2,$$
$$a_{14}\sigma_x + a_{24}\sigma_y + a_{34}\sigma_z + a_{44}\tau_{yz} + a_{45}\tau_{xz} + a_{46}\tau_{xy} - \frac{\partial W_0}{\partial y} = -\alpha x + \omega_1 \tag{1.60}$$

where $\alpha, \omega_1, \omega_2$ are the new arbitrary constants. Substituting the equations (1.60) and (1.58) into (1.54) one can obtain the general expressions of displacements as follows:

$$u = -\frac{Aa_{33}}{2}z^2 - \alpha yz + U(x,y) + \omega_2 z - \omega_3 y + u_0,$$
$$v = -\frac{Ba_{33}}{2}z^2 + \alpha xz + V(x,y) + \omega_3 x - \omega_1 z + v_0, \tag{1.61}$$
$$w = -(Ax + By + C)a_{33}z + W(x,y) + \omega_1 y - \omega_2 x + w_0$$

where the new functions U, V, W are related to U_0, V_0, W_0 by following relations:

$$U_0 = U - \omega_3 y + u_0,$$
$$V_0 = V + \omega_3 x + v_0, \tag{1.62}$$
$$W_0 = W + \omega_1 y - \omega_2 x + w_0.$$

In the general equation (1.61), the constants u_0, v_0, w_0 are the rigid-body displacements and $\omega_1, \omega_2, \omega_3$ are the rotations with respect to the *x, y,* and *z* axes; *α* is the relative angle of rotation about the *z*-axis which relates the torsion problems, i.e., the angle of twist per unit length; *A* and *B* characterize the bending of the body in the *x*–*z* and *y*–*z* planes.

In order to determine U, V and W, substituting Eq. (1.59) into Eqs. (1.57) and (1.60) one obtains the following expressions:

$$
\begin{aligned}
\frac{\partial U}{\partial x} &= (s_{11}\sigma_x + s_{12}\sigma_y + s_{13}\sigma_z + s_{14}\tau_{yz} + s_{15}\tau_{xz} + s_{16}\tau_{xy} + a_{13}(Ax+By+C), \\
\frac{\partial V}{\partial y} &= (s_{12}\sigma_x + s_{22}\sigma_y + s_{23}\sigma_z + s_{24}\tau_{yz} + s_{25}\tau_{xz} + s_{26}\tau_{xy} + a_{23}(Ax+By+C), \\
\frac{\partial U}{\partial y} + \frac{\partial V}{\partial x} &= (s_{16}\sigma_x + s_{26}\sigma_y + s_{36}\sigma_z + s_{46}\tau_{yz} + s_{56}\tau_{xz} + s_{66}\tau_{xy} + a_{36}(Ax+By+C).
\end{aligned}
\tag{1.63}
$$

and

$$
\begin{aligned}
\frac{\partial W}{\partial x} &= (s_{15}\sigma_x + s_{25}\sigma_y + s_{35}\sigma_z + s_{45}\tau_{yz} + s_{55}\tau_{xz} + s_{56}\tau_{xy} + a_{35}(Ax+By+C) + \alpha y, \\
\frac{\partial W}{\partial y} &= (s_{14}\sigma_x + s_{24}\sigma_y + s_{34}\sigma_z + s_{44}\tau_{yz} + s_{45}\tau_{xz} + s_{46}\tau_{xy} + a_{34}(Ax+By+C) - \alpha x,
\end{aligned}
\tag{1.64}
$$

where:

$$
s_{ij} = a_{ij} - \frac{a_{i3}a_{j3}}{a_{33}}
\tag{1.65}
$$

are the reduced elastic compliances.

It is noted that, both plane stress and plane strain problems are resolved by the same equations presented above. When one concerns the plane stress problems, the compliance is used and the reduced compliance for the plane strain problem.

It should be highlighted that, for the plane problem in elasticity using the Airy stress function approach is very convenient. Following that, it reduces the field equations to a single partial differential equation. According to Lekhnitskii (1963), the stress components can be identified from the functions called Airy stress functions, which satisfies the equilibrium equation presented in Eq. (1.48):

$$
\sigma_x = \frac{\partial^2 F}{\partial y^2} + \overline{U},\ \sigma_y = \frac{\partial^2 F}{\partial x^2} + \overline{U},\ \tau_{xy} = -\frac{\partial^2 F}{\partial x \partial y},\ \tau_{xz} = \frac{\partial^2 \psi}{\partial y},\ \tau_{yz} = -\frac{\partial^2 \psi}{\partial x}
\tag{1.66}
$$

By differentiating, addition and subtraction the equations in (1.63) and (1.64), one can eliminate U, V and W. Thereafter, by substituting stress components in (1.66), one obtains the following equations that called Beltrami-Michell equation of compatibility for an anisotropic body:

$$
\begin{aligned}
L_4(F) + L_3(\psi) &= -(s_{12} + s_{22})\frac{\partial^2 \overline{U}}{\partial x^2} + (s_{16} + s_{26})\frac{\partial^2 \overline{U}}{\partial x \partial y} - (s_{11} + s_{12})\frac{\partial^2 \overline{U}}{\partial y^2}, \\
L_3(F) + L_2(\psi) &= -2\alpha + As_{34} - Bs_{35} + (s_{14} + s_{24})\frac{\partial \overline{U}}{\partial x} + (s_{15} + s_{25})\frac{\partial \overline{U}}{\partial y},
\end{aligned}
\tag{1.67}
$$

where the linear differential operators of the fourth, third and second orders L_4, L_3 and L_2 are defined as:

$$L_4 = s_{22}\frac{\partial^4}{\partial x^4} - 2s_{26}\frac{\partial^4}{\partial x^3 \partial y} + 2(s_{12}+s_{66})\frac{\partial^4}{\partial x^2 \partial y^2} - 2s_{16}\frac{\partial^4}{\partial x \partial y^3} + s_{11}\frac{\partial^4}{\partial y^4},$$
$$L_3 = -s_{24}\frac{\partial^3}{\partial x^3} + (s_{25}+s_{46})\frac{\partial^3}{\partial x^2 \partial y} - (s_{14}+s_{56})\frac{\partial^3}{\partial x \partial y^2} + s_{15}\frac{\partial^3}{\partial y^3}, \tag{1.68}$$
$$L_2 = s_{44}\frac{\partial^2}{\partial x^2} - 2s_{45}\frac{\partial^2}{\partial x \partial y} + s_{55}\frac{\partial^2}{\partial y^2}$$

It can be seen that, the system of differential equations obtained in (1.67) is the combined result of the 15 basic equations shown in (1.48), (1.50) and (1.51).

Briefly, determining the stress functions in the Eq. (1.67), one can find the stresses from Eqs. (1.66) and (1.59), the strains and displacements from Eqs. (1.51), (1.63), (1.64), (1.62) and (1.61). The solution of the problem must satisfy the condition of the unique solution of the elasticity problem. Therefore, the boundary conditions and the requirement of the single-valued displacement should be satisfied.

b. General Solutions

In this section, we will present the method to find the general solution of the problem as mentioned in previously.

It can be seen that, the general solution of Eq. (1.67) includes a homogeneous solution corresponding the homogeneous equations without right-hand side and a particular solution that corresponds the nonhomogeneous equations with right-hand side. Hence, it can be written in the form:

$$F = F_h + F_p, \; \psi = \psi_h + \psi_p \tag{1.69}$$

in wich:

$$\begin{aligned} L_4(F_h) + L_3(\psi_h) = 0, \\ L_3(F_h) + L_2(\psi_h) = 0 \end{aligned} \tag{1.70}$$

The form of the known functions of the right-hand sides of the nonhomogeneous equations will decide the form of the particular solutions. If the right-hand sides are simple, the particular solutions are usually not difficult to find. Consequently, we only focus on the method to determine the general solutions of the homogeneous system (1.70) hereafter. Concerning determination the particular solution of the equation system, we will present in details in the next part that devotes to resolve one hydro-mechanical coupling problem.

Solving the system of (1.70) simultaneously gives the expression in term of the stress functions F_h, ψ_h, respectively:

$$(L_4L_2 - L_3^2)F_h = 0,$$
$$(L_3^2 - L_4L_2)\psi_h = 0, \tag{1.71}$$

These are linear partial differential equations of the sixth-order with constant coefficients which can be solved by the method of characteristics (Milne-Thomson, 1960). The first equation of the (1.71) will be satisfied if:

$$f(\mu) = l_4(\mu)l_2(\mu) - l_3^2(\mu) = 0 \tag{1.72}$$

where

$$\begin{aligned} l_4(\mu) &= s_{11}\mu^4 - 2s_{16}\mu^3 + (2s_{12} + s_{66})\mu^2 - 2s_{26}\mu + s_{22} \\ l_3(\mu) &= s_{15}\mu^3 - (s_{14} + s_{56})\mu^2 + (s_{25} + s_{46})\mu^2 - s_{24} \\ l_2(\mu) &= s_{55}\mu^2 - 2s_{45}\mu + s_{44} \end{aligned} \tag{1.73}$$

The function in Eq. (1.72) is called the characteristic function, and the equation $f(\mu) = 0$ the characteristic equation and μ the root of the characteristic equation. Let $\mu_1, \mu_2, \mu_3, \mu_4, \mu_5, \mu_6$ be the six roots of the characteristic equation, one can rewrite Eq. (1.72) in the following form:

$$f(\mu) = (s_{11}s_{55} - s_{15}^2)(\mu - \mu_1)(\mu - \mu_2)(\mu - \mu_3)(\mu - \mu_4)(\mu - \mu_5)(\mu - \mu_6) = 0 \tag{1.74}$$

In general, $(s_{11}s_{55} - s_{15}^2) \neq 0$ and inferring Eq.(1.72) the first equation of (1.71) can be written in the form:

$$(D_6D_5D_4D_3D_2D_1)F_h = 0, \tag{1.75}$$

where

$$D_k = \frac{\partial}{\partial y} - \mu_k \frac{\partial}{\partial x} \tag{1.76}$$

The equation (1.74) has the roots μ_k that are distinct, thus Eq. (1.75) can be solved by considering the following six equations of the first order:

$$\begin{aligned} &D_6F_h = \varphi_5, \quad D_5D_6F_h = \varphi_4, \quad D_4D_5D_6F_h = \varphi_3, \\ &D_3D_4D_5D_6F_h = \varphi_2, \quad D_2D_3D_4D_5D_6F_h = \varphi_1 \end{aligned} \tag{1.77}$$

so that

$$\begin{aligned} &D_1\varphi_1 = 0, \quad D_2\varphi_2 = \varphi_1, \quad D_3\varphi_3 = \varphi_2, \\ &D_4\varphi_4 = \varphi_3, \quad D_5\varphi_5 = \varphi_4, \quad D_6\varphi_6 = \varphi_5 \end{aligned} \tag{1.78}$$

Solving (1.78) respectively in the order of $\varphi_6, \varphi_5, \varphi_4, \varphi_3, \varphi_2, F_h$ one obtains the general expression for the stress function, F, and with the same manner the general expression of the stress function ψ is inferred. These expressions and the relation between F_k and ψ_k as follows:

$$
\begin{aligned}
F_h &= \sum_{k=1}^{6} F_k(z_k), \\
\psi_h &= \sum_{k=1}^{6} \psi_k(z_k), \\
\psi_k(z_k) &= -\frac{l_3(\mu_k)}{l_2(\mu_k)} F_k'(z_k),
\end{aligned}
\tag{1.79}
$$

where $F_k(z_k)$ and $\psi_k(z_k)$ are analytic functions of complex variables $z_k = x + \mu_k y$ and prime denotes differentiation with respect to z_k.

Lekhnitskii (1963) proved that, the roots of characteristic equation (1.74) are either complex, or purely imaginary and it cannot have real roots in the case of any ideal elastic body with real constants $s_{11}, 2s_{11} + s_{66}, s_{22}$ not equal to zero. Lekhnitskii proved also that three of them are being the conjugate of the other three.

Let μ_1, μ_2, μ_3 be these roots and $\bar{\mu}_1, \bar{\mu}_2, \bar{\mu}_3$ their conjugates; one has the expression of the stress function F from the first equation of (1.79) as:

$$
F_h = F_1(z_1) + F_2(z_2) + F_3(z_3) + F_1(\bar{z}_1) + F_2(\bar{z}_2) + F_3(\bar{z}_3) \tag{1.80}
$$

In addition, one has the following relation in the complex variable theory:

$$
2\, Re\{A\} = A + \bar{A} \tag{1.81}
$$

in which A is a complex number and ***Re*** stands for the its real part.

Therefore, one obtains also:

$$
F_h = 2\,\mathrm{Re}\{F_1(z_1) + F_2(z_2) + F_3(z_3)\} \tag{1.82}
$$

One has also the analogous general expression for the stress function ψ as:

$$
\psi_h = 2\,\mathrm{Re}\{\psi_1(z_1) + \psi_2(z_2) + \psi_3(z_3)\} \tag{1.83}
$$

The relations between $F_k(z_k)$ and $\psi_k(z_k)$ showed in the third equation of (1.79) can be expanded under explicit forms as follows:

$$
\begin{aligned}
&\psi_1 = -\frac{l_3(\mu_1)}{l_2(\mu_1)}\frac{\partial F_1}{\partial z_1}, \quad \psi_2 = -\frac{l_3(\mu_2)}{l_2(\mu_2)}\frac{\partial F_2}{\partial z_2}, \\
&\psi_3 = -\frac{l_3(\mu_3)}{l_2(\mu_3)}\frac{\partial F_3}{\partial z_3} = -\frac{l_4(\mu_3)}{l_3(\mu_3)}\frac{\partial F_3}{\partial z_3}
\end{aligned}
\tag{1.84}
$$

Introducing three complex number that are defined in the forms:

$$
\lambda_1 = -\frac{l_3(\mu_1)}{l_2(\mu_1)}, \quad \lambda_2 = -\frac{l_3(\mu_2)}{l_2(\mu_2)}, \quad \lambda_3 = -\frac{l_3(\mu_3)}{l_4(\mu_3)} \tag{1.85}
$$

and substituting (1.85) along with (1.84) into (1.83) one has the general expression of the stress function ψ:

$$\psi_h = 2\,\mathrm{Re}\{\lambda_1 F_1'(z_1) + \lambda_2 F_2'(z_2) + \frac{1}{\lambda_3} F_3'(z_3)\} \tag{1.86}$$

Therefore, one can obtain now the general solution of Eq. (1.67) that takes the following form:

$$\begin{aligned} F &= 2\,\mathrm{Re}\{F_1(z_1) + F_2(z_2) + F_3(z_3)\} + F_p, \\ \psi &= 2\,\mathrm{Re}\{\lambda_1 F_1'(z_1) + \lambda_2 F_2'(z_2) + \frac{1}{\lambda_3} F_3'(z_3)\} + \psi_p \end{aligned} \tag{1.87}$$

Lekhnitskii introduced three analytic functions so-called complex potentials that are defined as follows:

$$\Phi_1(z_1) = \frac{\partial F_1(z_1)}{\partial z_1} = F_1'(z_1), \quad \Phi_2(z_2) = \frac{\partial F_2(z_2)}{\partial z_2} = F_2'(z_2), \quad \Phi_3(z_3) = \frac{\partial F_3(z_3)}{\partial z_3} = F_3'(z_3) \tag{1.88}$$

From the definition of complex variable $z_k = x + \mu_k y$, one has following relations:

$$\begin{aligned} &\frac{\partial G_k}{\partial x} = \frac{\partial G_k}{\partial z_k}\frac{\partial z_k}{\partial x} = \frac{\partial G_k}{\partial z_k}, \quad \frac{\partial G_k}{\partial y} = \frac{\partial G_k}{\partial z_k}\frac{\partial z_k}{\partial y} = \mu_k \frac{\partial G_k}{\partial z_k} \\ &\frac{\partial^2 G_k}{\partial x^2} = \frac{\partial^2 G_k}{\partial z_k^{\,2}}\frac{\partial z_k^{\,2}}{\partial x^2} = \frac{\partial G_k}{\partial z_k^{\,2}}, \quad \frac{\partial^2 G_k}{\partial y^2} = \frac{\partial^2 G_k}{\partial z_k^{\,2}}\frac{\partial z_k^{\,2}}{\partial y^2} = \mu_k^{\,2} \frac{\partial^2 G_k}{\partial z_k^{\,2}} \end{aligned} \tag{1.89}$$

in which G_k is an arbitrary function which can either be F_k or ψ_k for the present case. By replacing G_k with F_k and ψ_k, substituting Eq. (1.88) into Eq. (1.89) and using Eq. (1.87) one can obtain the expression for the first derivatives of the stress function F with respect the coordinates x and y and the expression for ψ:

$$\begin{aligned} \frac{\partial F}{\partial x} &= 2\,\mathrm{Re}[\Phi_1(z_1) + \Phi_2(z_2) + \lambda_3 \Phi_3(z_3)] + \frac{\partial F_p}{\partial x} \\ \frac{\partial F}{\partial y} &= 2\,\mathrm{Re}[\mu_1 \Phi_1(z_1) + \mu_2 \Phi_2(z_2) + \lambda_3 \mu_3 \Phi_3(z_3)] + \frac{\partial F_p}{\partial y} \\ \psi &= 2\,\mathrm{Re}[\lambda_1 \Phi_1(z_1) + \lambda_2 \Phi_2(z_2) + \Phi_3(z_3)] + \psi_p \end{aligned} \tag{1.90}$$

Based on the basis of Eq. (1.90) and the relations between the stress components and the stress functions in Eq. (1.66) one has the general expression of the stresses as follows:

$$\sigma_x = 2\,\mathrm{Re}\{\mu_1^2\Phi_1'(z_1)+\mu_2^2\Phi_2'(z_2)+\mu_3^2\lambda_3\Phi_3'(z_3)\}+\frac{\partial^2 F_p}{\partial^2 y}+\overline{U}$$

$$\sigma_y = 2\,\mathrm{Re}\{\Phi_1'(z_1)+\Phi_2'(z_2)+\lambda_3\Phi_3'(z_3)\}+\frac{\partial^2 F_p}{\partial^2 x}+\overline{U}$$

$$\tau_{xy} = -2\,\mathrm{Re}\{\mu_1\Phi_1'(z_1)+\mu_2\Phi_2'(z_2)+\mu_3\lambda_3\Phi_3'(z_3)\}-\frac{\partial^2 F_p}{\partial x\partial y} \tag{1.91}$$

$$\tau_{xz} = 2\,\mathrm{Re}\{\mu_1\lambda_1\Phi_1'(z_1)+\mu_2\lambda_2\Phi_2'(z_2)+\mu_3\Phi_3'(z_3)\}+\frac{\partial \psi_p}{\partial y}$$

$$\tau_{yz} = -2\,\mathrm{Re}\{\lambda_1\Phi_1'(z_1)+\lambda_2\Phi_2'(z_2)+\Phi_3'(z_3)\}-\frac{\partial \psi_p}{\partial x}$$

It can be seen that once the derivatives of the analytic functions $\Phi_k(z_k)$ are obtained, the solutions of the stress distributions is analytically derived.

Substituting Eq. (1.91) into (1.63) and (1.64) and integrating the resulting equations, one obtains the expressions of the functions *U, V,* and *W* as:

$$\begin{aligned} U &= 2\,\mathrm{Re}[p_1\Phi_1(z_1)+p_2\Phi_2(z_2)+p_3\Phi_3(z_3)]+U_p, \\ V &= 2\,\mathrm{Re}[q_1\Phi_1(z_1)+q_2\Phi_2(z_2)+q_3\Phi_3(z_3)]+V_p, \\ W &= 2\,\mathrm{Re}[r_1\Phi_1(z_1)+r_2\Phi_2(z_2)+r_3\Phi_3(z_3)]+W_p \end{aligned} \tag{1.92}$$

in which

$$\begin{aligned} p_k &= s_{11}\mu_k^2+s_{12}-s_{16}\mu_k+\lambda_k(s_{15}\mu_k-s_{14}), \\ q_k &= s_{12}\mu_k+\frac{s_{22}}{\mu_k}-s_{26}+\lambda_k(s_{25}-\frac{s_{24}}{\mu_k}), \qquad k=1,2,3 \\ r_k &= s_{14}\mu_k+\frac{s_{24}}{\mu_k}-s_{46}+\lambda_k(s_{45}-\frac{s_{44}}{\mu_k}) \end{aligned} \tag{1.93}$$

and

$$\begin{aligned} p_3 &= \lambda_3(s_{11}\mu_3^2+s_{12}-s_{16}\mu_3)+s_{15}\mu_3-s_{14}, \\ q_3 &= \lambda_3(s_{12}\mu_3+\frac{s_{22}}{\mu_3}-s_{26})+s_{25}-\frac{s_{24}}{\mu_3}, \\ r_3 &= \lambda_3(s_{14}\mu_3+\frac{s_{24}}{\mu_3}-s_{46})+s_{45}-\frac{s_{44}}{\mu_3} \end{aligned} \tag{1.94}$$

In Eq. (1.92), U_p, V_p, W_p are the solutions of (1.63) and (1.64) corresponding to the functions $F_p, \psi_p, \overline{U}$ and to the linear functions $a_{ij}\,(Ax + By + C)$, αy, αx which contain the constants *α*, *A, B, C.*

The equation (1.92) shows that, the functions *U, V,* and *W* and hence the displacements in Eq. (1.61) are also obtained through the analytic functions $\Phi_k(z_k)$.

In brief, in order to determine the fields of stresses and displacements in the body one has to first determine the analytic functions so-called complex potentials, i.e., three potential functions $\Phi_k(z_k)$ of three different complex variables $z_k = x + \mu_k y$ in the region S of the cross section. These functions must satisfy the single-valued conditions with respect to the coordinates *x* and *y*, and continuous condition on the contour of the body for the stresses and displacements.

c. Boundary conditions

The stresses and displacements expressed in (1.91), (1.92), and (1.61) depend on the arbitrary complex analytic functions $\Phi_k(z_k)$. For the purpose of determination of these functions one has to impose the boundary conditions on the lateral surface. There are two types of boundary conditions. The first one mentions the prescribed tractions (that is often known the Newmann condition) and the other describes prescribed displacements (that is often called Dirichlet condition). It is known that the general expressions for the stresses and displacements are expressed in terms of the complex analytic functions $\Phi_k(z_k)$. Therefore, it is now more convenient to express the boundary conditions in terms of $\Phi_k(z_k)$.

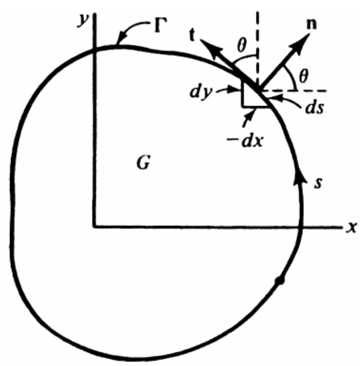

Fig. 1-8: Tangential and normal directions of boundary surfaces (Boresi, 1965)

➢ *First fundamental problem:*

The first fundamental problem mentions determination the stresses and displacements within the elastic body in statics induced by surface and body forces. If the external forces $Z_n = 0, X_n, Y_n$ prescribed on the contour of the body cross section are functions of the coordinates x and y, the boundary conditions along the contour of the body are given by:

$$\begin{aligned} &\sigma_x \cos(\vec{n},x) + \tau_{xy} \cos(\vec{n},y) + \tau_{xz} \cos(\vec{n},z) = X_n, \\ &\tau_{yx} \cos(\vec{n},x) + \sigma_y \cos(\vec{n},y) + \tau_{yz} \cos(\vec{n},z) = Y_n, \\ &\tau_{zx} \cos(\vec{n},x) + \tau_{zy} \cos(\vec{n},y) + \sigma_z \cos(\vec{n},z) = Z_n = 0 \end{aligned} \tag{1.95}$$

where $\vec{n}$ is the outward unit vector normal to the contour (see Figure. 1.8).

For a plane problem, the direction cosine, $\cos(\vec{n},z)$, is equal to zero whereas the others direction cosines $\cos(\vec{n},x)$ and $\cos(\vec{n},y)$ can be expressed in terms of the arc length, s. The equation of s can be written under parametric form as: $x = x(s)$, $y = y(s)$.The length of arc, s, is often taken from the arbitrary starting point on the contour ($s = 0$) and in the positive direction. The positive direction of the length of arc obeys counterclockwise convention.

One has the expression of the direction cosines as follows:

$$\cos(\vec{n}, x) = -\frac{dy}{ds}, \qquad \cos(\vec{n}, y) = \frac{dx}{ds} \tag{1.96}$$

Substituting Eq. (1.96) and Eq. (1.66) into the Eq. (1.95) and integrating the resulting equations with respect to the length of arc s yields a differential form of boundary conditions below:

$$\begin{aligned}
&\frac{\partial}{\partial y}\left(\frac{\partial F}{\partial y}\right)\frac{\partial y}{\partial s} + \frac{\partial}{\partial x}\left(\frac{\partial F}{\partial y}\right)\frac{\partial x}{\partial s} = -X_n - \bar{U} \\
&\frac{\partial}{\partial y}\left(\frac{\partial F}{\partial x}\right)\frac{\partial y}{\partial s} + \frac{\partial}{\partial x}\left(\frac{\partial F}{\partial x}\right)\frac{\partial x}{\partial s} = Y_n - \bar{U}, \\
&\frac{\partial \psi}{\partial y}\frac{\partial y}{\partial s} + \frac{\partial \psi}{\partial x}\frac{\partial x}{\partial s} = -Z_n
\end{aligned} \tag{1.97}$$

Multiplying two sides of Eq. (1.97) with ds and by using the exact differential notation for the functions $\frac{\partial F}{\partial y}, \frac{\partial F}{\partial x}$ and $\partial \psi$ one can rewrite Eq. (1.97) as follows:

$$\begin{aligned}
&d\left(\frac{\partial F}{\partial y}\right) = -(X_n + \bar{U}\frac{dx}{ds})ds \\
&d\left(\frac{\partial F}{\partial x}\right) = (Y_n - \bar{U}\frac{dy}{ds})ds, \\
&d(\partial \psi) = -Z_n ds
\end{aligned} \tag{1.98}$$

Thence, integrating Eq. (1.98) with respect to the length of arc s and taking the limits from the certain point ($s = 0$), one obtains:

$$\begin{aligned}
&\frac{\partial F}{\partial y} = \int_0^s -\left(X_n + \bar{U}\frac{dx}{ds}\right)ds + C_1 \\
&\frac{\partial F}{\partial x} = \int_0^s \left(Y_n - \bar{U}\frac{dy}{ds}\right)ds + C_2 \\
&\psi = \int_0^s -Z_n ds + C_3
\end{aligned} \tag{1.99}$$

where C_1, C_2 and C_3 are the integration constants.

Using Eqs. (1.87) and (1.88) into Eq. (1.99) one obtains the general expressions of boundary conditions in terms the complex potentials as follows:

$$2\,\mathrm{Re}[\mu_1\Phi_1(z_1)+\mu_2\Phi_2(z_2)+\lambda_3\mu_3\Phi_3(z_3)]=-\int_0^s\left(X_n+\bar{U}\frac{dx}{ds}\right)ds-\frac{\partial F_p}{\partial y}+C_1$$
$$2\,\mathrm{Re}[\Phi_1(z_1)+\Phi_2(z_2)+\lambda_3\Phi_3(z_3)]=\int_0^s\left(Y_n-\bar{U}\frac{dy}{ds}\right)ds-\frac{\partial F_p}{\partial x}+C_2 \qquad (1.100)$$
$$2\,\mathrm{Re}[\lambda_1\Phi_1(z_1)+\lambda_2\Phi_2(z_2)+\Phi_3(z_3)]=-\int_0^s Z_n ds+C_3$$

For a finite simply connected region, because linear terms in F and ψ do not distribute to the stress components, one can set the integration constants equal to zero.

- *Second fundamental problem:*

The second fundamental problem devotes to determine the stresses and displacements in the elastic body in statics induced by prescribed displacements.

Let $\hat{u},\hat{v},\hat{w}$ be the prescribed displacements on the lateral surface of the cross section contour. One has the boundary condition (Dirichlet condition) as below:

$$u=\hat{u},\qquad v=\hat{v},\qquad w=\hat{w} \qquad (1.101)$$

Substituting Eq. (1.61), Eq. (1.92) into Eq. (1.101) one obtains:

$$2\,\mathrm{Re}[p_1\Phi_1(z_1)+p_2\Phi_2(z_2)+p_3\Phi_3(z_3)]=-U_p+\hat{U}+\omega_3 y-u_0,$$
$$2\,\mathrm{Re}[q_1\Phi_1(z_1)+q_2\Phi_2(z_2)+q_3\Phi_3(z_3)]=-V_p+\hat{V}+\omega_3 x-v_0, \qquad (1.102)$$
$$2\,\mathrm{Re}[r_1\Phi_1(z_1)+r_2\Phi_2(z_2)+r_3\Phi_3(z_3)]=-W_p+\hat{W}-w_0$$

in which $\hat{U},\hat{V},\hat{W}$ are given as:

$$\hat{U}=\hat{u}+\frac{Aa_{33}}{2}z^2+\alpha yz-\omega_2 z,$$
$$\hat{V}=\hat{v}+\frac{Ba_{33}}{2}z^2+\alpha xz-\omega_1 z, \qquad (1.103)$$
$$\hat{W}=\hat{w}-(Ax+By+C)a_{33}z-\omega_1 y+\omega_2 x$$

d. Conformal mapping technique and the potentials

As presented above, the present problem of the equilibrium of a body bounded by the cylindrical surface is reduced to that of determination the complex potentials, i.e., three potential functions $\Phi_k(z_k)$ in the region S of the cross section. The stresses and displacements due to these potential functions must satisfy the single-valued conditions at any point in the body, and, moreover, the boundary conditions on the contour of the cross section. In other words, three potential functions and their conjugates functions are given on the contour.

The potential functions $\Phi_k(z_k)$ of three complex variables $z_k = x + \mu_k y$ ($k = 1,2,3$) may be considered in the ordinary complex plane, $z_k = x_k + iy_k$. According to Lekhnitskii (1963) μ_k is either complex or imaginary, thus one can write the affine transformation as:

$$z_k = x + \mu_k y = x + (\alpha_k + i\beta_k)y = x_k + iy_k \tag{1.104}$$

in which

$$x_k = x + \alpha_k y, \, y_k = \beta_k y, \; k = 1,2,3 \tag{1.105}$$

Lekhniskii (1963) indicated that, if based on this standpoint, the complex potentials $\Phi_k(z_k)$ must be determined not in the region of the cross-section S, but in the regions S_1, S_2, S_3 obtained from S by the affine transformation (1.105).

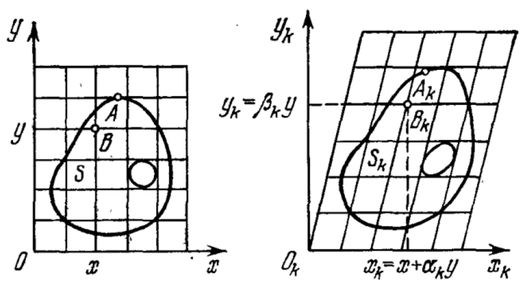

Fig. 1-9: Geometric representation of an affine transformation (Lekhnitskii, 1963)

Figure 1-9 shows how the regions S_k ($k = 1,2,3$) are obtained from the region S. The determination of potential functions $\Phi_k(z_k)$ on the regions $S_k (k = 1,2,3)$ usually encounters many difficulties because the shape of the regions may be complicated. One method employed to overcome these difficulties is to use an affine transformation, i.e., instead of determination the potential functions of the regions S_k, one determines potential functions on the regions which are the mapping images of S_k by an affine transformation. The complete solution of the potential functions in the domain of interest is accomplished by a reverse transformation.

In many elasticity problems, such as plane problems (plane strain or plane stress problems), the potential functions are complex and harmonic. The affine transformation for the defined set of complex harmonic functions is known as the conformal mapping.

This affine transformation provides a useful tool to find elasticity solutions for interior and exterior problems of complicated shape. Many plane elasticity problems based on solutions which relate to the unit circle, and thus the conformal mapping of the regions S_k in the plane of interest into a unit circle in the conformed plane is commonly used.

The critical problem now is to find the complex potentials. Lekhnitskii proposed these potentials for problem of a cavity of elliptical shape cross section. In order to search for the potentials, Lekhnitskii used conformal mapping technique which transforms the region outside the ellipse in original plane onto the region outside unit circle in the transformed plane. The conformal mapping is performed by relation below:

$$z_k = w(\zeta_k) = \frac{a - i\mu_k b}{2}\zeta_k + \frac{a + i\mu_k b}{2}\zeta_k^{-1} \tag{1.106}$$

or reciprocal form:

$$\zeta_k = \frac{z_k + \sqrt{z_k^2 - (a + \mu_k^2 b)}}{a - i\mu_k b} \tag{1.107}$$

where a and b are respectively the major and minor axis of the ellipse.

For the elliptical cavity, Lekhnitskii proposed two potentials as follows:

$$\begin{aligned} \Phi_1(z_1) &= A_1 \ln\zeta_1 + \sum_{m=1}^{\infty} \frac{\overline{b}_m - \mu_2 \overline{a}_m}{\mu_1 - \mu_2}\zeta_1^{-m}; \\ \Phi_2(z_2) &= A_2 \ln\zeta_2 - \sum_{m=1}^{\infty} \frac{\overline{b}_m - \mu_1 \overline{a}_m}{\mu_1 - \mu_2}\zeta_2^{-m} \end{aligned} \tag{1.108}$$

where $\overline{a}_m, \overline{b}_m$ are complex constants which are determined from the stresses applied on the wall of the cavity, the constants A_m depend on the boundary condition and the condition for single-valuedness of displacement. Lekhnitskii (1963) indicated that, for normal cavity problems, the constants A_m take the value of zero.

It is noted that, these complex potentials in Eqs. (1.108) satisfy automatically the condition of zero stresses at infinity.

Lekhnitskii presented the values of $\overline{a}_m, \overline{b}_m$ for three special cases of loading condition as follows (Fig.1-10):

- Normal pressure distributed uniformly over the surface of cavity (Fig.1-10 a):

$$\begin{aligned} \overline{a}_1 = -\frac{qa}{2}, \quad \overline{b}_1 = -\frac{qib}{2}; \\ \overline{a}_m = \overline{b}_m = 0 \text{ for } m = 2,3,4,... \end{aligned} \tag{1.109}$$

where q is pressure per unit area.

- Tangential forces distributed uniformly over the surface of cavity and acting in the planes parallel to x-y plane (Fig.1-10 b):

$$\bar{a}_1 = \frac{tbi}{2}, \qquad \bar{b}_1 = -\frac{ta}{2};$$
$$\bar{a}_m = \bar{b}_m = 0 \text{ for } m = 2,3,4,... \tag{1.110}$$

where t is force per unit area.

- Tension. At a large distance from the cavity there are tensile forces acting at an angle φ to the axis 2a of the ellipse (Fig.1-10c):

$$\bar{a}_1 = -\frac{p}{2}\sin\varphi(a\sin\varphi - b\cos\varphi);$$
$$\bar{b}_1 = -\frac{p}{2}\cos\varphi(a\sin\varphi - ib\cos\varphi); \tag{1.111}$$
$$\bar{a}_m = \bar{b}_m = 0 \text{ for } m = 2,3,4,...$$

in which p is tensile force per unit area.

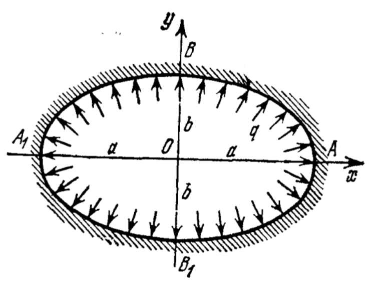

(a)

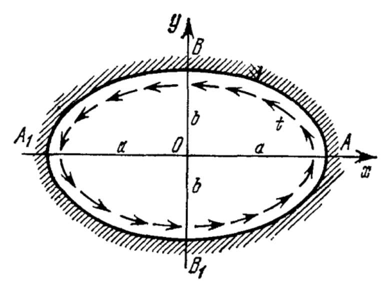

(b)

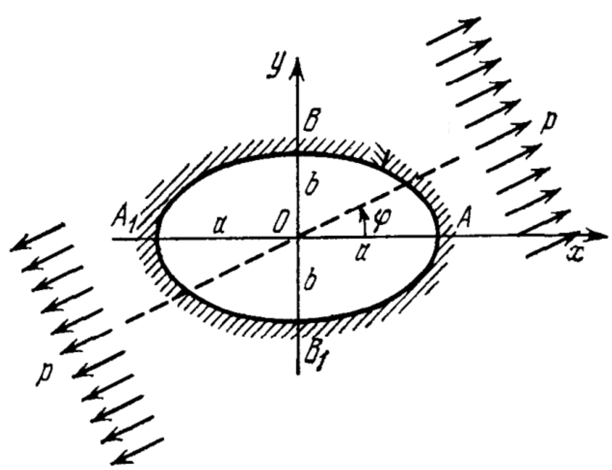

(c)

Fig. 1-10: Elliptical cavity considered by Lekhnitskii

In the chapter 2, we will present applications of the Lekhnitskii approach to find the solution of a specific problem, i.e., the solution of a deep tunnel in poroelastic medium.

1.4.3 Solution of Green et Zerna

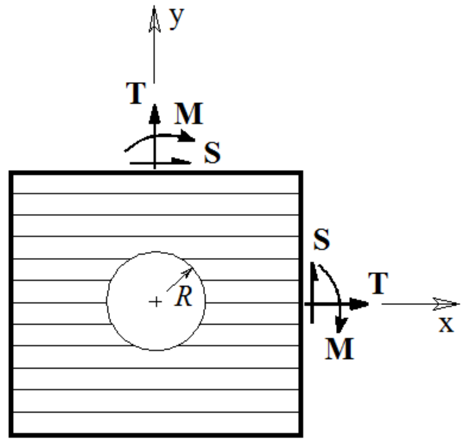

Fig. 1-11: The excavation in the anisotropic medium- Green and Zerna's solution

Considering a cavity with circular cross-section in the elastic anisotropy medium (Fig.1-11), assuming the cavity satisfies the plane strain condition; one has the simplification constitutive equations as follows:

$$\begin{pmatrix} \varepsilon_x \\ \varepsilon_y \\ \varepsilon_{xy} \end{pmatrix} = \begin{pmatrix} s_{11} & s_{12} & 0 \\ s_{21} & s_{22} & 0 \\ 0 & 0 & s_{33} \end{pmatrix} \begin{pmatrix} \sigma_x \\ \sigma_y \\ \tau_{xy} \end{pmatrix} \tag{1.112}$$

in which $s_{11}, s_{12}, s_{21}, s_{22}, s_{33}$ are the compliance constants and defined by Eq. (1.65) and relate to the material constants as below:

$$s_{11} = \frac{1-\nu_{xz}^2}{E_x}, s_{12} = s_{21} = -\frac{\nu_{xy}(1+\nu_{xz})}{E_x}, s_{22} = \frac{1-\nu_{xy}\nu_{yx}}{E_y}, s_{33} = \frac{1}{G_{xy}}, \nu_{yx} = \frac{\nu_{xy}E_y}{E_x} \tag{1.113}$$

With the stress function as defined in Eq. (1.66), the equilibrium equations are automatically satisfied. For the compatibility deformation equations, the Airy function must be verified by the following bi-harmonic equation:

$$s_{11}\frac{\partial^4 F}{\partial y^4} + (2s_{12}+s_{33})\frac{\partial^4 F}{\partial y^2 \partial x^2} + s_{22}\frac{\partial^4 F}{\partial x^4} = 0 \tag{1.114}$$

The bi-harmonic (1.114) equation is transformed into the form:

$$\left(\frac{\partial^2}{\partial x^2} + \alpha_1 \frac{\partial^2}{\partial y^2}\right)\left(\frac{\partial^2}{\partial x^2} + \alpha_2 \frac{\partial^2}{\partial y^2}\right)F = 0 \tag{1.115}$$

where

$$\alpha_1\alpha_2 = \frac{s_{11}}{s_{22}}, \qquad \alpha_1 + \alpha_2 = \frac{s_{33}+2s_{12}}{s_{22}} \tag{1.116}$$

One introduces two new complex variables $z_k (k = 1, 2)$:

$$\overline{z}_k = (\overline{z} + \overline{\gamma}_k z), \quad \gamma_k = \frac{\sqrt{\alpha_k} - 1}{\sqrt{\alpha_k} + 1} \tag{1.117}$$

Green and Zerna assumed that the real function *F* is the sum of two functions $\Omega_1(z_1)$ and $\Omega_2(z_2)$ which are the unique functions of the complex variables z_1 and z_2, and their conjugated functions:

$$F = \sum_{k=1}^{2} \left(\Omega_k(z_k) + \overline{\Omega_k(z_k)} \right) \tag{1.118}$$

where $\overline{\Omega_k(z_k)}$ are conjugate functions of $\Omega_k(z_k)$.

The displacement is written in complex form:

$$D = u + iv = \sum_{k=1}^{2} \left(\delta_k \Omega_k'(z_k) + \overline{\rho}_k \overline{\Omega_k'}(\overline{z}_k) \right) \tag{1.119}$$

where u and v are displacements in the horizontal and vertical directions respectively. The constants δ_k, ρ_k in (…) are determined as follows:

$$\begin{aligned} \delta_1 &= (1+\gamma_1)\beta_2 - (1-\gamma_1)\beta_1; \qquad \delta_2 = (1+\gamma_2)\beta_1 - (1-\gamma_2)\beta_2; \\ \rho_1 &= (1+\gamma_1)\beta_2 + (1-\gamma_1)\beta_1; \qquad \rho_1 = (1+\gamma_2)\beta_1 + (1-\gamma_2)\beta_2 \end{aligned} \tag{1.120}$$

in which:

$$\beta_1 = S_{12} - S_{22}\alpha_1; \qquad \beta_2 = S_{12} - S_{22}\alpha_2 \tag{1.121}$$

Green and Zerna also showed that all the functions $\ln z_k$ and z_k^{2n} satisfy automatically the conditions of compatibility deformations and they are sufficient to verify the boundary conditions. In the case of a circular cavity in an infinite medium, Green and Zerna proposed the following formulas for the stresses functions:

$$\begin{aligned} \Omega_1''(z_1) &= B + iC + \frac{H}{2\pi z_1} + O\left(\frac{1}{z_1^2}\right); \\ \Omega_2''(z_2) &= B' + iC' + \frac{K}{2\pi z_2} + O\left(\frac{1}{z_2^2}\right) \end{aligned} \tag{1.122}$$

where $O\left(\frac{1}{z_k^2}\right)$ are functions of $\frac{1}{z_k^2}$ which tends to zero at infinity. The coefficients B, C, B', C', H, K are then determined by the boundary conditions at infinity for the problem of the cavity with radius *R*.

According to Green and Zerna, the hoop stress at the perimeter of the cavity is given by:

- in the case of an uniform tension T at infinity:

$$\sigma_\theta = \frac{T(1+\gamma_1)(1+\gamma_2)(1+\gamma_1+\gamma_2-\gamma_1\gamma_2-2\cos 2\theta)}{(1+\gamma_1^2-2\gamma_1\cos 2\theta)(1+\gamma_2^2-2\gamma_2\cos 2\theta)}; \tag{1.123}$$

- in the case of a shear stress S at infinity:

$$\sigma_\theta = \frac{4S(\gamma_1\gamma_2-1)\sin 2\theta}{(1+\gamma_1^2-2\gamma_1\cos 2\theta)(1+\gamma_2^2-2\gamma_2\cos 2\theta)}; \tag{1.124}$$

- in the case of a moment M at infinity:

$$\frac{b^3\sigma_\theta}{RM} = \frac{3(1+\gamma_1)(1+\gamma_2)\left[(1+\gamma_1+\gamma_2)\sin\theta-\sin 3\theta\right]}{(1+\gamma_1^2-2\gamma_1\cos 2\theta)(1+\gamma_2^2-2\gamma_2\cos 2\theta)}; \tag{1.125}$$

In the formulas above, θ denotes the anticlockwise angle from the horizontal direction to the considered point.

Based on the work of Green and Zerna, Hefny and Lo (1999) proposed a solution to a circular unlined deep tunnel with radius *R* in a transverse isotropic medium with an anisotropic initial stress state. Hefny and Lo (1999) obtained the expression of hoop stress at the tunnel wall as follows:

$$\begin{aligned}\sigma_\theta &= \frac{4(\gamma_1+\gamma_2)-4(1-\gamma_1\gamma_2)\cos 2\theta}{(1+\gamma_1^2-2\gamma_1\cos 2\theta)(1+\gamma_2^2-2\gamma_2\cos 2\theta)}Q_0 \\ &+\frac{2+2(\gamma_1+\gamma_2)^2-2\gamma_1^2\gamma_2^2-4(\gamma_1+\gamma_2)\cos 2\theta}{(1+\gamma_1^2-2\gamma_1\cos 2\theta)(1+\gamma_2^2-2\gamma_2\cos 2\theta)}P_0\end{aligned} \tag{1.126}$$

and the radial and ortho-radial displacements respectively:

$$\begin{aligned}u_R &= \frac{R}{2(\gamma_1-\gamma_2)}\times \\ &\left\{\left[Q_0(\delta_1-\delta_2)+P_0(\gamma_2\delta_1-\gamma_1\delta_2)P_0\right]\cos 2\theta+Q_0(\rho_1-\rho_2)+P_0(\gamma_2\rho_1-\gamma_1\rho_2)\right\}; \\ u_\theta &= \frac{R}{2(\gamma_1-\gamma_2)}\left[Q_0(\delta_1-\delta_2)+P_0(\gamma_1\delta_2-\gamma_2\delta_1)P_0\right]\sin 2\theta\end{aligned} \tag{1.127}$$

where P_0 and Q_0 are the hydrostatic and deviatory stresses of the initial stresses respectively. Some works based also on this solution of Green and Zerna to develop and extend for different tunnel problems such as Zhang and Sun (2011), Vu et al. (2013), Tran et al. (2015a).

1.5 Summary

This chapter presents the necessity of taking into account the anisotropic properties of the medium in the analysis of the tunnel, the motivation of the thesis. Chapter 1 also revisited the description as well as some fundamental concepts of poroelastic. The constitutive equations of the poroelastic model which will be employed thereafter in this work have been presented. The inherent anisotropy of rocks has been discussed on the basis of rock mechanics. Finally, a literature review has been presented by synthetizing the works in literature that relate to the study objective of the thesis.

Résumé:

Ce chapitre, résolument bibliographique a présenté quelques notions de bases de la poroélasticité dans le contexte anisotrope en justifiant la nécessité de la prise en compte de cette anisotropie dans le dimensionnement des tunnels. Le chapitre résume les concepts fondamentaux des milieux poroélastique, les équations constitutives du comportement du solide, du fluide et de leur couplage qui seront utilisées par la suite dans ce travail. L'anisotropie inhérente de roches a été discutée sur la base de la mécanique des roches. Enfin, une revue de la littérature décrivant les tunnels dans les milieux anisotropes a été présentée.

CHAPTER 2: DEEP TUNNEL IN ANISTROPIC POROELASTIC ROCK: ANALYTICAL SOLUTION USING THE COMPLEX POTENTIALS APPROACH

2.1.Introduction

As mentioned in Chapter 1, in many cases, the rock mass exhibits usually an anisotropic behavior and the transversely isotropic rock is frequently encountered in the practice.

The existent analytical solutions for deep tunnels in anisotropic medium refer primarily to the elastic behavior with the circular or non-circular cross section shapes of the tunnels.

A hydro-mechanical closed-form solution for the deep tunnels in anisotropic porous medium is still not mentioned in the literature, and hence, in this chapter we devote to develop an analytical solution which takes into account the effect of the pore pressure distribution on the mechanical responses. In this study, we account also for the liner in the interaction with the surrounding rock, whereby, to clarify the reciprocal impact of them.

Once the solution derived, we conduct parametric estimations to elucidate the effect of the hydro-mechanical parameters of the anisotropic material on the behavior of the tunnel, thereby, understanding the nature of work of the tunnel in anisotropic rock. On these basis, some comments and initial conclusions are given.

The study could provide a quick analysis tool for design and evaluation of the stresses and displacements of the tunnels as well as the recommendations as basis for studies in the same subject.

2.2.Problem statement

Let us consider a deep tunnel with circular cross section of radius r_0 excavated in a transversely isotropic porous elastic medium which is saturated with an initial pore pressure p_{ff} . The longitudinal axis of tunnel is parallel to the *z*- axis in the cartesian coordinates and the cross section lies on the vertical plane (x-y plane) which corresponds to the anisotropic plane of the medium. Otherwise, the axes of the elastic symmetry can be inclined an angle β with respect to the axes of principal stresses applied at far-field which consists of the vertical and horizontal stressed $\sigma_v^{ff}, \sigma_h^{ff}$ as illustrated in Fig. 2.4a. The adopted hypothesis of deep tunnel allows considering that these stresses are uniform. Then by taking a rotation of angle β the considered problem can be studied in the coordinate system of elastic symmetry with the following stresses imposed at far-field (see Fig.2.4b):

$$\sigma_v = \frac{1}{2}\left(\sigma_v^{ff} + \sigma_h^{ff}\right) + \frac{1}{2}\left(\sigma_v^{ff} - \sigma_h^{ff}\right)\cos 2\beta,$$
$$\sigma_h = \frac{1}{2}\left(\sigma_v^{ff} + \sigma_h^{ff}\right) - \frac{1}{2}\left(\sigma_v^{ff} - \sigma_h^{ff}\right)\cos 2\beta, \qquad (2.1)$$
$$\tau_{vh} = \frac{1}{2}\left(\sigma_v^{ff} - \sigma_h^{ff}\right) sin 2\beta$$

The excavation will induce a redistribution of pore pressure, stresses and displacements around the tunnel. Particularly, depending on the hydraulic conditions behind the liner of tunnel, the pore pressure can be uniform if the liner is impermeable or it can decrease to the ambient pressure if the system of drainage is put on the extrados of liner. Thus, in a general manner we consider that the pore pressure behind the liner is p_0. Therefore, the tunnel excavated in dry rock is a particular case with the pore pressure being uniform and equal to zero in all the medium.

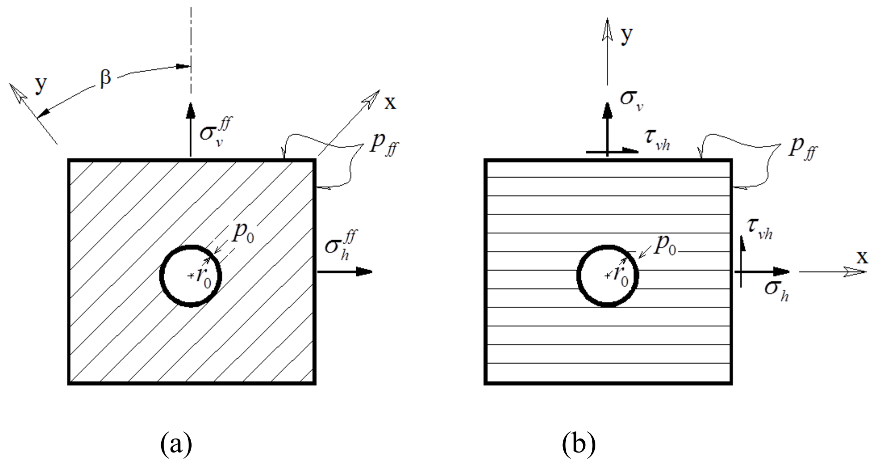

Fig. 2-1: The initial problem of deep tunnel excavated in a transversely anisotropic ground whose axes of elastic symmetry make an angle β with the principle stress axis at far-field (a). The equivalent problem after a rotation of angle β (b).

Solving this problem consists of the determination of stresses, strains and displacement distribution in the surrounding rock mass as well as in the liner of tunnel. As usual, the analytical solution is only obtained under some degree of simplification represented in different hypothesis. For the sake of clarity, the following assumptions are considered throughout this study: the tunnel with circular section is deep which allows neglecting the gravity effect (1); the anisotropic elastic behavior of rock mass belongs to the transversely isotropic class (2); the homogeneous elastic liner is installed simultaneously with the excavation and its thickness is small with respect to the radius of tunnel (3); contact between the liner and surrounding rock mass is perfect. i.e., no slip and no detachment at the contact between the rock and the liner, (4); and plane strain conditions are adopted along the tunnel axis (5).

The results obtained from these assumptions may be limited in the realistic application; however, this study does not aim to find a general solution which is unworkable due to the complexity of tunnel problems but rather to develop an explicit formulation for the preliminary calculations and may be useful for the further analysis or even to clarify the work mechanism of the tunnel by obtained computational tool.

Under these hypotheses and in the framework of the hydro-mechanical coupling, the solution of the considered problem must satisfy the following well-known equations for plane strain problem (Detournay and Cheng, 1993; Cheng, 1998). It should be noted that, the general expression of these equations were outlined in Chapter 1, however, we present them again in detail for the purpose of employing for plane strain problem:

- the equilibrium equation:

$$\begin{aligned}\frac{\partial \sigma_x}{\partial x}+\frac{\partial \tau_{xy}}{\partial y}=0\\ \frac{\partial \tau_{\mathrm{yx}}}{\partial x}+\frac{\partial \sigma_y}{\partial y}=0\end{aligned} \tag{2.2}$$

- the elastic constitutive equation:

$$\begin{pmatrix}\varepsilon_x\\ \varepsilon_y\\ \varepsilon_{xy}\end{pmatrix}=\begin{pmatrix}s_{11} & s_{12} & 0\\ s_{21} & s_{22} & 0\\ 0 & 0 & s_{33}\end{pmatrix}\begin{pmatrix}\sigma'_x\\ \sigma'_y\\ \tau'_{xy}\end{pmatrix} \tag{2.3}$$

- the strain compatibility equation:

$$2\frac{\partial^2 \varepsilon_{xy}}{\partial x\partial y}=\frac{\partial^2 \varepsilon_x}{\partial y^2}+\frac{\partial^2 \varepsilon_y}{\partial x^2} \tag{2.4}$$

- the fluid flow equation (by combining the Darcy law and the mass conservation):

$$k_x\frac{\partial^2 p}{\partial x^2}+k_y\frac{\partial^2 p}{\partial y^2}=\rho_{\mathrm{w}}\frac{\partial \chi}{\partial t} \tag{2.5}$$

In Eq. (2.2) σ_x,σ_y are the total stress in the x and y directions. Respectively in Eq. (2.3) σ'_x,σ'_y are the effective stresses which are related to the total stresses and pore pressure through the well-known Biot's theory:

$$\begin{aligned}\sigma'_x=\sigma_x+b_x p\\ \sigma'_y=\sigma_y+b_y p\end{aligned} \tag{2.6}$$

where b_x, b_y indicate the Biot coefficients in two directions x and y. Note that, in this study, the mechanical sign convention is used where the tension is taken as positive.

In addition to the two Biot coefficients (b_x,b_y), the hydro-mechanical properties of the medium consist of two different values of permeability (k_x, k_y) and five elastic parameters which are respectively the horizontal and vertical Young's modulus (E_x, E_y), the Poisson's ratios in the isotropic plane and anisotropic plane of the medium (ν_{xz}, ν_{xy}) and the shear modulus G_{xy}. These five elastic parameters are related to the compliance coefficients appeared in Eq. (2.3) through the following relationships (Lekhnitskii, 1963):

$$s_{11} = \frac{1-\nu_{xz}^2}{E_x}, s_{12} = s_{21} = -\frac{\nu_{xy}(1+\nu_{xz})}{E_x}, s_{22} = \frac{1-\nu_{xy}\nu_{yx}}{E_y}, s_{33} = \frac{1}{G_{xy}}, \nu_{yx} = \frac{\nu_{xy}E_y}{E_x} \quad (2.7)$$

Moreover, in Eq. (2.5) ρ_w is the unit weight of the pore fluid and χ indicates the change of fluid volume (per unit volume of material) which is related to the pore pressure and volumetric strain of the medium as follows:

$$p = M(\chi - b_x\varepsilon_x - b_y\varepsilon_y) \quad (2.8)$$

with M the Biot's modulus.

2.3. Analytical solution for deep tunnel excavated in anisotropic poroelastic medium with steady-state groundwater flow

In this section we consider the behavior of the tunnel excavated in the anisotropic and saturated medium and focus on the influence of groundwater flow at steady-state. Precisely, by limiting our study to a long period of time, when the groundwater flow attains the steady-state with a pore pressure p_0 on the extrados of liner, we will show that a closed-form solution can be deduced. For this purpose, at the first stage, the analytical solution of pore pressure at the steady flow will be introduced and at the second stage, we will detail the obtained closed-form solution of stresses and displacements distributions around the tunnel in the framework of hydro-mechanical coupling. The resolution of this last problem is done by using the complex potential approach.

2.3.1. Analytical solution for the steady-state pore pressure

A steady state of pore pressure will be obtained for long time, when the excess pore pressures dissipate. The pore pressure distribution around a tunnel in steady fluid flow must verify the fluid flow equation (see Eq. (2.5)) without right-hand side:

$$k_x\frac{\partial^2 p}{\partial x^2} + k_y\frac{\partial^2 p}{\partial y^2} = 0 \quad (2.9)$$

Multiplying two sides of this equation with $\sqrt{\frac{k_y}{k_x}}$, we have:

$$\sqrt{k_x k_y}\frac{\partial^2 p}{\partial x^2} + k_y\sqrt{\frac{k_y}{k_x}}\frac{\partial^2 p}{\partial y^2} = 0 \quad (2.10)$$

$$\Leftrightarrow \sqrt{k_x k_y}\frac{\partial^2 p}{\partial x^2}+\sqrt{k_x k_y}\frac{\partial^2 p}{\frac{k_x}{k_y}\partial y^2}=0 \tag{2.11}$$

$$\Leftrightarrow k_e\frac{\partial^2 p}{\partial x^2}+k_e\frac{\partial^2 p}{\partial\left(y\sqrt{\frac{k_x}{k_y}}\right)^2}=0 \tag{2.12}$$

in wich $k_e=\sqrt{k_x k_y}$

Introducing $X=x, Y=y\sqrt{k_x/k_y}$ and substituting in Eq. (2.9) yields the Laplace equation written in the new coordinate system (X, Y) as:

$$k_e\frac{\partial^2 p}{\partial X^2}+k_e\frac{\partial^2 p}{\partial Y^2}=0 \tag{2.13}$$

It should be noted that, the diffusion equation in anisotropic medium Eq. (2.9) is transformed into Eq. (2.13) in the equivalent isotropic medium.

In this new coordinate system, the cross section of the tunnel degenerates to an ellipse with two semi-axes $a=r_0$ and $b=r_0\sqrt{k_x/k_y}$. To solve the Eq. (2.13), we can use the conformal mapping technique to transform the outside region of the ellipse in the Z_w plane (the complex variable Z_w is defined as $Z_w=X+iY$) onto the outside region of unit circle in ζ_w plane. Mathematically, the conformal mapping can be written (Lekhnitskii, 1963):

$$Z_w=w(\zeta_w)=\frac{a+b}{2}\zeta_w+\frac{a-b}{2}\zeta_w^{-1} \tag{2.14}$$

or reciprocally one has:

$$\zeta_w=\frac{Z_w+\sqrt{Z_w^2-a^2+b^2}}{a+b} \tag{2.15}$$

In the plane ζ_w the solution of the Eq. (2.13) is the radial flow and can be expressed as function of the radius ρ (Fitts, 2006):

$$p=C_1+C_2\log\rho \tag{2.16}$$

where the constants C_1 and C_2 are determined from the boundary conditions: the pore pressure is equal to p_0 at the tunnel wall (corresponding to the circle with radius $\rho=1$ on the ζ_w plane) and equal to p_{ff} at infinity.

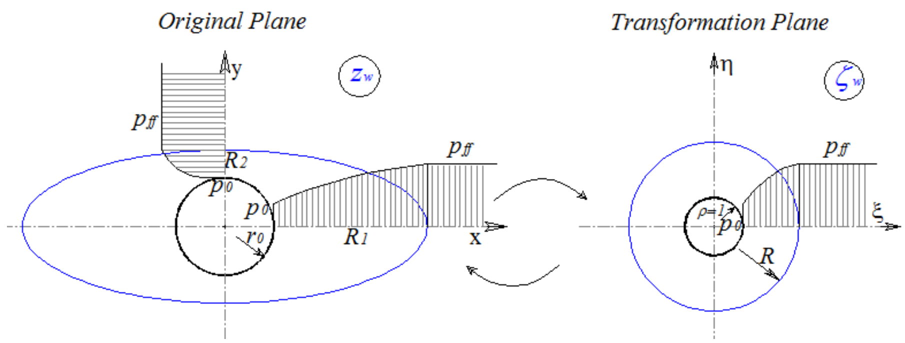

Fig. 2-2: The distribution of pore pressure in the original plane and in the transformation plane

However, beyond a distance far enough from the tunnel wall we could consider that pore pressure does not change (Fig.2-2), i.e, it is restored like initial pressure ($p = p_{ff}$) as discussed in different contributions (Carranza-Torres and Zhao, 2009; Wang and Wang, 2013; Bobet and Yu, 2015). In the ζ_w-plane one considers that this distance is represented by a circle with radius $\rho = R >> 1$. Therefore, from these boundary conditions, one can obtain straightforwardly the two constants C_1 and C_2 as follows:

$$\begin{cases} C_1 = p_0 \\ C_2 = \dfrac{p_{ff} - p_0}{\log R} \end{cases} \tag{2.17}$$

Because the complex variable can be written in the form $\zeta_w = \rho e^{i\theta}$, we obtain the final expression of pore pressure distribution in the rock mass in the following:

$$p = p_{ff} - \frac{p_0 - p_{ff}}{\log R} \mathrm{Re}\left[\log\left(\frac{\zeta_w}{R} \right) \right] \tag{2.18}$$

2.3.2. Closed-form solution of stress and displacement of deep tunnel

As previously presented, we limit our study in this part to a long period of time when the fluid flow toward the opening attains the steady-state. The interest is focused not only on the influence of the initial stresses but also on the effect of pore pressure distribution in the rock mass on the tunnel behavior which is characterized through the redistribution of stresses and displacements of the surrounding medium as well as the liner behavior. In comparison with different contributions in the literature (e.g. Carranza-Torres and Zhao, 2009; Wang and Wang, 2013; Bobet, 2011), the solution developed in this part can be considered as an extension by taking into account the anisotropic aspect of poroelastic rock. This solution is also regarded as an extension of the solution presented in Tran et al. (2016) which address a tunnel without liner in anisotropic poro-elastic ground.

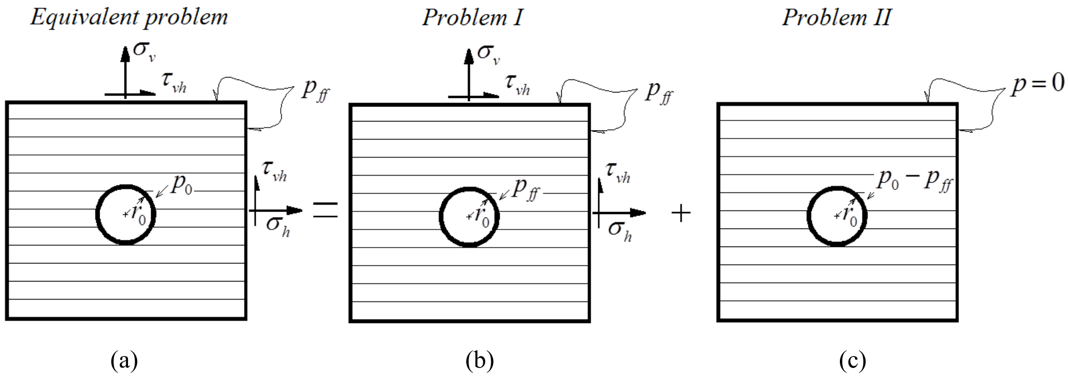

Fig. 2-3: Decomposition of the equivalent problem into two sub-problems.

As illustrated in Fig. 2-3, one can decompose the considered problem into two sub-problems called respectively as problem I and problem II because of its linear elasticity characteristic. In the problem I (Fig. 2-3b) one considers that the tunnel is excavated in the saturated porous medium with a uniform distribution of pore pressure ($p = p_{ff}$) and the total stress ($\sigma_v, \sigma_h, \tau_{vh}$) imposed at far-field. In the second problem (Fig 2.3c) one will study the tunnel behavior under the steady fluid flow of groundwater but the pore pressure distributes now from zero at infinity to $p = p_0 - p_{ff}$ at the tunnel wall. Once the solutions of problem I and problem II obtained, one has the complete solution for the original problem based on the principles of superposition of linear elasticity.

2.3.2.1. Solving the problem I:

As pointed out in the contribution of Bobet (2011), this problem corresponds to the case of the tunnel excavated in the porous medium below the water table with impermeable liner. The author showed that the solutions of the displacement and total stress in the rock mass as well as in the liner are the same as the ones obtained in case where the tunnel is excavated in the dry rock as long as the far-field total stresses are the same. Thus, if the problem of excavation in dry rock is solved, the solutions (displacements and total stresses) of the problem of the tunnel below the water table are straightforward while the effective stresses can be calculated from the total stresses and pore pressure using the Biot's theory as presented in Eq. (2.6).

Note that the closed-form solution of the tunnel excavated in an anisotropic and dry rock was detailed by Bobet (2011) in which the author used the complex potential approach firstly presented by Lekhnitskii (1963). In fact, in order to solve this problem, Bobet (2011) proposed to decompose it into four sub-problems noted respectively problems Ia, Ib, Ic and Id as illustrated in Fig. 2-4. In the problem Ia, the medium, as before the excavation, is homogeneous and is subjected to the total stress ($\sigma_v, \sigma_h, \tau_{vh}$) at far-field. The problem Ib corresponds to the case of a borehole without liner which is excavated in the infinite medium and subjected only to the radial and shear stresses (σ_{r_0}, τ_{r_0}) on its circumference. These radial and shear stresses are equivalent to ones determined on the tunnel wall of the problem Ia but with opposite sign:

$$\sigma_{r0} = -\frac{1}{2}(\sigma_h + \sigma_v) + \frac{1}{2}(\sigma_v - \sigma_h)cos2\theta - \tau_{vh}sin2\theta,$$
$$\tau_0 = -\frac{1}{2}(\sigma_v - \sigma_h)sin2\theta - \tau_{vh}cos2\theta \tag{2.19}$$

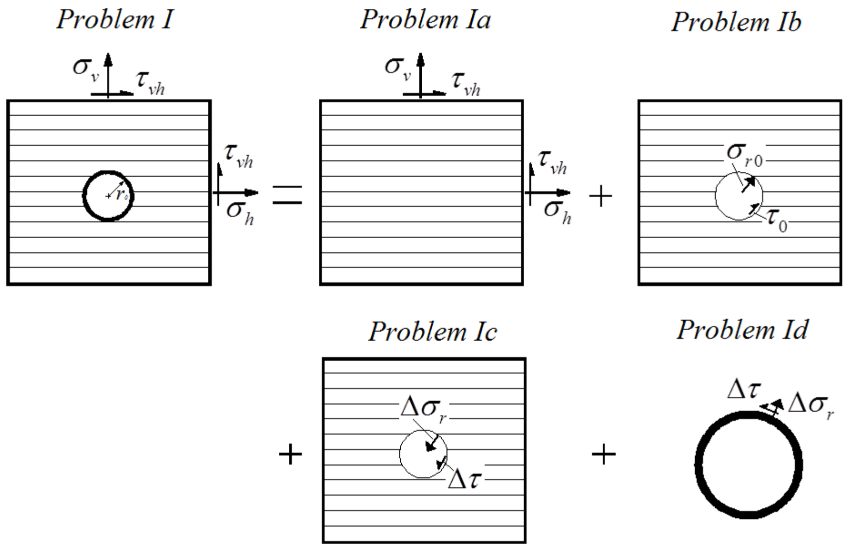

Fig. 2-4: Deep tunnel in anisotropic dry rock and its decomposition into four sub-problems (Bobet, 2011).

The problem Ic takes into account the interaction of the liner on the surrounding rock mass represented by the interactive radial and shear stresses ($\Delta\sigma_r, \Delta\tau$) applied to the tunnel wall. These same stresses (but with opposite sign), are applied to the liner from the rock mass (problem Id) as consequence of the perfect contact hypothesis between the liner and rock. The symmetry of the problem and the loading, and, the even and odd characteristic of the functions of $\Delta\sigma_r, \Delta\tau$ respectively, allow writing theses stresses in Fourier series forms (Bobet, 2011):

$$\Delta\sigma_r = \sigma_0 + \sum_{n=2,4,6}^{\infty} \sigma_n^a \cos n\theta + \sum_{n=2,4,6}^{\infty} \sigma_n^b \sin n\theta,$$
$$\Delta\tau = \sum_{n=2,4,6}^{\infty} \tau_n^a \sin n\theta + \sum_{n=2,4,6}^{\infty} \tau_n^b \cos n\theta \tag{2.20}$$

where the constants $\sigma_0, \sigma_n^a, \sigma_n^b, \tau_n^a, \tau_n^b$ are determined from the compatibility of displacements (hypothesis of perfect contact) between the rock and the liner:

$$U_{x,r_0}^{Id} = U_{x,r_0}^{Ia} + U_{x,r_0}^{Ib} + U_{x,r_0}^{Ic},$$
$$U_{y,r_0}^{Id} = U_{y,r_0}^{Ia} + U_{y,r_0}^{Ib} + U_{y,r_0}^{Ic} \tag{2.21}$$

and θ is the rotation angle from the springline to the considered point on the circumference of the tunnel wall with the anticlockwise positive direction.

In Eq. (2.21) the right-hand side terms present the displacements of rock mass at the perimeter of tunnel wall (sum of the solutions of problems Ia, Ib and Ic) whereas the left-hand side terms are the displacements of the liner evaluated at the contact surface with the ground (solution of the problem Id). It should be noted that, this tied contact condition is only achieved when the radial total stress on the interface between the liner and the rock mass is compressive. If the radial total stress is tensile, it would violate the assumption of perfect contact.

It should also be noted that, because of the assumption of perfect contact, the equation (2.21) must be validated to any point on the liner-rock mass interface. Therefore, in order to solve this equation, one has to impose the identical condition of term-by-term in two sides of the equation, i.e., for the constant term and for the factors of $\cos\theta$, $\sin\theta$, $\cos 2\theta$, $\sin 2\theta$ and so forth.

The solutions of the stresses and displacements in the homogeneous medium in the problem Ia are trivial where:

$$\begin{aligned} &\sigma_x^{Ia} = \sigma_h, \\ &\sigma_y^{Ia} = \sigma_v, \\ &\tau_{xy}^{Ia} = \tau_{vh}, \\ &U_x^{Ia} = U_y^{Ia} = 0 \end{aligned} \tag{2.22}$$

It can be observe that solving the problem Ib is similar to that of the problem Ic because both problems correspond to the case of a circular borehole subjected to the radial and shear stresses on its circumference. This last problem has been widely discussed in the literature since the pioneered work of Lekhnitskii (1963) in which the stresses and displacements around the excavation can be determined analytically by using the complex potentials. According to Lekhnitskii (1963), the stress components can be identified from the function so-called Airy stress function, $F(x, y)$ which satisfies the equilibrium equation presented in Eq. (2.2):

$$\sigma_x = \frac{\partial^2 F(x,y)}{\partial y^2}; \sigma_y = \frac{\partial^2 F(x,y)}{\partial x^2}; \tau_{xy} = -\frac{\partial^2 F(x,y)}{\partial x \partial y} \tag{2.23}$$

Note that by substituting the Eqs. (2.6), (2.2) and (2.23) in Eq. (2.3) we obtain the following expression of the compatibility equation that the stress function must verify:

$$s_{11}\frac{\partial^4 F}{\partial y^4} + (2s_{12} + s_{33})\frac{\partial^4 F}{\partial y^2 \partial x^2} + s_{22}\frac{\partial^4 F}{\partial x^4} = -(s_{11}b_x + s_{12}b_y)\frac{\partial^2 p}{\partial y^2} - (s_{21}b_x + s_{22}b_y)\frac{\partial^2 p}{\partial x^2} \tag{2.24}$$

Eq. (2.24) is the compatibility equation written in terms of Airy function. In the framework of the pure mechanical problem (as the problem Ib and Ic) where the right-hand side of Eq. (2.24) is equal to zero, Lekhnitskii (1963) proposed a solution by introducing two complex functions, namely complex potentials that are defined as follows:

$$\Phi_1(z_1) = F'(z_1) = \frac{\partial F(z_1)}{\partial z_1},\ \Phi_2(z_2) = F'(z_2) = \frac{\partial F(z_2)}{\partial z_2}, \tag{2.25}$$

In Eq. (2.25) two complex variables $z_k = x + \mu_k y$ were used where μ_k (*k=1,2*) are roots with positive imaginary parts of the following characteristic equation:

$$s_{11}\mu^4 + (2s_{12} + s_{33})\mu^2 + s_{22} = 0 \tag{2.26}$$

Lekhnitskii (1963) proved also that the roots of the characteristic equation (2.26) are either complex, or pure imaginary and they consist of two pairs of complex conjugates since the characteristic equation is a fourth order algebraic equation with real coefficients. From the two potential functions, the author showed that stresses and displacements around the cavity can be determined through the following relationships:

$$\begin{aligned} \sigma_x &= 2\,\mathrm{Re}[\mu_1^2\Phi_1'(z_1) + \mu_2^2\Phi_2'(z_2)]; \\ \sigma_y &= 2\,\mathrm{Re}[\Phi_1'(z_1) + \Phi_2'(z_2)]; \\ \tau_{xy} &= -2\,\mathrm{Re}[\mu_1\Phi_1(z_1) + \mu_2\Phi_1(z_1)]; \\ U_x &= 2\,\mathrm{Re}[p_1\Phi_1(z_1) + p_2\Phi_2(z_2)]; \\ U_y &= 2\,\mathrm{Re}[q_1\Phi_1(z_1) + q_2\Phi_2(z_2)] \end{aligned} \tag{2.27}$$

where the coefficients p_1, p_2, q_1, q_2 are defined as:

$$p_1 = s_{11}\mu_1^2 + s_{12},\ p_2 = s_{11}\mu_2^2 + s_{12}; \qquad q_1 = s_{12}\mu_1 + \frac{s_{22}}{\mu_1},\ q_2 = s_{12}\mu_2 + \frac{s_{22}}{\mu_2} \tag{2.28}$$

and '***Re***' stands for the real part.

In fact, to determine these two complex potentials, the conformal mapping technique which transforms the infinite domain outside the tunnel (of radius r_0) in the z_k planes to the infinite domain outside the unit circle in the ζ_k planes was used. Mathematically, this transformation is written as Eq. (1.106) with $a = b = r_0$ (Lekhnitskii, 1963, 1968):

$$z_k = w(\zeta_k) = \frac{r_0(1 - i\mu_k)}{2}\zeta_k + \frac{r_0(1 + i\mu_k)}{2}\zeta_k^{-1}, \qquad (k = 1, 2) \tag{2.29}$$

or reciprocally, one has:

$$\zeta_k = \frac{z_k + \sqrt{z_k^2 - r_0^2(1 + \mu_k^2)}}{r_0(1 - i\mu_k)}, \qquad (k = 1, 2) \tag{2.30}$$

For the circular opening subjected to the distributed forces on its circumference, Lekhnitskii (1963) proposed the general form of the two complex potentials as in Eqs. (1.108) with the constants $A_1 = A_2 = 0$, and so, one has:

$$\Phi_1(z_1) = \frac{1}{\mu_1 - \mu_2} \sum_{n=1}^{\infty} \left(\bar{b}_n - \mu_2 \bar{a}_n \right) \zeta_1^{-n}$$
$$\Phi_2(z_2) = -\frac{1}{\mu_1 - \mu_2} \sum_{n=1}^{\infty} \left(\bar{b}_n - \mu_1 \bar{a}_n \right) \zeta_2^{-n} \tag{2.31}$$

These complex potentials satisfy the condition of vanished stresses at infinity (in fact their derivatives tend to zero as $z_k \to \infty$). The constants $\bar{a}_n$ and $\bar{b}_n$ are the conjugates of the complex number a_n and b_n which are calculated from the boundary conditions at the tunnel wall.

Imposing the boundary condition on the tunnel circumference (the interface between the rock mass and the liner) as presented in Eq. (1.100) with eliminating the body forces we have following relation:

$$\sum_{n=1}^{\infty} \bar{b}_n e^{-n\theta i} = \int_0^{\theta} (\sigma_r \cos\theta - \tau \sin\theta) r_0 d\theta,$$
$$\sum_{n=1}^{\infty} \bar{a}_n e^{-n\theta i} = \int_0^{\theta} (-\sigma_r \sin\theta - \tau \cos\theta) r_0 d\theta \tag{2.32}$$

where the angle θ is defined in the Fig. 2-5. It should be noted that, on the tunnel circumference, i.e., $r = r_0$, $\zeta_k = \cos\theta + i\sin\theta = e^{i\theta}$ and $\bar{a}_n = \bar{b}_n = 0 \quad (n = 2, 3, 4, ...)$.

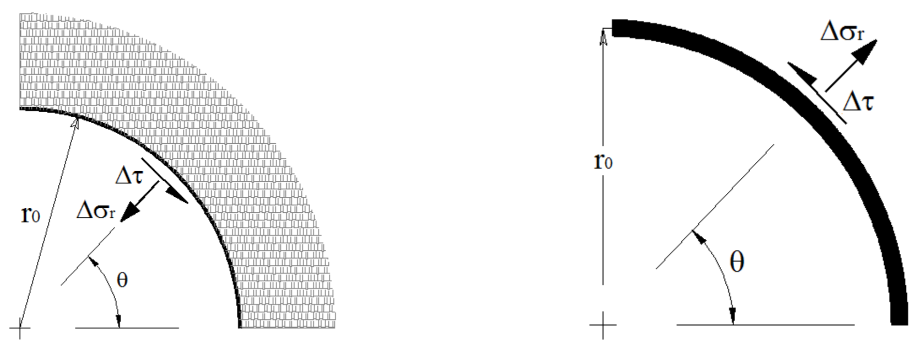

Fig. 2-5: Stresses at the rock-liner interface

Applying these boundary conditions, therefore, one obtains the two complex functions $\Phi_1(z_1)$ and $\Phi_2(z_2)$ (see Bobet, 2011) as follows:

$$\Phi_1 = \frac{1}{2} \frac{r_0}{\mu_1 - \mu_2} \left[(1 - i\mu_2)\tau_{vh} + \mu_2 \sigma_v - i\sigma_h \right] \frac{1}{\zeta_1},$$
$$\Phi_2 = -\frac{1}{2} \frac{r_0}{\mu_1 - \mu_2} \left[(1 - i\mu_1)\tau_{vh} + \mu_1 \sigma_v - i\sigma_h \right] \frac{1}{\zeta_2} \tag{2.33}$$

for the problem Ib and:

$$\Phi_1 = \frac{1}{4}\frac{r_0}{\mu_1-\mu_2}\left([2(i-\mu_2)\sigma_0 + (\sigma_2^a - \tau_2^a)(i+\mu_2) + (\sigma_2^b + \tau_2^b)(i+\mu_2)i]\frac{1}{\zeta_1} + \right.$$
$$\left.\sum_{n=3,5,7}^{\infty}\frac{1}{n}\left[(i-\mu_2)(\sigma_{n-1}^a + \tau_{n-1}^a + i\sigma_{n-1}^b - i\tau_{n-1}^b) + (i+\mu_2)(\sigma_{n-1}^a - \tau_{n-1}^a + i\sigma_{n-1}^b + i\tau_{n-1}^b)\right]\frac{1}{\zeta_1^n}\right);$$
$$\Phi_2 = -\frac{1}{4}\frac{r_0}{\mu_1-\mu_2}\left([2(i-\mu_2)\sigma_0 + (\sigma_2^a - \tau_2^a)(i+\mu_2) + (\sigma_2^b + \tau_2^b)(i+\mu_2)i]\frac{1}{\zeta_1} + \right. \tag{2.34}$$
$$\left.\sum_{n=3,5,7}^{\infty}\frac{1}{n}\left[(i-\mu_1)(\sigma_{n-1}^a + \tau_{n-1}^a + i\sigma_{n-1}^b - i\tau_{n-1}^b) + (i+\mu_2)(\sigma_{n-1}^a - \tau_{n-1}^a + i\sigma_{n-1}^b + i\tau_{n-1}^b)\right]\frac{1}{\zeta_2^n}\right);$$

for the problem Ic.

Concerning the problem Id, the displacement in the liner can be calculated from the following relationship (Flügge, 1966; Bobet, 2011):

$$\begin{aligned}
&\frac{\partial^2 U_\theta^s}{\partial\theta^2} + \frac{\partial U_\theta^s}{\partial\theta} = \frac{(1-\nu_s^2)}{E_s A_s} r_0^2 \tau^s, \\
&\frac{\partial U_\theta^s}{\partial\theta} + U_r^s + \frac{I_s}{r_0^s}\left(\frac{\partial^4 U_r^s}{\partial\theta^4} + 2\frac{\partial^2 U_r^s}{\partial\theta^2} + U_r^s\right) = \frac{(1-\nu_s^2)}{E_s A_s} r_0^2 \sigma_r^s
\end{aligned} \tag{2.35}$$

where U_θ^s and U_r^s are the radial and tangential displacements of the liner, σ_r^s and τ^s are the radial and shear stresses acting on the liner. It should be noted that here $U_\theta^s = U_\theta^{Id}$ and $U_r^s = U_r^{Id}$, $\tau^s = \Delta\tau$ and $\sigma_r^s = \Delta\sigma_r$ mentioned in Eqs. (2.20) and (2.21) because of the perfect rock mass-liner contact condition. E_s, ν_s are the elastic modulus and Poisson coefficient; A_s, I_s are the cross-section area and moment of inertia of the liner which are calculated from the thickness t_s ($A_s = t_s, I_s = t_s^3/12$). These relations are established based on the assumption that the liner is thin in comparison with the radius of tunnel and, thereby, the cylindrical shell theory is applied. Thus, this Eq. (2.35) allows determining the radial and tangential displacements U_r^s, U_θ^s from the radial and shear stresses (σ_r^s, τ^s) that applied to the liner.

To simplify the presentation, the expressions of displacements on the interface, i.e., the displacement solutions of the problem Ib, Ic and Id at $r = r_0$ as mentioned in Eq. (2.21), are not detailed here but are given in appendix A (see also in appendix II of Bobet, 2011).

One has relations between the thrust force $T^{s,Id}$ and the moment distribution $M^{s,Id}$ in the liner with the stresses applied to the liner as following expressions (Bobet 2011):

$$\begin{aligned}
&r_0\frac{\partial T^{s,Id}}{\partial\theta} - \frac{\partial M^{s,Id}}{\partial\theta} = -r_0^2\tau^{s,Id}, \\
&r_0 T^{s,Id} + \frac{\partial^2 M^{s,Id}}{\partial\theta^2} = r_0^2\sigma_r^{s,Id}
\end{aligned} \tag{2.36}$$

Substituting Eq. (2.20) into (2.36) and then integrating the resulting equations one obtains the general expression for the thrust load $T^{s,Id}$ and the moment distribution $M^{s,Id}$ as follows (Bobet 2011):

$$\begin{aligned} T^{s,Id} &= \sigma_0 r_0 - \sum_{n=2,4,6}^{\infty} \left\{ \left(\frac{\sigma_n^a - n\tau_n^a}{n^2-1} \right) r_0 \cos n\theta + \left(\frac{n\sigma_n^b + \tau_n^b}{n(n^2-1)} + \frac{\tau_n^b}{n} \right) r_0 \sin n\theta \right\} \\ M^{s,Id} &= - \sum_{n=2,4,6}^{\infty} \left\{ \left(\frac{n\sigma_n^a - \tau_n^a}{n(n^2-1)} \right) r_0^2 \cos n\theta + \left(\frac{n\sigma_n^b + \tau_n^b}{n(n^2-1)} \right) r_0^2 \sin n\theta \right\} \end{aligned} \tag{2.37}$$

Thenceforth, one has the tangential stresses in the interior and exterior fibers as well as the strains in the liner respectively as:

$$\begin{aligned} \sigma_\theta^{s,Id} &= \frac{T^{s,Id}}{A_s} \pm \frac{M^{s,Id} t_s}{2I_s}, \\ \varepsilon_\theta^{s,Id} &\approx \frac{1-\nu_s^2}{E_s} \sigma_\theta^{s,Id} \end{aligned} \tag{2.38}$$

2.3.2.2. Solving the problem II:

We consider now the problem II that focuses on the influence of the steady fluid flow on the mechanical response of the tunnel. This problem was discussed in different works (Carranza-Torres and Zhao, 2009; Bobet, 2003) but limited only in case of the isotropic behavior of the porous medium.

Like the previous problem, to solve this problem we will use the complex potential approach but in this case, it needs both the hydraulic and hydro-mechanical potentials. Note that this approach was successfully applied by Bobet and Yu (2015) to determine the stress field near the tip of a crack in the transversely isotropic saturated rock. More precisely, knowing the distribution of pore pressure around the crack at the steady-state and, hence, the hydraulic potential, these authors proposed the hydro-mechanical potentials owing to the same form as ones of the hydraulics. After some developments, these authors showed that the displacements as well as the stress around the crack tip can be deduced. In the present study, sharing the same idea, this method is used to study the deep tunnel taking into account the interaction between the liner and the rock mass. Concretely, to solve the problem II, one decomposes it in three sub-problems as shown in Fig. 2-6. In the problem IIa, one determines the stresses and displacements in the surrounding rock mass due to the steady-state groundwater flow. Thus, in this problem, the liner of tunnel is not accounted for and the tunnel behavior is controlled by the steady-flow of the groundwater with pore pressure ranging from (p_0-p_{ff}) at the surface of tunnel to zero at infinity. The presence of liner is considered through its interaction with the surrounding rock mass in the problem IIb and IIc. Similarly to the problem Ic and Id, this interaction is represented by the radial and shear stresses ($\Delta\sigma_r^p, \Delta\tau_r^p$) applied respectively to the tunnel wall or the liner (with opposite sign) as illustrated in Fig. 2-6:

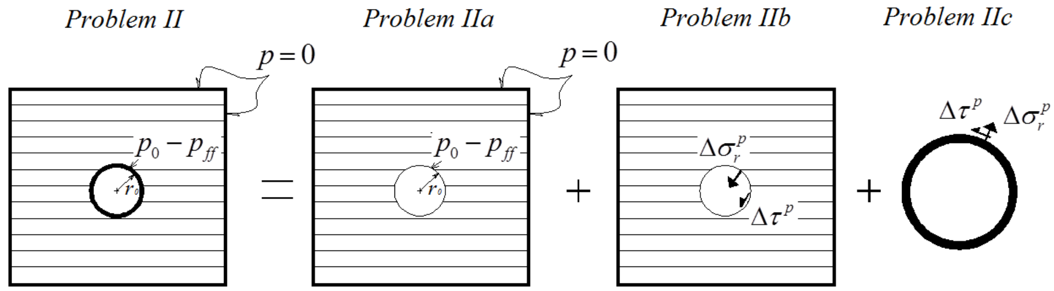

Fig. 2-6: Decomposition of the problem II into three sub-problems

Considering firstly the problem IIa, in order to search its solution one has to resolve the compatibility equation Eq. (2.24) with right-hand side for determination the Airy stress function F. The general solution of this equation consists of two components, a homogeneous solution (F_h^*) and a particular solution (F_p^*) corresponding respectively to the mechanical and hydro-mechanical effects.

For this purpose, as the first step, one will determine the particular solution F_p^* by substituting the solution of pore pressure distribution into the compatibility equation (Eq. 2.23). Note that the distribution of pore pressure in this problem II can be deduced directly from Eq. (2.18) with a small modification because of the fact that the pore pressure ranges now from (p_0-p_{ff}) at the tunnel wall (corresponds to $\rho=1$ on the ζ_w plane) to zero at far-field (corresponds to $\rho=R>>1$ on the ζ_w plane as discussed previously). Therefore without difficulty, one obtains the following expression:

$$F_p^{*''}(z_w)=2\,\mathrm{Re}\{\eta\Phi_w^{*\prime}(z_w)\}=\frac{p_0-p_{ff}}{\log R}\mathrm{Re}\left[\eta.\log\frac{\zeta_w}{R}\right] \tag{2.39}$$

with:

$$\eta=-\frac{\beta_1\mu_w^2+\beta_2}{s_{11}\mu_w^4+(2s_{12}+s_{33})\mu_w^2+s_{22}},\quad \beta_1=s_{11}b_x+s_{12}b,\quad \beta_2=s_{21}b_x+s_{22}b_y \tag{2.40}$$

Owing to the fact that the hydraulic and hydro-mechanical potentials have the same order of effect on the displacements and stresses of tunnel, thus one can propose, in the second step, two hydro-mechanical potentials $\Phi_1^{*p}(z_1),\Phi_2^{*p}(z_2)$ whose derivatives take the same form as the hydraulic potential:

$$\begin{aligned}\Phi_1^{*p}{}'(z_1)&=\frac{1}{2}\frac{p_0-p_{ff}}{\log R}N_1\log\left(\frac{\zeta_1}{R}\right),\\ \Phi_2^{*p}{}'(z_2)&=\frac{1}{2}\frac{p_0-p_{ff}}{\log R}N_2\log\left(\frac{\zeta_2}{R}\right)\end{aligned} \tag{2.41}$$

where N_1 and N_2 are two complex constants that one has to determine.

From these hydraulic and hydro-mechanical potentials, the stresses and displacements can be computed according to the following relations:

$$\begin{cases} \sigma_x^{IIa,p} = 2\,\mathrm{Re}[\mu_1^2 \Phi_1^{*p}\,'(z_1) + \mu_2^2 \Phi_2^{*p}\,'(z_2)] + 2\,\mathrm{Re}[\eta \mu_w^2 \Phi_w^{*}\,'(z_w)] \\ \sigma_y^{IIa,p} = 2\,\mathrm{Re}[\Phi_1^{*p}\,'(z_1) + \Phi_2^{*p}\,'(z_2)] + 2\,\mathrm{Re}[\eta \Phi_w^{*}\,'(z_w)] \\ \tau_{xy}^{IIa,p} = -2\,\mathrm{Re}[\mu_1 \Phi_1^{*p}\,'(z_1) + \mu_2 \Phi_2^{*p}\,'(z_2)] + 2\,\mathrm{Re}[\eta \mu_w \Phi_w^{*}\,'(z_w)] \\ U_x^{IIa,p} = 2\,\mathrm{Re}[p_1 \Phi_1^{*p}(z_1) + p_2 \Phi_2^{*p}(z_2)] + 2\,\mathrm{Re}[p_w \Phi_w^{*}(z_w)] \\ U_y^{IIa,p} = 2\,\mathrm{Re}[q_1 \Phi_1^{*p}(z_1) + q_2 \Phi_2^{*p}(z_2)] + 2\,\mathrm{Re}[q_w \Phi_w^{*}(z_w)] \end{cases} \tag{2.42}$$

in which:

$$p_w = s_{11}\mu_w^2 + s_{12}; \qquad q_w = s_{12}\mu_w + \frac{s_{22}}{\mu_w} \tag{2.43}$$

Substituting Eqs. (2.39) and (2.41) into Eq. (2.42) yields the expressions of stress components:

$$\begin{aligned} \sigma_x^{IIa,p} &= \frac{p_0 - p_{ff}}{logR}\mathrm{Re}\left[N_1\mu_1^2 log\frac{\zeta_1}{R} + N_2\mu_2^2 log\frac{\zeta_2}{R} + \eta\mu_w^2 log\frac{\zeta_w}{R}\right]; \\ \sigma_y^{IIa,p} &= \frac{p_0 - p_{ff}}{logR}\mathrm{Re}\left[N_1 log\frac{\zeta_1}{R} + N_2 log\frac{\zeta_2}{R} + \eta log\frac{\zeta_3}{R}\right]; \\ \tau_{xy}^{IIa,p} &= -\frac{p_0 - p_{ff}}{logR}\mathrm{Re}\left[N_1\mu_1 log\frac{\zeta_1}{R} + N_2\mu_2 log\frac{\zeta_2}{R} + \eta\mu_3 log\frac{\zeta_3}{R}\right] \end{aligned} \tag{2.44}$$

as well as the expressions of displacement components:

$$\begin{aligned} U_x^{IIa,p} &= \frac{r_0}{2}\frac{p_0 - p_{ff}}{logR}\mathrm{Re}\left\{ p_1 N_1 \frac{1}{\zeta_1}\left[\left(log\frac{\zeta_1}{R} - 1\right)\zeta_1^2(1 - \mathrm{i}\mu_1) + \left(log\frac{\zeta_1}{R} + 1\right)(1 + \mathrm{i}\mu_1)\right] + \right. \\ & p_2 N_2 \frac{1}{\zeta_2}\left[\left(log\frac{\zeta_2}{R} - 1\right)\zeta_2^2(1 - \mathrm{i}\mu_2) + \left(log\frac{\zeta_2}{R} + 1\right)(1 + \mathrm{i}\mu_2)\right] \\ & \left. + (p_w\eta - \beta_1)\frac{1}{\zeta_w}\left[\left(log\frac{\zeta_w}{R} - 1\right)\zeta_w^2(1 - \mathrm{i}\mu_w) + \left(log\frac{\zeta_w}{R} + 1\right)(1 + \mathrm{i}\mu_w)\right]\right\}; \\ U_y^{IIa,p} &= \frac{r_0}{2}\frac{p_0 - p_{ff}}{logR}\mathrm{Re}\left\{ q_1 N_1 \frac{1}{\zeta_1}\left[\left(log\frac{\zeta_1}{R} - 1\right)\zeta_1^2(1 - \mathrm{i}\mu_1) + \left(log\frac{\zeta_1}{R} + 1\right)(1 + \mathrm{i}\mu_1)\right] + \right. \\ & q_2 N_2 \frac{1}{\zeta_2}\left[\left(log\frac{\zeta_2}{R} - 1\right)\zeta_2^2(1 - \mathrm{i}\mu_2) + \left(log\frac{\zeta_2}{R} + 1\right)(1 + \mathrm{i}\mu_2)\right] \\ & \left. + \left(q_w\eta - \frac{\beta_1}{\mu_w}\right)\frac{1}{\zeta_w}\left[\left(log\frac{\zeta_w}{R} - 1\right)\zeta_w^2(1 - \mathrm{i}\mu_w) + \left(log\frac{\zeta_w}{R} + 1\right)(1 + \mathrm{i}\mu_w)\right]\right\} \end{aligned} \tag{2.45}$$

These expressions show that the displacements and stresses are calculated from the logarithmic functions of the complex variables $\zeta_1, \zeta_2, \zeta_w$. However, it is important to note that the logarithmic functions of the complex variables are multi-valued in angle θ (periodic functions of angle θ) which is expressed as (Churchill, 1960; Kreyszig, 1999):

$$\log\Omega = \log(\rho e^{i(\theta+2n\pi)}) = \log\rho + i(\theta+2n\pi) \tag{2.46}$$

in wich Ω is complex number and n is integer number. Therefore, the requirement of single-valuedness of the displacements in Eq. (2.45), i.e., the sum of factors of imaginary numbers equal to zero, provides the following system of equations:

$$\begin{aligned}
&\mathrm{Im}[p_1N_1 + p_2N_2 + p_w\eta - \beta_1] = 0,\\
&\mathrm{Im}[p_1N_1\mu_1 + p_2N_2\mu_2 + (p_w\eta - \beta_1)\mu_w] = 0,\\
&\mathrm{Im}[q_1N_1 + q_2N_2 + q_w\eta - \beta_2 / \mu_w] = 0,\\
&\mathrm{Im}[q_1N_1\mu_1 + q_2N_2\mu_2 + (q_w\eta - \beta_2 / \mu_w)\mu_w] = 0
\end{aligned} \tag{2.47}$$

where "***Im***" stands for the imaginary parts.

It should be noted that, the single-valuedness condition of displacements infers also the single-valuedness condition of the stresses.

Furthermore, by writing the complex numbers in the form: $\kappa_i = \kappa_{i1} + i\kappa_{i2}$, for example $\eta = \eta_1 + i\eta_2$, we can express the Eq. (2.47) as follows:

$$\begin{aligned}
&N_{12}p_{11} + N_{11}p_{12} + N_{22}p_{21} + N_{21}p_{22} + \eta_2 p_{w1} + \eta_1 p_{w2} = 0,\\
&(N_{12}p_{11} + N_{11}p_{12})\mu_{11} + (N_{11}p_{11} - N_{12}p_{12})\mu_{12} + (N_{22}p_{21} + N_{21}p_{22})\mu_{21}\\
&+(N_{21}p_{21} - N_{22}p_{22})\mu_{22} + (\eta_2 p_{w1} + \eta_1 p_{w2})\mu_{31} + (\eta_1 p_{w1} - \eta_2 p_{w2})\mu_{32} - \beta_1\mu_{32} = 0,\\
&N_{12}q_{11} + N_{11}q_{12} + N_{22}q_{21} + N_{21}q_{22} + \eta_2 q_{w1} + \eta_1 q_{w2} + \frac{\beta_2\mu_{32}}{\mu_{31}^2 + \mu_{32}^2} = 0,\\
&(N_{12}q_{11} + N_{11}q_{12})\mu_{11} + (N_{11}q_{11} - A_{12}q_{12})\mu_{12} + (N_{22}q_{21} + N_{21}q_{22})\mu_{21}\\
&+(N_{21}q_{21} - N_{22}q_{22})\mu_{22} + (\eta_2 q_{w1} + \eta_1 q_{w2})\mu_{31} + (\eta_1 q_{w1} - \eta_2 q_{w2})\mu_{32} = 0
\end{aligned} \tag{2.48}$$

This last system of four linear equations allows calculating the real and imaginary parts of two complex constants N_1, N_2 (which are N_{11}, N_{12} and N_{21}, N_{22} respectively). It is worth noting that, this system of equation is still validated in the general case of an elliptical tunnel. Particularly, as a special case when one semi-axis of ellipse is equal to zero, Eq. (2.48) is degenerated to one presented in the previous work of Bobet and Yu (see Eq. (39) in Bobet and Yu, 2015). However, in this later contribution, to derive the system of equations, Bobet and Yu (2015) used the compatibility condition of displacements and stresses at the common boundary of crack.

Once the two complex constants N_1, N_2 are calculated, it is straightforward to determine the derivatives of complex potentials in Eq. (2.41) as well as the stresses and displacements from Eq. (2.44) and (2.45). The stresses given by Eq. (2.44) satisfy the boundary conditions of zero total stresses far from the tunnel, i.e., at $\zeta_k = R\mathrm{e}^{i\theta}(k = 1, 2, w)$ but introduce non-zero total normal and shear stresses on the surface of the tunnel wall. Thus, to satisfy the condition of vanished stresses on the perimeter surface of the tunnel, at this place one imposes the same normal and shear stresses but with opposite sign. Expressions of these imposed stresses on the surface of the tunnel wall are:

$$\begin{aligned}\sigma_{r0}^{p} &= -\frac{1}{2}(\Sigma_x+\Sigma_y)+\frac{1}{2}(\Sigma_y-\Sigma_x)cos2\theta-\mathrm{T}_{xy}sin2\theta,\\ \tau_0^{p} &= -\frac{1}{2}(\Sigma_y-\Sigma_x)sin2\theta-\mathrm{T}_{xy}cos2\theta\end{aligned} \tag{2.49}$$

where $\Sigma_x,\Sigma_y,\mathrm{T}_{xy}$ are stress components on the tunnel wall obtained from Eq.(2.44):

$$\begin{aligned}\Sigma_x &= -(p_0-p_{ff})\,\mathrm{Re}[N_1\mu_1^2+N_2\mu_2^2+\eta\mu_w^2],\\ \Sigma_y &= -(p_0-p_{ff})\,\mathrm{Re}[N_1+N_2+\eta],\\ \mathrm{T}_{xy} &= (p_0-p_{ff})\,\mathrm{Re}[\mu_1N_1+\mu_2N_2+\mu_w\eta]\end{aligned} \tag{2.50}$$

This case, as mentioned above, belongs to one of the well-known problem solved in the work of Lekhnitskii (1963) and can be also found in Amadei (1983), and is analogical to the problem Ib. Therefore, the solution of the problem Ib, previously presented can be used here. For example one can directly deduce the two complex potential functions from the Eq. (2.33) but replacing the stresses ($\sigma_h,\sigma_v,\tau_{vh}$) by ($\Sigma_x,\Sigma_y,\mathrm{T}_{xy}$):

$$\begin{aligned}\Phi_1^{*h} &= \frac{1}{2}\frac{r_0}{\mu_1-\mu_2}\left[(1-i\mu_2)T_{xy}+\mu_2\Sigma_y-i\Sigma_x\right]\frac{1}{\zeta_1},\\ \Phi_2^{*h} &= -\frac{1}{2}\frac{r_0}{\mu_1-\mu_2}\left[(1-i\mu_1)T_{xy}+\mu_1\Sigma_y-i\Sigma_x\right]\frac{1}{\zeta_2}\end{aligned} \tag{2.51}$$

Consequently, the complete solution of stresses and displacements of the problem IIa is:

$$\begin{aligned}\sigma_x^{IIa} &= \sigma_x^{IIa,p}+\sigma_x^{IIa,h},\\ \sigma_y^{IIa} &= \sigma_y^{IIa,p}+\sigma_y^{IIa,h},\\ \tau_{xy}^{IIa} &= \tau_{xy}^{IIa,p}+\tau_{xy}^{IIa,h},\\ U_x^{IIa} &= U_x^{IIa,p}+U_x^{IIa,h},\\ U_y^{IIa} &= U_y^{IIa,p}+U_y^{IIa,h}\end{aligned} \tag{2.52}$$

where the stresses $\sigma_x^{IIa,h},\sigma_y^{IIa,h},\tau_{xy}^{IIa,h}$ and displacement $U_x^{IIa,h},U_y^{IIa,h}$ are calculated from the complex potentials in Eq. (2.51) by using the Eq. (2.27).

Let us treat now the two other problems IIb and IIc in which the interaction between the liner and the rock mass is taken into account. As mentioned above, these two problems are similar to the problem Ic and Id where the interaction between the liner and the rock mass can be represented through the radial and shear stresse ($\Delta\sigma_r^p,\Delta\tau_r^p$) acting on the tunnel wall and liner. Using the similar process as in case of the dry rock (problem Ic and Id) one can write these radial and shear stresses in form of the Fourier series:

$$\Delta\sigma_r^p = \sigma_0^p + \sum_{n=2,4,6}^{\infty} \sigma_n^{a,p}\cos n\theta + \sum_{n=2,4,6}^{\infty} \sigma_n^{b,p}\sin n\theta,$$
$$\Delta\tau^p = \sum_{n=2,4,6}^{\infty} \tau_n^{a,p}\sin n\theta + \sum_{n=2,4,6}^{\infty} \tau_n^{b,p}\cos n\theta \tag{2.53}$$

where the constants $\sigma_0^p, \sigma_n^{a,p}, \sigma_n^{b,p}, \tau_n^{a,p}, \tau_n^{b,p}$ are determined from the compatibility of displacements at the liner–rock mass contact (assumption of no slip and no detachment). Concretely, these parameters can be found from the following conditions:

$$U_{x,r_0}^{IIc} = U_{x,r_0}^{IIa} + U_{x,r_0}^{IIb};$$
$$U_{y,r_0}^{IIc} = U_{y,r_0}^{IIa} + U_{y,r_0}^{IIb} \tag{2.54}$$

Consequently, the same procedure as used in problem Ic and Id can be used here to solve the problem IIb and IIc. Note that the expressions of the displacements U^{IIa}, U^{IIb} and U^{IIc} at the liner-rock mass contact are detailed in appendix A in which the displacements of problem IIa are reduced by using the single-valuedness condition.

The general expression for thrust load $T^{s,IIc}$ and moment distribution $M^{s,IIc}$ in the liner for the problem *IIc* which are analogous with the problem *Id* as:

$$T^{s,IIc} = \sigma_0 r_0 - \sum_{n=2,4,6}^{\infty}\left\{\left(\frac{\sigma_n^{a,p} - n\tau_n^{a,p}}{n^2-1}\right) r_0 \cos n\theta + \left(\frac{n\sigma_n^{b,p} + \tau_n^{b,p}}{n(n^2-1)} + \frac{\tau_n^{b,p}}{n}\right) r_0 \sin n\theta\right\}$$
$$M^{s,IIc} = -\sum_{n=2,4,6}^{\infty}\left\{\left(\frac{n\sigma_n^{a,p} - \tau_n^{a,p}}{n(n^2-1)}\right) r_0^2 \cos n\theta + \left(\frac{n\sigma_n^{b,p} + \tau_n^{b,p}}{n(n^2-1)}\right) r_0^2 \sin n\theta\right\} \tag{2.55}$$

One has also the tangential stresses in the interior and exterior fibers and the strains in the liner respectively as:

$$\sigma_\theta^{s,IIc} = \frac{T^{s,IIc}}{A_s} \pm \frac{M^{s,IIc} t_s}{2I_s},$$
$$\varepsilon_\theta^{s,IIc} \approx \frac{1-\nu_s^2}{E_s}\sigma_\theta^{s,IIc} \tag{2.56}$$

2.3.2.3. Final results:

The final results of the original problem are then calculated from the solutions of the problem I and problem II by using the superposition principle.

More precisely, in rock mass we can calculate the displacements:

$$U_x = U_x^{Ia} + U_x^{Ib} + U_x^{Ic} + U_x^{IIa} + U_x^{IIb};$$
$$U_y = U_y^{Ia} + U_y^{Ib} + U_y^{Ic} + U_y^{IIa} + U_y^{IIb}; \tag{2.57}$$

and the total stresses:

$$\sigma_x = \sigma_x^{Ia} + \sigma_x^{Ib} + \sigma_x^{Ic} + \sigma_x^{IIa} + \sigma_x^{IIb};$$
$$\sigma_y = \sigma_y^{Ia} + \sigma_y^{Ib} + \sigma_y^{Ic} + \sigma_y^{IIa} + \sigma_y^{IIb}; \tag{2.58}$$

while the effective stresses can be determined from the total stresses in Eq. (2.58) and the pore pressure in Eq. (2.18) by using the Biot's theory Eq. (2.6).

In the liner, we can compute the tangential stress and the strain as follows:

$$\sigma_\theta^s = \sigma_\theta^{s,Id} + \sigma_\theta^{s,IIc}$$
$$\varepsilon_\theta^s \approx \varepsilon_\theta^{s,Id} + \varepsilon_\theta^{s,IIc} \tag{2.59}$$

2.4.Numerical applications

Some numerical applications are presented in this section. In the first stage, we will validate the analytical solution by comparing with one obtained from the numerical simulation based on the finite element method (FEM). In the second stage, the validated analytical solution will be employed to elucidate the anisotropic effect on the hydro-mechanical behavior of tunnel through a parametric study.

2.4.1. Validation of the analytical solution

For the validation purpose, the numerical simulation using FEM is carried out and compared with the analytical results. For that, a 2D model is built in the Aster_Code using the plane strain elements with 4 nodes for displacement and 4 nodes corresponding to middle points of 4 edges for pore pressure. Owing to the symmetry of the considered problem, only one quarter of the tunnel is used in the simulation as illustrated in Fig. 2-7. The dimension of the model is taken equal to 60m from the center of the circular hole of radius $r_0 = 1m$. The hydro-mechanical properties of the Callovo-Oxfordian clay-stone at depth of 500m are chosen as follows (Charlier et al., 2013; Armand et al., 2013): $E_x = 5600MPa$, $E_y = 4000MPa$, $\nu_{xz} = 0.3$, $\nu_{yx} = 0.142$, $G_{xy} = 1600MPa$, $k_x = 4\times10^{-13} m/s$, $k_y = 1.33\times10^{-13} m/s$ and $b_x = b_y = 0.6$. Concerning the liner (with thickness $t_s = 0.05m$), the mechanical properties are chosen $E_s = 20GPa$ and $\nu_s = 0.3$ (Carranza-Torres and Zhao, 2009). The boundary conditions consist of imposing the initial horizontal, vertical stresses ($\sigma_h = 12.5MPa, \sigma_v = 12.5MPa$) following the elastic symmetry of medium ($\beta = 0$) and pore pressure $p_{ff} = 4.7MPa$ on the right lateral and top boundary while on the two other boundaries no normal displacement and flux are allowed. Furthermore, the pore pressure p_0 is imposed at the interface of liner and ground while beyond an elliptical zone around the tunnel, pore pressure is kept constant at $p = p_{ff} = 4.7MPa$. This elliptical zone with two semi-axes of $a = 45m$ and $b = a\sqrt{k_x / k_y} = 25m$ corresponds to the chosen distance $R = 30m$ from the center of unit circle in the ζ_w plane of the analytical solution at which the pore pressure is considered not to be influenced by groundwater flow toward opening. It was confirmed from our results that these dimensions are far enough that beyond which no significant improvement in the solution of the stresses and displacements near the tunnel can be stated. Depending on the study purpose, the pore pressure on the circumference of tunnel can be equal to the ambient pressure $p_0 = 0$ (case of tunnel excavated in drained rock due to the implementation of drainage system at extrados of liner and we note hereafter as *case 1*) or equal to the initial pressure $p_0 = p_{ff}$ (known as case of tunnel excavated in saturated rock with impermeable liner and is noted as *case 2*). From physical point of view, the behavior of the tunnel in the former case is controlled by the purely mechanical mechanism while in the latter case the hydro-mechanical coupling is considered.

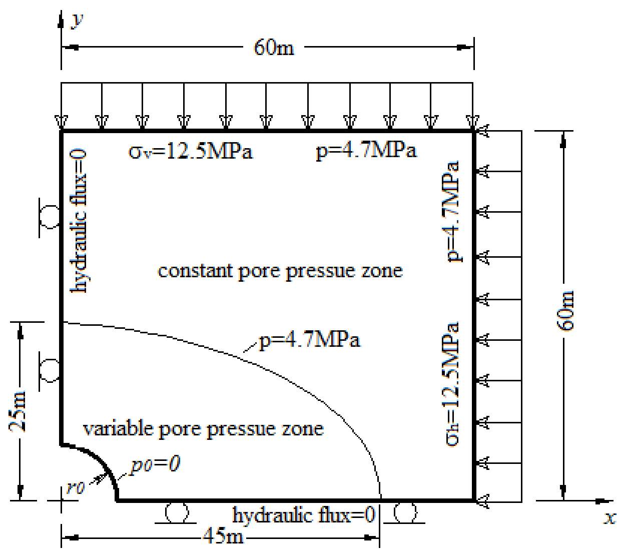

Fig. 2-7: 2D plane strain model used in the numerical simulation by FEM

The numerical simulation process is described by two steps below:

- *The first step:*

The entire medium is discretized by the elements described above. In this step, the elements corresponding to the excavation and liner are active with the same material parameters as the rock mass, i.e. the tunnel has not been excavated yet. The initial stresses and pore pressure are created and they dominate all the medium, whereas the displacements of the medium are equal to zero. This procedure is ensured by a feature of ASTER which allows zeroing all displacements while maintaining the initial stresses. In this step, all the elements of the medium have a same effective horizontal stress, effective vertical stress, and pore pressure equal to the initial stresses applied. Imposing the zero displacements ensures also that, the elements corresponding to the liner do not deform in this step, i.e., the liner should deform only when the tunnel is excavated.

- *The second step:*

This step is for the excavation of the tunnel and installation of the liner. Therefore, the elements corresponding to the excavation are not active and the material parameters of the elements corresponding to the liner are changed by those of concrete. The pore pressure at the liner-rock mass interface is imposed according to the study case of drainage condition. This means that, for the case 1, the pore pressure at this place is equals to zero while it takes the initial value for the case 2.

Fig. 2-8 presents the numerical results obtained at the final equilibrium state (steady-state of groundwater flow) in comparison with the analytical ones.

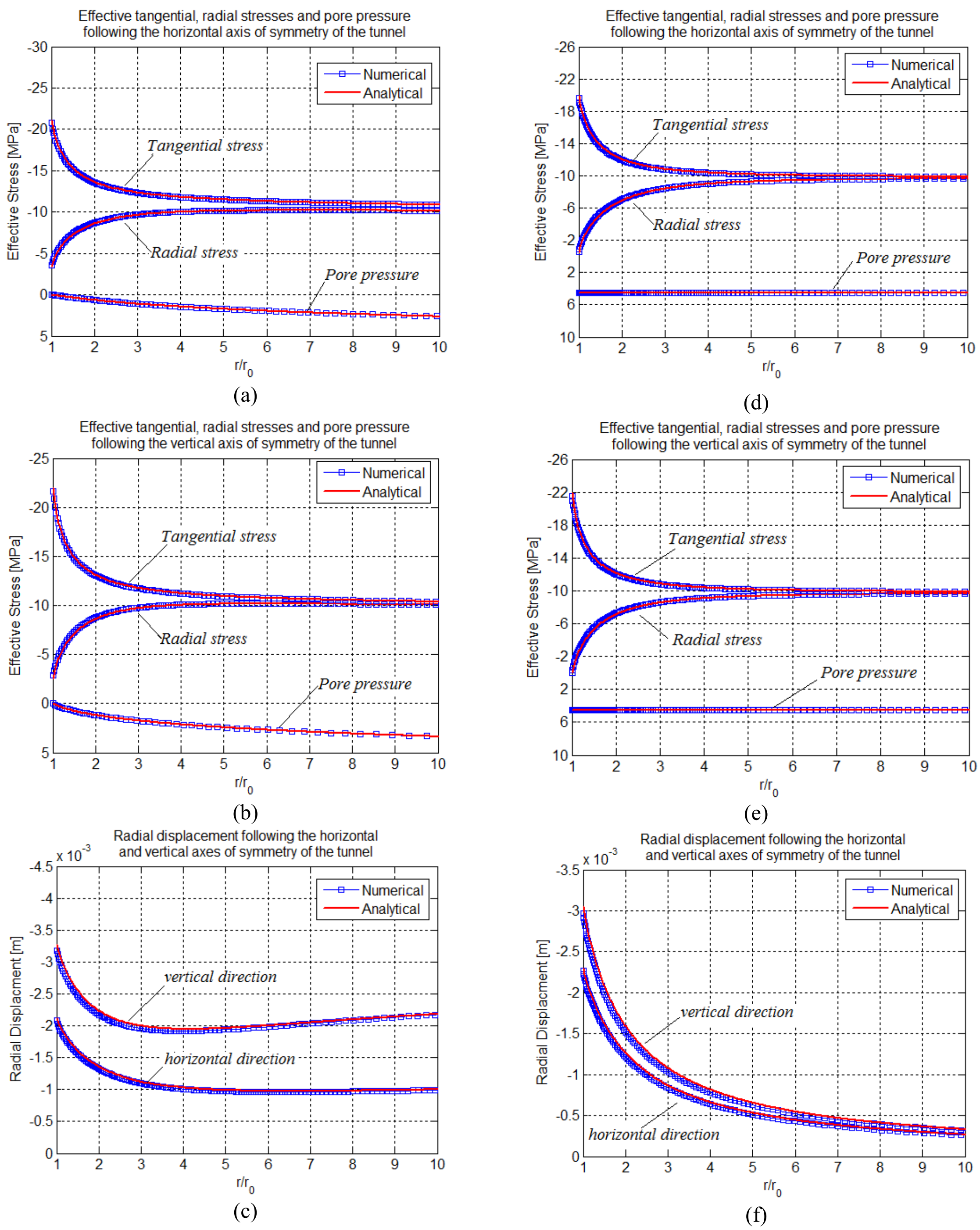

Fig. 2-8: Effective radial stress, effective tangential stress, pore pressure and radial displacements determined on the horizontal and vertical axes of symmetry of tunnel: comparison between the analytical and numerical solutions. These results are calculated for the case of excavation: in drained rock (a,b,c) and in saturated rock with uniform pore pressure (d,e,f).

In both cases, a very good agreement is noted for all results of the pore pressure, effective radial or tangential stresses and displacement. A tiny difference with a relative error is inferior to 3%. Different calculations highlight that the error increases with respect to the higher thickness of the liner. This could be explained by the fact that the increase of thickness of liner at a certain value can violate the hypothesis of thin liner at which the cylindrical shell theory is no longer validated.

Through these results, the anisotropic behavior of tunnel is well captured by the difference of effective hoop stress and particularly the convergence determined on the horizontal and vertical axes of symmetry of tunnel (Fig. 2.8c).

2.4.2. Extreme conditions of drainage behind the tunnel liner

If a deep tunnel is placed under the ground water table, the surrounding medium is fully saturated. In the topic of tunnel studies, two extreme conditions at the rock–liner interface are usually considered: full drainage, or no-drainage (Fig. 2-9). For the full drainage case, the pore pressures, p, at the contact are equal to zero and fluid flow towards the opening occurs; for the no-drainage case, the pore pressures in all the medium around the tunnel are uniform and equal to the far-field pore pressures, p_{ff}, so, there is no flow. The permeabilities of rock mass and the liner decide the condition of full drainage or no-drainage at the contact. In fact, the lining system for a deep tunnel is designed either impermeable or permeable. In the case of impermeable liner, water cannot flow through the liner and, thus, the liner has to support the pressure transferred from the ground as well as the water pressure at the liner-ground interface. Hence, one has the no-drainage condition at the ground-liner interface. When a drain is installed on the extrados of the liner to collect and remove water from the ground, one has the full drainage condition at the ground-liner contact. For the case of permeable liner, partial drainage may occur.

One considers only the two extreme conditions in the following evaluations. Differences in the displacement and rock tangential stress at the ground-liner interface as well as the liner stresses in each of the two drainage conditions are investigated. Fig. 2-9 shows a tunnel with full drainage or no drainage at the ground–liner interface.

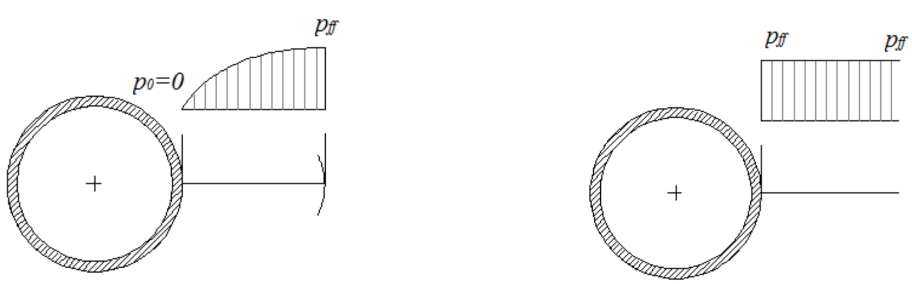

a) Full-drainage case

b) No-drainage case

Fig. 2-9: Two cases of drainage conditions considered for the tunnel problem

Several results below for several quantities with hydro-mechanical properties given as previous section indicate the differences between two cases.

The iso-value contours of radial displacement presented in Fig. 2-10 help to give insight to the anisotropic effect on the tunnel behavior in which a more pronounced displacement in magnitude can be stated with the highest convergence at the crown.

It is also worth noting here that the radial displacement on the perimeter of tunnel is different in the two cases of study (see, for example, the displacement at the springline and at the crown of the tunnel in Fig. 2-8c,f corresponding to the position $r=r_0$). Discussions in the literature (for instance, Bobet, 2003; Carranza-Torres and Zhao, 2009) showed that in the isotropic poroelastic medium framework the stresses and displacement in the liner and, hence, the radial displacement at the ground-liner interface are independent on drainage condition; instead they depend only on the total stress at far-field.

In order to show that whether the radial displacement and stresses of the liner depend on the drainage condition at the ground-liner contact or not, henceforth one will evaluate theses quantities in all the study cases.

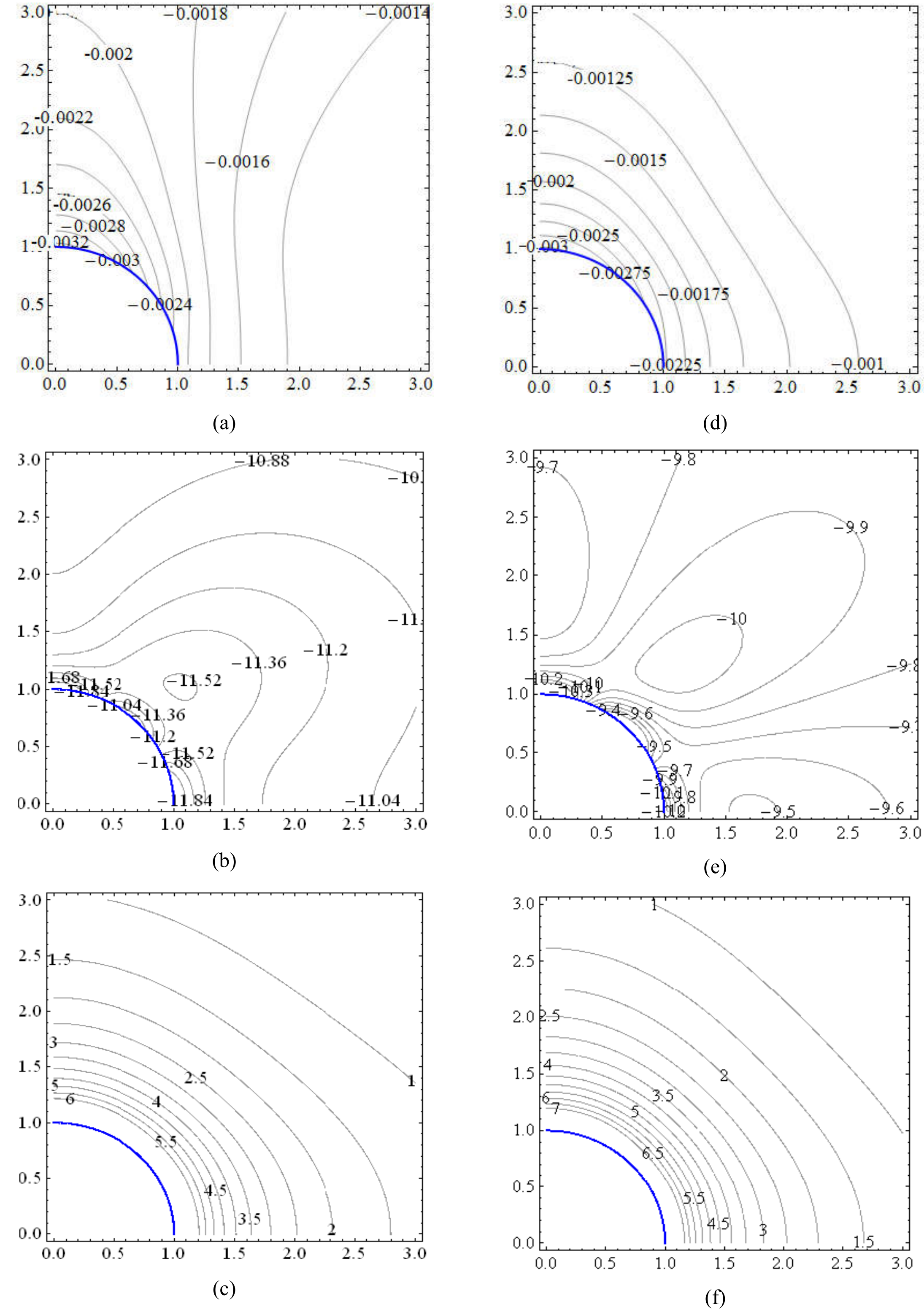

Fig. 2-10: Isovalue contours of radial displacement, mean stress and deviatory stress respectively in rock mass for the case of drained rock (a,b,c) and for the case of uniform pore pressure (d, e, f).

2.4.3. Parametric study

The goal of this part is to elucidate the influence of the different poroelastic properties on the anisotropic hydro-mechanical behavior of tunnel. Concretely, the studies will be conducted with respect to the Poisson's ratio, the shear modulus, the ratio of Young's modulus, the permeabilities and Biot coefficient and the far-field pore pressure of the porous medium. This could be done by changing the value of the interested parameter while the other parameters are kept constants. Moreover, it is known in the literature (Chen and Yu, 2015) that the tunnel behavior depends on the initial stresses, particularly on its anisotropy as well as its inclination with respect to the axes of elastic symmetry of medium. These effects will be also considered in this part. In order to analyze reciprocal impact between the liner and the rock mass, some studies are carried out by using different values of liner thickness and stiffness.

The obtained results are detailed as belows.

2.4.3.1. Influence of Poisson ratios

The first results that we will detail here allow elucidating the effect of Poisson's ratio on the tunnel behavior. In Fig. 2.11a, b, c, e, f, g are presented the distribution of rock effective tangential stress, the interior fiber tangential stress of the liner and radial displacement on the circumference of tunnel calculated with different values of the Poisson's ratio ν_{yx} for two cases of drainage condition. Because of the same variation tendency of the tangential stresses in the interior and exterior fibers of the liner from the springline to the crown of the tunnel, henceforward in the figures we present only the interior fiber tangential stresses.

In these figures, angle θ is measured from the springline to the crown of the tunnel. More precisely, by changing the Poisson's ratio ν_{yx} of the vertical plane, which is also the anisotropic plane of the medium, we can observe that its effect is quite significant on the rock tangential stress, the liner tangential stress (Fig. 2.11a, b, e, f) and on the radial displacement (Fig. 2.11c, g). For the case 1 (drained rock case), the rock tangential stress changes more importantly at the middle point between the springline and the crown of the tunnel while it changes more importantly at the crown for the case 2 (uniform pore pressure case).

In general, the decrease of the vertical Poisson's ratio ν_{yx} will decrease the liner tangential stress at the crown and change slightly liner tangential stress at the springline of the tunnel whereas it will decrease the radial displacement at the springline (noted hereafter as U_x) and increase slightly the radial displacement at the crown of the tunnel (noted as U_y). These tendencies are reciprocal because of the mechanism: the more deformation, the less take the load and vice versa. Consequently, the anisotropic behavior of the tunnel represented by the ratio of radial displacements evaluated at the crown and at the springline respectively (U_y/U_x) is higher if the Poisson's ratio ν_{yx} is smaller and they are highly sensitive to the change of the Poisson ratio ν_{yx} (Fig. 2.11d, h). Otherwise, by comparing the results obtained from both cases of study in Fig. 2.11b,c and in Fig. 2.11f, g we can observe the same tendency but the influence seems more pronounced in *case 1* illustrated by the higher differences of liner tangential stress and radial displacement between the srpingline and the crown as well as a higher magnitude of rock tangential stress at both the springline and the crown.

This can be explained by the fact that in *case 2*, only the mechanical mechanism determines the behavior of tunnel (purely mechanical response) while in *case 1*, the contribution of the hydraulic mechanism, consequence of the steady flow of groundwater, is also taken into accounted (hydro-mechanical response).

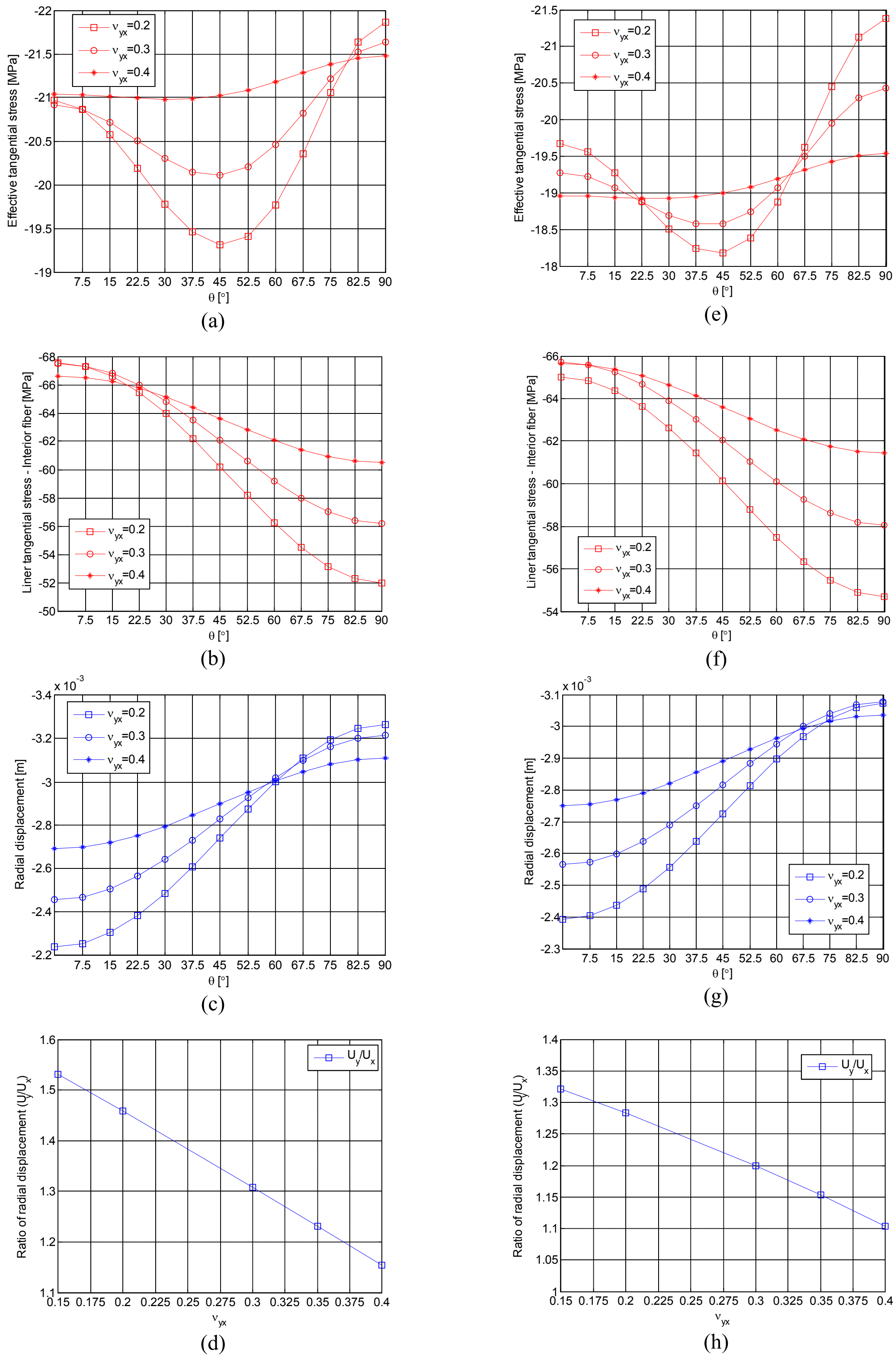

Fig. 2-11: Influence of the Poisson's ratio ν_{yx} on the rock effective tangential stress, the liner tangential stress, the radial displacement, and the ratio of radial displacement respectively at the circumference of tunnel which is excavated: in drained rock (a, b, c, d) or in saturated rock with uniform pore pressure (e,f,g,h)

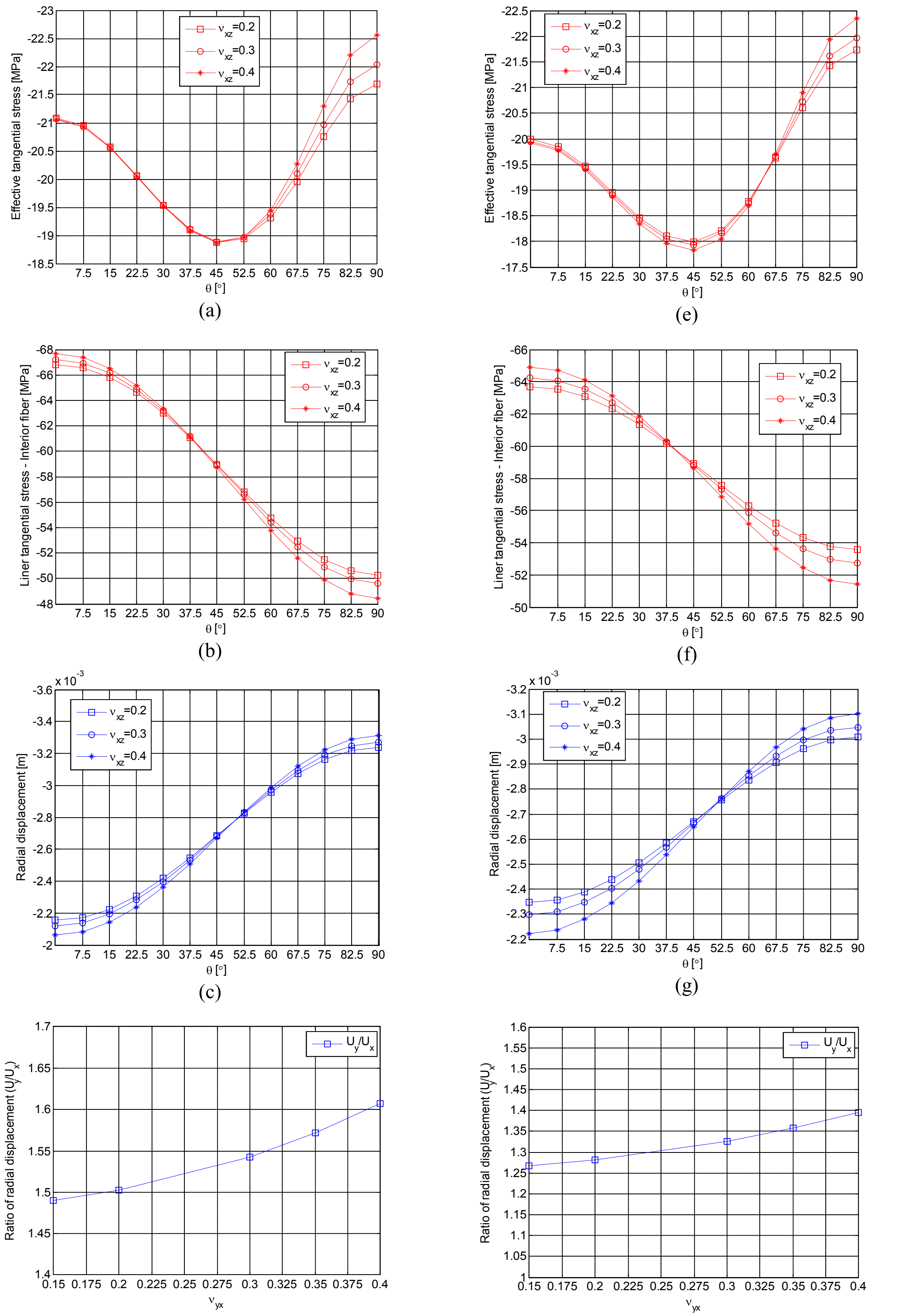

Fig. 2-12: Influence of the Poisson's ratio ν_{xz} on the rock effective tangential stress, the liner tangential stress, the radial displacement, and the ratio of radial displacement respectively at the circumference of tunnel which is excavated: in drained rock (a, b, c, d) or in saturated rock with uniform pore pressure (e, f, g, h).

Concerning the influence of the other Poisson's ratio which lies on the isotropic plane of the medium (ν_{xz}), the results are showed in the Fig. 2-12.

It can be seen from Fig.2-12 that the effect of ν_{xz} on the rock tangential stress, the liner tangential stress, the radial displacement as well as the ratio of radial displacement is small, i.e., the Poisson's ratio in the isotropic plane has a negligible effect on the tunnel behavior.

2.4.3.2. Influence of the shear modulus

The effect of the shear modulus G_{xy}, highlighted in Fig. 2-13, is done by changing the ratio E_x / G_{xy} while E_x is kept constant. It shows that the decrease of shear modulus, represented by the higher ratio E_x / G_{xy}, affects strongly the distribution of stress and displacement around the tunnel. For example, smaller shear modulus induces a higher compressive rock tangential stress at the springline as well as at the crown of the tunnel while it can decrease this stress at the middle portion between the springline and the crown (Fig. 2-13a, e). Furthermore, the decrease of shear modulus results in an increase of the liner tangential stress on the perimeter of the tunnel. In the same trend, there is an increase of radial displacement on the perimeter of the tunnel but the rate is more pronounced at the springline illustrated by a slightly decrease of the ratio U_y/U_x (Fig. 2-13c,f). In addition, the larger magnitude of the liner tangential stress corresponds the smaller magnitude of radial displacement at the springline and vice versa at the crown. It can be seen from Fig. 2-13 that the magnitude variations of the stresses and the radial displacement are highly sensitive to the value of G_{xy}.Therefore, E_x / G_{xy} is an important deformation parameter to consider in predicting displacements. Similarly to the previous parametric study case, the variation of the rock effective tangential stress, the liner tangential stress and the radial displacement as well as the ratio of radial displacement along the perimeter of the tunnel is more important for the tunnel excavation in drained rock.

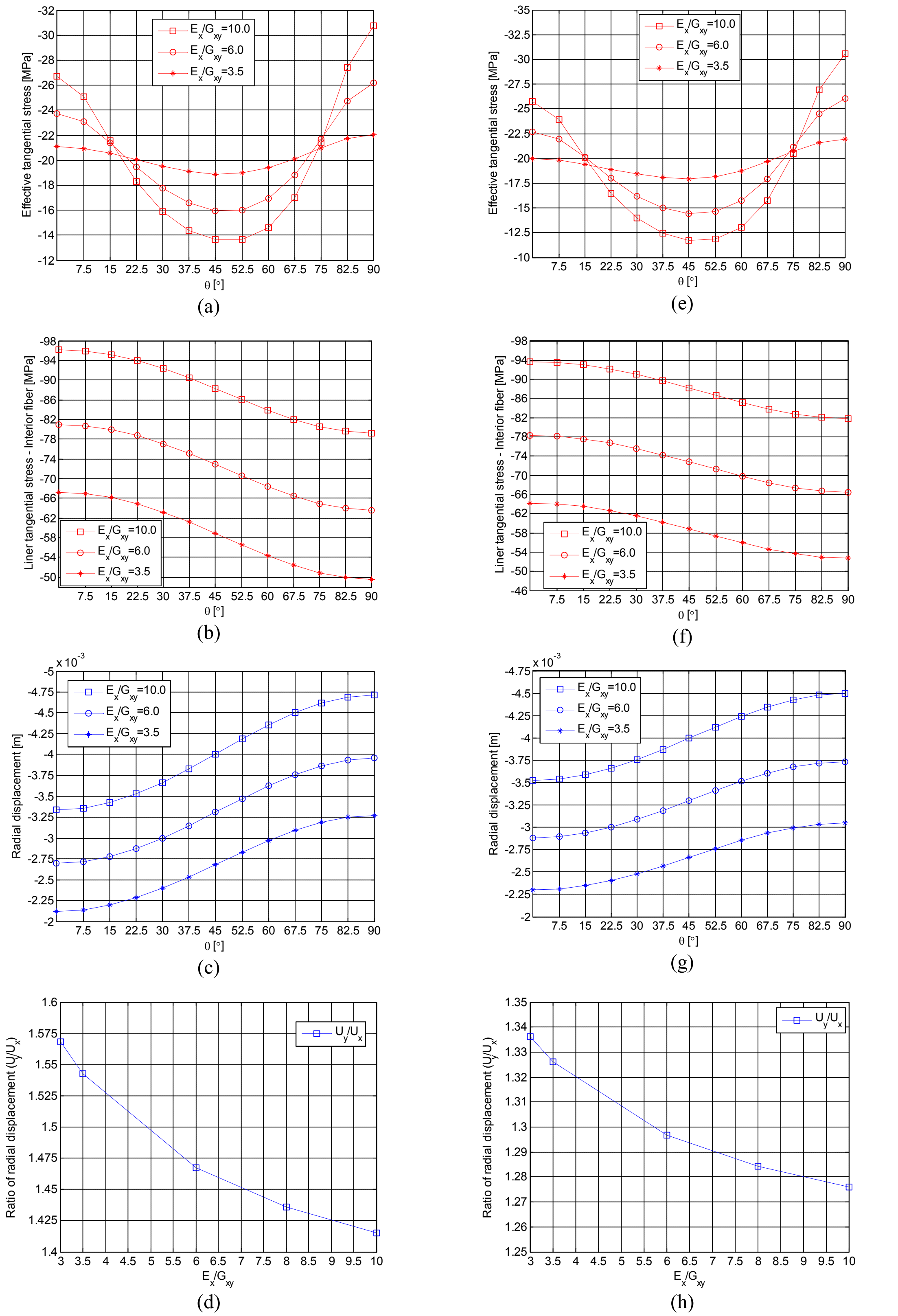

Fig. 2-13: Influence of the shear modulus G_{xy} on the rock effective tangential stress, the liner tangential stress, the radial displacement, and the ratio of radial displacement respectively at the circumference of tunnel which is excavated: in drained rock (a, b, c, d) or in saturated rock with uniform pore pressure (e, f, g, h).

2.4.3.3. Influence of the Young's modulus ratio

Fig. 2-14 presents the rock effective tangential stress, the liner tangential stress and radial displacement evaluated on the tunnel wall with different values of Young's modulus ratio E_x / E_y. The results show that the ratio E_x / E_y could contribute to a significant effect on the distribution of the tangential stresses in both the rock mass and the liner notably near the crown when the increase of this ratio yields a greater compressive rock tangential stress and a smaller liner tangential stress (Fig. 2.14a, b, e, f). Otherwise, as expected, an increase of Young's modulus in the horizontal direction E_x with respect to one in the vertical direction E_y, will induce a decrease of the radial displacement at the springline and an increase at the crown (Fig. 2-14c, g). As a result, the higher the Young's modulus ratio E_x / E_y the greater the radial displacement ratio U_y/U_x (Fig. 2-14d, h). On the contrary, the variation of liner tangential stress is inverse with respect to one of radial displacement. This is because, in the uniform far-field stresses condition, the larger radial deformations (in the smaller stiffness direction) the smaller radial stresses (the stress applies to the liner), i.e., larger unloading, occur at the crown than at the springline. The rock mass in the smaller deformation direction, i.e., here the horizontal direction, takes more load. The tendencies are similar in both cases of study but a more significant variation in magnitude is also marked in *case 1*.

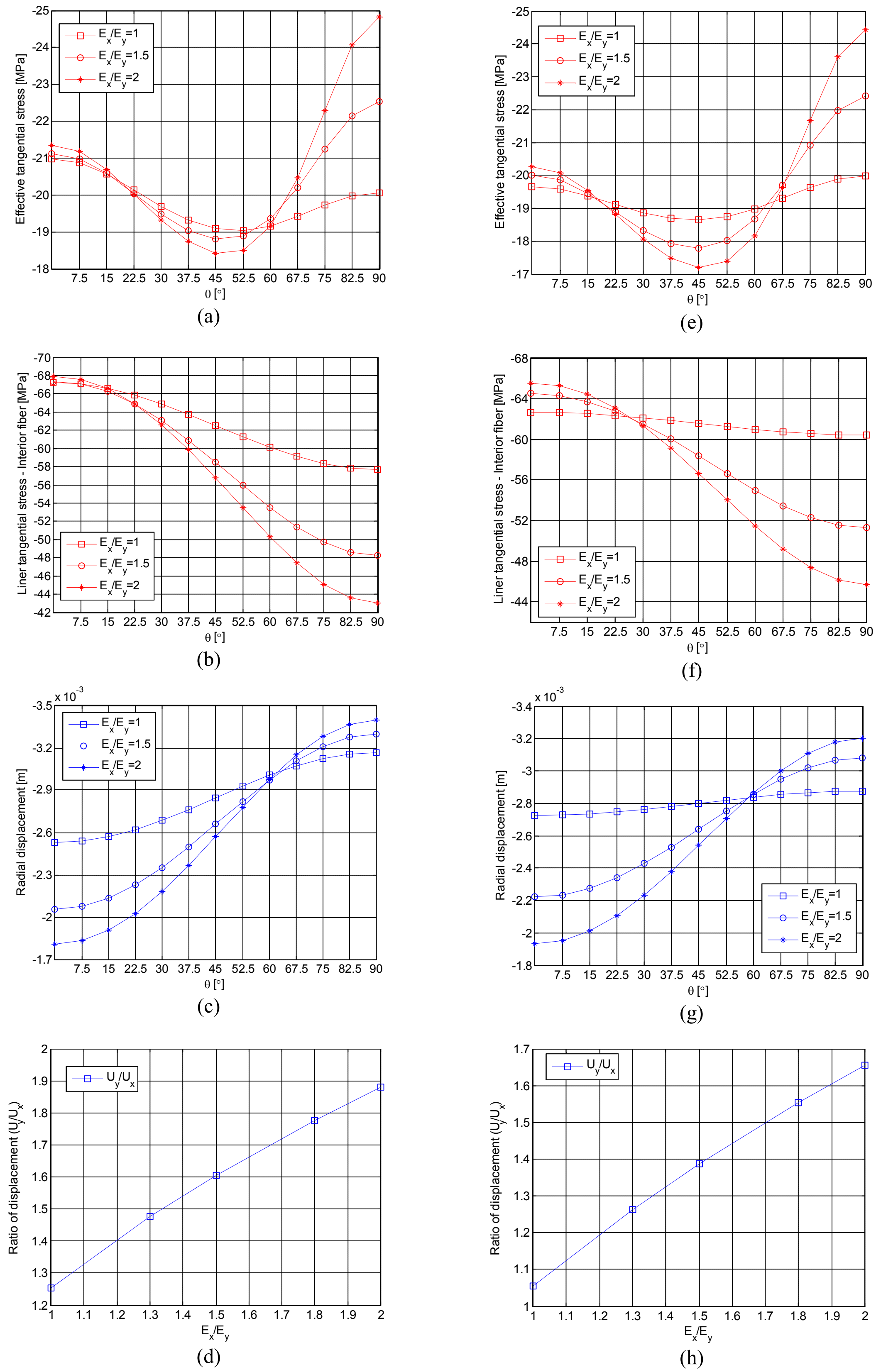

Fig. 2-14: Influence of the Young's modulus ratio (E_x / E_y) on the rock effective tangential stress, liner tangential stress, radial displacement, and the ratio of radial displacement respectively at the circumference of tunnel which is excavated: in drained rock (a, b, c, d) or in saturated rock with uniform pore pressure (e, f, g, h).

2.4.3.4. Influence of the anisotropic permeability and Biot coefficient

To better understand the hydraulic effect on the tunnel behavior, this parametric study case addresses the influence of the permeability and the Biot coefficient. The corresponding results with respect to each effect of parameter are illustrated respectively in Fig. 2-15, Fig. 2-17. As expected, the excavation in saturated medium with uniform pore pressure (*case 2*) does not change the tunnel displacement if we change the hydraulic properties of the medium (the permeabilities and Biot coefficients). As being discussed previously, in the case of no drainage, the purely mechanical responses of the tunnel are similar to those of the tunnel excavated in the dry rock in terms of total stress and displacement. Consequently, changing of, for example, the Biot coefficient can change only the effective stress but it does not impact on the radial displacement (Fig 2-17g, h). In contrast, the influence of the anisotropic permeability and Biot coefficient in combination with mechanical anisotropy is well illustrated in *case 1* where the excavation is conducted in the drained rock. More precisely, if the anisotropy of permeability increases, which is represented by a higher ratio k_x/k_y, we can state that the magnitudes of the rock effective tangential stress and the liner tangential stress increase at the springline and decrease at the the crown (Fig. 2-15a). The permeabilities can also affect the radial displacement. Indeed the higher anisotropic degree of permeability produces a higher convergence at the crown and a smaller one at the the springline (Fig. 2-15c) which is well illustrated by a more pronounced displacement ratio U_y/U_x as shown in Fig. 2-15d. This is explained as follows. When the ratio of permeabilities k_x/k_y increases, the zone of isovalue of pore pressure around the opening tunnel, with an elliptical shape, extends toward the horizontal axe as illustrated in Fig. 2-16. Therefore, gradient of pore pressure increases in the vertical direction while it decreases in the horizontal one, i.e., the larger seepage force occurs at the crown than at the springline. The higher seepage force induces the higher radial displacement at the crown than at the springline. It should be also noted that, in the steady state condition of fluid flow, the zone of pore pressure distribution surrounding the opening depends only on the ratio of permeabilities but does not depend on the magnitude of them.

The same remarks can be noted by regarding the influence of the Biot coefficients (concurrently in two directions) on the radial displacement in drained rock. Following that, the increase of Biot coefficients corresponding to the decrease of effective stress (Fig. 2-17 a) results in a higher radial displacement at the crown and a smaller radial displacement at the springline (Fig. 2-17 c) and, hence, an increase radial displacement ratio U_y/U_x (Fig. 2-17 d). On the other hand, by comparing the results of *case 1* and *case 2*, it is confirmed that a more pronounced radial displacement ratio is produced in *case 1*. The results discussed here demonstrate the essential role of pore pressure distribution on the tunnel's responses and particularly the importance to account for the anisotropic hydro-mechanical coupling on the analysis of tunnel behavior.

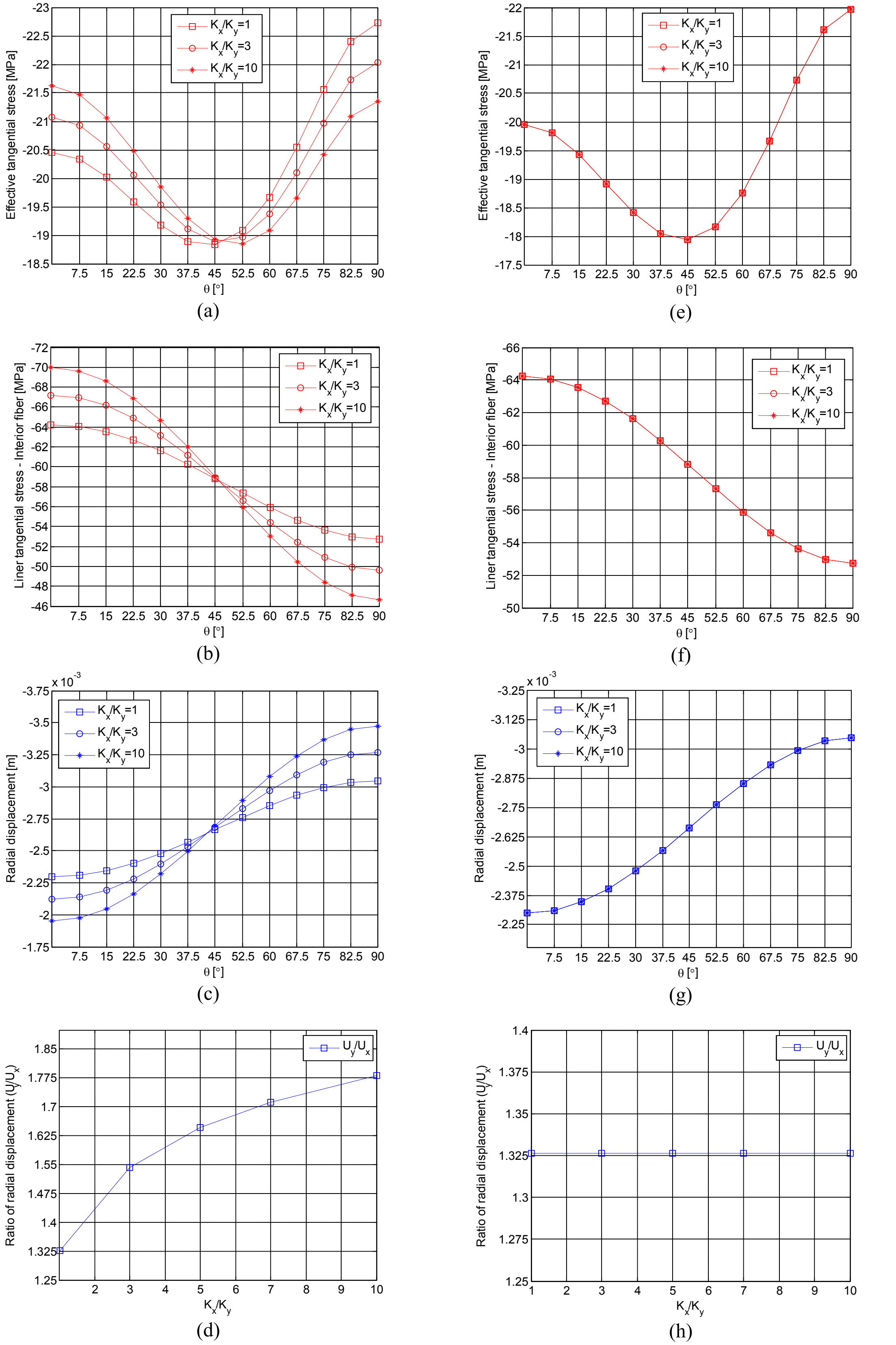

Fig. 2-15: Influence of the anisotropic permeability (k_x / k_y) on the rock effective tangential stress, liner tangential stress, radial displacement, and the ratio of radial displacement respectively at the circumference of tunnel which is excavated: in drained rock (a, b, c, d) or in saturated rock with uniform pore pressure (e, f, g, h).

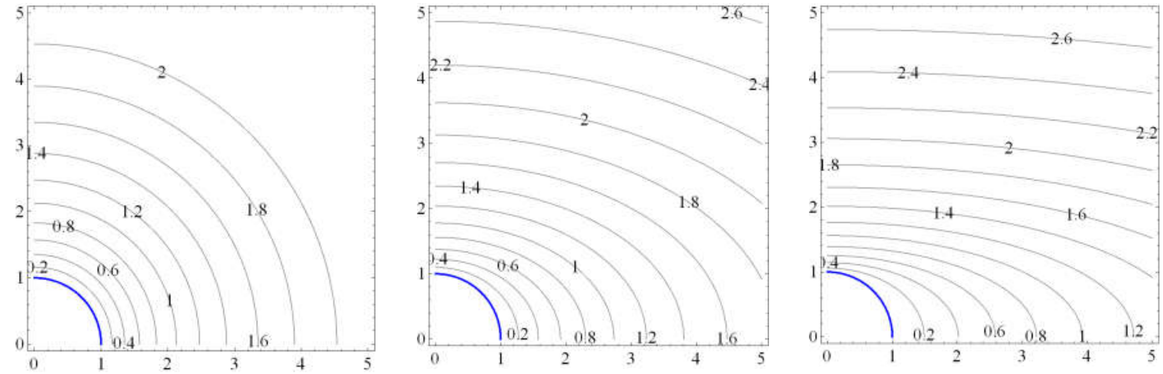

(a) (b) (c)

Fig. 2-16: Contours of the pore pressure around the opening tunnel in the cases: $k_x / k_y = 1$(a), $k_x / k_y = 3$(b), $k_x / k_y = 10$(c)

On the other hand, Fig. 2-15 b, c and Fig. 2-15 f, g indicate also that, when the ratio of permeabilities is equal to 1, i.e., the hydraulic property is isotropic, the tangential stress and radial displacement of the liner in two conditions of drainage at the rock-liner contact are exactly the same. Therefore, it is hydraulic anisotropy that induces the difference of the radial displacement and tangential stress of the liner between two conditions of drainage. This will be still evaluated in the study cases following.

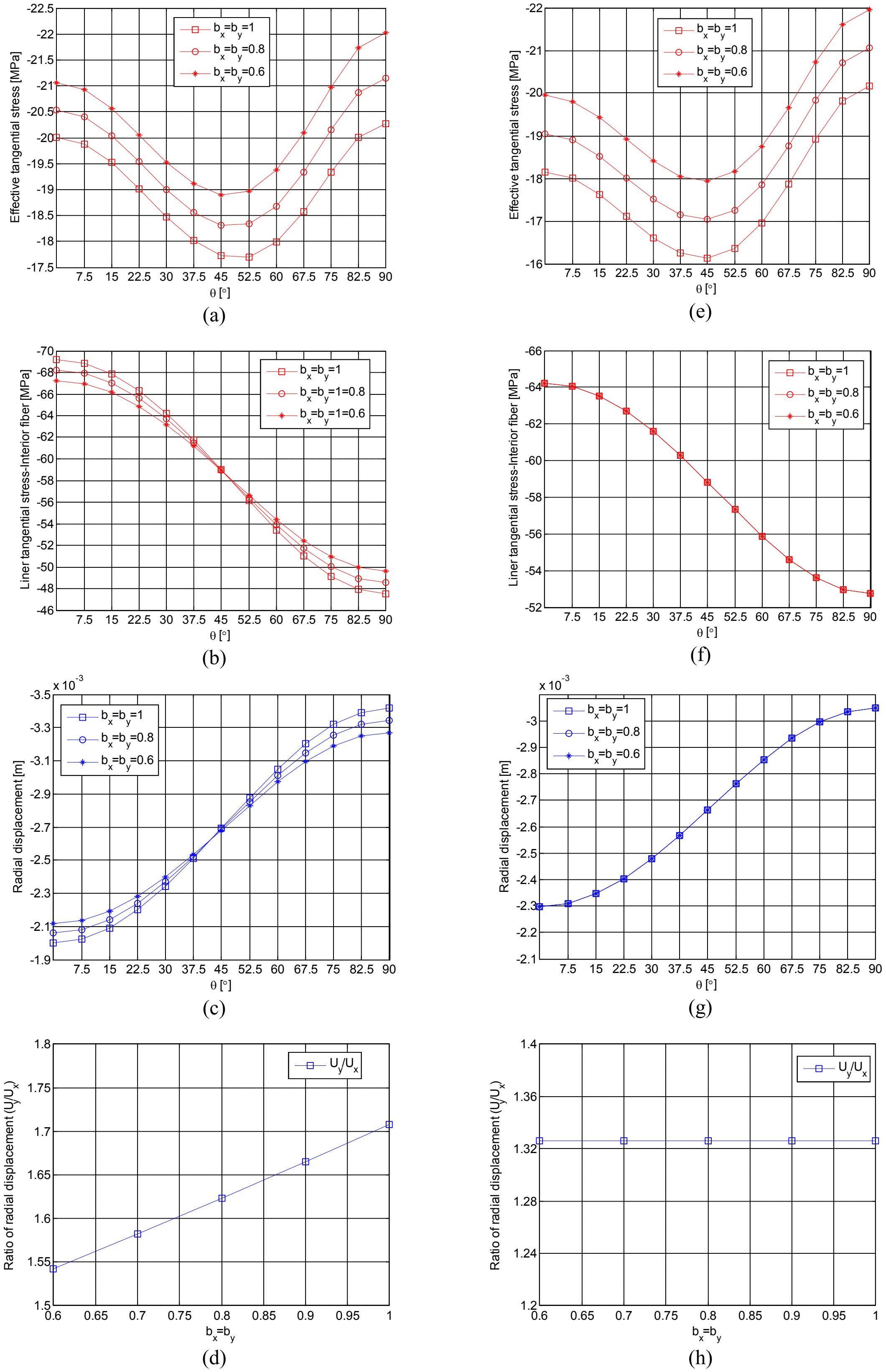

Fig. 2-17: Influence of of the Biot coefficients ($b_x = b_y$) on the rock effective tangential stress, the liner tangential stress, the radial displacement, and the ratio of radial displacement respectively at the circumference of tunnel which is excavated: in drained rock (a, b, c, d) or in saturated rock with uniform pore pressure (e, f, g, h).

For the purpose of elucidating the effects of anisotropic Biot coefficients, one keeps the Biot coefficient constant in isotropic plane, i.e., in the horizontal direction while changing it in anisotropic plane, i.e, in the vertical direction. The results of the estimated quantities are presented in Fig. 2-18. The figure shows that, in combination with the mechanical anisotropy, for the case 1, the anisotropy of Biot coefficient influences the rock effective tangential stress at both the springline and the crown and more importantly at the springline that lies on the direction kept the Biot coefficient constant whereas the rock effective tangential stress only changes at the springline but keeps unchanged at the crown.

With regard to the radial displacement, for the case 1, it can be seen that, there is a slightly decrease at the crown while it does not vary at the springline. The liner tangential stress decreases slightly at the springline and increases slightly at the crown corresponding to the diminution of Biot coefficient in the vertical direction. In the previous study case, there is not any impact on the radial displacement as well as the liner tangential stress in the case of uniform pore pressure distribution.

In summary, the anisotropy of Biot coefficient affects primarily on the tangential stress in the rock whereas it has a negligible effect on the displacement and liner tangential stress.

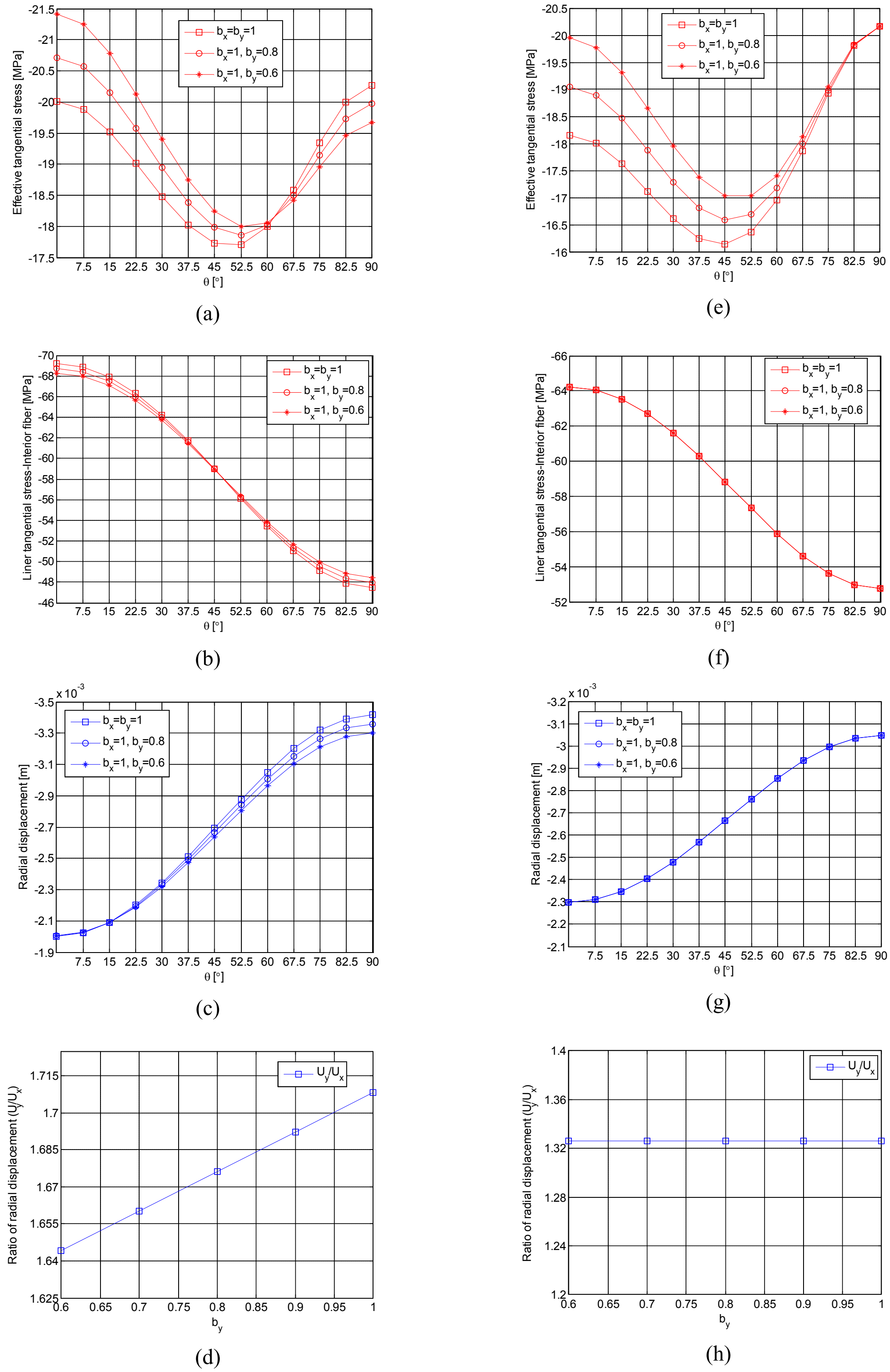

Fig. 2-18: Influence of the Biot coefficients ($b_x \neq b_y$) on the rock effective tangential stress, the liner tangential stress, the radial displacement, and the ratio of radial displacement respectively at the circumference of tunnel which is excavated: in drained rock (a, b, c, d) or in saturated rock with uniform pore pressure (e, f, g, h).

2.4.3.5. *Influence of the far-field pore pressure*

In an attempt to acquire additional insight into the influence of pore pressure field around the tunnel, we analyze the tangential stress and radial displacement in the rock as well as in the liner under different pore pressure magnitudes. The results are investigated with three values far-field pore presures: p_{ff} = 1 MPa, p_{ff} = 3 MPa and p_{ff} = 4.7 MPa while the total far-field stresses remain constant at 12.5 MPa. The results are plotted in the following Fig. 2-19.

It is observed in the Fig. 2-19 (a, e) that, when the far-field pore pressure increases the rock effective tangential stress decreases at the entire circumference of the tunnel wall. It is interesting that, moreover, in comparison between two cases, full-drainage and no-drainage cases, at the same magnitude of far-field pore pressure, the change of the rock tangential stress occurs primarily at the springline while it keeps almost constant at the crown. This shows that, the fluid flow influences almost at the springline where belongs to the greater stiffness direction, i.e., the rock carries more the seepage forces in the larger stiffness direction.

The Fig. 2-19 (f, g) shows also that, when there is no fluid flow, no-drainage cases, there is no change in displacement and tangential stress in the liner. This may be explained that, the displacement and tangential stress of the liner depend only on the total stresses at the contact between the liner and the rock mass (interaction stresses) which depend only the total far-field stresses not on the far-field pore pressure.

For the case with the fluid flow, the liner tangential stress increases slightly at the springline and decreases slightly at the crown, i.e., there is an increase of the liner tangential stress in the greater stiffness direction and a decrease of it in the smaller stiffness direction (Fig. 2-19b). In this case, the total stresses at the contact are equal to the effective stresses because of the zero pore pressure at this place.

The variation of radial displacement has an invert tendency with respect to liner tangential stress; as a consequence, the ratio of radial displacement on the tunnel wall increases together with the far-field pore pressure (Fig. 2-19c, d).

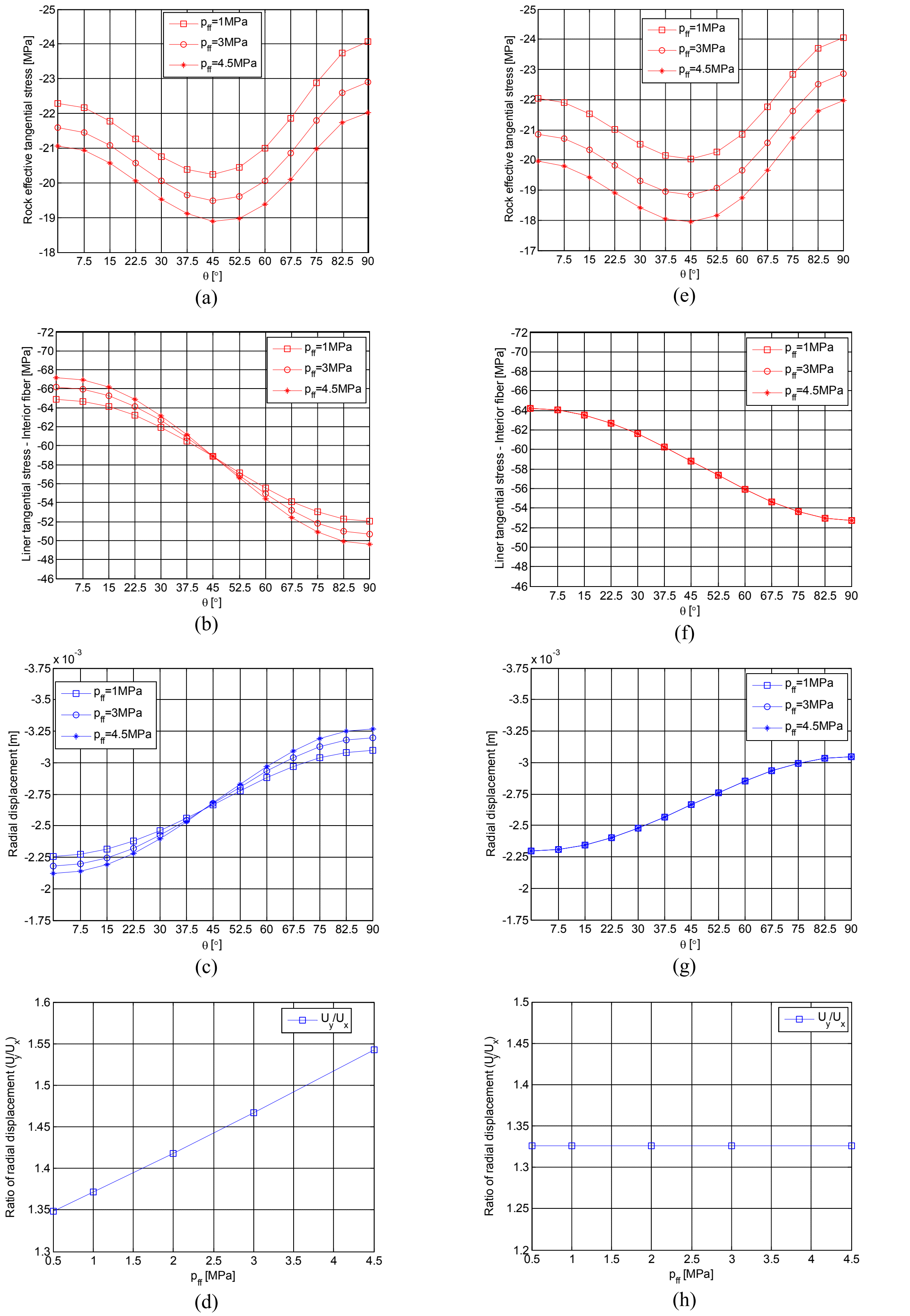

Fig. 2-19: Influence of the far-field pore pressure (p_{ff}) on the rock effective tangential stress, the liner tangential stress, the radial displacement, and the ratio of radial displacement respectively at the circumference of tunnel which is excavated: in drained rock (a, b, c, d) or in saturated rock with uniform pore pressure (e, f, g, h).

2.4.3.6. *Influence of the anisotropy and inclination of initial stress*

Our next parametric study case aims to investigate the effect of anisotropic of initial stresses which is represented through the parameter $K_0 = \sigma_h^{ff} / \sigma_v^{ff}$. As shown in Fig. 2-20 (a, d) even if the initial stresses are isotropic ($K_0 = 1$) the tangential stress and radial displacement on the tunnel wall are not uniformed, as a result of the anisotropic behavior of the poroelastic rock mass. The additional anisotropic effect of initial stress contributes to a significant role on the tunnel behavior illustrated by a strong variation of tangential stresses and displacement around the tunnel as highlighted in Fig. 2-20 (a, b, d, e). Concretely, when one increases the horizontal stress σ_h^{ff} with respect to the vertical stress σ_v^{ff}, both the compressive tangential stress of the rock and of the liner increase strongly at the crown of the tunnel whereas they decrease slightly at the springline (Fig. 2-20a, e). Concerning the radial displacement, an inverse tendency can be stated following the mechanism mentioned in the previous studies. The increase of horizontal initial stress σ_h^{ff} induces an increase of radial displacement at the springline and makes it decrease at the crown (Fig. 2-20c, g). Consequently, the anisotropic response of the tunnel, represented by the ratio U_y/U_x, decreases strongly with respect to the anisotropic degree of initial stress K_0 (see Fig. 2-20d, h).

These phenomena could be explained as follows. When the initial horizontal stress increases, the rock deforms more and takes less load in the horizontal direction. Therefore, the load transmitted to the liner is smaller which induces the smaller liner tangential stress at the springline. Meanwhile, the invert process occurs at the crown. This mechanism can be observed in Fig. 2-20 (b, c, f, g).

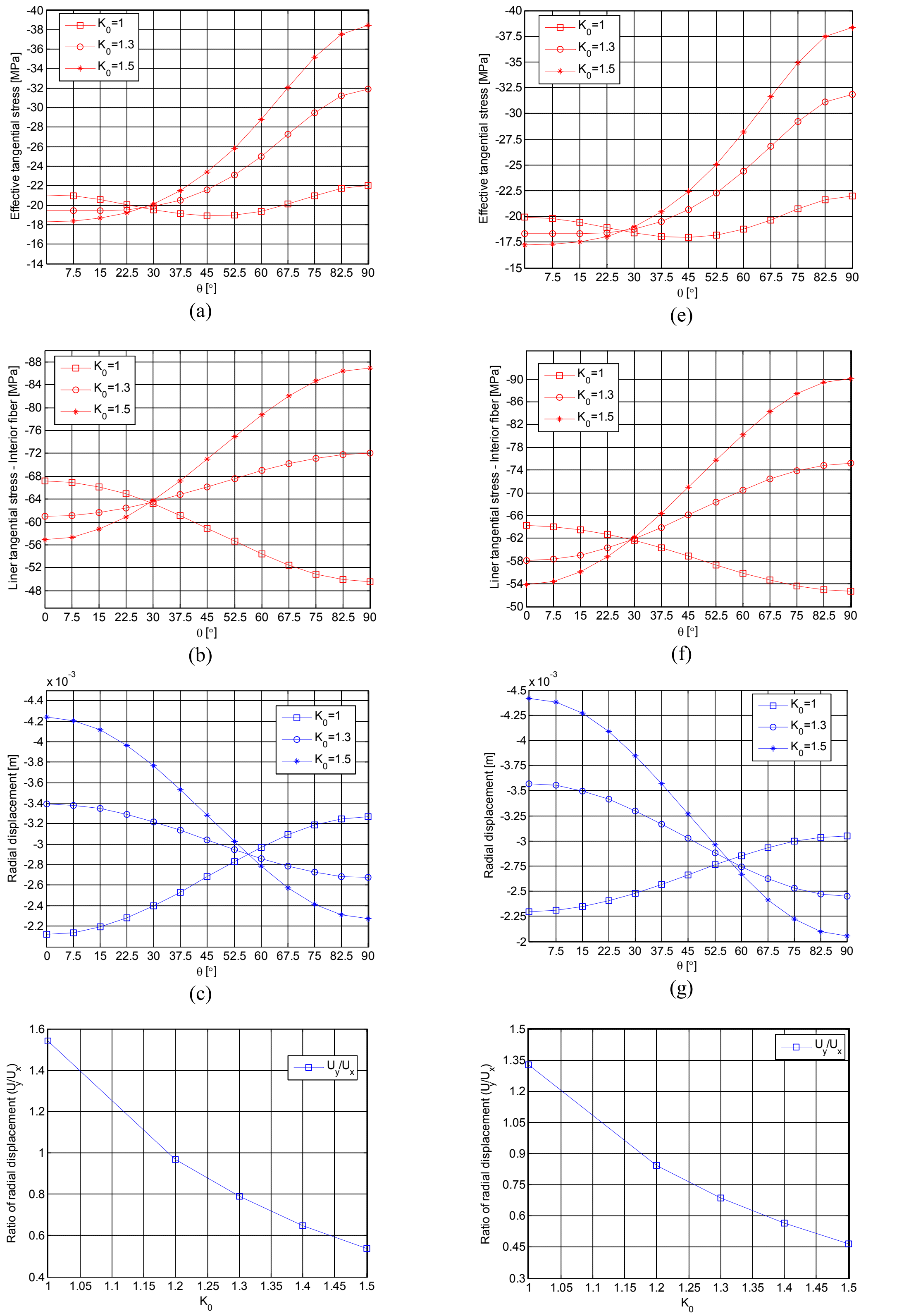

Fig. 2-20: Influence of the initial stresses ($K_0 = \sigma_h^{ff} / \sigma_v^{ff}$) on the rock effective tangential stress, liner tangential stress, radial displacement, and the ratio of radial displacement respectively at the circumference of tunnel which is excavated: in drained rock (a, b, c, d) or in saturated rock with uniform pore pressure (e, f, g, h).

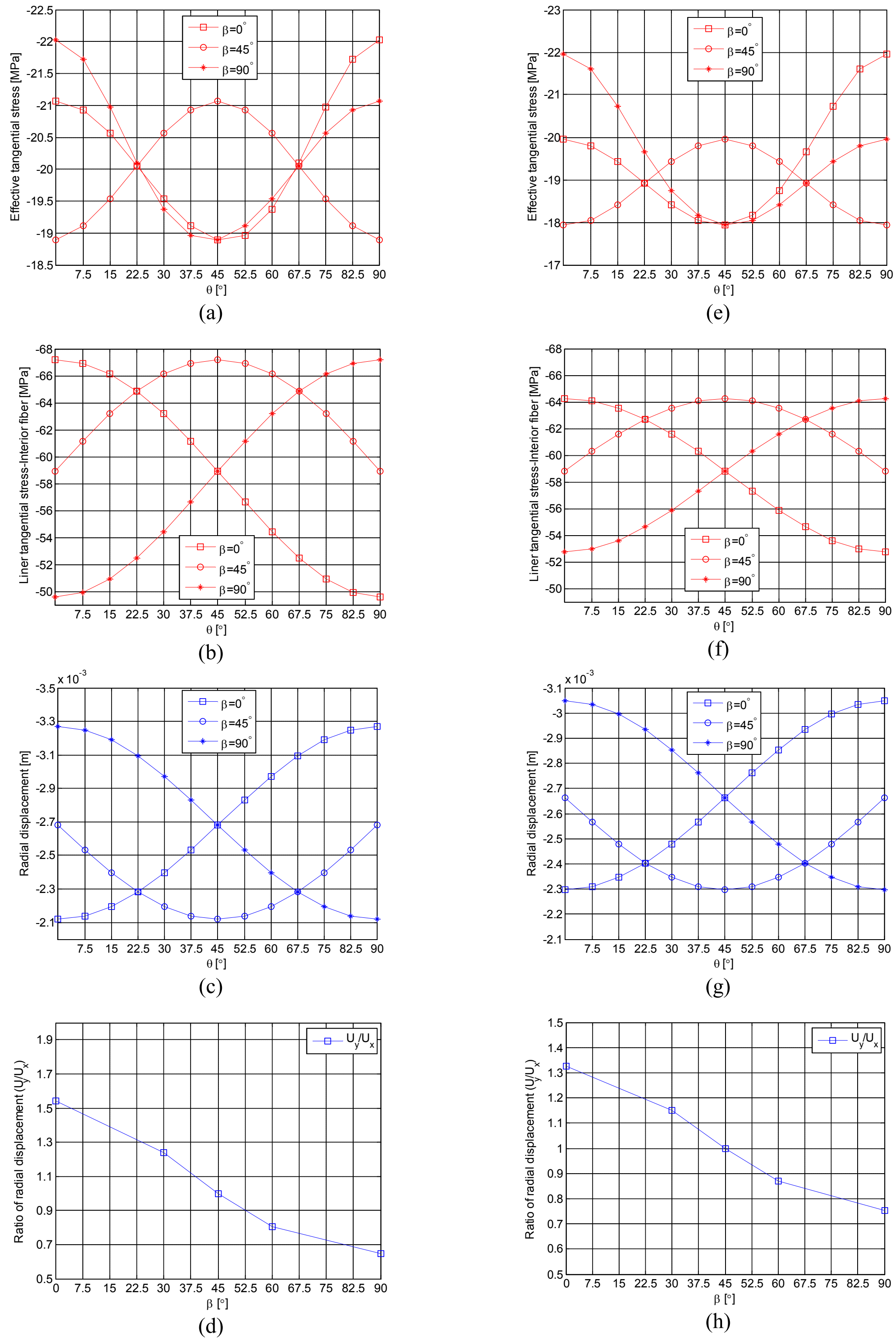

Fig. 2-21: Influence of the inclination of initial stresses (*β*) on the rock effective tangential stress, liner tangential stress, radial displacement, and the ratio of radial displacement respectively at the circumference of tunnel which is excavated: in drained rock (a, b, c, d) or in saturated rock with uniform pore pressure (e, f, g, h).

To clarify the impact of the foliation direction of the rock on the tunnel behavior, we investigated the influence of the inclination of discontinuous plane with respect to horizontal direction on the displacement and stresses distributions of the tunnel. As shown in Fig. 2-21 (a, b, c, e, f, g) the rock effective tangential stress, the liner tangential stress and radial displacement on the tunnel wall change significantly if the inclined angle β varies. Fig. 2-21 (a, b, e, f) shows that when β=45°the tangential stresses and radial displacement at the sprinline and the crown take the magnitude of those at the middle point between the springline and the crown (the point creates an angle θ=45° with respect to the springline) in case of β=0°. This is because of the symmetry of them through discontinuous plane. At that point, the compressive rock tangential stresses are smallest in case of inclined angle β=0° while they are highest in case of β=45° (Fig. 2-21 a, e).

On the other hand, one can observe that, the tangential stresses and radial displacement at the springline in the case β=90° take the magnitude of those at the crown in the case β=0° and vice versa. This is explained that, when the elastic symmetric axes of the rock rotate an angle 90°, the larger stiffness direction turns over the smaller stiffness direction and inversely.

In comparison with the convergence at the springline, a higher convergence at the crown is observed in case β=0° but a smaller value is stated in case β=90° (Fig. 2-21 c, f). Therefore, the radial displacement ratio U_y/U_x which represents the anisotropic behavior of the tunnel can vary in the large range from a superior value in the case of β=0° to an inferior value in the case β=90°.

2.4.3.7. Influence of the liner

Knowing the impact of the liner on the tunnel behavior is an important issue, particularly in engineering design framework where the conception of liner's thickness and stiffness to ensure the stability of tunnel is important. Hence, in the followings, we will highlight the influence of these parameters on the behavior of tunnel. As expected the higher thickness or stiffness of the liner will decrease the radial displacement on the tunnel wall (see Fig. 2-22c, f and Fig. 2-23 c, f). It is also the case of the rock effective compressive tangential stress (Fig. 2.22 a, e and Fig. 2.23a, e). These results also confirm that the rock tangential stresses in the case of full-drainage at the ground-liner contact are always superior to those in the case of no drainage at the contact. However, the difference is very small at the crown and larger at the springline which lies on the larger stiffness direction of the rock mass.

On the other hand, it is interesting to note that the displacement ratio U_y/U_x decreases with regard to the increase of thickness and/or stiffness (modulus) of the liner in *case 2* (tunnel in saturated rock with uniform pore pressure) but it tends to increase in *case 1* (tunnel in drained rock).

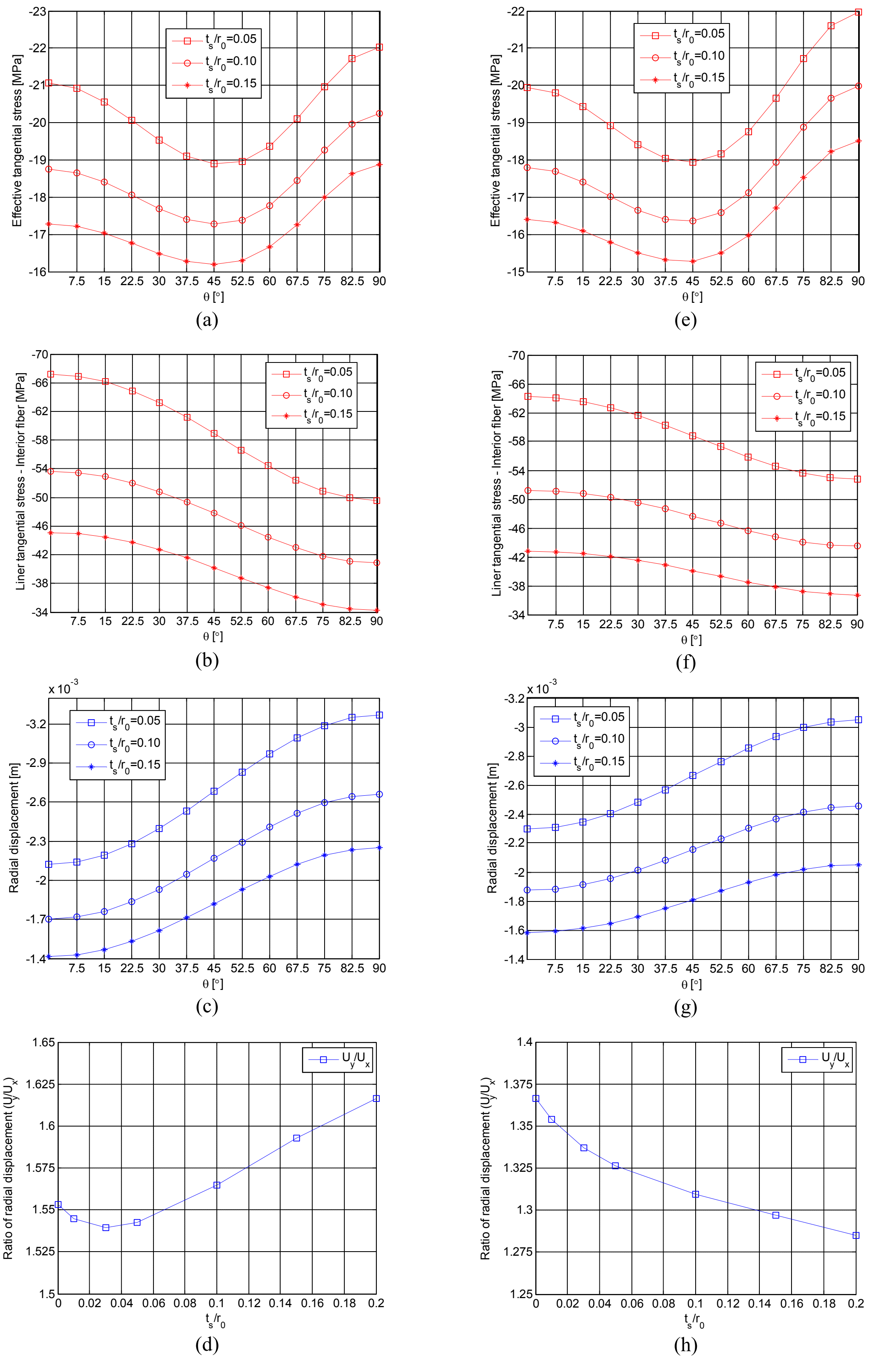

Fig. 2-22: Influence of the liner thickness (t_s / r_0) on the rock effective tangential stress, the liner tangential stress, the radial displacement, and the ratio of radial displacement respectively at the circumference of tunnel which is excavated: in drained rock (a, b, c, d) or in saturated rock with uniform pore pressure (e, f, g, h).

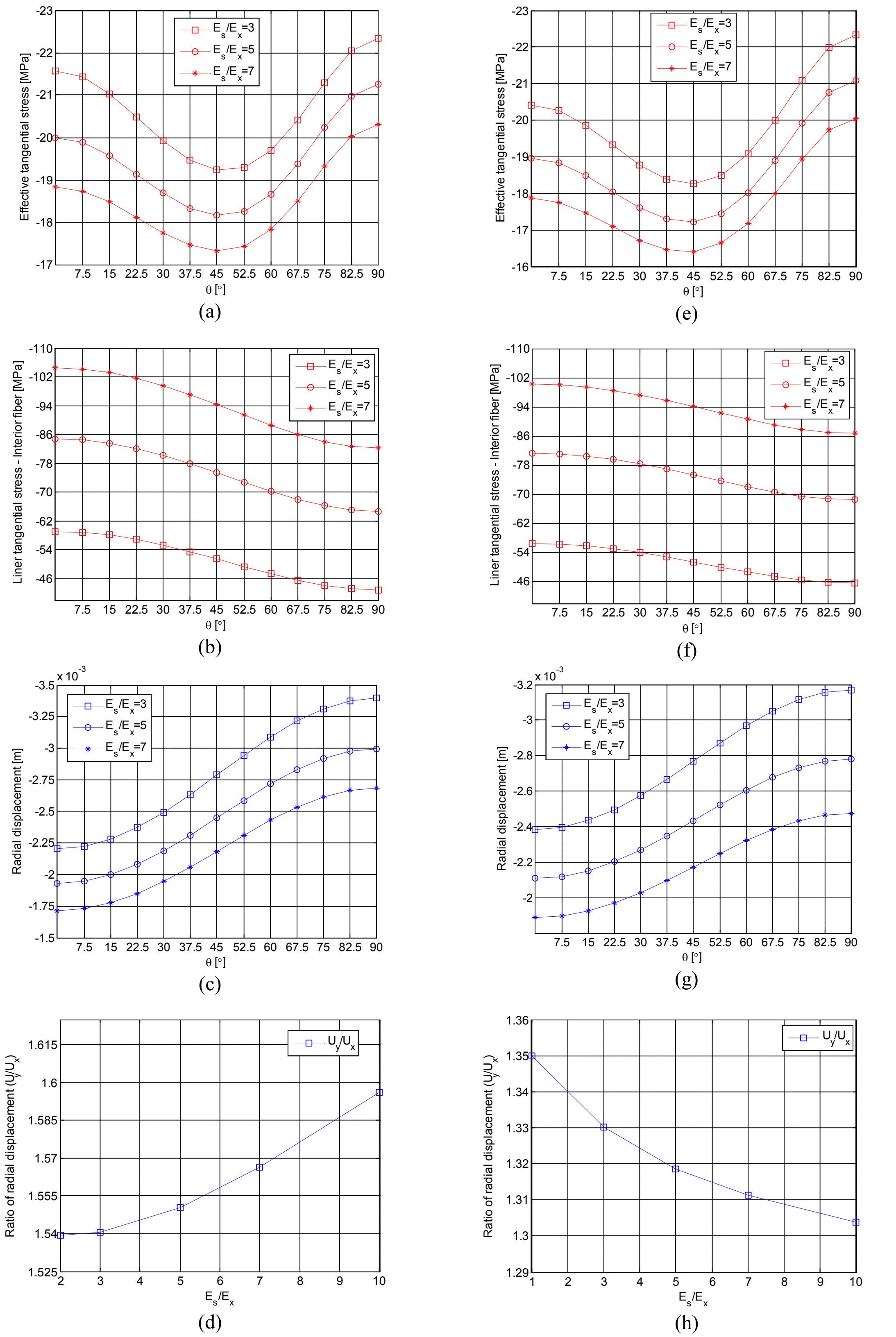

Fig. 2-23: Influence of the liner stiffness (E_s / E_x) on the rock effective tangential stress, the liner tangential stress, the radial displacement, and the ratio of radial displacement respectively at the circumference of tunnel which is excavated: in drained rock (a, b, c, d) or in saturated rock with uniform pore pressure (e, f, g, h).

In addition, when the thickness of the liner increases, the tangential stress in the liner are reduced. However, an increase of liner stiffness may result in an increase of liner stress. This is explained by the mechanical mechanism, the large stiffness liner carries more load.

To further elucidate the impact of the liner to the distribution of stresses and displacement in the rock, we compare several results in the case of full drainage at the rock–liner interface whether there is liner or not. The results given in figure 2-24.

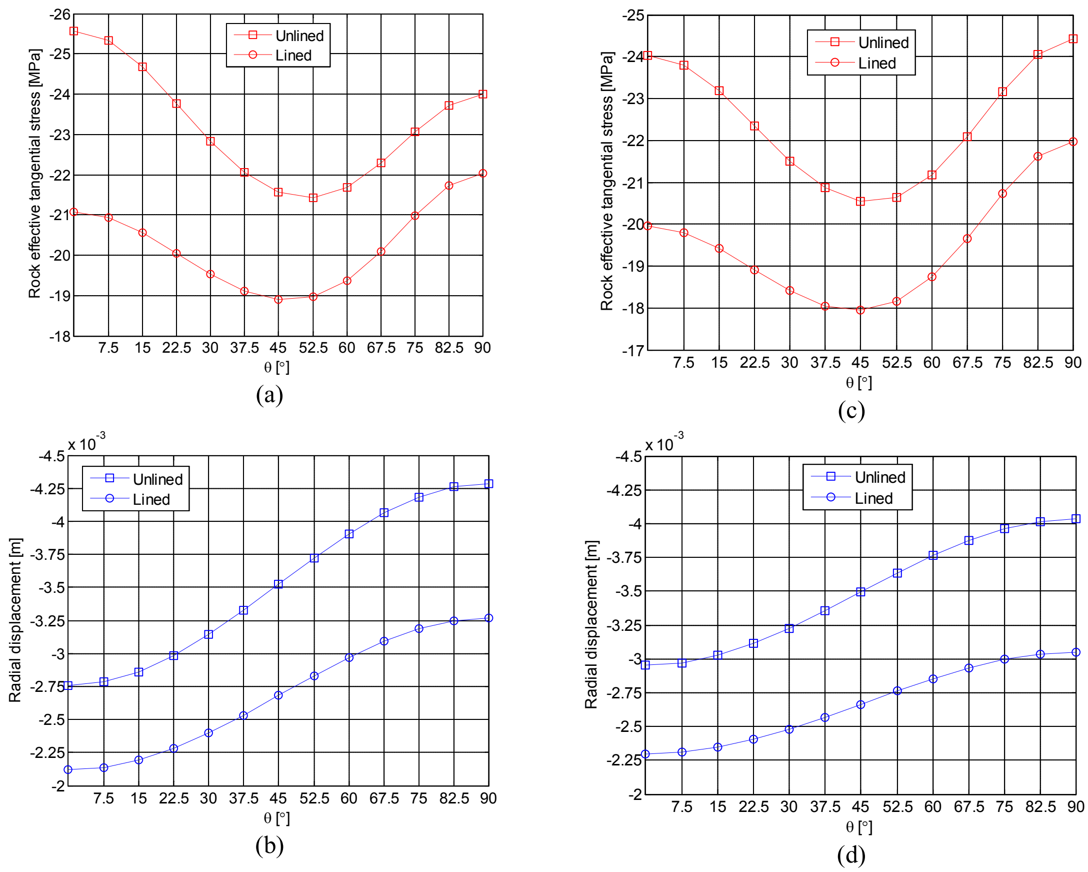

Fig. 2-24: Rock effective tangential stress and radial displacement on the rock-liner contact whether there is liner or not

The figure indicates that, the liner redistributes the radial displacement and the rock tangential stresses on the contact rock-liner. Concretely, the liner reduces more the rock tangential stress at the springline than at the crown and vice versa for radial displacement.

It is important to note that, as all the studies before, the radial displacement and tangential stress of the liner in the full drainage condition are always different from those in the no drainage condition at the rock-liner contact. Concretely, in the case of full-drainage the radial displacement is always smaller at the springline and greater at the crown than those of the no drainage condition. For the liner stress, the tendency is invert. This can be explained as follows. Provided the same total initial stresses, the work of the liner in the case of no-drainage equilibrates that in the dry rock, i.e., the total stresses applied to the liner take the same values in two cases. In the full-drainage condition, the liner is not only subjected to far-field total stresses but also the fluid flow in the rock.

It is also highlighted that, this is not the case for tunnels excavated in isotropic rock. According to Bobet (2003), the drainage conditions at the rock–liner interface do not affect the displacement and stresses in the liner, i.e., the displacement and stresses in the liner are exactly the same whether there is drainage or not at the ground–liner interface. This is because the total stresses at the ground–liner interface (interaction stress) do not depend on the drainage conditions.

2.5. Conclusions

In this chapter, we developed an analytical solution to determine stresses and displacements around the lined tunnel excavated in an anisotropic saturated rock. The fully anisotropic aspect is considered which consists of not only the anisotropic effect of initial stress but also the anisotropic characteristic of the surrounding poroelastic medium. The complex potential approach which has been successfully used in the literature to study the tunnel behavior in dry rock is utilized and extended in the context of anisotropic hydro-mechanical coupling. Our closed-form solution is then validated by comparing with the numerical solution based on the finite element method. A very good agreement was stated for two study cases corresponding respectively to the case of excavation in saturated rock with uniform pore pressure and in drained rock.

A parametric study is then carried out, allowing us to elucidate impact of each parameter on the distribution of stresses and displacements around the tunnel as well as in the liner. It showed that the decrease of shear modulus in isotropic plane can increase significantly the magnitude of radial displacement at the circumference of the tunnel. The radial displacement at the springline is sensitive to the variation of the Poisson ratio in anisotropic plane ν_{yx} and the ratio of Young's modulus E_x / E_y while the influence of Poisson ratio in the isotropic plane ν_{xz} could be negligeable. In case of the excavation in full drainage condition at the rock-liner interface, the variations of the permeabilities and Biot coefficients do not change much the radial displacement, the rock effective tangential stress, the liner tangential stress and only a moderate increase of the displacement ratio U_y/U_x is observed. However, in comparison with the other case (excavation in uniform pore pressure rock), a significant difference is stated which demonstrates the important role of the pore pressure distribution on the anisotropic hydro-mechanical behavior of the tunnel. The investigation also highlighted a strong dependence of the stress and displacement on the anisotropy and inclination of initial stresses. The anisotropic degree of tunnel behavior represented by the displacement ratio U_y/U_x can vary largely when one increases the ratio K_0 or the inclined angle β. Thereafter the impact of the liner's thickness and stiffness is elucidated. The increase of these parameters will decrease the compressive rock hoop stress as well as radial displacement but it increase the ratio U_y/U_x at the perimeter of the tunnel. In addition, one evaluated the effects of far-field pore pressure on the distribution of displacement and the stresses. The results show that, the fluid flow induced by far-field pore pressure influences primarily on rock tangential stress at the springline which belongs to the larger stiffness direction. A common observation from all parametric study cases is that the hydro-mechanical coupling induces a higher anisotropy of convergence of the tunnel wall in comparison with one obtained in the purely mechanical case (case of uniform pore pressure) whereas they are always the same when the tunnel is in isotropic medium. It confirms the necessity to account for effect of the distribution of pore pressure on the study and design of tunnel. It should be also emphasized that, when the fluid flow exhibits an isotropic property, i.e., the permeabilities are the same in two direction, this characteristic is recovered. It proves that, it is hydraulic anisotropy which controle the difference of radial displacement and liner tangential stress in two condition of drainage at the rock-liner interface. There is a noteworthy point that, in all the study cases, the radial displacement is always more important in the direction where the rock stiffness is smaller.

Conclusions

Dans ce chapitre, nous avons développé une solution analytique pour déterminer les contraintes et les déplacements autour d'un tunnel soutenu creusé dans une roche saturée anisotrope. Nous avons considéré, à la fois les effets de l'anisotropie du mileu poroélastique et celle de la contrainte initiale. L'approche par potentiel complexe qui a été utilisé avec succès dans la littérature pour étudier le comportement du tunnel dans la roche sèche a été utilisée et étendu dans le cadre du couplage hydro-mécanique anisotrope. La solution analytique est ensuite validée en comparant les résultats obtenus analytiquement avec les résultats numériques basés sur la méthode des éléments finis. Un très bon accord a été remarqué pour les deux cas d'étude correspondant respectivement aux cas d'excavation dans une roche saturée avec une pression de pore uniforme (cas non-drainé) et dans le cas du régime stationnaire et une roche drainée (la condition de drainage entière au niveau du contact le massif et le revêtement).

Une série d'étude paramétrique a été ensuite réalisée, afin d'élucider l'impact de chaque paramètre sur la distribution des contraintes et des déplacements autour du tunnel et dans le revêtement. Elle a montré que la diminution du module de cisaillement dans le plan d'isotrope peut augmenter de manière significative l'ampleur du déplacement radial en paroi du tunnel. Le déplacement radial au à la paroi est sensible à la variation du coefficient de Poisson ν_{yx} dans le plan anisotrope et le rapport du module de Young E_x / E_y tandis que l'influence du coefficient de Poisson ν_{xz} dans le plan isotrope pourrait être négligeable. Dans le cas d'excavation en condition de drainage complet à l'interface roche-revêtement, les variations des perméabilités et de coefficient de Biot ne conduisent que très peu de variations du déplacement radial, de la contrainte tangentielle effective de la roche et de la contrainte tangentielle du revêtement, et seulement une augmentation modérée du rapport de déplacement Uy/Ux a été observée. Cependant, en comparaison avec l'autre cas (excavation dans une roche à pression interstitielle uniforme), une différence significative a été remarquée qui démontre le rôle important de la distribution de la pression interstitielle sur le comportement anisotrope hydro-mécanique du tunnel.

L'étude a été également mise en évidence une forte dépendance des champs de contrainte et de déplacement à l'anisotropie et à l'inclinaison des contraintes initiales. Le degré d'anisotropie de la réponse de tunnel, représenté par le rapport de déplacement Uy/Ux, peut varier largement lorsque on augmente le rapport K_0 ou l'angle d'inclinaison β. Par la suite l'impact de l'épaisseur du revêtement et de sa rigidité a été étudié. L'augmentation de ces paramètres va diminuer la contrainte tangentielle àl'interface avec la roche ainsi que le déplacement radial mais augmente le rapport Uy/Ux en la paroi du tunnel. En plus, nous avons évalué les effets de la pression interstitielle initiale sur la distribution des déplacements et des contraintes. Les résultats montrent que, l'écoulement induit par la pression interstitielle initiale influe sur la contrainte tangentielle à l'ensemble des directions. Une observation commune de tous les cas d'étude paramétrique est que le couplage hydromécanique induit une anisotropie de convergence plus élevé de la paroi du tunnel par rapport à celui obtenu dans le cas purement mécanique (cas de pression de pore uniforme. Il confirme la nécessité à tenir compte de l'effet de la répartition de la pression interstitielle sur l'étude et la conception du tunnel. Il convient également de souligner que, lorsque l'écoulement de fluide est isotrope, cette différence diminue. Cela prouve que, l'anisotropie hydraulique est le mécanisme qui contrôle la différence des déplacements radiaux et de la contrainte tangentielle de revêtement à l'interface roche-revêtement. Il y a un point à noter que, dans tous les cas d'étude, le déplacement radial est toujours plus important dans le sens où la rigidité de la roche est plus petite.

CHAPTER 3: DEEP TUNNEL BEHAVIOUR IN ANISTROPIC POROELASTIC ROCK WITH TRANSIENT GROUNDWATER FLOW

3.1.Introduction

The study conducted in the previous chapter revealed the important effect of the anisotropic poroelastic rock mass on the response of tunnel. Due to the fact that the problem is considered in the context of steady flow of groundwater, only some particular (or extreme) cases are investigated such that the uniform pore pressure case and the steady distribution of pore pressure (at the very long period of time). Thus it seems necessary to complete the study by extending the problem in the context of the transient flow which could contribute a crucial role on the behavior of tunnel. The challenge of this new problem lies on the time effect which appears in the diffusion equation. Very often, to solve this type of problem, the Laplace transform will be used which contribute however the drawback of this approach because in time domain, only numerical results can be obtained through a numerically inverted procedure. To overcome this difficulty, in this work we will use a simplified method introduced in the literature by approximating the transient solution with ones of a successive equivalent steady flow. Based on this obtained analytical expression of pore pressure, we will propose the complex hydraulic and hydro-mechanical potentials through which the mechanical response (stress, displacement) of tunnel can be determined. This closed form solution is limited however in the one way hydro-mechanical coupling (H→M coupling). To take into account the fully coupled (H↔M) on the behavior of tunnel, the numerical simulations using FEM are chosen. Different numerical applications will be presented during this work with aim to validate the closed form solution in the one way hydro-mechanical coupling case and to highlight the contribution of each method of coupling on the final hydro-mechanical behavior of deep tunnel.

3.2.Deep tunnel behavior in saturated rock with transient groundwater flow: analytical solution of the one way poroelastic coupling

In this part, the influence of transient pore pressure on the mechanical behavior of tunnel will be considered throughout the one way coupling (H→M coupling). For this purpose, in the first step, we will detail the analytical solution of the groundwater flow in the transient state of the saturated medium with isotropic hydraulic properties based on a simplified method. Knowing the distribution of pore pressure, in the second step, we will apply the complex potential approach to deduce the mechanical response of the deep tunnel. An extension of this analytical solution in the general case of anisotropic behavior will be introduced in the final step.

3.2.1. Distribution of transient pore pressure in saturated rock with isotropic hydraulic properties: analytical solution using the simplified method

The horizontal flow towards a tunnel or well discharge under constant drawdown is the well known classical problem that was studied analytically in the first time by Jacob and Lohman (1952). Since then this solution has been used as the reference formula to evaluate the transient discharge at well or tunnels. However, based on the Green's function and integral transforms, this analytical solution is expressed as function of the first and second kind zero-order Bassel functions which makes it complicated and difficult for the practical and mathematical manipulation. To overcome these drawbacks, recently, Perrrochet (2005) presented an alternative approach which is simpler in nature but yields essentially the same results as ones of Jacob and Lohman (1952). The principal idea of this approach is that, since at a given time, the pore pressure at a distance is almost unperturbed, then the transient solution of the radial diffusion equation can be computed as successive steady-state snapshots using a time dependent radius $R_w(t)$. More precisely, it means that at each instant the perturbation of pore pressure induced by the opening is only occurred in the interior region of the circle with radius $R_w(t)$ from the center of opening and beyond this distance, the pore pressure equals to the initial water pore pressure. As a function of time, this influenced radius $R_w(t)$ will expand from zero (case of the tunnel instantaneously excavated) to the value $R=R_w(t=\infty)$. This latter corresponds to the influenced radius at the steady state, a distance far enough from the tunnel wall as indicated in the previous chapter.

This simplified method introduced by Perrochet (2005) presents a powerful tool, particularly useful for the practical and mathematical manipulation and will be utilized in this study.

As illustrated in Figure (3.1), our purely hydraulic problem consists in studying the transient distribution of pore pressure p which decreases suddenly to p_0 on the perimeter of the tunnel while it is equal to initial pore pressure p_{ff} at the infinity. The considered problem can be solved by decomposing it into two sub-problems: the first problem (problem Ip) corresponds to the case that the tunnel is excavated instantaneously in the saturated porous medium with a uniform distribution of pore pressure ($p = p_{ff}$) while in the second problem (problem IIp), the transient flow induces a variation of pore pressure ranging from ($p_0 - p_{ff}$) at the tunnel wall to zero at infinity. The solution of the problem Ip is trivial where distribution of pore pressure is uniform in surrounding rock mass, so we concentrate only on the problem IIp whose solution has to verify the mentioned boundary conditions for all instant of time. Thereby, based on the principles of superposition, we have the complete solution of the original hydraulic diffusion in the transient state.

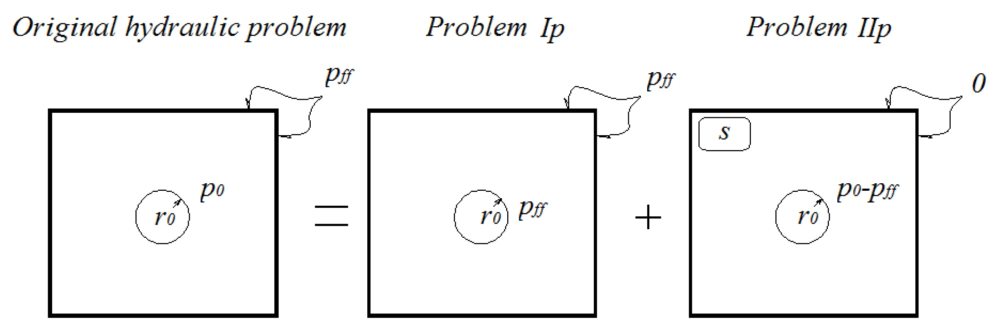

Fig. 3-1: Decomposition the original purely hydraulic diffusion in the transient state into two sub-problems

The transient fluid flow equation of the problem IIp as shown in Eq. (2.5) is rewritten now in the context of the isotropic medium as follows:

$$k\frac{\partial^2 s}{\partial x^2}+k\frac{\partial^2 s}{\partial y^2}=\gamma_{\mathrm{w}}\frac{\partial \chi}{\partial t} \tag{3.1}$$

In Eq. (3.1), k is the isotropic permeability of the medium while the pore pressure is noted as s to distinguish with the total pore pressure p. The boundary conditions of the problem consist of the constants pore pressures ($s_{ff}=0$) at infinity and ($s_0=p_0-p_{ff}$) at the tunnel wall while the pressure at initial state is equal to zero:

$$s(r,0)=0, \qquad s(r_0,t)=s_0, \qquad s(\infty,t)=s_{ff}=0 \tag{3.2}$$

Otherwise, in the one way coupling context, the change of fluid volume (per unit volume of material) χ is related to the pore pressure and the Biot modulus M as follows:

$$s=M\chi \tag{3.3}$$

Substituting Eq. (3.3) into Eq. (3.1) we have:

$$k\frac{\partial^2 s}{\partial x^2}+k\frac{\partial^2 s}{\partial y^2}=\frac{\gamma_{\mathrm{w}}}{M}\frac{\partial s}{\partial t} \tag{3.4}$$

Under the hypothesis of isotropic medium, the fluid flow is radial and hence in the polar coordinate system the diffusion equation can be rewritten in form:

$$\frac{1}{r}\frac{\partial}{\partial r}\left(rk\frac{\partial s}{\partial r}\right)=S^*\frac{\partial s}{\partial t} \tag{3.5}$$

where

$$S^*=\frac{\gamma_w}{M} \text{ and } r_0\le r\le\infty, \qquad 0\le t\le\infty \tag{3.6}$$

By multiplying two sides of Eq. (3.5) with 2π, this last equation can be developed as follows:

$$\partial\left(2\pi rk\frac{\partial s}{\partial r}\right)=\frac{\partial}{\partial t}\left(2\pi rsS^*\right)\partial r \tag{3.8}$$

Moreover, according to Darcy's law, we have the discharge of fluid flow across the perimeter of the tunnel as below:

$$Q(t)=-2\pi r_0k\frac{\partial s}{\partial r}(r_0,t) \tag{3.9}$$

As proposed by Perrochet (2005), the transient solution of Eq. (3.5) can be solved as successive steady state snapshots of the function $s(r,t)$ over a time dependent distance $R_w(t)$. This distance is known as the no-flow moving boundary beyond which the specified pore pressure strictly vanishes. So the interested domain in which the perturbation of pore pressure can take place is restricted in the range $r_0 \le r \le R_w(t)$ and the boundary conditions of the problem II are can be modified as follows:

$$s(r_0,t)=s_0, \qquad \frac{\partial s}{\partial r}(R_w(t),t)=0, \qquad s(R_w(t),t)=0 \tag{3.10}$$

By integrating Eq. (3.8) over this domain, it yields the following relationship:

$$-2\pi r_0k\frac{\partial s}{\partial r}(r_0,t)=\frac{\partial}{\partial t}\int_{r_0}^{R_w(t)}2\pi rsS^*dr \tag{3.11}$$

Therefore, by taking into account Eq. (3.9) we have:

$$Q(t)=\frac{\partial}{\partial t}\int_{r_0}^{R_w(t)}2\pi rsS^*dr=\frac{\partial V(t)}{\partial t} \tag{3.12}$$

where $V(t)$ is the cumulative volume of extracted water.

According to the simplified approach of Perrochet (2005), one can replace the right-hand side of Eq. (3.5) by a uniform source term that depends on time. Hence, the diffusion equation (3.5) to resolve is written in the following form:

$$\frac{1}{r}\frac{\partial}{\partial r}\left(rk\frac{\partial s}{\partial r}\right)=I(t), \qquad r_0 \le r \le R_w(t) \tag{3.13}$$

The Eq. (3.13) can be solved now by taking into account the boundary conditions (3.10) and the conditions in Eq. (3.12), we can obtain the uniform time dependent source term I(t):

$$I(t)=\frac{4ks_0}{2R_w(t)^2\ln\dfrac{R_w(t)}{r_0}-R_w(t)^2+r_0^2} \tag{3.14}$$

as well as the distribution of the pore pressure in following form:

$$s(r,t)=s_0\left(1-\frac{2R_w(t)^2\ln\dfrac{r}{r_0}-r^2+r_0^2}{2R_w(t)^2\ln\dfrac{R_w(t)}{r_0}-R_w(t)^2+r_0^2}\right) \tag{3.15}$$

Substituting this solution in Eqs. (3.9) and (3.11) the global quantities *Q(t)* and *V(t)* can be expressed as (see also Perrochet, 2005):

$$Q(t)=2\pi k s_0\left[\ln\left(\lambda^{\frac{\lambda^2}{\lambda^2-1}}\right)-\frac{1}{2}\right]^{-1} \tag{3.16}$$

and

$$V(t)=\pi r_0 S^* s_0\left[\lambda^2-4\ln\left(\lambda^{\frac{\lambda^2}{\lambda^2-1}}\right)+1\right]\left[4\ln\left(\lambda^{\frac{\lambda^2}{\lambda^2-1}}\right)-2\right]^{-1} \tag{3.17}$$

where $\lambda = R_w(t)/r_0$.

Considering Eq. (3.12) and the variation of $V(t)$ with respect to $R_w(t)$, one can write:

$$Q=\frac{\partial V}{\partial R_w}\frac{\partial R_w}{\partial t} \tag{3.18}$$

After some manipulations, we can obtain the following relation (see Perrochet, 2005):

$$\frac{kt}{S^* s_0^2}=\int_1^{\lambda}\frac{\ln\left(u^{\frac{u^2+1}{u^2-1}}\right)-1}{4\ln\left(u^{\frac{u^2}{u^2-1}}\right)-2}\,u\,du \tag{3.19}$$

The complexity of the term under the integral sign in Eq. (3.19) makes it not to be fully integrated. To overcome this problem, Perrochet (2005) used the following approximation based on the polynomial analysis:

$$\frac{kt}{S^* s_0^2}\cong\frac{1}{\pi e}\left(\lambda^{\frac{\lambda^2}{\lambda^2-1}}-\sqrt{e}\right)^2 \tag{3.20}$$

where e (mathematical constant) is Euler's number

Without difficulty one can determine the ratio λ:

$$\lambda^{\frac{\lambda^2}{\lambda^2-1}}\cong\sqrt{e}\left(1+\sqrt{\frac{\pi k t}{S^* r_0^2}}\right) \tag{3.21}$$

through which the radius $R_w(t)$ can be evaluated:

$$R_w(t) = \lambda r_0 \tag{3.22}$$

Thus, at each instant, the transient fluid flow of the isotropic saturated medium can be solved analytically where the solution of pore pressure (Eq. 3.15) varies from ($s_0 = p_0 - p_{ff}$) at the tunnel wall (*r=r0*) to ($s_{ff} = 0$) at (*r=Rw(t)*) with *Rw(t)* is determined from Eqs. (3.21) and (3.22).

3.2.2. Mechanical behavior of deep tunnel under the transient fluid flow

We investigate now the mechanical behavior of the tunnel taking into account the effect of transient flow of groundwater (so only the one way H->M is considered). The same procedure as mentioned in chapter 2 is used to solve analytically this problem. More precisely, the problem is also decomposed into two problems: problem I and problem II as illustrated in Fig. 3.2 which is similar as Fig. 2.6. However, it is important to emphasize that the problem II in this chapter is studied in the context of transient fluid flow yielding a variation of pore pressure as a function of time. The solution of the problem I which corresponds to the case of the tunnel excavated in the saturated rock with uniform pore pressure (*p=pff*) was detailed in the chapter 2. As consequence, in this sub-section the detail is focused only on the problem II.

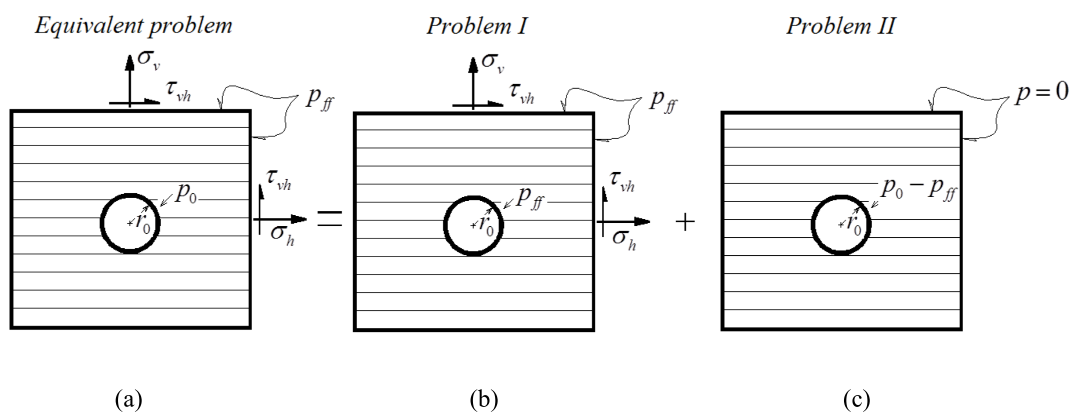

Fig. 3-2: Decomposition of the equivalent problem into two sub-problems (which is similar as one presented in chapter 2, see Fig. 2.6): problem I and problem II. In this latter problem the transient flow of groundwater is considered.

To solve the problem II, the complex potential approach, presented previously in chapter 2 is used. Concretely, at each instant *t*, the same procedure is applied and the problem is treated similarly as one in the steady state. To recall, in the complex potential approach (see section 2.3 of chapter 2), it is essential to determine the complex hydraulic and hydro-mechanical potentials from which the stress and displacement around the tunnel can be calculated. For this purpose, the conformal mapping technique is used which transforms the region outside the tunnel of radius r_0 in *z*-plane ($z_k = x + \mu_k y$) into the region outside the unit circle in the ζ_k-plane ($\zeta_k = \xi_k + i\eta_k$) ($k = 1, 2, w$) (see Eq. (2.29) in section 2.3 of chapter 2).

Now one will study the problem *IIa* with the pore pressure distribution in transient state.

In the particular case of the isotropic hydraulic behavior of the saturated rock, one has:

$$\mu_w = i \text{, and so } z_w = x + iy \tag{3.23}$$

and hence, the conformal mapping generates into:

$$z_w = w(\zeta_w) = r_0 \zeta_w \tag{3.24}$$

Thus in the conformal mapping (3.24), any circle with radius r that is concentric with the tunnel in z_w-plane is transformed into a circle of radius $\rho = r / r_0$ that is also concentric with the unit circle in ζ_w- plane. In this latter plane, the diffusion equation (3.4) can be rewritten with respect to the coordinate $\xi_w = x / r_0, \eta_w = y / r_0$ as follows:

$$k \frac{\partial^2 s}{\partial \xi_w^2} + k \frac{\partial^2 s}{\partial \eta_w^2} = \frac{\gamma_w}{M} \frac{\partial s}{\partial t_e} \tag{3.25}$$

where the variable t_e is defined:

$$t_e = t / r_0^2 \tag{3.26}$$

It can be seen here that, there is a change of time variable, i.e., if we have a certain instant t in z_w-plane, it will correspond to the instant $t_e = t / r_0^2$ in ζ_w- plane.

Otherwise, in the polar coordinate system of the ζ_w- plane, the diffusion equation (3.25) can be expressed in form:

$$k \frac{\partial^2 s}{\partial \rho^2} + k \frac{1}{\rho} \frac{\partial s}{\partial \rho} = I_e(t_e) \tag{3.27}$$

where ρ is polar radius.

And the boundary conditions that the water pore pressure field $s(\rho, t_e)$ must satisfy are:

$$s(\rho_0 = 1, t_e = 0) = s_0; \qquad \frac{\partial s(R_e, t_e)}{\partial \rho} = 0; \qquad s(R_e, t_e) = 0 \tag{3.28}$$

where $R_e(t_e)$ is the time dependent radius in ζ_w- plane beyond which no flow can occur.

From the solution of pore pressure obtained in z_w-plane (Eq. (3.15), it is straightforward to write the solution $s(\rho, t_e)$ in ζ_w- plane as follows:

$$s(\rho, t_e) = s_0 \left(1 - \frac{2R_e(t_e)^2 \ln \rho - \rho^2 + 1}{2R_e(t_e)^2 \ln R_e(t_e) - R_e(t_e)^2 + 1} \right) \tag{3.29}$$

and:

$$I_e(t_e)=\frac{4ks_0}{2R_e(t_e)^2\ln R_e(t_e)-R_e(t_e)^2+1} \tag{3.30}$$

After some developments, one can deduce the final expression of pore pressure in the problem II:

$$s=u_{ff}-\frac{u_0-u_{ff}}{\log R_e}\log\left(\frac{\rho}{R_e}\right)+\frac{I_e(t_e)}{4k}\rho^2 \tag{3.31}$$

with:

$$\begin{cases} u_0=s_0-\dfrac{I_e(t_e)}{4k}\rho_0^2=p_0-p_{ff}-\dfrac{I_e(t_e)}{4k} \\ u_{ff}=s_{ff}-\dfrac{I_e(t_e)}{4k}R_e(t_e)^2=-\dfrac{I_e(t_e)}{4k}R_e(t_e)^2 \end{cases} \tag{3.32}$$

Hence the total solution of pore pressure in the original problem is:

$$p=p_{ff}+s=p_{ff}+u_{ff}-\frac{u_0-u_{ff}}{\log R_e}\log\left(\frac{\rho}{R_e}\right)+\frac{I_e(t_e)}{4k}\rho^2 \tag{3.33}$$

Concerning the influence radius $R_e(t_e)$, it can be deduced directly from the equation (3.21) accounting for the fact that the radius of the borehole in the transformation plane ζ_w is equal to unit ($\rho_0=1$), one obtains:

$$R_e^{\frac{R_e^2}{R_e^2-1}}\cong\sqrt{e}\left(1+\sqrt{\frac{\pi k t_e}{S^*}}\right) \tag{3.34}$$

Therefore, corresponding to each instant *t*, the influence radius $R_e(t_e)$ can be evaluated from Eq. (3.34) and the distribution of total pore pressure is determined from Eq. (3.33).

Now for the aim of determination the complex potentials, we can express the transient solution of pore pressure (3.31) in a general form with respect to the complex variable $\zeta_w=\rho e^{i\theta}$:

$$s=u_{ff}-\frac{u_0-u_{ff}}{\log R_e}\mathrm{Re}\left[\log\left(\frac{\zeta_w}{R_e}\right)\right]+\frac{I_e(t_e)}{4k}\mathrm{Re}\left[\left(\frac{\zeta_w}{e^{i\theta}}\right)^2\right] \tag{3.35}$$

Knowing the solution of the purely hydraulic problem, we aim to solve the hydro-mechanical problem. It should be noted that, the first component in the right hand side of Eq. (3.35) induces a uniform distribution of pore pressure ($s=u_{ff}$) in the studied region around the tunnel ($\rho_0=1\le\rho\le R_e$), so it does not change of total stresses as well as displacement (as the problem I with uniform pore pressure $p=p_{ff}$) but it influences the effective stresses. Meanwhile, only the other terms in the right hand side of Eq. (3.35) can result in a variation of total stresses and displacement in the interested region ($\rho_0 = 1 \le \rho \le R_e$) around the tunnel. Consequently, the interest lies only on the effect of these terms on the mechanical behavior of tunnel. As mentioned above, the procedure is similar as one presented of chapter 2 in which the problem II is also decomposed into the three sub-problems as illustrated in Fig. 3.3. The main difference is that in the present study case, we treat the problem in the transient state of fluid flow while in chapter 2 the influence of the pore pressure on the mechanical behavior of tunnel (problem II of chapter 2) is only investigated in the steady state. Thus here to simplify the presentation, we capture only the principal results of each sub-problems of the problem II and the detail of the procedure will not be repeated.

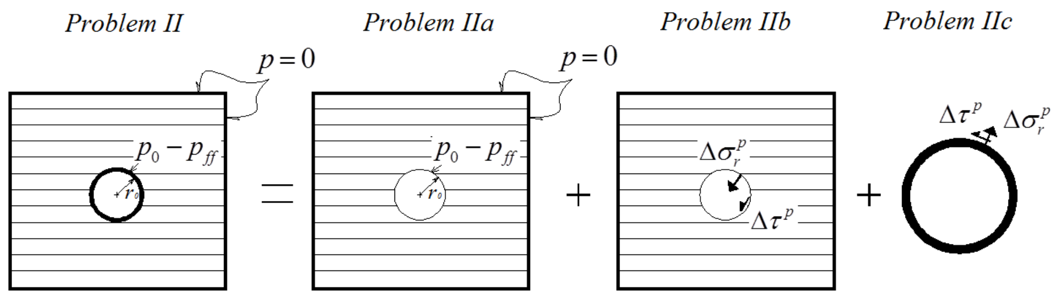

Fig. 3-3: Decomposition of the problem II into three sub-problems as ones detailed in chapter 2.

For example, by substituting the expression of pore pressure in Eq. (3.35) without the first term in the compatibility equation (2.24), the particular solution $F_p''(z_w)$ can be determined as follows:

$$F_p''(z_w) = 2\,\mathrm{Re}\left[\Phi_w'(z_w)\right] = \frac{u_0 - u_{ff}}{\log R_e}\eta\,\mathrm{Re}\left[\log\frac{\zeta_w}{R_e} - \frac{I_e(t_e)}{4k}\mathrm{Re}\left[\left(\frac{\zeta_w}{e^{i\theta}}\right)^2\right]\right] \tag{3.36}$$

or the derivate of the hydraulic potential can be found as:

$$\Phi_w'(z_w) = \frac{1}{2}\frac{u_0 - u_{ff}}{\log R_e}\eta\,\mathrm{Re}\left[\log\frac{\zeta_w}{R_e} - \frac{I_e(t_e)}{4k}\mathrm{Re}\left[\left(\frac{\zeta_w}{e^{i\theta}}\right)^2\right]\right] \tag{3.37}$$

where the complex coefficient η is defined in Eq. (2.40).

The same order of effect on the displacements and stresses around the tunnel of the hydraulic and hydro-mechanical potentials allows us to propose the two following hydro-mechanical potentials whose derivatives take the same form as one of the hydraulic potential:

$$\begin{aligned}
\Phi_1'(z_1) &= \frac{1}{2}\left[N_1\frac{u_0 - u_{ff}}{\log R_e(t)}\log\left(\frac{\zeta_1}{R_e(t)}\right) - P_1\frac{I_e(t)}{4k}\left(\frac{\zeta_1}{e^{i\theta}}\right)^2\right] \\
\Phi_2'(z_2) &= \frac{1}{2}\left[N_2\frac{u_0 - u_{ff}}{\log R_e(t)}\log\left(\frac{\zeta_2}{R_e(t)}\right) - P_2\frac{I_e(t)}{4k}\left(\frac{\zeta_2}{e^{i\theta}}\right)^2\right]
\end{aligned} \tag{3.38}$$

In Eq. (3.38) N_1, N_2 and P_1, P_2 are the complex constants to be determined.

The complex potentials are inferred from their derivatives by the following integrations:

$$\begin{aligned}
\Phi_w(\zeta_w) &= \int \Phi'_w(\zeta_w) w'(\zeta_w) d\zeta_w \\
\Phi_1(\zeta_1) &= \int \Phi'_1(\zeta_1) w'(\zeta_1) d\zeta_1 \\
\Phi_2(\zeta_2) &= \int \Phi'_2(\zeta_2) w'(\zeta_2) d\zeta_2
\end{aligned} \tag{3.39}$$

in which the transformation functions $w(\zeta_1), w(\zeta_2)$ are defined in Eq. (2.29).

Thus, the expressions of the complex potentials are deduced as below:

$$\begin{aligned}
\Phi_w(\zeta_w) &= \frac{r_0(u_0 - u_{ff})\left[1-\zeta_w^2 + (1+\zeta_w^2) log\dfrac{\zeta_w}{R_e(t_e)} + \mathrm{i}\left(1+\zeta_w^2 + (1-\zeta_w^2) log\dfrac{\zeta_w}{R_e(t_e)}\right)\mu_w\right]}{4\zeta_w log R_e(t_e)} \\
&\quad - \frac{I_e(t_e)}{12k} \mathrm{e}^{-2\mathrm{i}\theta} r_0 (1-\mathrm{i}\mu_w)\zeta_w^3; \\
\Phi_1(\zeta_1) &= \frac{r_0(u_0 - u_{ff})N_1\left[1-\zeta_1^2 + (1+\zeta_1^2) log\dfrac{\zeta_1}{R_e(t_e)} + \mathrm{i}\left(1+\zeta_1^2 + (1-\zeta_1^2) log\dfrac{\zeta_1}{R_e(t_e)}\right)\mu_1\right]}{4\zeta_1 log R_e(t_e)} \\
&\quad - \frac{I_e(t_e)}{12k} P_1 \mathrm{e}^{-2\mathrm{i}\theta} r_0 (1-\mathrm{i}\mu_1)\zeta_1^3; \\
\Phi_2(\zeta_2) &= \frac{r_0(u_0 - u_{ff})N_2\left[1-\zeta_2^2 + (1+\zeta_2^2) log\dfrac{\zeta_2}{R_e(t_e)} + \mathrm{i}\left(1+\zeta_2^2 + (1-\zeta_2^2) log\dfrac{\zeta_2}{R_e(t_e)}\right)\mu_2\right]}{4\zeta_2 log R_e(t_e)} \\
&\quad - \frac{I_e(t_e)}{12k} P_2 \mathrm{e}^{-2\mathrm{i}\theta} r_0 (1-\mathrm{i}\mu_2)\zeta_2^3.
\end{aligned} \tag{3.40}$$

Respectively, the stresses and displacements corresponding to the particular solution can be computed from these hydraulic and hydro-mechanical potentials by using the relations expressed in Eq. (2.42):

$$\sigma_x^{IIa,p} = \mathrm{Re}\left\{ \begin{array}{l} \dfrac{(u_0 - u_{ff})\left[log\dfrac{\zeta_1}{R_e(t_e)} N_1\mu_1^2 + log\dfrac{\zeta_2}{R_e(t_e)} N_2\mu_2^2 + \eta log\dfrac{\zeta_3}{R_e(t_e)}\mu_w^2 \right]}{logR_e(t_e)} \\ -\left[\mathrm{e}^{-2\mathrm{i}\theta}\dfrac{I_e(t_e)}{4k}(P_1\zeta_1^2\mu_1^2 + P_2\zeta_2^2\mu_2^2 + \eta\zeta_3^2\mu_w^2) \right] \end{array} \right\};$$

$$\sigma_y^{IIa,p} = \mathrm{Re}\left\{ \begin{array}{l} \dfrac{(u_0 - u_{ff})\left[log\dfrac{\zeta_1}{R_e(t_e)} N_1 + log\dfrac{\zeta_2}{R_e(t)} N_2 + \eta log\dfrac{\zeta_3}{R_e(t_e)} \right]}{logR_e(t_e)} \\ -\left[\mathrm{e}^{-2\mathrm{i}\theta}\dfrac{I_e(t_e)}{4k}(P_1\zeta_1^2 + P_2\zeta_2^2 + \eta\zeta_3^2) \right] \end{array} \right\}; \qquad (3.41)$$

$$\tau_{xy}^{IIa,p} = \mathrm{Re}\left\{ \begin{array}{l} \dfrac{(u_0 - u_{ff})\left[log\dfrac{\zeta_1}{R_e(t_e)} N_1\mu_1 + log\dfrac{\zeta_2}{R_e(t_e)} N_2\mu_2 + \eta log\dfrac{\zeta_3}{R_e(t_e)}\mu_w \right]}{logR_e(t_e)} \\ -\left[\mathrm{e}^{-2\mathrm{i}\theta}\dfrac{I_e(t_e)}{4k}(P_1\zeta_1^2\mu_1 + P_2\zeta_2^2\mu_2 + \eta\zeta_3^2\mu_w) \right] \end{array} \right\}$$

$$U_x^{IIa,p}=\mathrm{Re}\left\{\frac{N_1p_1\left[1-\zeta_1^{\,2}+(1+\zeta_1^{\,2})log\dfrac{\zeta_1}{R_e(t_e)}+\mathrm{i}\left(1+\zeta_1^{\,2}+(\zeta_1^{\,2}-1)log\dfrac{\zeta_1}{R_e(t_e)}\right)\mu_1\right]}{2\zeta_1 logR_e(t_e)}\right.$$

$$\times(u_0-u_{ff})+p_1P_1\frac{I_e(t_e)}{6}\mathrm{e}^{-2\mathrm{i}\theta}(i\mu_1-1)\zeta_1^{\,3}+$$

$$+\frac{N_2p_2\left[1-\zeta_2^{\,2}+(1+\zeta_2^{\,2})log\dfrac{\zeta_2}{R_e(t_e)}+\mathrm{i}\left(1+\zeta_2^{\,2}+(\zeta_2^{\,2}-1)log\dfrac{\zeta_2}{R_e(t_e)}\right)\mu_2\right]}{2\zeta_2 logR_e(t_e)}$$

$$\times(u_0-u_{ff})+p_2P_2\frac{I_e(t_e)}{6}\mathrm{e}^{-2\mathrm{i}\theta}(i\mu_2-1)\zeta_2^{\,3}+$$

$$+\frac{\eta p_w\left[1-\zeta_w^{\,2}+(1+\zeta_w^{\,2})log\dfrac{\zeta_w}{R_e(t_e)}+\mathrm{i}\left(1+\zeta_w^{\,2}+(\zeta_w^{\,2}-1)log\dfrac{\zeta_w}{R_e(t_e)}\right)\mu_w\right]}{2\zeta_w logR_e(t_e)}$$

$$\left.\times(u_0-u_{ff})+p_w\frac{I_e(t_e)}{6}\mathrm{e}^{-2\mathrm{i}\theta}(i\mu_w-1)\zeta_w^{\,3}\right\}r_0(u_0-u_{ff});$$

$$\tag{3.42}$$

$$U_y^{IIa,p}=\mathrm{Re}\left\{\frac{N_1q_1\left[1-\zeta_1^{\,2}+(1+\zeta_1^{\,2})log\dfrac{\zeta_1}{R_e(t_e)}+\mathrm{i}\left(1+\zeta_1^{\,2}+(\zeta_1^{\,2}-1)log\dfrac{\zeta_1}{R_e(t_e)}\right)\mu_1\right]}{2\zeta_1 logR_e(t_e)}\right.$$

$$\times(u_0-u_{ff})+q_1P_1\frac{I_e(t_e)}{6}\mathrm{e}^{-2\mathrm{i}\theta}(i\mu_1-1)\zeta_1^{\,3}+$$

$$+\frac{N_2q_2\left[1-\zeta_2^{\,2}+(1+\zeta_2^{\,2})log\dfrac{\zeta_2}{R_e(t_e)}+\mathrm{i}\left(1+\zeta_2^{\,2}+(\zeta_2^{\,2}-1)log\dfrac{\zeta_2}{R_e(t_e)}\right)\mu_2\right]}{2\zeta_2 logR_e(t_e)}$$

$$\times(u_0-u_{ff})+q_2P_2\frac{I_e(t_e)}{6}\mathrm{e}^{-2\mathrm{i}\theta}r_0(i\mu_2-1)\zeta_2^{\,3}+$$

$$+\frac{\eta q_w\left[1-\zeta_w^{\,2}+(1+\zeta_w^{\,2})log\dfrac{\zeta_w}{R_e(t_e)}+\mathrm{i}\left(1+\zeta_w^{\,2}+(\zeta_w^{\,2}-1)log\dfrac{\zeta_w}{R_e(t_e)}\right)\mu_w\right]}{2\zeta_w logR_e(t_e)}$$

$$\left.\times(u_0-u_{ff})+q_w\frac{I_e(t_e)}{6}\mathrm{e}^{-2\mathrm{i}\theta}(i\mu_w-1)\zeta_w^{\,3}\right\}r_0;$$

It can be seen that, the expressions of the displacements and stresses include the polynomial functions and the logarithmic functions of the complex variables ζ_1,ζ_2,ζ_w. As discussed in chapter 2, one important characteristic of the logarithmic function with respect to the complex variables is its multi-value, i.e., periodic functions of angle (Kreyszig, 1999). Hence the imposed condition of single-valued displacement yields the same system of equation as written in Eq. (2.48) through which we can determine two complex constants N_1,N_2.

Concerning the two others constants P_1, P_2, they can be calculated from the condition of zero stresses at $\rho = R_e(t_e)$. In effect, as discussed previously, beyond this latter distance, no flow occurs meaning that the pore pressure is not disturbed and hence it does not affect the mechanical behavior of tunnel in the region with $\rho \geq R_e(t_e)$. More precisely, by using the condition of zero stresses at $\rho = R_e(t_e)$, we obtain the other system of equations (Eq. 3.43) through which the real (P_{11}, P_{21}) and imaginary (P_{12}, P_{22}) parts of two complex numbers P_1, P_2 can be evaluated.

$$
\begin{aligned}
& P_{11} + P_{21} + \eta_1 = 0; \\
& P_{12} i\mu_{11} + P_{22} i\mu_{21} + \eta_2 i\mu_{w1} = 0; \\
& P_{11}\mu_{11}^2 + P_{21}\mu_{21}^2 + \eta_1\mu_{w1}^2 = 0; \\
& P_{12} = 0
\end{aligned}
\tag{3.43}
$$

It is worth noting that the stresses given by Eq. (3.41) satisfy the boundary conditions of zero total stresses at the distance $\rho = R_e(t_e)$ but result the non-zero total normal and shear stresses on the surface of the tunnel wall. Therefore, the same normal and shear stresses but with opposite sign are applied on the perimeter of the tunnel to satisfy the condition of zero stresses at this place. The expression of these normal and shear stresses was expressed in Eq. (2.49) as function of $\Sigma_x, \Sigma_y, \mathrm{T}_{xy}$, the stress components on the tunnel calculated from Eq.(3.44):

$$
\begin{aligned}
& \Sigma_x = -(u_0 - u_{ff})\,\mathrm{Re}[N_1\mu_1^2 + N_2\mu_2^2 + \eta\mu_w^2] - \frac{I_e(t_e)}{4k}\mathrm{Re}[(P_1\mu_1^2 + P_2\mu_2^2 + \eta\mu_w^2)]; \\
& \Sigma_y = -(u_0 - u_{ff})\,\mathrm{Re}[N_1 + N_2 + \eta] - \frac{I_e(t_e)}{4k}\mathrm{Re}[P_1 + P_2 + \eta]; \\
& \mathrm{T}_{xy} = (u_0 - u_{ff})\,\mathrm{Re}[\mu_1 N_1 + \mu_2 N_2 + \mu_w \eta] + \frac{I_e(t_e)}{4k}\mathrm{Re}[P_1\mu_1 + P_2\mu_2 + \eta\mu_w]
\end{aligned}
\tag{3.44}
$$

The solution of stresses $\sigma_x^{IIa,h}, \sigma_y^{IIa,h}, \tau_{xy}^{IIa,h}$ and displacement $U_x^{IIa,h}, U_y^{IIa,h}$ of this latter problem are calculated from the complex potentials Φ_1^{*h}, Φ_2^{*h} expressed in Eq. (2.51) by using the Eq. (2.27). So on, the final solution of the problem *IIa* can be evaluated from Eq. (2.52).

Concerning the problem *IIb* and *IIc*, the procedure is strictly similar as ones in chapter 2 and hence all formula developed in chapter 2 will be applied straightforwardly here. For example, to account for the interaction between the liner and rock mass, the compatibility condition of displacement at the liner-rock mass contact as written in Eq. (2.54) is used directly here. Note that to simplify the presentation, the expression of displacement of the problem *IIa*, *IIb*, and *IIc* are detailed in appendix B.

The final results of the original problem are calculated from the solutions of the problem I and problem II based on the superposition principle as expressed from Eq. (2.57) to Eq. (2.59).

3.2.3. Extension in case of saturated rock with anisotropic hydraulic properties

The solution as presented in the previous section 3.2.2 will be extended now in a more general context in which the hydraulic behavior of saturated rock is anisotropic.

Specifically, in the hydrological field, accounting for the anisotropic aspect in the analytical solution of the transient diffusion problem is an interesting topic and a lot of contributions were dedicated the last two decades. For example, by using the Laplace transform, Mathias and Butler (2007) deduced the analytical solution for the problem of flow to a finite diameter well in a horizontally anisotropic aquifer. The analytical solution is written in the Laplace domain in terms of Mathieu functions and then a numerically inverted procedure is used to evaluate the time response. Otherwise, these authors showed that for large times, the problem can be approximated as ones in an equivalent isotropic domain by coordinate transformations. The approximation agrees well with the exact solution for moderately anisotropic systems (with the anisotropic ratio $k_x / k_y \leq 25$). This observation was also confirmed in the contribution of Cihan *et al*. (2014) who studied the problem of flow in horizontally anisotropic multilayered aquifer systems. In addition, Cihan *et al*. (2014) highlighted that the equivalent isotropic solution can give satisfactory results at observation points away from the injection/pumping wells even for highly anisotropic aquifer systems (with the ansitropic degree can reach to $k_x / k_y = 1000)$.

Returning to our problem, our idea coming from this brief literature is that we aim to replace the initial anisotropic diffusion of groundwater by one in the equivalent isotropic medium. Hence the hydro-mechanical solution as developed in section 3.2.2 will be applied directly.

Considering the problem of transient flow of groundwater in the problem *IIp* as described in section 3.2.1 which is now extended in the general context of anisotropic permeable medium:

$$k_x \frac{\partial^2 s}{\partial x^2} + k_y \frac{\partial^2 s}{\partial y^2} = \frac{\gamma_w}{M} \frac{\partial s}{\partial t} \tag{3.45}$$

The pore pressure *s*, solution of this diffusion equation, must satisfy the initial and boundary conditions as noted in Eq. (3.2).

By introducing the transformation coordinate (Mathias and Butler, 2007):

$$X = x, Y = y\sqrt{\frac{k_x}{k_y}} \tag{3.46}$$

the diffusion equation (3.45) can be written in the new coordinate system X-Y as follows:

$$k_e \frac{\partial^2 s}{\partial X^2} + k_e \frac{\partial^2 s}{\partial Y^2} = S^* \sqrt{\frac{k_y}{k_x}} \frac{\partial s}{\partial t} \tag{3.47}$$

where $S^* = \gamma_w / M$ and $k_e = \sqrt{k_x k_y}$ is the equivalent isotropic permeability.

Therefore, the initially anisotropic diffusion problem is now degenerated to the equivalent isotropic problem in the transformed domain. It is important to note that, as pointed out by Fitts (2006), Mathias and Butler (2007) and Cihan *et al.* (2014), with coordinate transformation, the circular tunnel of radius r_0 becomes an ellipse and in the transformed domain, the pore pressure contours in the immediate vicinity of the tunnel have also elliptical shapes.

Using the conformal mapping technique as introduced in section 2.3, the diffusion equation (3.47) is written in the ζ_w plane, which is related to the complex variable z_w through the expression noted in Eq. (2.15), as follows:

$$k_e \frac{\partial^2 s}{\partial \xi_w^2} + k_e \frac{\partial^2 s}{\partial \eta_w^2} = \frac{1}{\left| d\zeta_w / dz_w \right|^2} S^* \sqrt{\frac{k_y}{k_x}} \frac{\partial s}{\partial t} \tag{3.48}$$

Mathematically, Eq. (3.48) owns the same form as ones written in Eq.(3.25) which means that we can directly apply the solution of the isotropic diffusion problem whose permeability is now $k=k_e$. However, it is essential to point out that the solution of the isotropic diffusion in the transient state as detailed in section 3.2.1 based on the assumption of uniform source term, the right hand side of the diffusion equation depends only on time and is uniform in space. This assumption is not verified in the present problem where the term $\left| d\zeta_w / dz_w \right|$ in Eq. (3.48) is function of the spatial variables (ξ_w, η_w) meaning that the right hand side of the diffusion equation (Eq. 3.48) is not uniform. To overcome this problem, we use the following approximation:

$$k_e \frac{\partial^2 s}{\partial \xi_w^2} + k_e \frac{\partial^2 s}{\partial \eta_w^2} = (r_0')^2 S^* \sqrt{\frac{k_y}{k_x}} \frac{\partial s}{\partial t} \tag{3.49}$$

where the parameter r_0' is defined as:

$$r_0' = \lim_{z_w \to \infty} \frac{1}{\left| d\zeta_w / dz_w \right|} = \frac{r_0 (1 + \sqrt{k_x / k_y})}{2} \tag{3.50}$$

It is interesting to note that, this latter parameter is similar as one introduced by Kucuk and Brigham (1979) as well as by Mathias and Butler (2007). In fact, these authors called this parameter the effective radius of the equivalent circular opening to approximate the elliptical tunnel in the (X, Y) coordinate. And in their contribution, Mathias and Butler (2007) showed that this approximation is good for large times but it can work well for small times as long as the anisotropic degree is moderate, i.e., $k_a=k_x/k_y<25$.

With this approximation, our diffusion problem in Eq. (3.49) represents the radial fluid flow in the conformal mapping plane of an equivalent isotropic medium with permeability k_e. Thus, the solution of transient flow obtained from the simplified approach presented in section 3.2.1 can be straightforwardly applied. For example, the total solution of pore pressure in the original problem as shown in Eq. (3.33) is now calculated with respect to the time-dependent influence radius $R_e(t_e)$ and $I_e(t_e)$ which are defined in ζ_w-plane as follow:

$$R_e^{\frac{R_e^2}{R_e^2-1}} \cong \sqrt{e}\left(1+\sqrt{\frac{\pi k_e t_e}{S^{**}}}\right); \quad I_e(t_e) = \frac{4k_e s_0}{2R_e(t_e)^2 \ln R_e(t_e) - R_e(t_e)^2 + 1} \tag{3.51}$$

while two parameters S^{**} and t_e are respectively equal to $S^{**} = S^* \sqrt{k_y / k_x}$ and $t_e = t/(r_0')^2$.

3.2.4. Numerical validation

In this sub-section, the closed form solution of deep tunnel's behavior under the one way hydro-mechanical coupling will be validated by comparing with the ones obtained from the numerical modeling which were also conducted by using the Aster_Code. The geometry of the numerical model is exactly similar as ones used in chapter 2 in the context of the steady flow of groundwater. Otherwise, the boundary conditions as used in this latter context are retained in the present simulations meaning that we impose the horizontal and vertical initial stresses ($\sigma_h = 12.5MPa, \sigma_v = 12.5MPa$), the initial pore pressure ($p_{ff} = 4.7MPa$) on the right–hand lateral and top boundary of the model while on the two other boundaries no normal displacement and flux are allowed. Otherwise, at the interface of liner and ground the pore pressure is kept constant at atmospheric pressure ($p_0=0$). In Fig. 3.4 is illustrated the numerical model used in our numerical simulations. Concerning the mechanical properties of of materials, all parameters used in chapter 2 are hold in the present studies which are $E_x = 5600MPa$, $E_y = 4000MPa$, $\nu_{xz} = 0.3$, $\nu_{yx} = 0.142$, $G_{xy} = 1600MPa$ for the rock mass and $E_s = 20GPa$ and $\nu_s = 0.3$ for the liner.

Technically, to simulate the one way hydro-mechanical coupling in Code_Aster, a specific procedure is used. More precisely, in the first stage the transient distribution of pore pressure in the rock mass will be evaluated by activating the purely hydraulic model. Then, in the second stage, the pore pressure field at each interested instant of time will be extracted to inject into the mechanical model as a body force field. Through this procedure the distributions of stress and displacement can be determined as consequence of the change of pore pressure.

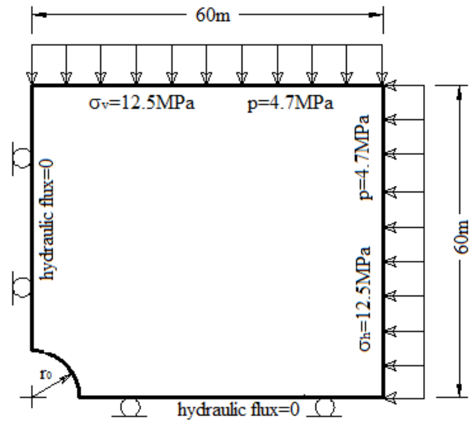

Fig.3-4: 2D plane strain model used in the numerical simulations by FEM

3.2.4.1. Case of saturated rock with isotropic hydraulic properties

As the first case of study, figures (Fig. 3-5 to Fig. 3-8) present the analytical results of pore pressure, radial displacement, effective radial and tangential stresses in comparison with the numerical ones in the context of the transient flow in the saturated rock with isotropic hydraulic properties. The isotropic permeability of saturated rock used in these calculations is $k=4\times10^{-13}(m/s)$. In general the comparison shows a very good agreement of the analytical and numerical results for different instants of time. For example in Fig. 3-5, one can state that the closed form solution of pore pressure fits quite well the curves obtained from the numerical simulations with the maximum relative error smaller than 5% at the very early instant of time ($t=1h$). With respect to the evolution of time, the relative error reduces representing a good agreement of the analytical and numerical simulation. The same remark can be noted for the displacement as well as effective radial and tangential stresses (Fig. 3-6 to Fig. 3-8). Otherwise, the results show that with respect to the evolution of time, displacement around the tunnel increases as consequence of the extension of the disturbed zone of pore pressure in the transient state (Fig. 3-6). This increase is significant at the distance far from the tunnel while the displacement is stable on the surface of tunnel. We can also observe that transient flow at small time can induce a drop in magnitude of effective radial stress in the zone near the tunnel (Fig. 3-7) which however retains in the compressional stress. This phenomenon will be considered in more details in the last subsection.

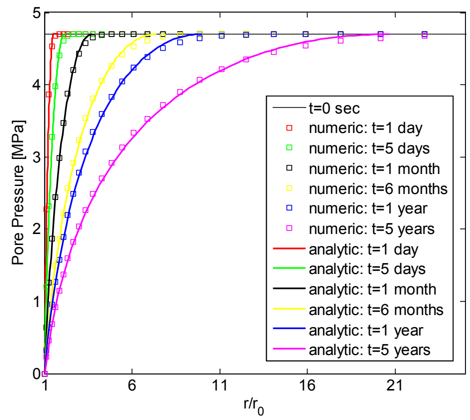

Fig. 3-5: Distribution of pore pressure in the radial direction (case of saturated rock with isotropic hydraulic properties $k_a=k_x/k_y=1$).

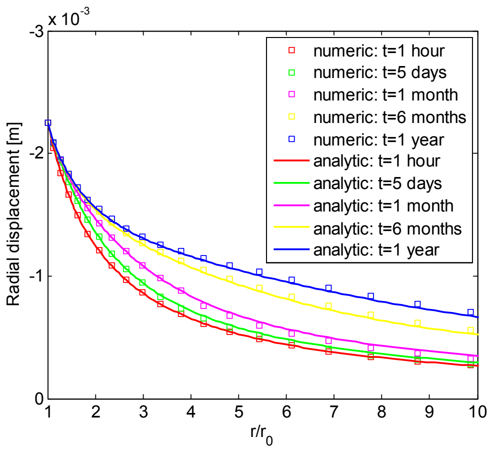

a) Radial displacement in the horizontal direction

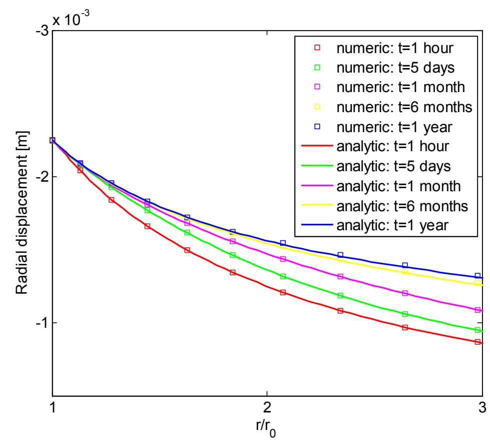

(b) Radial displacement in the horizontal direction (zoom around the tunnel)

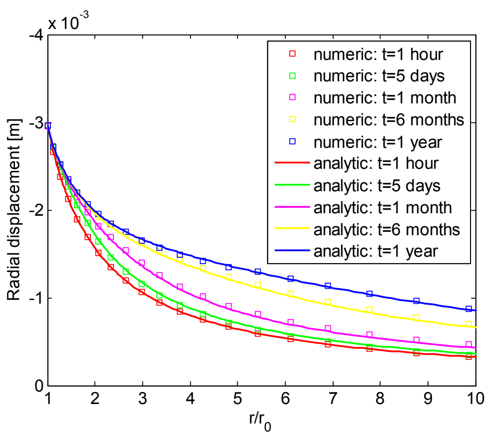

(c) Radial displacement in the vertical direction

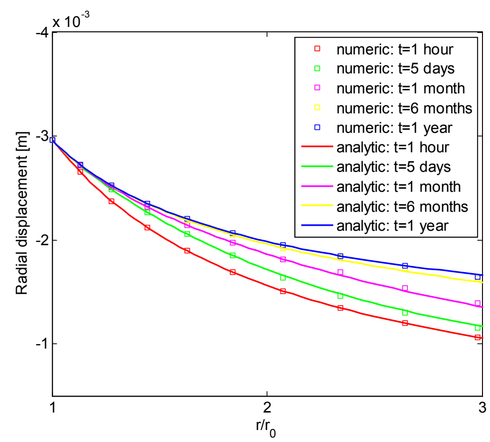

(d) Radial displacement in the vertical direction (zoom around the tunnel)

Fig.3-6: Radial displacement in the horizontal and vertical axes of symmetry of tunnel: comparison between the analytical and numerical solutions (case of saturated rock with isotropic hydraulic properties $k_a=k_x/k_y=1$).

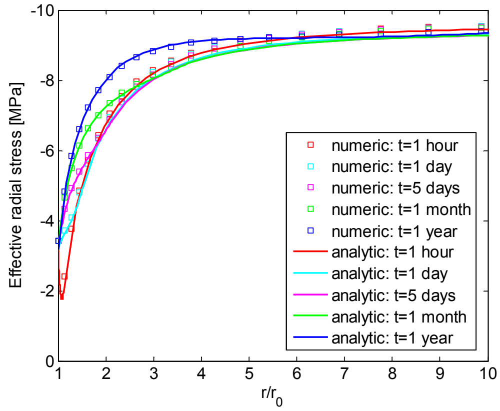

a) Effective radial stress in the horizontal direction

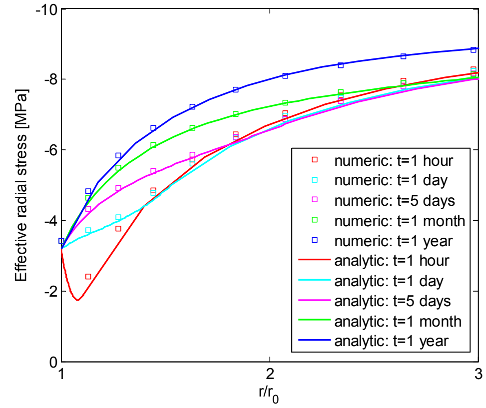

b) Effective radial stress in the horizontal direction (zoom around the tunnel)

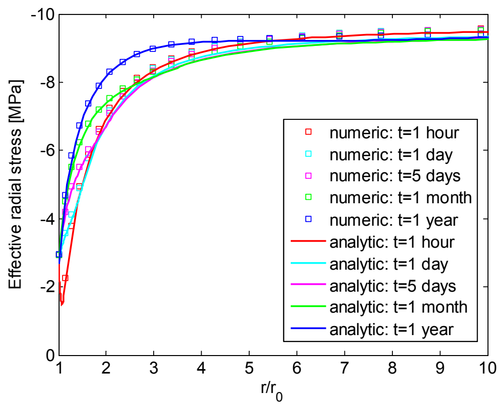

(c) Effective radial stress in the vertical direction

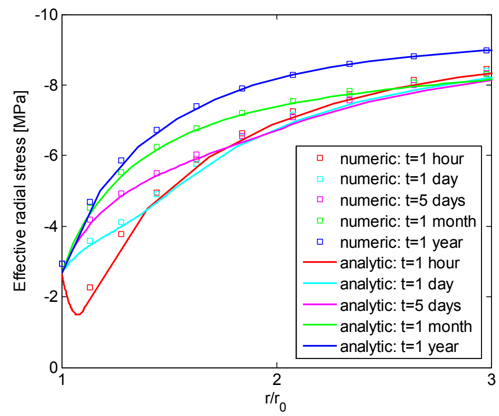

(c) Effective radial stress in the vertical direction (zoom around the tunnel)

Fig.3.7: Effective radial stress determined in the horizontal and vertical axes of symmetry of tunnel: comparison between the analytical and numerical solutions (case of saturated rock with isotropic hydraulic properties $k_a=k_x/k_y=1$).

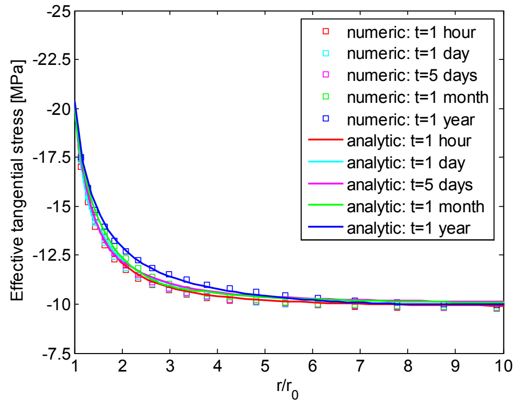

(a) Effective tangential stress in the horizontal direction

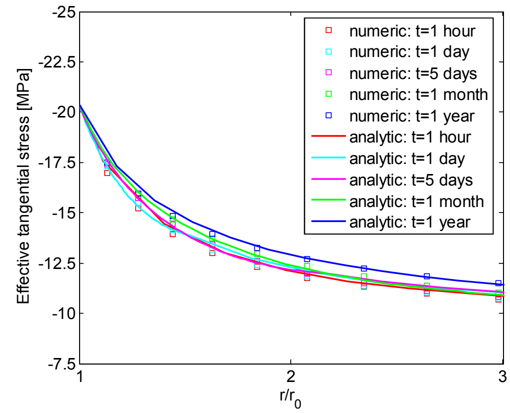

(b) Effective tangential stress in the horizontal direction (zoom around the tunnel)

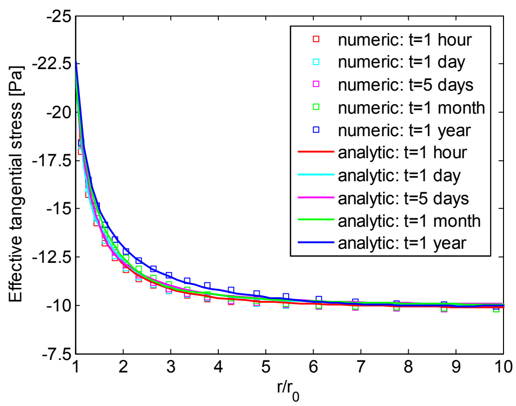

(c) Effective tangential stress in the vertical direction

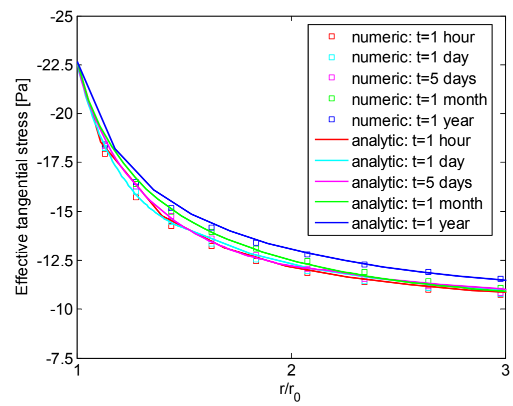

(d) Effective tangential stress in the vertical direction (zoom around the tunnel)

Fig.3.8: Effective tangential stress determined in the horizontal and vertical axes of symmetry of tunnel: comparison between the analytical and numerical solutions (case of saturated rock with isotropic hydraulic properties $k_a=k_x/k_y=1$).

3.2.4.2. Case of saturated rock with anisotropic hydraulic properties

The validation of the previous study case (saturated rock with isotropic hydraulic properties) allows us to investigate in this part the general case in which the anisotropic aspect of the hydraulic behavior of rock mass is accounted for. As detailed in subsection 3.2.3, the results of this latter case base principally on ones of the former case using the equivalent isotropic hydraulic medium.

Fig.3-9 are presented the results of the transient groundwater flow in saturated rock whose anisotropic hydraulic behavior is represented by two parameters $k_x = 4\times10^{-13} m/s$, $k_y = 1.33x10^{-13} m/s$ corresponding to an anisotropic degree $k_a=k_x/k_y=3$. For all instants, it shows that the analytical results of pore pressure match well with the numerical results. As consequence, no significant discrepancy is observed in term of displacement and stresses on the rock mass as illustrated in Fig.3-10 to Fig. 3-12. Similar to the previous case, it shows that the transient fluid flow will induce an increase of displacement in the surrounding rock, particular for the points far from the tunnel. However, following the horizontal symmetric axis, it exists a small zone near the tunnel ($r/r_0<1.5$) at which the displacement decreases slightly in time. In this zone, we also observe the drop in magnitude of effective radial stress for the first instants of time, the phenomenon noted in the previous study case. Concerning the effective tangential stress, a slight increase with time is observed. Thus, the variation of pore pressure due to transient flow induces primarily change of effective radial stress.

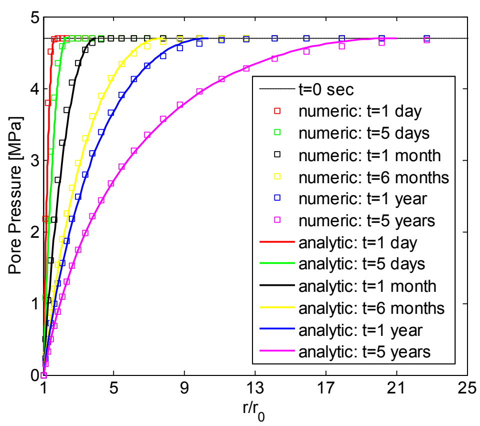

(a)

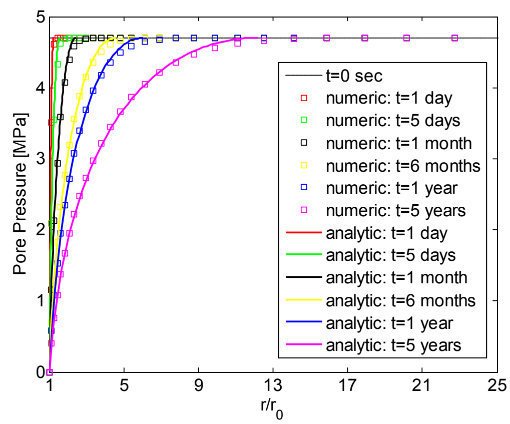

(b)

Fig. 3-9: Distribution of pore pressure: (a) in the horizontal direction, (b) in the vertical direction (case of saturated rock with anisotropic hydraulic properties $k_a=k_x/k_y=3$).

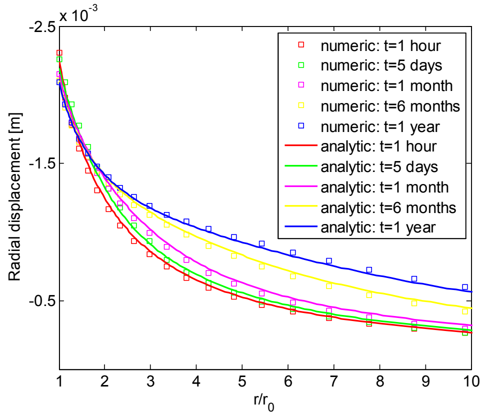

a) Radial displacement in the horizontal direction

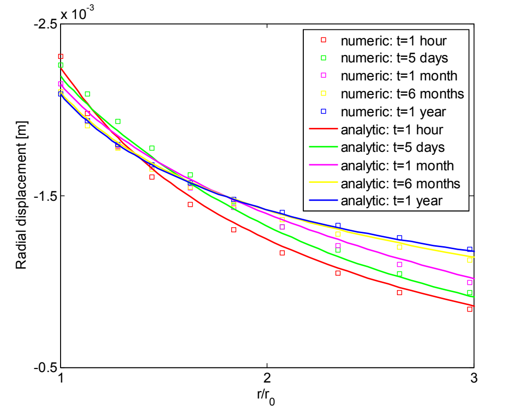

b) Radial displacement in the horizontal direction (zoom around the tunnel)

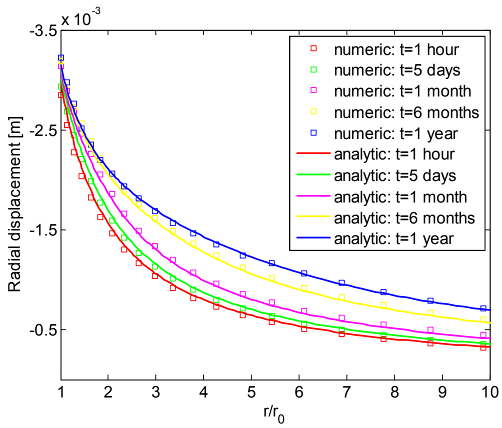

c) Radial displacement in the vertical direction

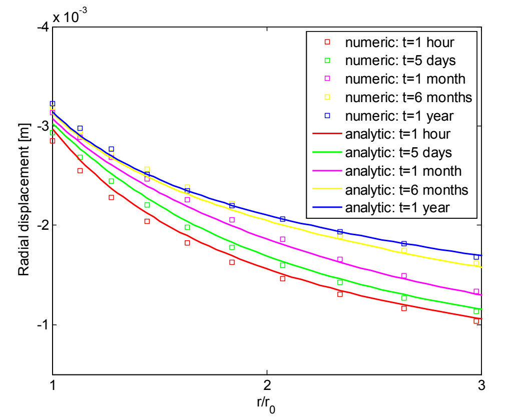

d) Radial displacement in the vertical direction (zoom around the tunnel)

Fig.3-10: Radial displacement in the horizontal and vertical axes of symmetry of tunnel: comparison between the analytical and numerical solutions (case of saturated rock with anisotropic hydraulic properties $k_a=k_x/k_y=3$).

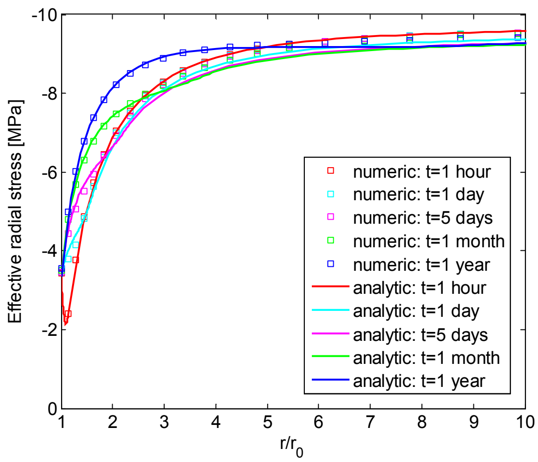

a) Effective radial stress in the horizontal direction

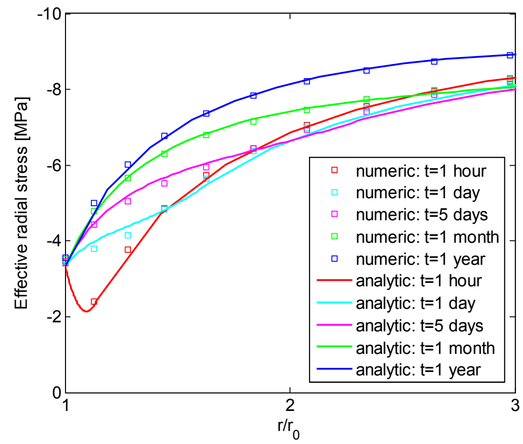

b) Effective radial stress in the vertical direction (zoom around the tunnel)

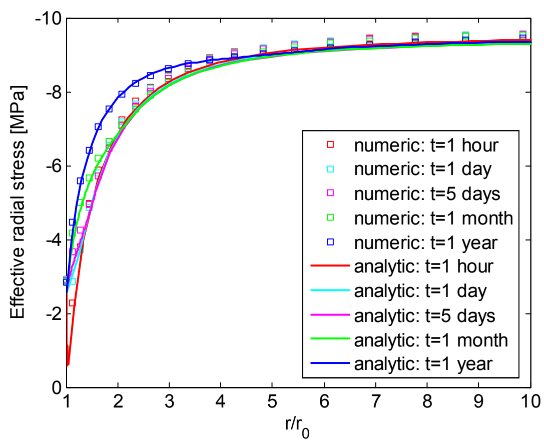

c) Effective radial stress in the vertical direction

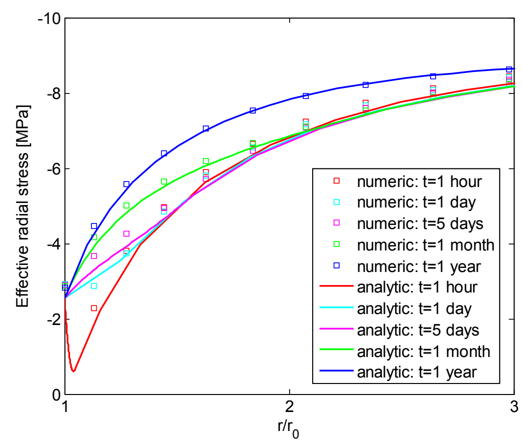

d) Effective radial stress in the vertical direction (zoom around the tunnel)

Fig.3-11: Effective radial stress determined in the horizontal and vertical axes of symmetry of tunnel: comparison between the analytical and numerical solutions (case of saturated rock with anisotropic hydraulic properties $k_a=k_x/k_y=3$).

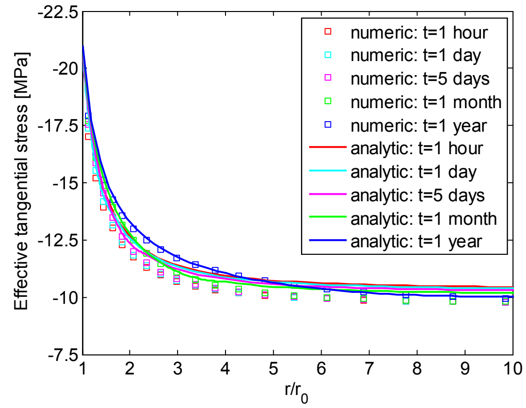

a) Effective tangential stress in the horizontal direction

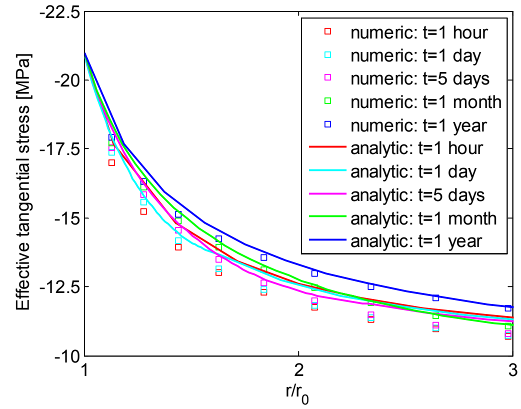

b) Effective tangential stress in the horizontal direction (zoom around the tunnel)

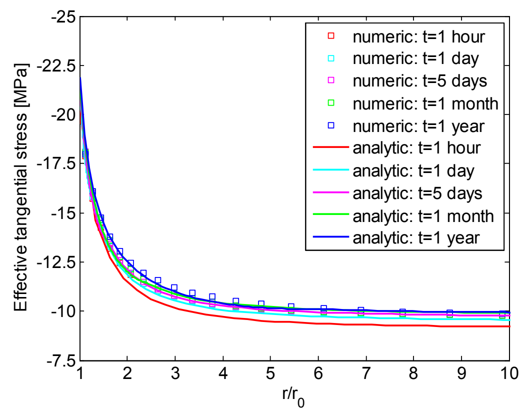

c) Effective tangential stress in the vertical direction

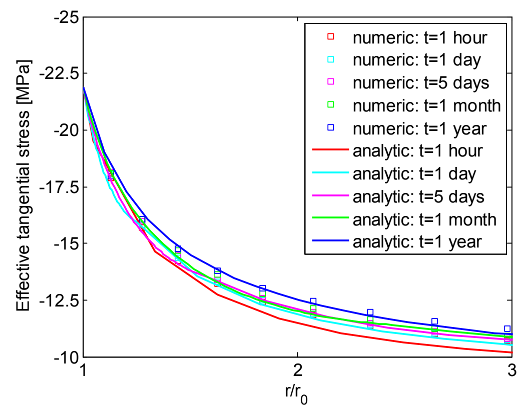

d) Effective tangential stress in the vertical direction (zoom around the tunnel)

Fig.3.12: Effective tangential stress determined in the horizontal and vertical axes of symmetry of tunnel: comparison between the analytical and numerical solutions (case of saturated rock with anisotropic hydraulic properties $k_a=k_x/k_y=3$).

As discussed by Mathias and Butler (2007) and Cihan *et al.* (2014), the approximation of the anisotropic diffusion problem by an equivalent isotropic ones matches well in case of moderate anisotropic ($k_x / k_y \leq 25$) while discrepancy can become significant (particular for the observed points near the bore well) with the increase of the anisotropic degree. Hence in what follow, this observation will be verified and we focus also on the mechanical response of tunnel as result of the hydro-mechanical coupling.

Figures (from Fig. 3-13 to Fig. 3-16) are illustrated the evolution of relative error (of pore pressure, effective radial and tangential stress and radial displacement) between the analytical and numerical with respect to time, to the anisotropic degree of the hydraulic properties and to the radius of tunnel. They were calculated at a point chosen near the surface of tunnel ($r/r_0=1.06$) at which we observe that the error is usually the most significant. The results show that, as a function of time, the relative error increases and attaints the maximum at an instant about $t=1h$ before decreasing. Otherwise, as expected, for all instants, the stronger anisotropic degree of the hydraulic properties will induce an increase of the relative error. It is also the case when the larger radius of tunnel will increase the error. As an example, at time $t=1h$, the relative error of pore pressure in case of radius $r_0=0.5m$ increases from 3.2% with anisotropic degree $k_a= 1$ to 13.5% when the anisotropy attaints $k_a=50$. The corresponding values for a larger radius of $r_0=1.5m$ are respectively 5% and 22%. Note that, at the same instant $t=1h$, the maximum relative error of pore pressure, radial displacement, effective radial and tangential stresses calculated with the smaller anisotropic degree $k_a=k_x/k_y=3$, as it is the case of Collovo Oxfordian rock, and with the radius $r_0=1m$ are respectively 7.4%, 6%, 7.4% and 4%. In addition, at the moderate anisotropy $k_a=k_x/k_y=25$ the relative error of all parameters (pore pressure, radial displacement, effective stresses) present the values inferior to 10%.

In our other investigations, the results show however that these relative errors will decrease importantly when the observed point goes far from the surface of tunnel. For instance, at the point $r/r_0=5$ the relative error can decrease two times with respect to the point shown above at $r/r_0=1.06$. For the sake of simplifying the presentation, the results calculated with this former point will not be detailed here.

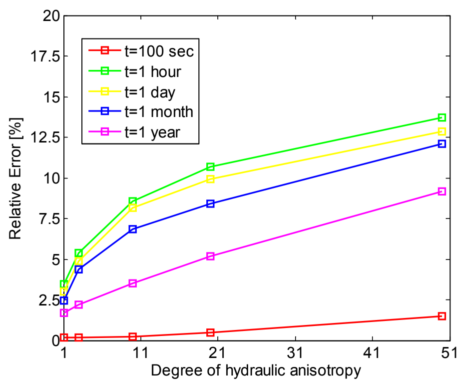

a) Relative error of pore pressure (case r_0=0.5m)

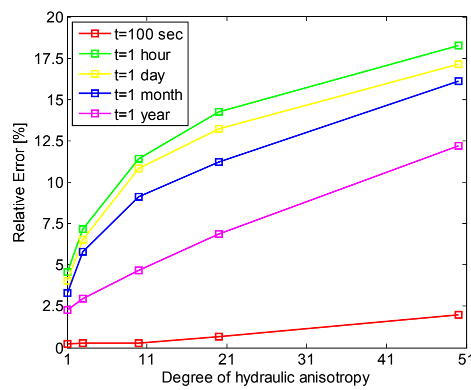

b) Relative error of pore pressure (case r_0=1.0m)

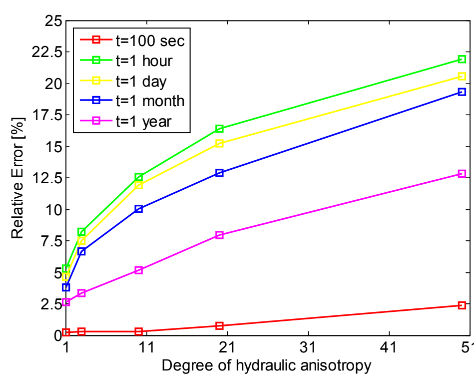

c) Relative error of pore pressure (case r_0=1.5m)

Fig.3-13: Relative error (%) between the analytical and numerical results of pore pressure in the horizontal direction as function of degree of hydraulic anisotropy ($k_a=k_x/k_y$) at different instants of time and with different radius r_0 of tunnel.

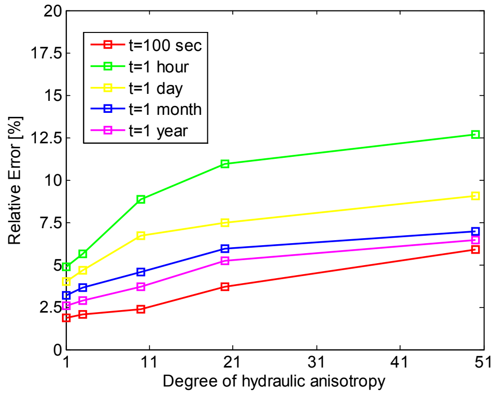

a) Relative error of effective radial stress (case r_0=0.5 m)

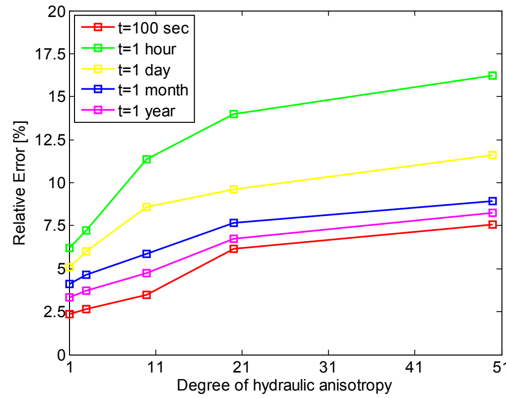

b) Relative error of effective radial stress (case r_0=1.0 m)

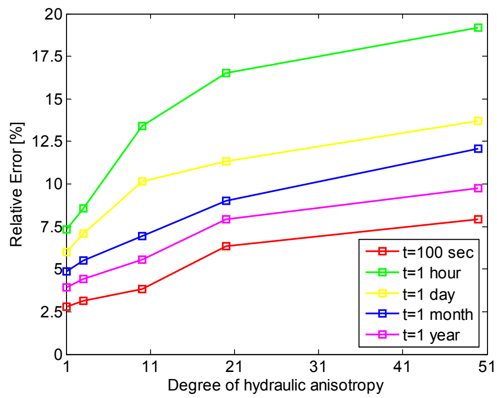

c) Relative error of effective radial stress (case r_0=1.5 m)

Fig.3-14: Relative error (%) between the analytical and numerical results of effective radial stress in the horizontal direction as function of degree of hydraulic anisotropy ($k_a=k_x/k_y$) at different instants of time and with different radius r_0 of tunnel.

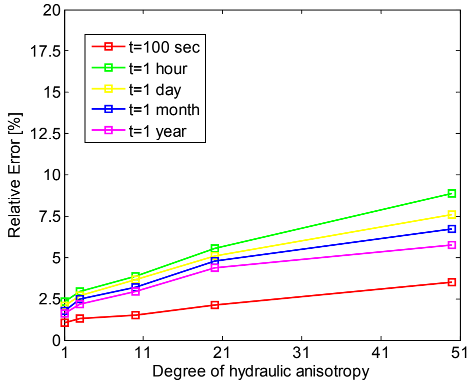

a) Relative error of effective tangential stress (case r_0=0.5 m)

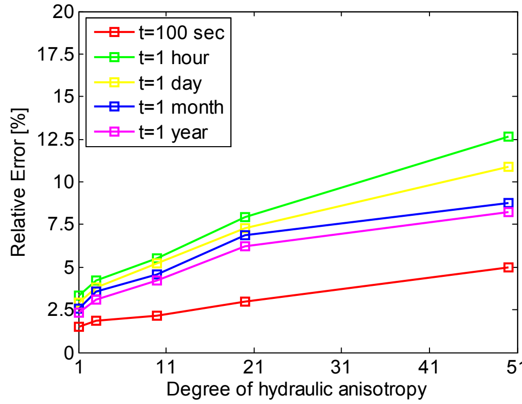

b) Relative error of effective tangential stress (case r_0=1.0 m)

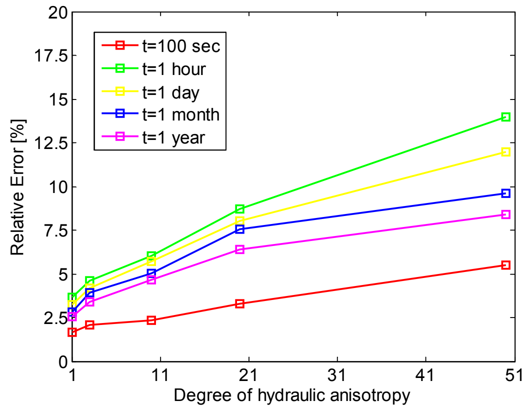

c) Relative error of effective tangential stress (case r_0=1.5 m)

Fig.3-15: Relative error (%) between the analytical and numerical results of effective tangential stress in the horizontal direction as function of degree of hydraulic anisotropy (k_a=k_x/k_y) at different instants of time and with different radius r_0 of tunnel.

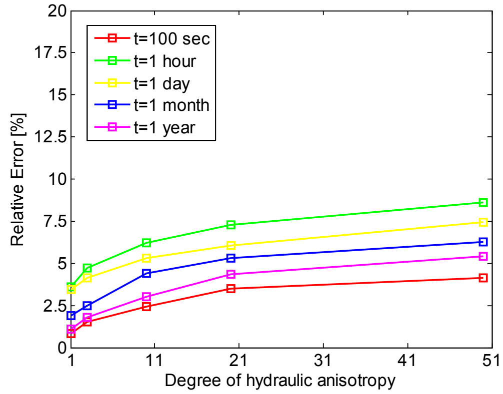

a) Relative error of radial displacement (case r_0=0.5 m)

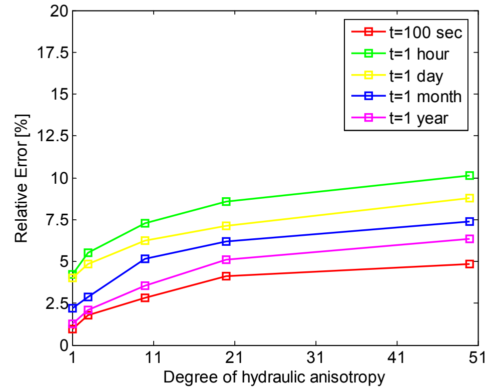

b) Relative error of radial displacement (case r_0=1.0 m)

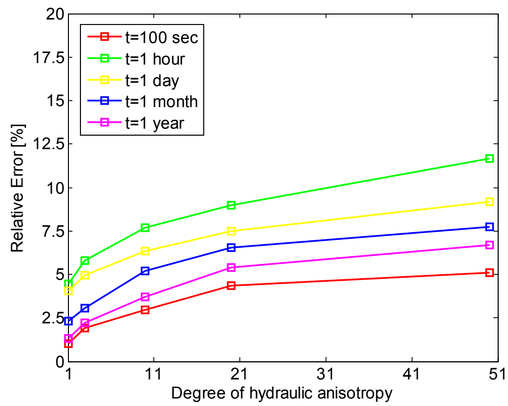

c) Relative error of radial displacement (case r_0=1.5 m)

Fig.3.16: Relative error (%) between the analytical and numerical results of radial displacement in the horizontal direction as function of degree of hydraulic anisotropy ($k_a=k_x/k_y$) at different instants of time and with different radius r_0 of tunnel.

3.2.4.3. Behavior of tunnel without liner

In all previous numerical validations, we observe that the transient flow of groundwater in small time can induce a drop in magnitude of the effective radial stress. The other studies show that this phenomenon can become significant particularly in case of unlined tunnel when a tensile stress can be observed near the surface of tunnel. The results highlighted in Fig. 3.17 show that the effective tensile radial stress appears all around the tunnel (not only in the horizontal but also in the vertical direction) at small time (t=100s and t=1h). Finally to demonstrate the effect of liner on the distribution of stress (particularly the effective radial stress) in Fig. 3.18 we compare the results obtained from two cases of unlined and lined tunnel. We state that the difference is remarkable in the zone near the tunnel and in case of unlined tunnel the transient fluid flow at small time can induce an effective tensile radial stress.

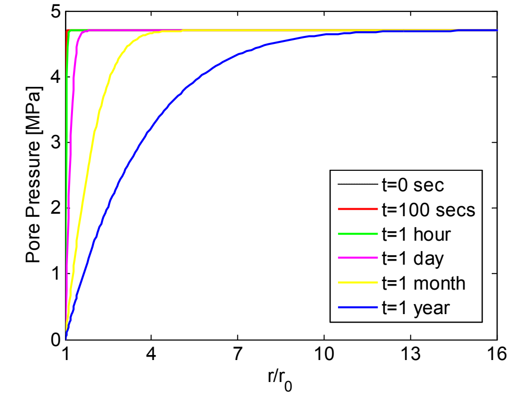

Pore pressure in the horizontal direction

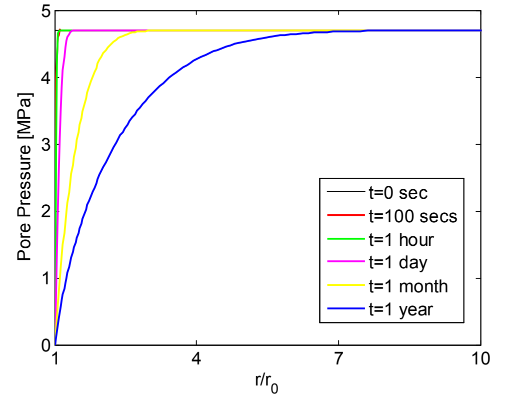

Pore pressure in the vertical direction

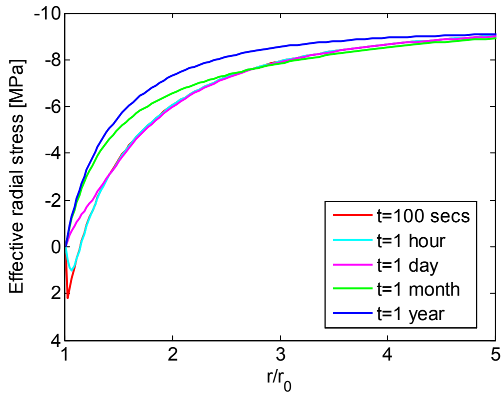

Effective radial stress in the horizontal direction

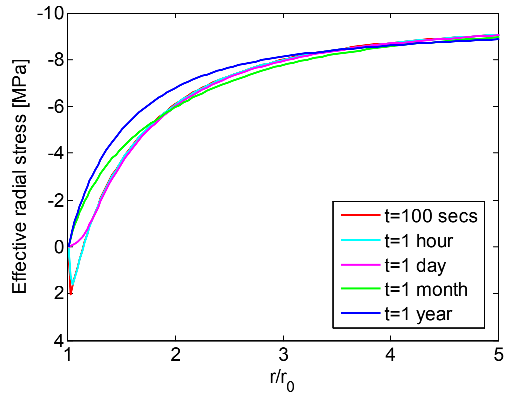

Effective radial stress in the vertical direction

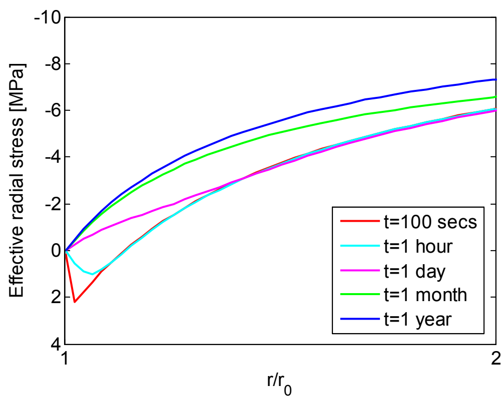

Effective radial stress in the horizontal direction (zoom in the range near the tunnel)

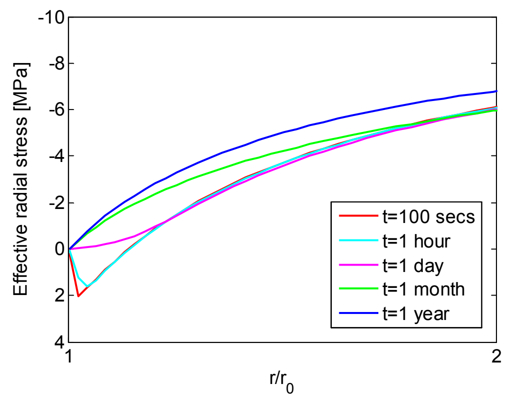

Effective radial stress in the vertical direction (zoom in the range near the tunnel)

Fig.3.17: Pore pressure and effective radial stress in the horizontal and vertical direction of unlined tunnel. The results calculated at different instants.

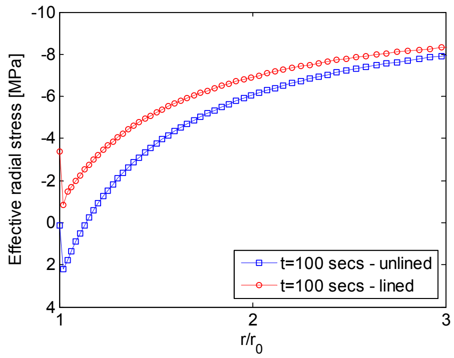

Effective radial stress in the horizontal direction

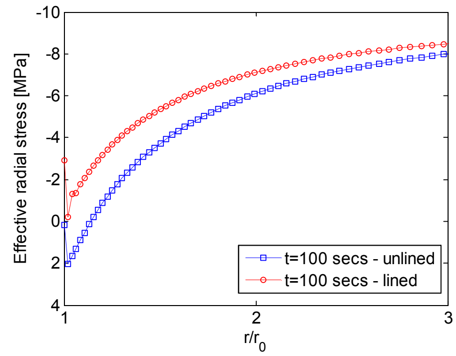

Effective radial stress in the vertical direction

(a) Instant t=100s

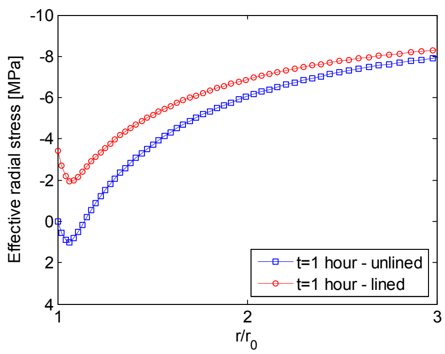

Effective radial stress in the horizontal direction

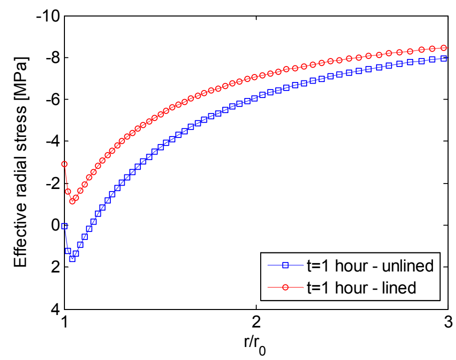

Effective radial stress in the vertical direction

(b) Instant t=1h

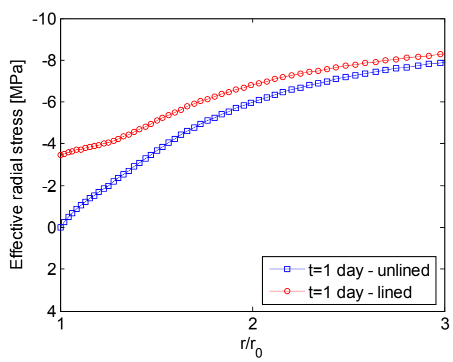

Effective radial stress in the horizontal direction

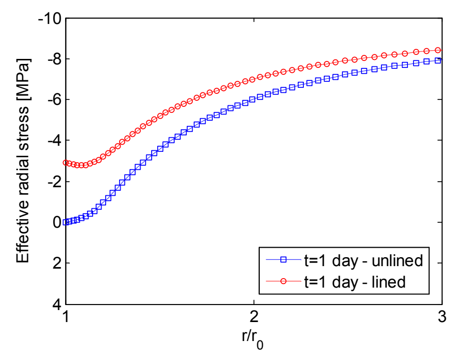

Effective radial stress in the vertical direction

(b) Instant t=1day

Fig.3.18: Comparison of effective radial stress in the horizontal and vertical directions between the unlined and lined tunnel.

3.3.Deep tunnel behaviour in saturated rock with transient groundwater flow: numerical solution in the context of two ways poroelastic coupling

One considered in the previous part the influence of the transient fluid flow as well as the anisotropic effect on the mechanical response of tunnel. A closed form solution was presented and validated but it is limited only in case of the one way hydro-mechanical coupling (H→M). In this latter context, it is known that only changes in the pore pressure field can induce changes in stresses and strains. This one way coupling is appropriable and particularly useful in case where the mass balance is mainly controlled by the pressure rather than by the stresses of the solid. However its application on studying the behavior of deep tunnel can be seen as a strong hypothesis due to the fact that for this kind of problem, changes of stress can have a significant effect on the changes of pore pressure and so on. Thus in this part, with aim to verify the importance of this latter effect (M→H), we will investigate the response of deep tunnel in the context of a fully (or two ways) hydro-mechanical coupling (H↔M). This could be done through the numerical simulations using the FEM Aster_Code. Note that the geometric model, the boundary and initial conditions as well as the hydro-mechanical properties of the materials are similar to the ones used in section 3.2.4 to validate the analytical solution. The only difference is that the fully hydro-mechanical coupling is chosen instead of one way coupling.

Figs. 3-19 and 3-20 illustrate the isovalues of pore pressures and effective radial stresses around the tunnel which are captured at first instants of time. As exhibited in Fig. 3.19, at the vicinity of tunnel, an overpressure zone appears with a maximum pore pressure observed at instant about 1hour. The overpressure takes place in both cases of unlined and lined tunnel while the presence of liner seems to reduce the magnitude of the overpressure. This phenomenon demonstrates the important effect of the M→H coupling where changes of stress will induce changes of pore pressure which cannot be observed in our previous study case of one way hydro-mechanical coupling.

Another noteworthy point as shown in Fig. 3.20 is that we can observe a domain of effective tensile radial stress which occurs in the vicinity of the unlined tunnel. This zone appears immediately after the simultaneous excavation. With regard to the considered material parameters and modeling hypothesis used here, the tensile stress takes the maximum magnitude about of 4.74 MPa (case of unlined tunnel) and 0.85 MPa (case of lined tunnel) in small time t=100s. This is because, in the vicinity of the tunnel, due to the instantaneous excavation, the total radial stress decreases strongly (and equal to zero on the tunnel's wall), whereas the pore pressure remains almost its initial value. Therefore, according to the Biot's effective stress theory, the radial effective stress can take the positive value in this region. Although the fact that this tensile stress is quite small, it can induce, in the surrounding rock mass (particularly in case of unlined tunnel) owning a low tensile resistance, a nucleation of crack. The contribution of the mechanical effect on the distribution of pore pressure and hence on the final response of tunnel is elucidated in figures (from Fig. 3.21 to Fig. 3.23) by comparing the numerical results conducted on the unlined tunnel using the one way and two ways coupling. Indeed, we can state an important gap in the distribution of pore pressure, stress and displacement mostly in the first days marked by an important overpressure and more significant effective tensile radial stress in the case of two ways coupling. As a function of time, gap reduces and at an instant about one month, the difference between the two methods of coupling becomes negligible.

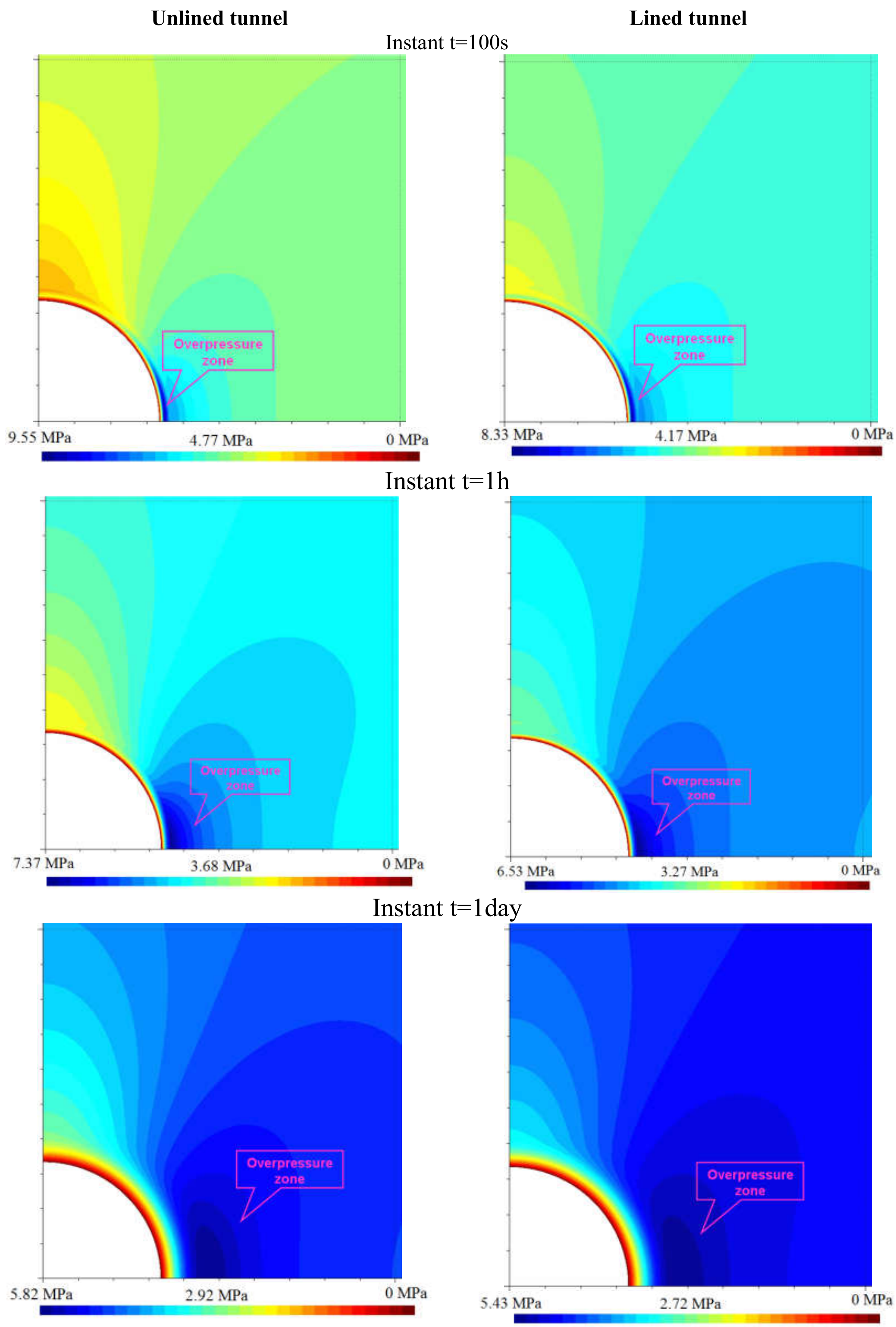

Fig.3-19: Distribution of pore pressure around the tunnel (with and without liner) at different instants. The results highlight the appearance of the overpressure zone near the tunnel when the two ways hydro-mechanical coupling is accounted for.

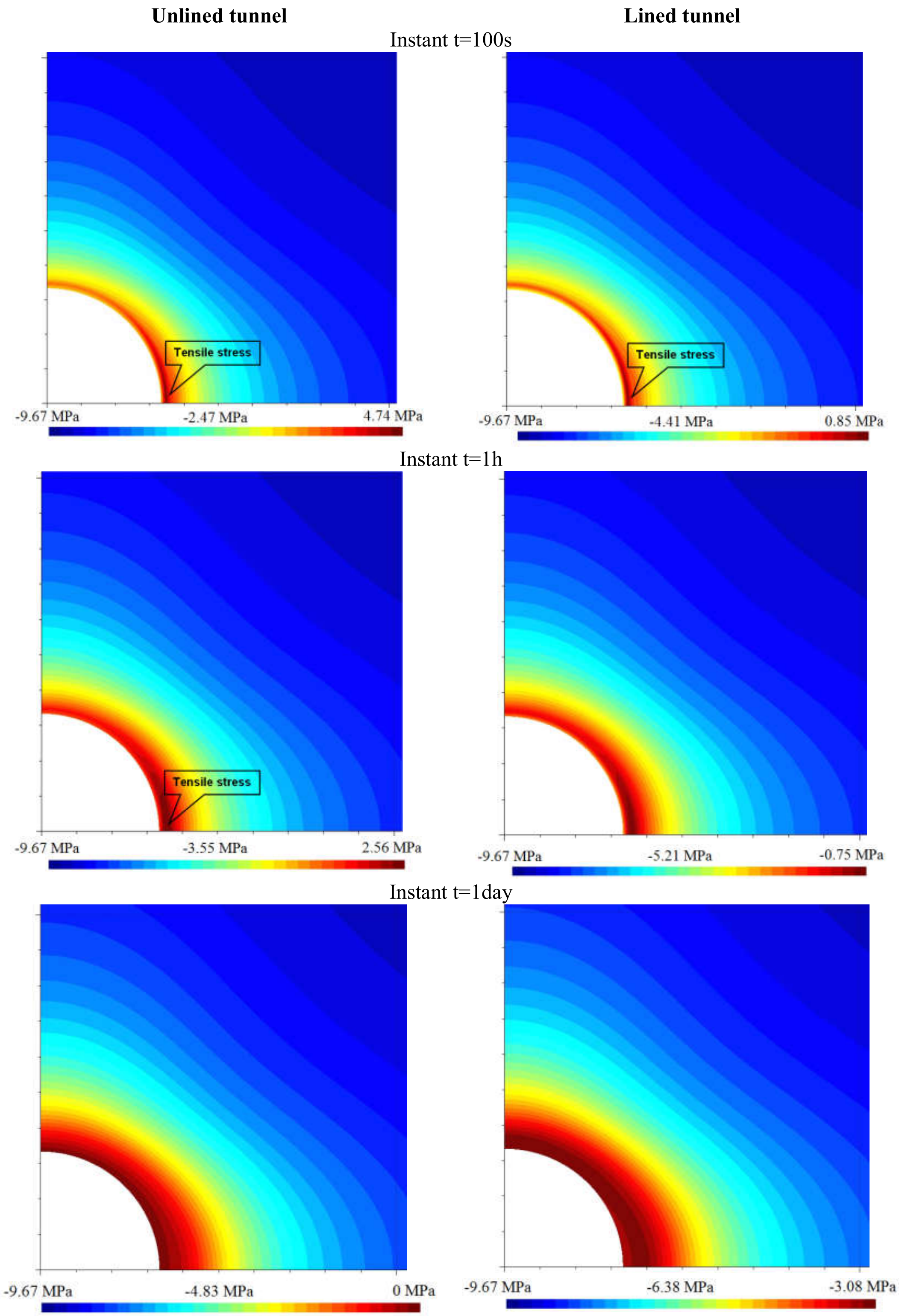

Fig.3-20: Distribution of effective radial stress around the tunnel (case with and without liner) at different instants. The results highlight the appearance of the tensile stress near the tunnel without liner at small times.

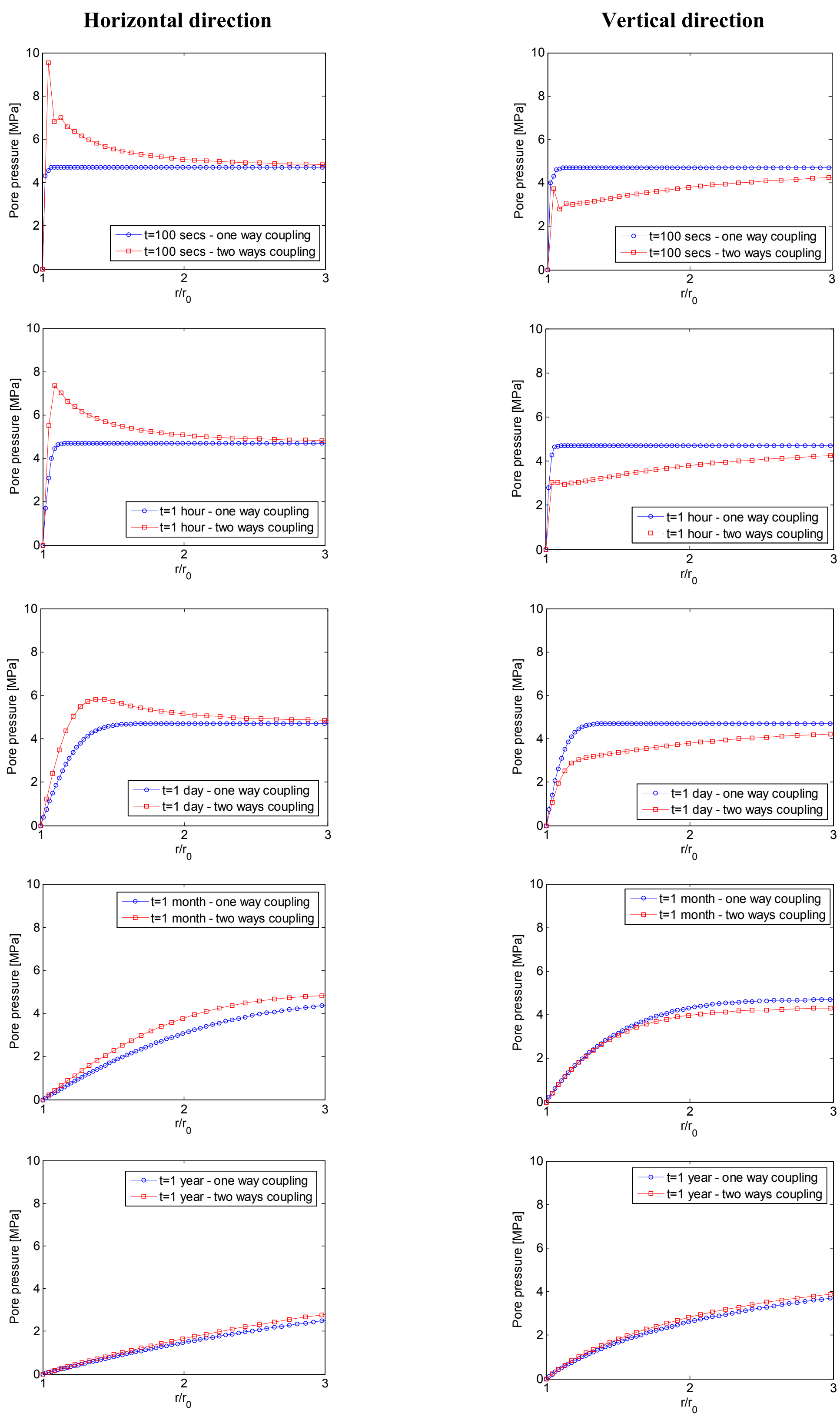

Fig.3-21: Distribution of pore pressure around the tunnel: comparison between the one way and two ways coupling at different instants.

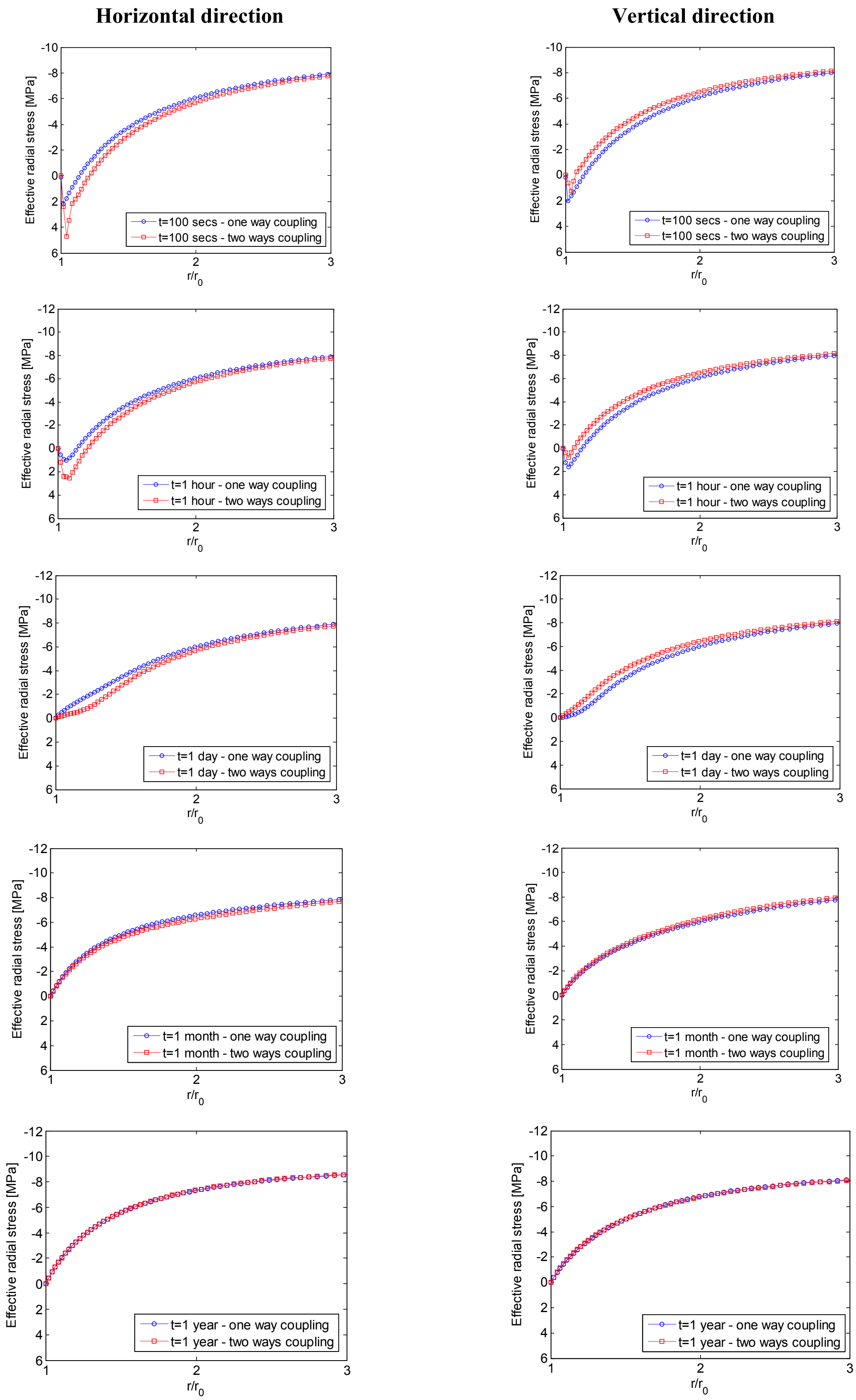

Fig.3-22: Distribution of effective radial stress around the tunnel: comparison between the one way and two ways coupling at different instants.

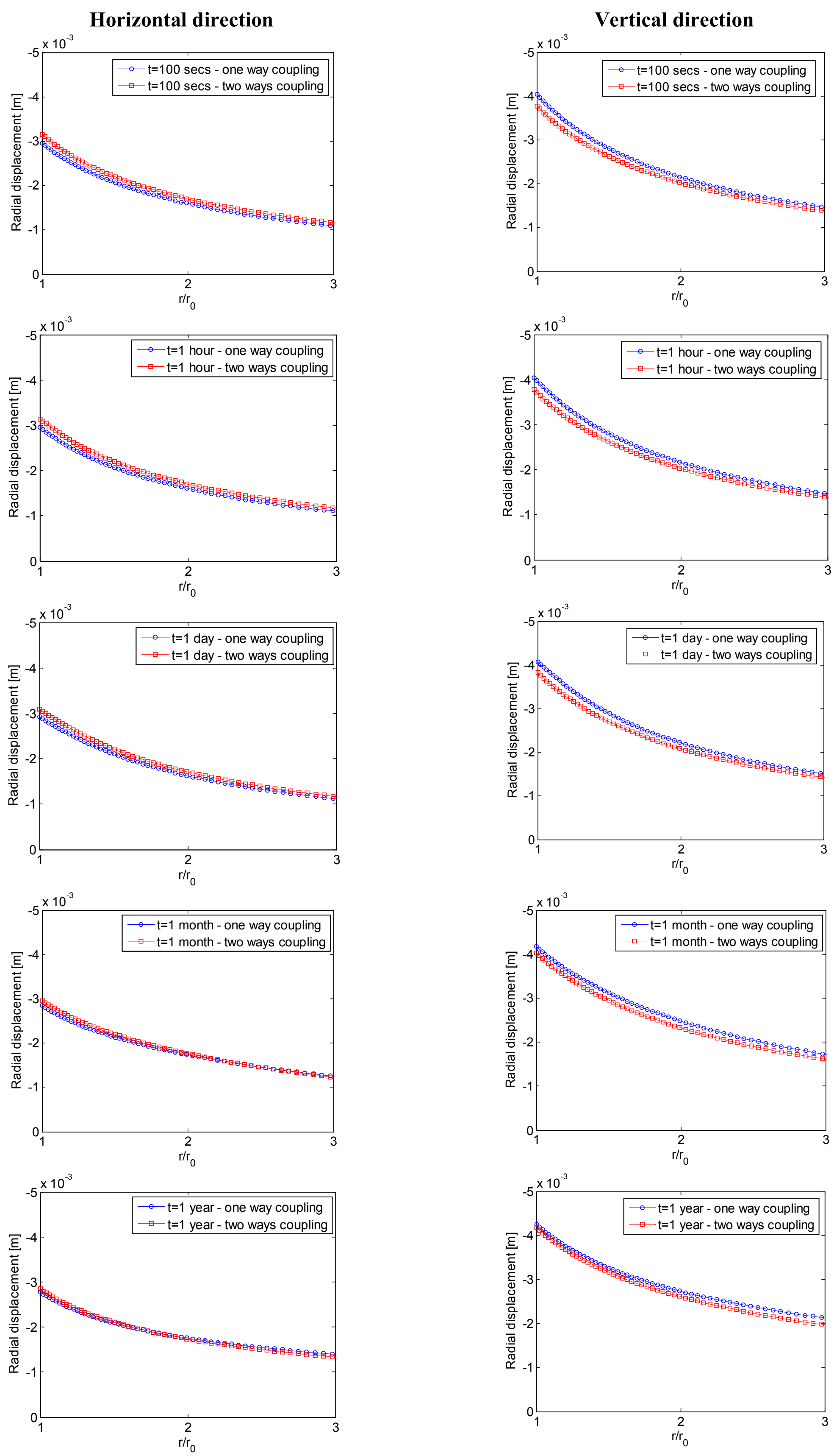

Fig.3-23: Distribution of radial displacement around the tunnel: comparison between the one way and two ways coupling at different instants.

The results presented above demonstrate the important role of the fully hydro-mechanical coupling on the distribution of pore pressure and mechanical response in the surrounding rock mass. More precisely, in case of the tunnel without liner, it exist a small zone near the surface of tunnel at which we observed the overpressure and the effective tensile radial stress in the first instants of transient flow of groundwater. To go insight, in the following study, our goal consists in investigating the influence of different hydro-mechanical properties on this phenomenon. Thanks to the previous parametric study conducted in chapter 2, it shows that the principal parameters like the hydraulic anisotropic degree, the Poisson ratio ν_{yz}, the shear modulus (G_{xy}) and the ratio of Young's modulus (E_y/E_x) could have an important effect on the response of tunnel and hence here our interest focuses only on these parameters.

In figures (from Fig. 3.24 to 3.27) are illustrated the influence of these parameters on the distribution of pore pressure and effective radial stress evaluated at instant t=1hour. From the results illustrated in Fig. 3.24 and Fig. 3.25, it seems that the changes in magnitude of the overpressure and the effective tensile radial stress do not depend on the anisotropic degree of permeability while the influence of the Poisson's ratio ν_{yz} is really moderate. Attention is dedicated to the two other parameters: the shear modulus (G_{xy}) and the ratio of Young's modulus (E_y/E_x) whose influence are respectively elucidated in Fig. 3.26 and 3.27. The results show that a decrease of the shear modulus (G_{xy}) can amplify the overpressure in the pore space as well as the tensile stress in the vicinity of the tunnel. For a quite small value of shear modulus, overpressure can appear all around the surface of the tunnel, not only in the horizontal but also in the vertical symmetric axis of tunnel as captured in Fig. 3.26. Quantitatively, a decrease of shear modulus from 1600MPa to 560MPa induces an increase of pore pressure from 7.8MPa to 12.2MPa, this latter is about 2.6 times the initial pore pressure, while tensile stress increases from 3.9MPa to 6.3MPa respectively. The variation in magnitude of overpressure as well as effective tensile radial stress is also remarkable with respect to the ratio of Young's modulus. More precisely, by fixing the Young modulus E_x and decreasing the other Young's modulus E_y, we can state a significant increase in magnitude of overpressure and tensile radial stress in the horizontal direction as exhibited in Fig. 3.27. As an example, we will compare the results calculated at the point near the surface of tunnel ($r/r_0=1.06$) with two ratios $E_y/E_x=1$ and $E_y/E_x=0.5$ who show that: the pore pressure changes from 6.2MPa to 9.9MPa in the horizontal direction (6.4MPa to 0.1MPa in the vertical direction) while the effective radial stress changes from 3.1MPa to 5MPa in the horizontal direction (3.1MPa to -0.3MPa in the vertical direction).

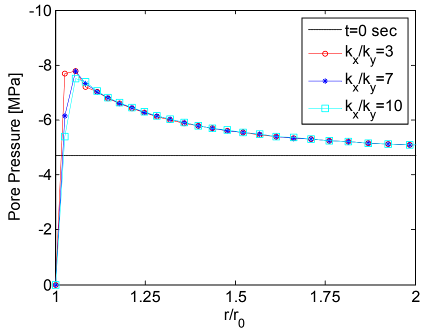

a) Pore pressure in the horizontal direction

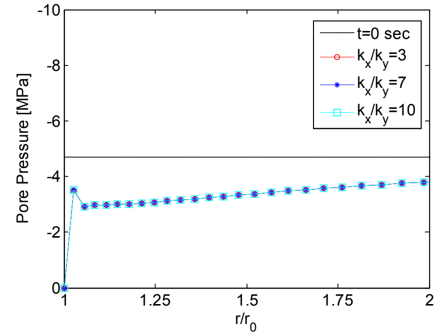

b) Pore pressure in the vertical direction

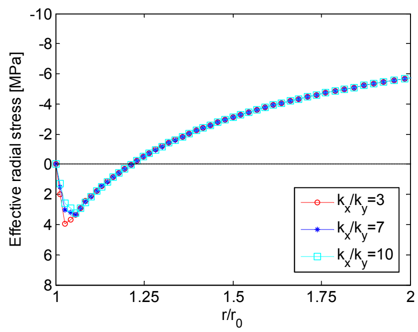

c) Effective radial stress in the horizontal direction

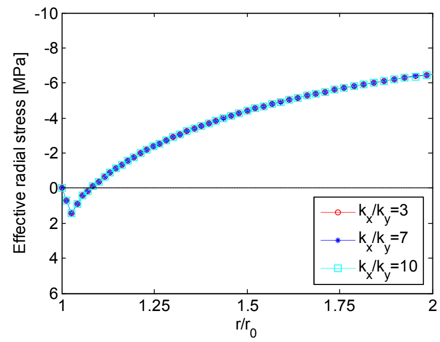

d) Effective radial stress in the vertical direction

Fig.3-24: Influence of the hydraulic anisotropic degree on the distribution of pore pressure and effective radial stress. The results calculated at instant t=1h.

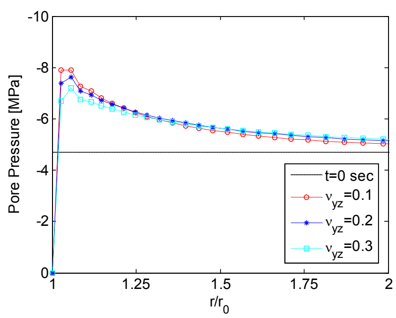

a) Pore pressure in the horizontal direction

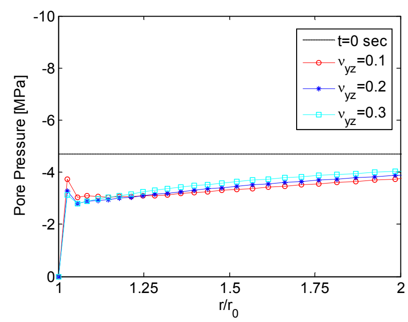

b) Pore pressure in the vertical direction

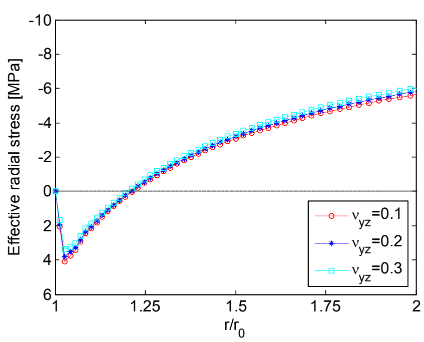

c) Effective radial stress in the horizontal direction

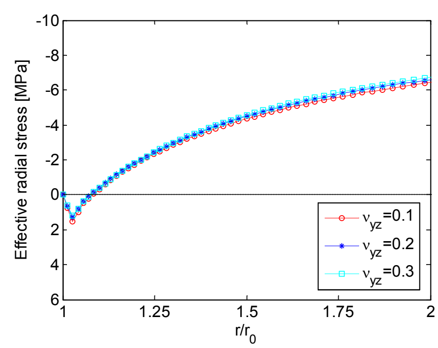

d) Effective radial stress in the vertical direction

Fig.3-25: Influence of the Poison's ratio ν_{yz} on the distribution of pore pressure and effective radial stress. The results calculated at instant t=1h.

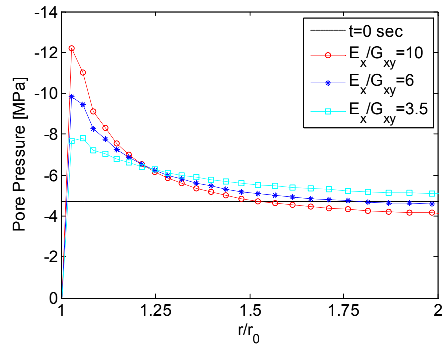

a) Pore pressure in the horizontal direction

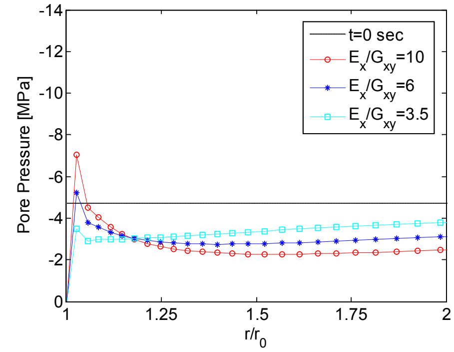

b) Pore pressure in the vertical direction

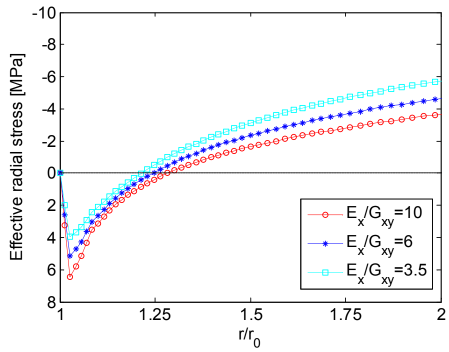

c) Effective radial stress in the horizontal direction

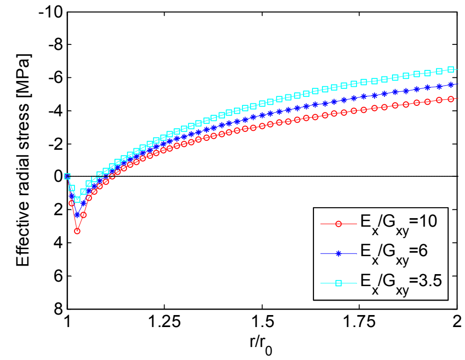

d) Effective radial stress in the vertical direction

Fig.3-26: Influence of shear modulus (G_{xy}) on the distribution of pore pressure and effective radial stress. The results calculated at instant t=1h.

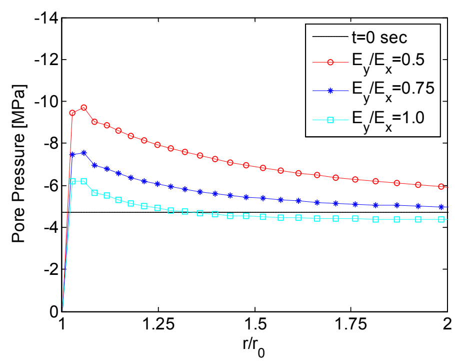

a) Pore pressure in the horizontal direction

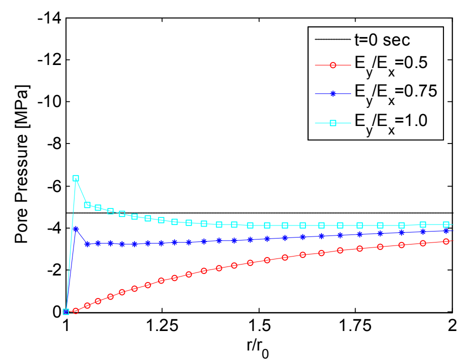

b) Pore pressure in the vertical direction

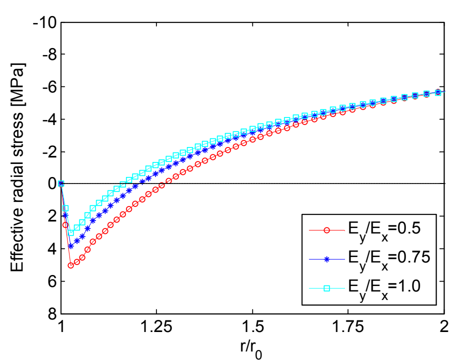

c) Effective radial stress in the horizontal direction

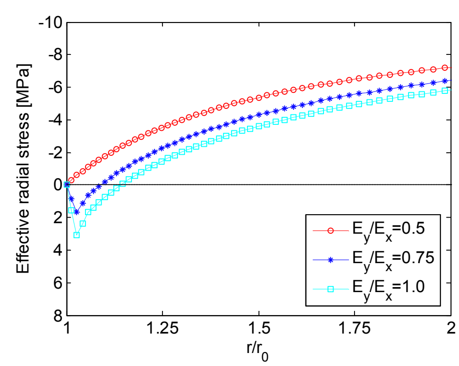

d) Effective radial stress in the vertical direction

Fig.3-27: Influence of the ratio of Young's modulus (E_y/ E_x) on the distribution of pore pressure and effective radial stress. The results calculated at instant t=1h.

3.4.Conclusions

Behavior of deep tunnel excavated in anisotropic saturated rock is investigated in this chapter in a general context by accounting for the water flow in the transient state. Firstly, our attention is focused on the effect of pore pressure during the transient fluid flow on the mechanical response of tunnel and the problem was solved by using the one-way hydro-mechanical coupling. For this purpose, the closed-form solution based on the complex potential approach, which was detailed in previous chapter in the context of steady flow, is now extended to take into account the time effect on the hydraulic diffusion equation. The principal idea relies on the way to treat this last equation by considering the transient solution as a successive steady state snapshots represented by a time dependent radius beyond which no flow can be occurred. Once the analytical solution of the pore pressure's distribution is obtained, the mechanical response of tunnel can be evaluated analytically thanks to using the complex potential approach whose procedure is similar as ones presented in the previous chapter. By comparing with the results obtained from the numerical simulations, a good agreement was noted when the anisotropic degree of the hydraulic properties of rock mass is moderate. The difference becomes significant, particularly for points near the surface of tunnel when this anisotropic degree of the hydraulic properties increases and/or the radius of tunnel is taken larger. In the second part, the interest relies on the behavior of tunnel in the framework of the fully hydro-mechanical coupling in which impact of the mechanical response on the distribution of pore pressured is accounted for. This study totally based on the numerical simulations highlighted that changes of stress can induce in the vicinity of tunnel an overpressure zone at short time, the phenomenon that is not observed when the one-way coupling is considered. By comparing the results obtained from two coupling methods (one way H→M and two ways H↔M), it is observed that the difference is essentially noted in short times (and ranging to about several days) represented by the overpressure phenomenon and a higher effective tensile radial stress in the case of two ways hydro-mechanical coupling. Particularly, in this latter context, the effective tensile radial stress appearing in the vicinity of the unlined tunnel exhibits a quite significant value which could induce a nucleation of crack in the rock mass due to a low tensile resistance.

Conclusions:

Comportement du tunnel profond creusé dans un massif rocheux saturé a été étudié dans ce chapitre dans un contexte général du couplage hydromécanique en tenant compte du régime hydraulique transitoire. Dans le premier temps, on porte une attention particulière à l'évolution de la distribution de pression de pores au cours de l'écoulement progressif. En suite le problème de l'effet de cette distribution sur la réponse mécanique du tunnel a été résolu en utilisant le couplage à sens unique. Dans ce but, la solution analytique basée sur l'approche du potentiel complexe, détaillée dans le chapitre précédent dans le contexte de l'écoulement en régime permanent, est maintenant étendue pour prendre en compte l'effet du temps sur l'équation de diffusion hydraulique. L'idée de base du traitement de l'équation d'écoulement est de considérer le régime transitoire comme une succession d'équilibres successifs de régimes permanents dont la zone perturbée hydrauliquement est représentée par un rayon qui évolue en fonction du temps. Pour un moment donné, au-delà de ce rayon aucun flux hydrique n'existe.

Une fois la solution analytique de la répartition de la pression interstitielle pour un temps donné est obtenue, la réponse mécanique du tunnel peut être évaluée analytiquement grâce à l'utilisation de l'approche du potentiel complexe dont la procédure est similaire à celle du chapitre précédent. En comparant les résultats obtenus par la solution analytique avec ceux des simulations numériques aux éléments finis, un bon accord a été noté lorsque le degré d'anisotropie des propriétés hydrauliques du massif rocheux est modéré. La différence devient importante, surtout pour les points proches de la paroi du tunnel lorsque ce degré d'anisotropie des propriétés hydrauliques augmente et/ou le rayon du tunnel est de plus en plus grand.

Dans un second temps, nous avons étudié plus en détails la différence entre couplage unilatérale et un couplage complet. Cette étude basée sur les simulations numériques a mis en évidence que les variations du stresses dans le voisinage de la paroi du tunnel peut induire, pendant la phase de creusement une zone de surpression aux premier instants et ce phénomène n'est pas observé lorsque le couplage à sens unique est considéré. En comparant les résultats obtenus des deux méthodes de couplage (à sens unique H→M et complete H↔M), on constate que les différences sont essentiellement observées dans les temps courts (à quelques jours) conduisant à des phénomènes de surpression et une contrainte radiale effective en traction plus élevée dans le cas du couplage hydro-mécanique complet. En particulier, dans ce dernier contexte, la contrainte radiale effective en traction apparaissant dans le voisinage du tunnel non soutenu présente une valeur significative qui pourrait induire une zone de fissuration initiale dans le massif rocheux en raison d'une résistance en traction faible de ce dernier.

CHAPTER 4: APPLICATION OF THE CLOSED FORM SOLUTION ON CONVERGENCE – CONFINEMENT METHOD

4.1. Introduction

The excavation of a tunnel taking into account the effect of the tunnel face is a three-dimensional problem. One of the methods to study the tunnel excavation by two-dimensional plane strain problem which can account for three-dimensional effect of the tunnel face to the sections behind and ahead of the face is convergence-confinement method (Panet and Guenot, 1982). Following that, the effect of the movement of the tunnel face is then equivalent to the reduction of an inner fictive pressure on the tunnel wall, from the initial pressure dominating the excavation to a zero pressure when the tunnel face advances far enough from the considered section. This method also takes into account the interaction between the rock mass and support.

This method applies to symmetric problem of deep, uniformly supported, circular tunnels embedded in an isotropic rock mass subjected to uniform in-situ stresses.

Extensions of the conventional convergence-confinement method have been tried for the case where the initial pre-stress is anisotropic by Einstein and Schwartz (1979) and then by Gill and Leite (1995) for an elastic material.

In this chapter, a solution based on the approach of the convergence-confinement method to study the interaction between the rock mass and the support for a deep tunnel in anisotropic poro-elastic medium will be presented. This solution is considered as an extension of the solution presented in chapter two which can take into account the influence of the tunnel face on the work of the support as well as the massif.

4.2. Principles of the convergence-confinement method

The theoretical study of a lined tunnel is usually complex because of the interaction ground-structure between the rock mass and the support. Among different methods, the convergence-confinement method is considered as a performance method thanks to its simplicity as well as its capacity to take into account fully ground-support interaction and conditions of installation the support behind the tunnel face.

Considering a section of tunnel near the tunnel face, its installed support will not take the entire load that redistributes around the tunnel due to the excavation. In fact, one part of this load induces deformation around the excavation and the tunnel face takes the other as consequence of the three dimensional effect. (Carranza-Torres and Fairhurst, 2000). By the time when the tunnel face advances, i.e., the tunnel is prolonged, the support carries more load that had been carried by the tunnel face earlier; the phenomenon finishes when the tunnel face has advanced at the far enough distant from the considered section (Carranza-Torres and Fairhurst, 2000).

Let us consider a circular tunnel of radius R excavated in an isotropic rock mass that is subject to the isotropic initial stresses, i.e., hydrostatic. Assuming that, at certain distance *L* behind the tunnel face (section A-A') one installs an annular support of unit length in the direction of the tunnel axis. One will determine interactive stresses at the rock mass-support interface from the instant of support installation until the moment when the face has advanced far enough so that the “face effect” vanishes. Once the stresses on the rock mass-support interface obtained, one can calculate the stresses and deformations in the support (Panet, 1995).

Figure 1.b shows a cross section of excavation at the position A-A' (the support has been 'removed' for clarity in this figure) in which the stress σ_0 represents the hydrostatic far field stress acting on the rock-mass, the radial displacement u_r and the reaction of the support on the rock mass p_i.

Figure 1.c illustrates a cross-section of the support in which t_s is the thickness of the support and the stress p_s that is transmit from the rock mass to the support.

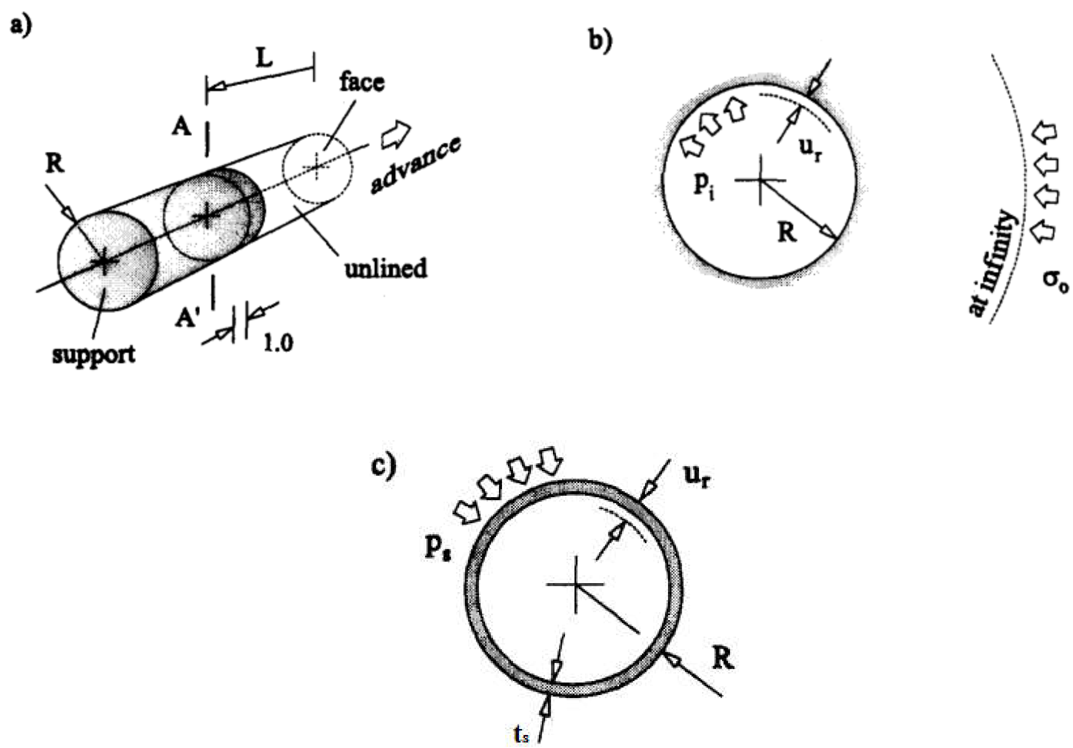

Fig. 4-1: a) Circular tunnel of radius R driven in the rock-mass; b) Cross-section of the rock-mass at section A-A'; c) Cross-section of the circular support installed at section A-A' (Carranza-Torres and Fairhurst, 2000).

To simplify the problem, the plane strain conditions can be adopted along the tunnel axis, i.e., all deformations occur in a plane perpendicular to the axis of the tunnel. This transformation from the 3D problem to the 2D problem is one of the principal ideas of the convergence-confinement method as illustrated in Figure 2. Following that, at the initial time t_0, the support is installed at the section A-A' (Fig. 2a) which is located at distance *L* from the tunnel face.

Corresponding to this latter instant, the tunnel surface at this section had converged radically by the amount u_d. The stresses from the rock mass have released partly while the tunnel face carries the other. Assuming that, the tunnel face does not advance ahead, so the support takes no load from the rock mass. i.e., $p_0^s = 0$ at this stage.

When the tunnel face advances ahead, the support takes more and more the load from the ground that has taken by the tunnel face previously. From this moment, the ground and the support deform together. Figure 2b shows the situation at time instant t when the section is located at the distance L_t from the tunnel face; at that moment, the ground has converged the amount $u_t > u_d$ and the pressure transmited to the support is p_t^s.

Once the face of the tunnel has moved ahead far enough (Fig. 4-2c), the support takes final (or design) load p_t^D and the ground-support system at the section A-A' is in equilibrium. At the corresponding instant t_D, the effect of the face has disappeared and the support and ground have converged together by the final amount u_r^D.

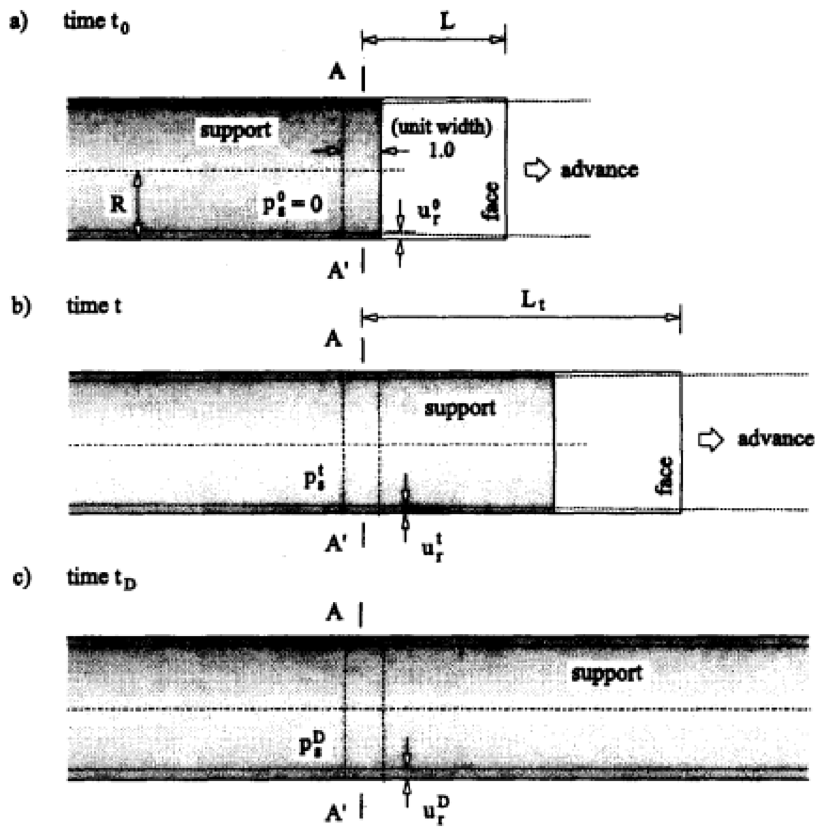

Fig. 4-2: Loading of the support at section A-A' due to progressive advance of the tunnel face (Carranza-Torres and Fairhurst, 2000)

Graphically, the Convergence-Confinement method can be represented by three curves obtained from three basic components, i.e., the Longitudinal Deformation Profile (LDP), the

Ground Reaction Curve (GRC) and the Support Characteristic Curve (SCC). In practice, the LDP is usually called as the curve of the deconfinement rate; and the GRC and SCC are known as the convergence and confinement curves respectively.

4.2.1. Construction of the Longitudinal Deformation Profile

Let us consider a plane section of a rock mass in which one wants to excavate a circular tunnel. This massif is subject to a natural stress corresponding to an isotropic initial state. To model the excavation of the tunnel, one first assumes that the cavity is subject to a pressure so-called fictive pressure corresponding to the isotropic initial state (Fig. 4-3). Thereafter, by reducing the fictive pressure, it causes a radial displacement corresponding to the decompression of the massif. This pressure decreases from the value of the initial hydrostatic pressure until the zero pressure. Once it takes the value of zero, the tunnel face has moved far enough so that the "face effect" has disappeared (Panet, 1995).

It is an artifice that permits to pass from the three-dimensional problem of the excavation to an equivalent plane strain problem based on the point of view of equality of tunnel wall convergences.

The deconfinement rate characterizing the reduction of the fictive pressure is determined as follows:

$$\lambda = 1 - \frac{p_f}{\sigma_0} \tag{4.1}$$

where σ_0 is the initial isotropic pre-stress of the massif. When the fictive pressure decreases from σ_0 to zero, the deconfinement rate increases from zero to 1 (Fig. 4-3).

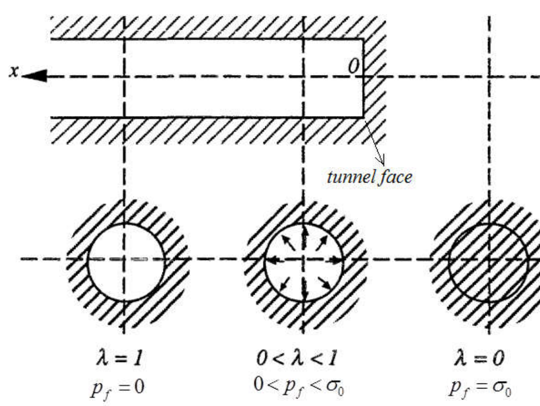

Fig. 4-3: Principle of deconfinement rate (Panet, 1995).

With respect to a given section of the tunnel, the parameter λ depends on the distance x to the tunnel face as well as the behavior law of the massif.

The deconfinement rate curve $\lambda(x)$ is usually constructed by numerical simulation which is described by following stages:

- The analytical calculation establishes a relationship between the fictive pressure applied to the tunnel wall p_f and the convergence u_r: $u_r = u_r(p_f)$

- Based on a 3D or 2D axisymmetric geometric model, a numerical calculation for the unsupported tunnel gives the convergence u_r as a function of the distance x to tunnel face: $u_r = u_r(x)$

From the above procedures one can obtain $p_f = p_f(x)$, and thereby, determine $\lambda(x)$ by using Eq. (4.1). On the contrary, the fictive pressure is deduced from deconfinement rate by:

$$p_f = [1-\lambda(x)]\sigma_0 \tag{4.2}$$

The LDP is the graphical representation of the radial displacement that occurs along the axis of an unsupported circular tunnel for sections located ahead and behind of the face.

As illustrated in Figure 4-4, at a distance x from behind of the tunnel face the radial displacement is u_r. At certain far enough distance x from behind of the tunnel face, the convergence of the tunnel wall attends the maximum value u_r^M. For sections ahead of the face, the distance x takes negative value. The displacement becomes essentially zero at some finite distance ahead of the face.

On the basis of the elastic models of the problem as represented in Figure 4-4a, Panet (1995) proposed following relationship between the radial displacements (convergence) and the distance to the tunnel face:

$$\frac{u_r}{u_r^M} = 0.25 + 0.75\left[1 - \left(\frac{0.75}{0.75 + x/R}\right)^2\right] \tag{4.3}$$

The plot of this relationship is presented in Figure 4-4b by the dashed curve. The horizontal axis of the diagram represents the ratio x/R and the vertical axis represents the rate of convergence u_r / u_r^M.

Observing the convergence of the tunnel wall in the vicinity of the tunnel face for a tunnel in the Mingtam Power Cavern project, Chern et al. (1998) obtained some data as illustrated in Figure 4b by the dots. Thereafter, based on this data, Hoek (1999) proposed the following empirical best-fit relationship between the convergence of the tunnel and the distance to the face:

$$\frac{u_r}{u_r^M} = \left[1 + \exp\left(\frac{-x/R}{1.10}\right)\right]^{-1.7} \tag{4.4}$$

The relationship (4.4) is also illustrated in Figure 4-4b by the continue curve.

It is observed in Figure 4-4b that, the maximum convergence attends at approximately 8 tunnel radii behind the face of the tunnel and the radial deformation is zero at approximately 4 tunnel radii ahead of the face. The relationships (4.3) and (4.4) indicate also that the convergence of the tunnel wall is approximately 30% of the maximum value at the tunnel face itself.

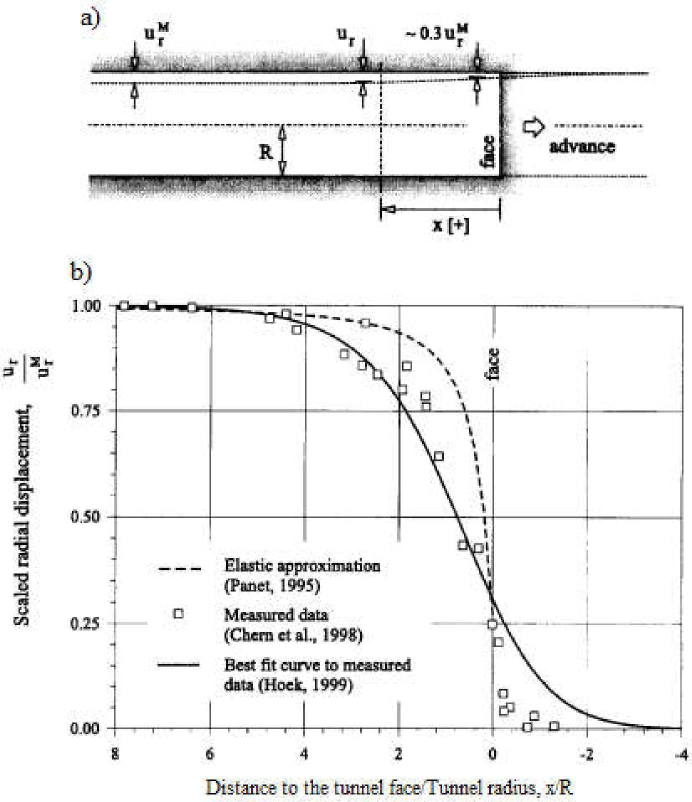

Fig. 4-4: Schematic representation of the Longitudinal Deformation Profile (LDP), Ground Reaction Curve (GRC) and Support Characteristic Curve (SCC) (Carranza-Torres and Fairhurst, 2000).

4.2.2. Ground Reaction Curve (GRC)-Convergence Curve

The Ground Reaction Curve (GRC) or Convergence Curve shows the relationship between the fictive pressure and the radial deformation on the tunnel wall. When the tunnel face moved sufficiently far from the interest cross-section, i.e., the fictive pressure decreases to zero value, the convergence reaches the maximum value.

The convergence curve is often constructed based on the elasto-plastic solutions of a circular opening subject to uniform (i.e., hydrostatic) far field stresses and uniform internal pressure. Some plasticity models are used, for example, Mohr-Coulomb and Hoek-Brown criterions (Carranza-Torres and Fairhurst, 2000; François, 2012).

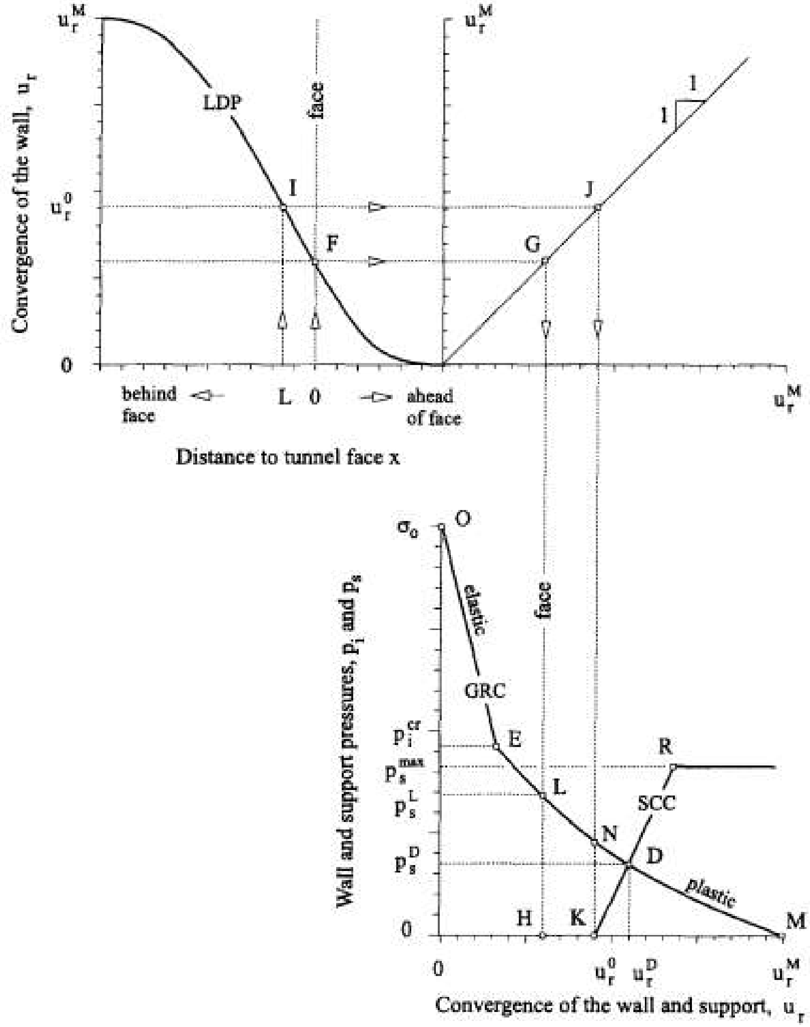

Fig. 4-5: Schematic representation of the Longitudinal Deformation Profile (LDP), Ground Reaction Curve (GRC) and Support Characteristic Curve (SCC) (Carrazane-Torres and Fairhurst, 2000)

As described in the lower of Figure 4-5, the GRC composes two portions OE and EM. The first one expresses an elastic behavior of the massif, so the pressure-displacement curve is linear from point O to point M. The second one corresponds to the second phase when the criterion of resistance of the material is reached on the wall of the cavity, and hence, a decompressed zone appears around the tunnel. It extends towards the interior of the massif when the internal pressure decreases. The curve OEM is called the characteristic curve of the excavation massif-Ground Reaction Curve (GRC) or the Convergence Curve.

4.2.3. Construction of Support Characteristic Curves

The confinement curve or Support Characteristic Curve (SCC) exhibits the relation between the applied stress p^s and the resulting closure u^s of a section of the support of unit length in the direction of the tunnel. Assuming that the support is composed by linear elastic material, so one has the relationship between the applied stress and the displacement of the support as follows:

$$p^s = K_s u^s \tag{4.5}$$

where K_s is the elastic stiffness of the support.

The support can be collapsed when the criterion of resistance of its material is reached, and the critical value of applied pressure corresponding to this state is $p_s^{\max}$. The perfect plastic part of the SCC is represented by the horizontal segment starting at point R.

It should be noted that, in the same coordinate system with the GRC, the SCC begin at its origin point corresponding the displacement u_d to account for the convergence that has already occurred before the installation of the support (at the instant t_0), i.e., the tunnel wall has converged by amount of u_d corresponding the rate of dis-confinement λ_d when one installs the support.

4.2.4. Application domain

The method is mainly used to calibrate the supports. The basic assumptions are rarely all verified in the reality; the ideal case being the deep circular tunnel in isotropic medium. Nevertheless, the approach is valid to calibrate the support/liner in the following cases (Panet, 1995; François, 2012):

- The rock mass must be represented as a homogeneous, isotropic and continuous medium. This satisfies the conditions of calculation in the framework of the continuum mechanics.
- The tunnel must satisfy the condition of the deep tunnel, i.e., the vertical initial stress variation between the upper and lower parts of the tunnel section (before excavation) is negligible compared to the initial vertical stress due to the weight of the ground to the average depth of the tunnel.
- The cross section of the tunnel is assumed to be circular in the method. In the case of a quasi-circular section, one will use an equivalent radius. The perfect circularity condition allows eliminating bending moments in the support.
- The initial stress state is isotropic.

4.3. Interaction ground-support in anisotropic case

4.3.1. Analytical solution for ground-support interaction

The purpose of this section is to develop an explicit solution for the ground-support interaction for an anisotropic medium tunnel. This problem was referred in chapter 2; however, this solution does not take into account the convergence of the tunnel wall which occurred before the installation of support, i.e., the liner is installed simultaneously with the excavation. In practice, the excavation is a successive process and the tunnel is prolonged in function of movement of tunnel face. At the instant of installation of the support (t_0), the interest section is located at a certain distance from the face, as presented previously. Therefore, the tunnel wall had converged by an amount (u_d) before the installation of the support. Thus, the interactive problem of rock-support considering the tunnel face effect (represented in 3D by the distance from the support cross-section to the tunnel face as well as the movement speed of this face) is an important issue not only to design the appropriate support but also to evaluate the work of rock mass before and after the installation of support.

It should be noted that the convergence-confinement method as detailed above is principally based on assumptions of the homogeneous, isotropic medium and isotropic in-situ stresses, i.e., hydrostatic pressure. With these assumptions, the interactive problem degenerates to the one-dimensional problem accounting for the symmetric conditions. In this case, the support works only in the pure compression and no bending moment is generated. However, this is not the case when the medium around the tunnel and/or the in-situ stresses are anisotropic. In this latter case, the behaviour of structures depends on the considered direction. The stresses applying on the extrados of the support include two components, the normal stress and shear stress, which vary with respect to the studied position. Therefore, the support is not only compressed but also bended and in this case the classical convergence-confinement method is not applied directly to the anisotropic problem. This could be done through some extensions as detailed below. Concretely during this work:

- The influence of three dimensional effect and the excavation process are considered through the fictive pressure on the tunnel wall that decreases progressively over time. The evolution of this fictive pressure is characterized by the deconfinement rate (λ) which is constant on the tunnel wall at each instant. This parameter as mentioned above depend on the distance between the considered section and the tunnel face (x) which is proportional to the excavation speed ($x=V.t$).
- In the context of the poroelastic behaviour of the massif, one assumes that if there is any change of pore pressure (depending on the hydraulic condition at the extrados of support) on the perimeter of tunnel, it is happening instantaneous when the tunnel face coincides with the studied section meaning that at the distance x=0. Figure 4-6 illustrates the evolution law of the pore pressure on the tunnel wall.
- The solution developed here considers only the condition of continuity at the interface between the rock mass and the support, i.e., perfect adhesion as adopted in chapter 2.

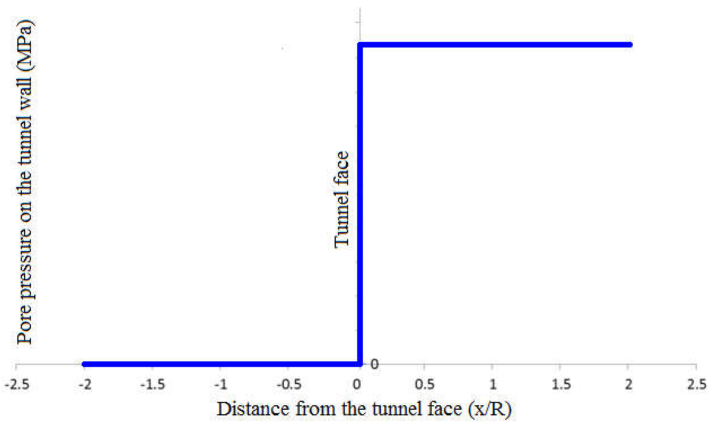

Fig. 4-6: Evolution of the pore pressure in function of distance from the study section to the tunnel face

In the convergence-confinement method, it is necessary to establish the convergence law of the ground that shows the relationship between the convergence of the tunnel wall and the stresses imposed, and the response of the support described by a relationship between the stresses applied to its extrados and the corresponding displacement (Fig. 4-7). For the clarity purpose, keep in mind that the elastic behavior of surrounding rock mass is transversely isotropic while the behavior of the support is isotropic.

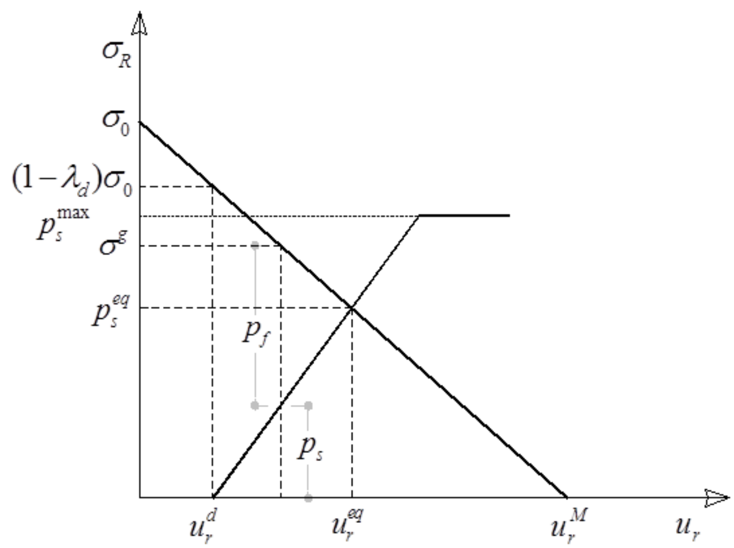

Fig.4-7: Relation between the stress on the tunnel wall and the stress applied to the extrados of the support after the support installation

<u>Characteristic of the rock:</u>

Let us consider a circular tunnel of radius R excavated in a transversely isotropic infinite medium characterized by five mechanical parameters $E_x, E_y, \nu_{xz}, \nu_{yz}, G_{xy}$ and the axis of the tunnel is parallel to discontinuity plane.

For the hydro-mechanical problem, normal and shear stresses on the tunnel wall consist of two components, the first one is induced by mechanical phenomenon and the other is due to the hydraulic phenomenon.

Because of the symmetry of the geometry and the loading of the problem, and thereby, the functions of normal and shear stresses on the tunnel wall exhibit the even and odd characteristic respectively. Therefore, one can expand them in Fourier series forms as follows (see equations 2.20 and 2.53):

$$\begin{aligned}\Delta\sigma_r &= (\sigma_0+\sigma_0^p)+\sum_{n=2,4,6}^{\infty}(\sigma_n^a+\sigma_n^{a,p})\cos n\theta+\sum_{n=2,4,6}^{\infty}(\sigma_n^b+\sigma_n^{b,p})\sin n\theta;\\ \Delta\tau &= \sum_{n=2,4,6}^{\infty}(\tau_n^a+\tau_n^{a,p})\sin n\theta+\sum_{n=2,4,6}^{\infty}(\tau_n^b+\tau_n^{b,p})\cos n\theta.\end{aligned} \tag{4.6}$$

in which the coefficients $\sigma_0, \sigma_n^a, \sigma_n^b, \tau_n^a, \tau_n^b$ are related to the mechanical problem and the coefficients $\sigma_0^p, \sigma_n^{a,p}, \sigma_n^{b,p}, \tau_n^{a,p}, \tau_n^{b,p}$ are related to hydraulic one. These coefficients are determined by using the boundary conditions and compatibility conditions of displacement at the rock mass – support contact (see equations 2.21 and 2.54).

Similarly, the displacements on the tunnel wall are written in the form (see Tran MH, 2014):

$$\begin{aligned}\frac{u_r}{R} &= (a_0+a_0^p)+\sum_{n=2,4,6}^{\infty}(a_n^a+a_n^{a,p})\cos n\theta+\sum_{n=2,4,6}^{\infty}(a_n^b+a_n^{b,p})\sin n\theta,\\ \frac{u_\theta}{R} &= (b_0+b_0^p)+\sum_{n=2,4,6}^{\infty}(b_n^a+b_n^{a,p})\sin n\theta+\sum_{n=2,4,6}^{\infty}(b_n^b+b_n^{b,p})\cos n\theta\end{aligned} \tag{4.7}$$

The coefficients of Eq. (4.7) can be determined by imposing the compatibility condition of displacement at the rock mass-support interface or can be found in Tran MH (2014).

From a practical point of view, it is not necessary to solve for all the terms of Eqs. (4.6) and (4.7), as the contributions from the higher terms will be negligible. By truncating the series expansion to the order of m, the relationship between the displacement and the variation of stress on the tunnel wall is written in matrix form (Tran MH, 2014):

$$\frac{1}{R}\begin{pmatrix}\mathbf{u}_r\\ \mathbf{u}_\theta\end{pmatrix}=\mathbf{G}\begin{pmatrix}\Delta\boldsymbol{\sigma}_r\\ \Delta\boldsymbol{\sigma}_\theta\end{pmatrix} \tag{4.8}$$

in which:

$$\begin{aligned}\mathbf{u}_r &= \{a_0+a_0^p, a_1^a+a_1^{a,p}, a_2^a+a_2^{a,p}\ldots, a_m^a+a_m^{a,p}, a_1^b+a_1^{b,p}, a_2^b+a_2^{b,p},\ldots, a_m^b+a_m^{b,p}\}^T;\\ \mathbf{u}_\theta &= \{b_1^a+b_1^{a,p}, b_2^a+b_2^{a,p}\ldots, b_m^a+b_m^{a,p}, b_1^b+b_1^{b,p}, b_2^b+b_2^{b,p},\ldots, b_m^b+b_m^{b,p}\}^T;\\ \Delta\boldsymbol{\sigma}_r &= \{\sigma_0+\sigma_0^p, \sigma_1^a+\sigma_1^{a,p}, \sigma_2^a+\sigma_2^{a,p},\ldots, \sigma_m^a+\sigma_m^{a,p}, \sigma_1^b+\sigma_1^{b,p}, \sigma_2^b+\sigma_2^{b,p},\ldots, \sigma_m^b+\sigma_m^{b,p}\}^T;\\ \Delta\boldsymbol{\sigma}_\theta &= \{\tau_0+\tau_0^p, \tau_1^a+\tau_1^{a,p}, \tau_2^a+\tau_2^{a,p},\ldots, \tau_m^a+\tau_m^{a,p}, \tau_1^b+\tau_1^{b,p}, \tau_2^b+\tau_2^{b,p},\ldots, \tau_m^b+\tau_m^{b,p}\}^T\end{aligned} \tag{4.9}$$

and $\mathbf{G}$ is the square matrix of order of $4m+1$ which characterizes the behavior of the ground. The relationship in Eq. (4.8) descripts the convergence curve.

Characteristic of the support:

The support is constituted by a circular annual of extrados radius R and of small thickness t_s. One assumes that the support material is characterized by a linear isotropic elastic model whose parameters are the Young modulus E_s and the Poisson coefficient ν_s. The relationship between the stresses that apply to the extrados and the displacement of the support is written (Flugge, 1967):

$$\begin{cases} K_f\left(\dfrac{1}{R}\dfrac{\partial^4 u_r}{\partial\theta^4}+\dfrac{2}{R}\dfrac{d^2u_r}{d\theta^2}+\dfrac{u_r}{R}\right)+K_n\left(\dfrac{u_r}{R}+\dfrac{1}{R}\dfrac{du_\theta}{d\theta}\right)=p_r^s; \\ -K_n\left(\dfrac{1}{R}\dfrac{du_r}{d\theta}+\dfrac{1}{R}\dfrac{\partial^2 u_\theta}{\partial\theta^2}\right)=p_\theta^s \end{cases} \tag{4.10}$$

where p_r^s and p_θ^s are respectively the radial stress and shear stress applied to the extrados of the support; u_r^s and u_θ^s are the radial displacement and ortho-radial displacement of the support; K_n and K_f are the normal stiffness and flexible stiffness moduli and they are given by the following expressions:

$$K_n=\frac{E_s}{1-\nu_s^2}\frac{t_s}{R};\qquad K_f=\frac{E_s}{1-\nu_s^2}\frac{I}{R};\qquad I=\frac{t_s^3}{12} \tag{4.11}$$

In the same way for the stresses applied to the tunnel wall, one has the Fourier expansions of the stresses applied to the extrados of the support as follows (Tran MH, 2014):

$$\begin{aligned} p_r^s &= p_0+\sum_{n=2,4,6}^{\infty} p_n^a\cos n\theta+\sum_{n=2,4,6}^{\infty} p_n^b\sin n\theta, \\ p_\theta^s &= \sum_{n=2,4,6}^{\infty} q_n^a\sin n\theta+\sum_{n=2,4,6}^{\infty} q_n^b\cos n\theta \end{aligned} \tag{4.12}$$

and with the same form, we have the following relations for displacements:

$$\begin{aligned} \frac{u_r^s}{R} &= c_0+\sum_{n=2,4,6}^{\infty} c_n^a\cos n\theta+\sum_{n=2,4,6}^{\infty} c_n^b\sin n\theta, \\ \frac{u_\theta^s}{R} &= d_0+\sum_{n=2,4,6}^{\infty} d_n^a\sin n\theta+\sum_{n=2,4,6}^{\infty} d_n^b\cos n\theta \end{aligned} \tag{4.13}$$

where $p_n^a, p_n^b, q_n^a, q_n^b$ and $c_0, c_n^a, c_n^b, d_0, d_n^a, d_n^b$ are the coefficients of the series that are determined by the compatibility of stresses and displacement at the massif-support contact (see expressions in Tran MH, 2014).

The relationship between the displacements and the stresses on the support can be also written in the matrix form as:

$$\frac{1}{R}\begin{pmatrix}\mathbf{u}_r^s\\ \mathbf{u}_\theta^s\end{pmatrix}=\mathbf{K}^s\begin{pmatrix}\mathbf{p}_r^s\\ \mathbf{p}_\theta^s\end{pmatrix} \tag{4.14}$$

in which

$$\mathbf{u}_r^s = \{c_0, c_1^a, c_2^a...c_m^a, c_1^b, c_2^b, ..., c_m^b\}^T; \quad \mathbf{u}_\theta^s = \{d_1^a, d_2^a...d_m^a, d_1^b, d_2^b, ..., d_m^b\}^T$$
$$\mathbf{p}_r^s = \{p_0, p_1^a, p_2^a..., p_m^a, p_1^b, p_2^b, ..., p_m^b\}^T; \quad \mathbf{p}_\theta^s = \{q_0, q_1^a, q_2^a..., q_m^a, q_1^b, q_2^b, ..., q_m^b\}^T \tag{4.15}$$

and $\mathbf{K}^s$ is the square matrix of order of $4m+1$ which characterizes the behavior of the support. The relationship in Eq. (4.13) descripts the confinement curve.

Analytical solution for ground-support interaction:

As presented, in the convergence-confinement method (see section 4.1), the influence of tunnel face on the considered section is taken into account by the fictive pressure p^f whose evolution is governed by the deconfinement rate $\lambda(x)$. In the case where the initial stress state is anisotropic, this fictive stress applying on the tunnel wall includes a normal stress and a shear stress as follows (Tran MH, 2014):

$$p_r^f = (1-\lambda)\left[\frac{1}{2}(\sigma_v - \sigma_h)cos2\theta - \frac{1}{2}(\sigma_h + \sigma_v) - \tau_{vh}sin2\theta\right];$$
$$p_\theta^f = (1-\lambda)\left[\frac{1}{2}(\sigma_h - \sigma_v)sin2\theta - \tau_{vh}cos2\theta\right] \tag{4.16}$$

where $\sigma_h, \sigma_v, \tau_{vh}$ are the far field initial stresses as defined in chapter 2 and 3. It assumes that, the deconfinement rate is $\lambda_d = \lambda(d)$, with d the distance from the tunnel face corresponding to the instant of installation of support (t_0), so one has stress variation on tunnel wall as follows:

$$\Delta\sigma_r^d = \lambda_d\left[\frac{1}{2}(\sigma_v - \sigma_h)cos2\theta - \frac{1}{2}(\sigma_h + \sigma_v) - \tau_{vh}sin2\theta\right];$$
$$\Delta\tau_\theta^d = \lambda_d\left[\frac{1}{2}(\sigma_h - \sigma_v)sin2\theta - \tau_{vh}cos2\theta\right] \tag{4.17}$$

Therefore, the corresponding displacements of the tunnel wall at this stage are determined by following relationship:

$$\frac{1}{R}\begin{pmatrix}\mathbf{u}_r^d \\ \mathbf{u}_\theta^d\end{pmatrix} = \mathbf{G}\begin{pmatrix}\Delta\boldsymbol{\sigma}_r^d \\ \Delta\boldsymbol{\tau}_\theta^d\end{pmatrix} = \lambda_d\mathbf{G}\begin{pmatrix}\Delta\boldsymbol{\sigma}_r^0 \\ \Delta\boldsymbol{\tau}_\theta^0\end{pmatrix} \tag{4.18}$$

After installation of the support, the relationship between the stresses on the tunnel wall and the stresses applied to the extrados of the tunnel is written (Fig 4-7):

$$\begin{pmatrix}\boldsymbol{\sigma}_r^g \\ \boldsymbol{\sigma}_\theta^g\end{pmatrix} = \begin{pmatrix}\mathbf{p}_r^s \\ \mathbf{p}_\theta^s\end{pmatrix} + \begin{pmatrix}\mathbf{p}_r^f \\ \mathbf{p}_\theta^f\end{pmatrix} \tag{4.19}$$

where $\boldsymbol{\sigma}_r^g, \boldsymbol{\sigma}_\theta^g$ are the stresses applied to the tunnel wall.

The final equilibrium state reaches when $\mathbf{p}^f = 0$ and hence:

$$\begin{pmatrix} \Delta\boldsymbol{\sigma}_r \\ \Delta\boldsymbol{\sigma}_\theta \end{pmatrix} = \begin{pmatrix} \boldsymbol{\sigma}_r^0 \\ \boldsymbol{\sigma}_\theta^0 \end{pmatrix} - \begin{pmatrix} \mathbf{p}_r^s \\ \mathbf{p}_\theta^s \end{pmatrix} \tag{4.20}$$

The perfect contact condition:

This condition implies the continuity of the radial and the tangential displacements between the ground and the support, so one has the relationship:

$$\begin{aligned} \mathbf{u}_r - \mathbf{u}_r^d &= \mathbf{u}_r^s \\ \mathbf{u}_\theta - \mathbf{u}_\theta^d &= \mathbf{u}_\theta^s \end{aligned} \tag{4.21}$$

Hence, one can infer the stresses applied on the extrados of the support:

$$\begin{pmatrix} \mathbf{p}_r^s \\ \mathbf{p}_\theta^s \end{pmatrix} = (1-\lambda_d)(\mathbf{G}+\mathbf{K}^s)^{-1} \begin{pmatrix} \boldsymbol{\sigma}_r^0 \\ \boldsymbol{\sigma}_\theta^0 \end{pmatrix} \tag{4.22}$$

and

$$\frac{1}{R}\begin{pmatrix} \mathbf{u}_r^s \\ \mathbf{u}_\theta^s \end{pmatrix} = \mathbf{K}^s \begin{pmatrix} \mathbf{p}_r^s \\ \mathbf{p}_\theta^s \end{pmatrix} \tag{4.23}$$

4.3.2. Application for GCS

In this section, one considers a specific example of the deep tunnel in anisotropic poro-elastic medium with the special attention on the interaction of rock-support. An example for this case is the tunnel so-called GCS in constructing the underground rock laboratory (URL) in the context of the underground storage of nuclear waste in Bure-France.

Digging and supporting of the GCS tunnel:

The GCS known as the gallery of flexible design, has been excavated in the direction of the major horizontal stress in the clay stone of Callovo-Oxfordien in Bure-France. The GCS drift has circular section with a 2.6m radius and the length of 63.32m with a concrete support of 18cm thickness in incorporating compressible wedges and trellis welded and completed by an aureole of radial bolts anchored in the ground. The average digging speed of the GCS for the reference section is 2.05 m/week (Armand et al., 2013).

One will carry out below some evaluations for GCS tunnel with its size given above. The material parameters of the clay stone and loading are the same as ones presented in chapters 2 and 3.

In an attempt to perform the relationship between the pressure acting on the tunnel wall and its convergence and the relationship between the stresses applying to the support and support displacement relied on the scheme of convergence – confinement method, one has some results illustrated in the Figures 4-8 and 4-9.

In order to estimate the influence of the digging speed on the interaction of rock mass-support, one will firstly consider two extreme cases. In the first case (noted as undrained case) one supposes that the tunnel is excavated with a very fast digging speed; hence, with low permeability of the rock, the pore fluid could not diffuse at the moment that the liner is installed. Therefore, the pore pressure in the rock mass is uniform and equal to the initial pore pressure. In this case, as already mentioned in chapter 2, the stresses applying to the support and its displacement as well as the total stresses and displacement of the rock are the same as those of the tunnel excavated in dry rock, solicited by the same initial far field total stresses. In the second extreme case (noted as drained case), the digging speed is so slow that at the installation moment of support, the fluid flow from the rock mass into the tunnel reaches its steady state. Consequently, the analysis is conducted based on the problem of the deep tunnel in the rock mass with the steady state groundwater flow. With the adopted hypothesis above, in this second case, the pore pressure at the tunnel wall is considered equal to the initial value when the tunnel face does not reach the considered section, and it falls immediately at atmospheric pressure ($p_0=0$) when the face passes through the study section. Thus, for the deconfinement rate ranging from 0 to 0.25 (value corresponding to the deconfinement rate at x=0), the results of two extreme cases coincide and the difference can be observed only when the tunnel face passed the studied section.

For the moderate excavation speed (case between the two extreme states), one could expect that the pressure-displacement relationships of the liner and the rock mass lie between the two extreme states. Technically, to construct the Convergence Curve in this latter, one can chose any constant deconfinement rate (which is beyond the value at x=0 thus $\lambda>0.25$). With the known value of λ, one calculates the distance d from the section to the tunnel face using Eq. (4.3) from which one determines the time interval ($\Delta t=t-t_0=d/V$) using the known digging speed (V). This time interval will be used as input in the closed form solution in the transient state as detailed in chapter 3. Hence, the second extreme case (corresponding to the very slow digging speed) is the particular case when one applies the closed form solution in the steady state as presented in chapter 2.

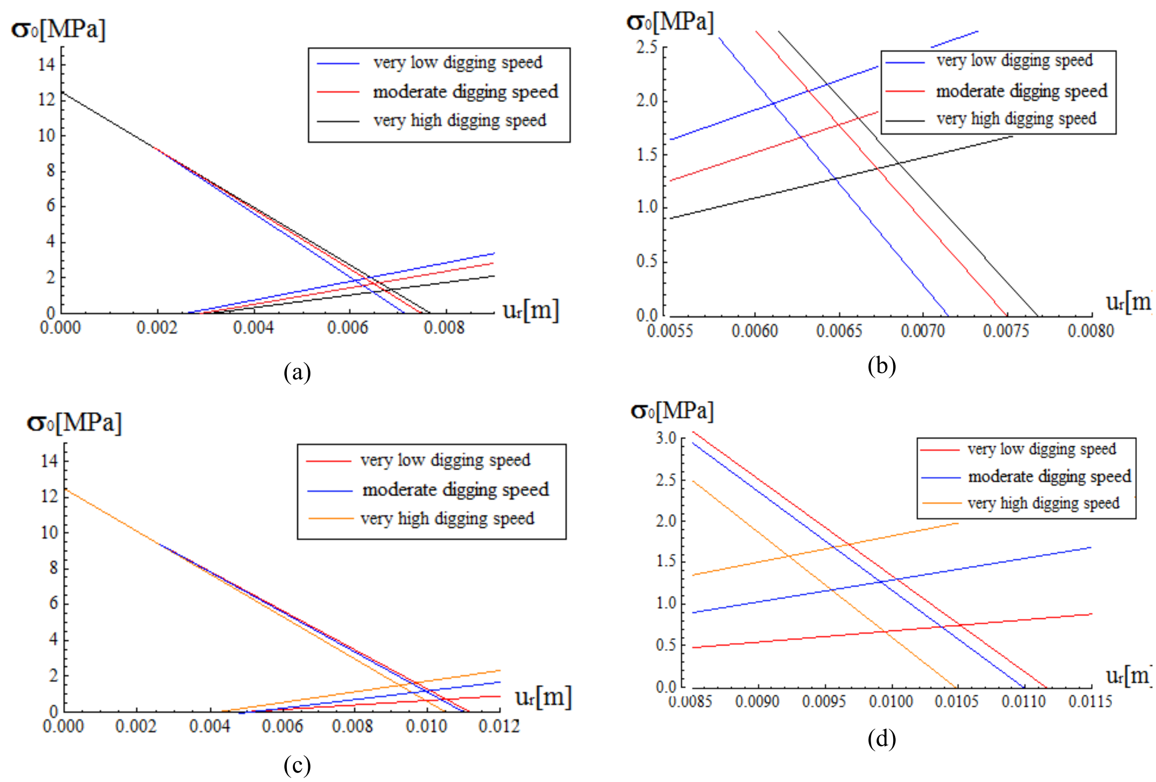

Fig. 4-8: Ground characteristic curve and support characteristic curve determined at two points in the tunnel wall a) at the springline of tunnel (θ=0), b) at the springline θ=0 with zoom around the equilibrium state, c) at the crown of tunnel (θ= π/2), d) at the crown of tunnel (θ= π/2) with zoom around the equilibrium state

Figure 4-9 illustrates diagrams of convergence-confinement method for 3 points on the perimeter of tunnel, corresponding to three directions 0, $\pi/4$ and $\pi/2$ with respect to the horizontal direction axis of tunnel, for the undrained case (Fig 4-9a, b) and the drained case with steady state fluid flow (Fig 4-9c, d). It is observed that, in the undrained case, the radial displacement of liner is larger at the crown than at the springline. For the drained case, i.e., the case of steady state fluid flow, the presence of anisotropic flow decreases the horizontal displacement while it increases vertical one. This is because of the distribution of pore pressure around the tunnel with greater hydraulic gradient in the vertical direction and smaller one in the horizontal direction (also indicated in chapter 2). It is the phenomenon that creates greater seepage forces in the vertical direction and smaller one in the horizontal direction, and hence, to induce an augmentation of vertical displacement and a diminution of horizontal displacement. For the stresses acting on the support, they have reverse trends.

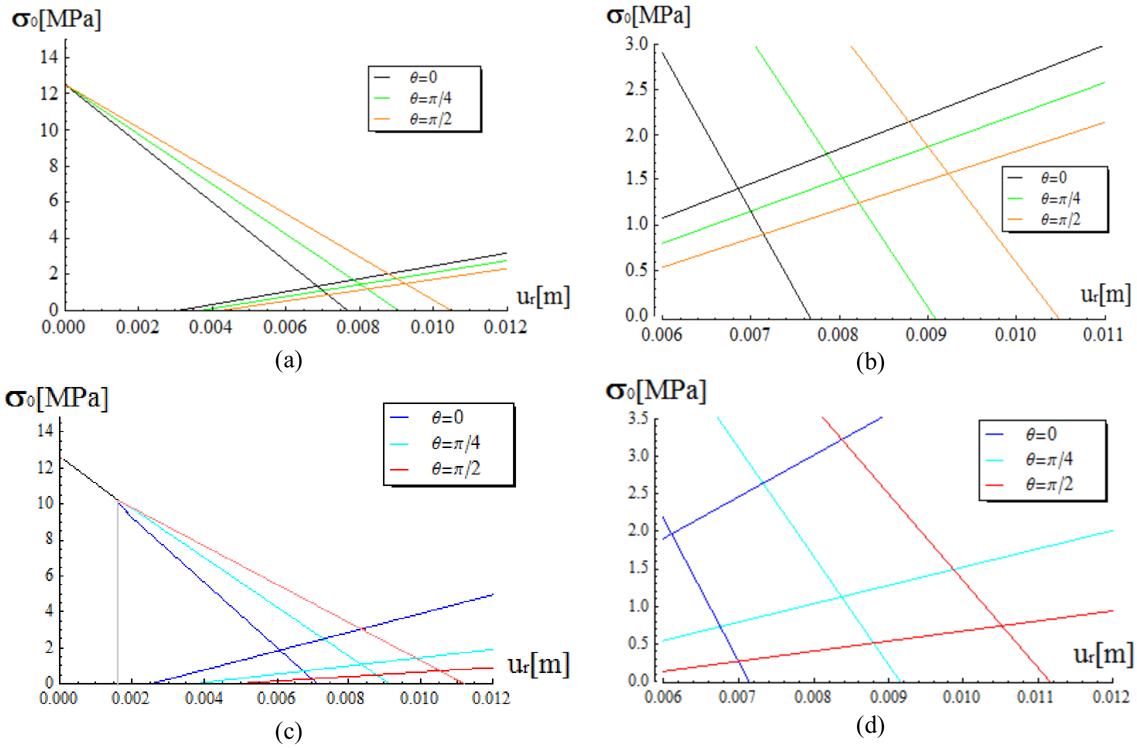

Fig. 4-9: Ground characteristic curve and support characteristic curve for three points in the perimeters of tunnel (corresponding to directions θ=0, π/4 and π/2) for: a) un-drained case; b) un-drained case with zoomaround the equilibrium state; c) drained case; d) drained case with zoomaround the equilibrium state

Figures 4-10 and 4-11 show thrust, moment in the support as well as the displacement and stresses in the interior and exterior fibres for two cases: undrained condition and drained condition in steady state. In these analyses, the support/liner is installed at the distance to the tunnel face corresponding to λ_d=0.4.

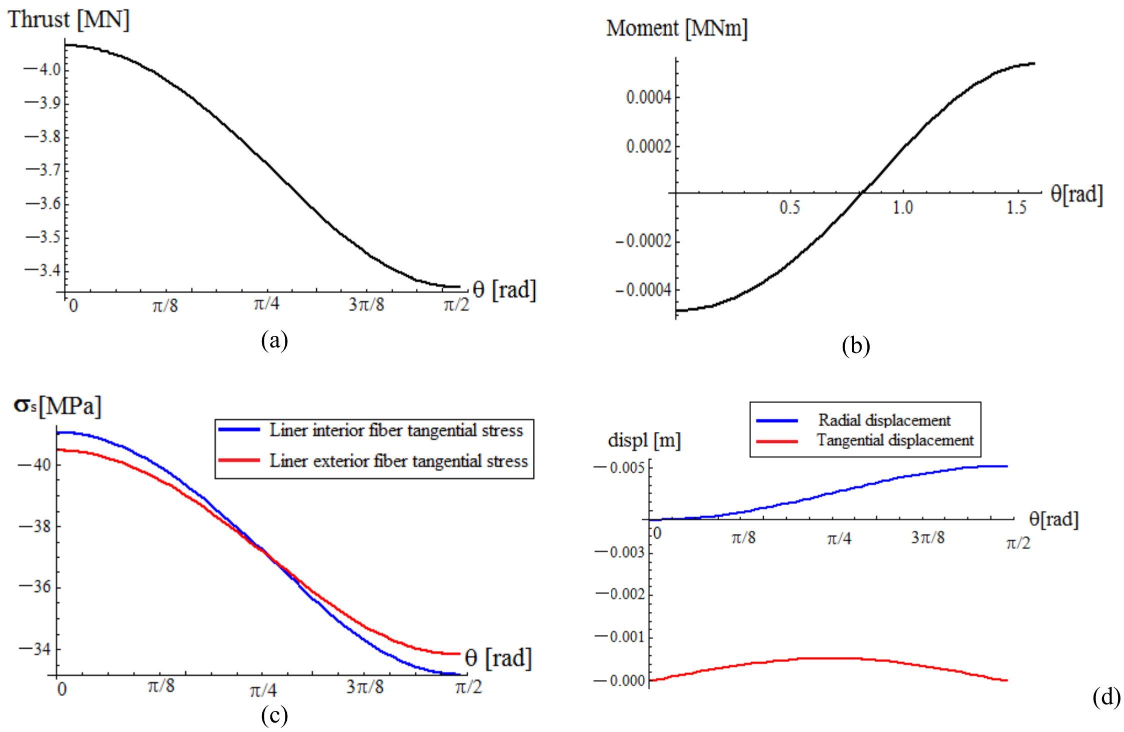

Fig. 4-10: The thrust, moment, stresses and the displacement of the liner in the case of λ_d=0.4 and un-drained condition

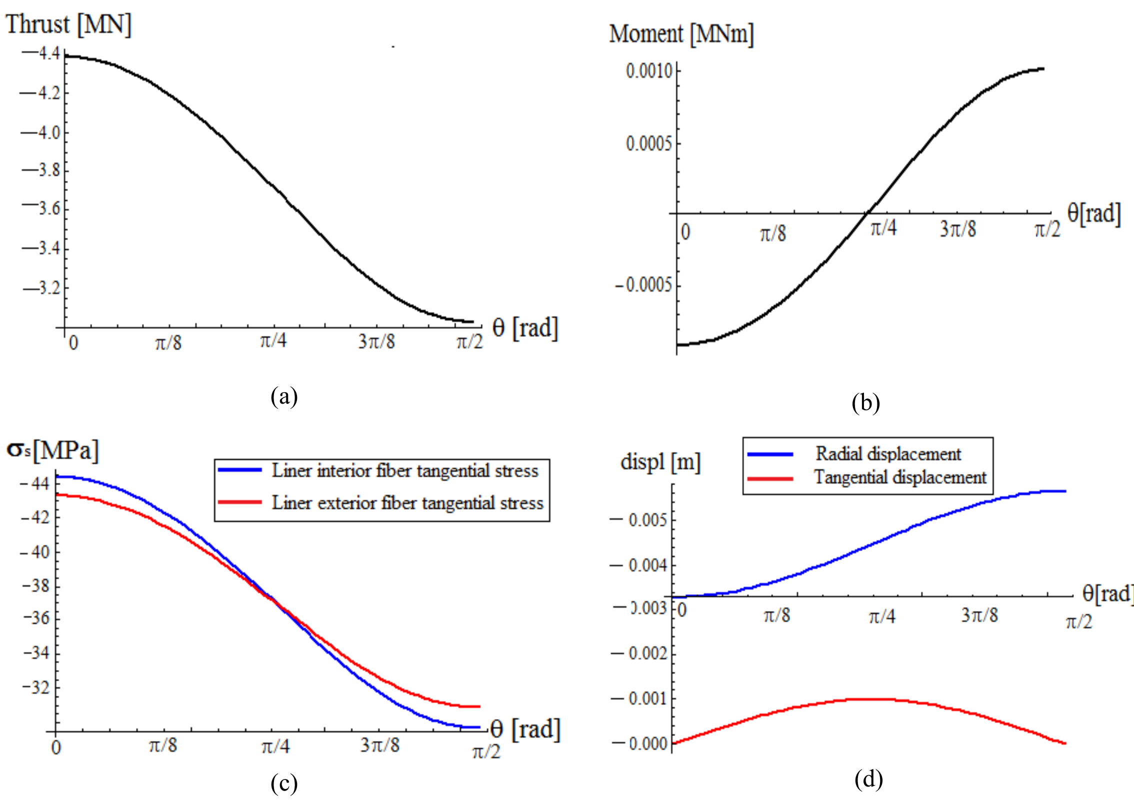

Fig. 4-11: The thrust, moment, stresses and the displacement of the liner in the case of λ_d=0.4 and drained condition in steady state

It can be seen that, in the case of drained condition, the variations of thrust, moment, stresses and the displacement of the support are always higher than those of undrained case due to the presence of the anisotropic fluid flow. In addition, the moment in the liner is always observed even the isotropic initial stresses. This suggests that, the anisotropic properties of the rock mass generates the moment and hence bend the support/liner.

One investigates now the influence of the instant of support installation, by varying the distance d (or by varying the deconfinement rate λ_d) to evaluate the variation of displacements and stresses in the support. Some results are presented in the Figures 4-12:

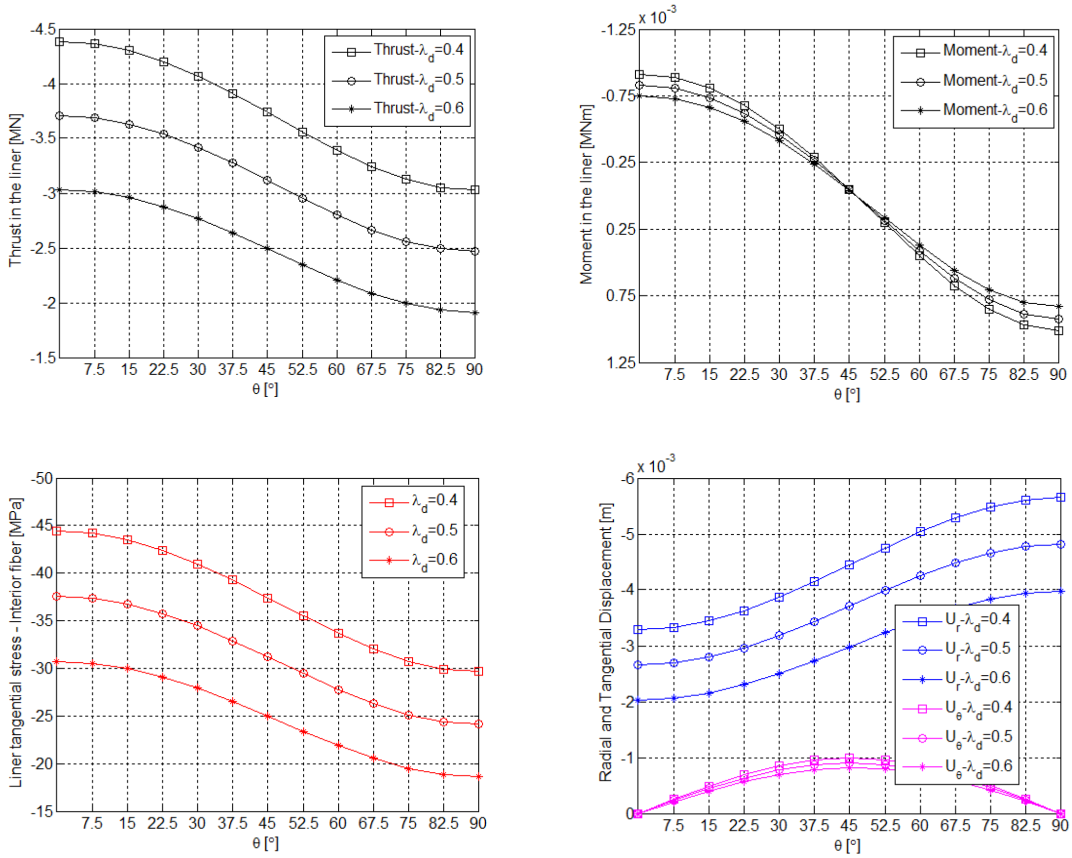

Fig. 4-12: The thrust (a), moment (b), stresses (c) and the displacement (d) of the liner corresponding to λ_d=0.4, λ_d=0.5 and λ_d=0.6 for the case of drained condition in steady state

The results indicates that, when the distance d increase (corresponding to the increase of deconfinement rate λ_d at the moment of support installation), the stresses as well as the displacement in the support decrease. This expected result explained that if the distance from the support installation section to the tunnel face is greater, the surrounding rock mass of the tunnel converged more significantly before placing the support. In other words, the internal forces are realised much more before support installation, and thus, the support is subject to smaller pressures.

Nevertheless, it is known that the principle role of the liner/support is to limit the convergence of the tunnel wall as well as plastic deformation zone generated around the tunnel. Therefore, determination the appropriate instant (or the distance *d*) to install the support is an important issue, which ensures at once the bearing capacity of the support and limiting the displacement of tunnel wall as well as limiting the plastic deformation zone around the tunnel.

Figures 4-10, 4-11 and 4-12 show that, the liner stresses is always larger at the springline where the stiffness of the rock is greater. Thus, in tunnel design, the results calculated at this last point will be utilized in the design of support/liner.

4.4. Conclusions

In this chapter, a solution is built for an interactive problem between the support and the massif of the deep tunnel in the hydro-mechanical anisotropic medium based on the approach of convergence-confinement method. The solution could be considered as a quick analysis tool for the preliminary support/liner tunnel design.

Some analysis pointed out that the cases of very fast and very slow digging speed, which correspond respectively the undrained and steady state flow conditions in the medium, are the extreme cases of the interactive problem of rock mass-support. Moreover, the stresses and deformations of the support/liner are always greater in the drained case. Some numerical results indicated also that, the greater stress of the support/liner occurs always in the larger stiffness direction, i.e., horizontal direction in this study. In addition, the instant of support/liner installation, i.e., the distance from the support installation section to tunnel face, influences strongly on the work of the support/liner in equilibrant state.

Therefore, the calibration of the tunnel support should be considered in the conditions of steady state flow in the massif with the stress state in larger stiffness direction as well as the instant of support installation so that the support/liner meets at once requirements of bearing and limiting the convergence and the plastic deformation zone around the tunnel.

The solution build on a convergence-confinement diagram for the deep tunnel in anisotropic medium could provide design engineers with a tool to analyse quickly the stress-strain state of the support/liner, and thereby, to calibrate preliminary the tunnel support/liner as well as its appropriate installation instant.

The solution is limited on the basis of the linear elastic model of the massif and; however, this study does not aim to find a solution which can take into account the plastic/visco-plastic material model but rather to provide a tool for determination the preliminary size of the support in tunnel design.

Conclusions :

Dans ce chapitre, une solution est construite pour un problème interactif entre le soutènement et le massif du tunnel profond dans le milieu anisotrope hydro-mécanique basé sur l'approche de la méthode convergence-confinement. La solution pourrait être considérée comme un outil d'analyse rapide pour la conception préliminaire le soutènement/revêtement des tunnels.

Certaines analyses ont souligné que les cas de vitesse de creusement très rapide et très lente, qui correspondent respectivement aux conditions non drainées et d'écoulement stable dans le milieu, sont les cas extrêmes du problème interactif des massif rocheux et soutènement. De plus, les contraintes et les déformations du soutènement/revêtement sont toujours plus grandes dans le cas de régime permanent d'écoulement. Certains résultats numériques indiquent également que, la plus grande contrainte du soutènement/revêtement se produit toujours dans la direction de rigidité plus grande, c'est-à-dire, la direction horizontale dans cette étude. Par ailleurs, l'instant d'installation soutènement/revêtement, c'est-à-dire, la distance entre la section d'installation de support et le front de taille, influence fortement le travail du soutènement/revêtement en état d'équilibre.

Par conséquent, le pré-dimensionnement du soutènement/revêtement du tunnel devrais être considéré dans les conditions d'écoulement stationnaire dans le massif avec l'état de contrainte dans la plus grande direction de rigidité aussi bien que l'instant de l'installation de soutènement afin que le soutènement/revêtement satisfasse à la fois aux exigences de la capacité de charge et de limitation la convergence et la zone de déformation plastique autour du tunnel.

La solution construite sur un diagramme de convergence-confinement pour le tunnel profond en milieu anisotrope pourrait fournir aux ingénieurs de conception un outil pour analyser rapidement et précisément l'état de contrainte-déformation du soutènement/revêtement et pour le pré-dimensionnement le soutènement/revêtement ainsi que son installation instantanée appropriée.

La solution est limitée sur la base du modèle élastique linéaire de la massif rocheux; cependant, cette étude n'a pas pour objectif de trouver une solution qui puisse prendre en compte le modèle de matière plastique/viscoplastique mais plutôt de fournir un outil pour le pré-dimensionnement le soutènement/revêtement dans la conception de tunnel.

CONCLUSIONS AND PERSPECTIVES

This work is an attempt to conduct a study of the behavior of a deep tunnel in anisotropic poroelastic medium with special attention on coupling between hydraulic and mechanical processes in fluid saturated porous media. The behavior of the tunnel is evaluated by determination of stresses, displacements and pore pressure distributions around tunnel.

The basic concepts in poroelasticity relevant to this work have been reviewed. The conservation principles of the continuum as well as the constitutive equations and relations between the material constants for poroelasticity, have been presented in their isotropic and anisotropic forms. The inherent anisotropy of rocks in which the tunnels built has been discussed on the basis of rock mechanics. The analytical solution was developed based on the complex potential approach of Lekhnitskii. Following that, a circular deep tunnel in anisotropic rock is resolved by the complex variable method, i.e., the solution of the problem is obtained through the complex potentials. Precisely, the original problem is sub-divided into simpler problems for which solutions are either known or can easily be obtained, i.e., the mechanical and hydraulic problems. With respect to mechanical problem, through the conformal mapping technique, the region outside the tunnel in original plane is transformed into the region outside the unit circle in transformed plane. The complex potential functions is determined in the transformed plane by using the solution of the boundary value problem with the specific boundary conditions. Thereafter, the actual solution of the mechanical problem is obtained by inverse transformation. The steady state hydraulic problem, is solved by finding the distribution of pore pressure, after that, it is expressed in term of hydraulic complex potential. The effect of pore pressure distribution on the mechanical response is considered by hydro-mechanical potentials.

The interaction between the rock mass and the liner is addressed by an interactive problem. Stress interaction between the liner and the rock mass is expanded under Fourier series. The constants of these series are determined by imposing the compatibility condition of displacement. It is noted that here, the condition of perfect contact between the rocks mass and the liner is applied, i.e., there is no slip and no detachment at the contact. Once the interaction stresses are determined, one can calculate the stresses and strains of the liner based on the elastic thin shell theory.

The results obtained by proposed analytical solution were compared with those obtained by the FEM code ASTER.

Based on the advantages of the analytical solution, i.e., quick and accurate analysis tool, the parametric studies are conducted. The parametric studies were done with all the parameters of anisotropic hydro-mechanical model. The results indicated that, the anisotropic behavior of the tunnel significantly depends on the degree of anisotropy of the medium. Contrary to widespread ideas, the convergence on the tunnel wall as well as the whole stress-strain state around the tunnel depend not only on the degree of anisotropy of Young moduli and permeability, but also (and sometimes as much as on these ones) on the Poisson coefficient and shear modulus in the isotropic plane and the degree of anisotropy of Biot's coefficient. In addition, the results showed that, the influence of stiffness and thickness of the liner on the anisotropic behavior of the rock mass is of nature to highly modify the behavior of the tunnel. In the parametric studies, the effect of the drainage condition at the liner-rock mass interface was evaluated. The results indicated that, when full drainage condition applied at the contact, a more pronounced anisotropic behavior is observed in comparison with the no-drainage case. Particularly, when the hydraulic is isotropic, i.e., the permeabilities are equal in two principle directions, the stresses and radial displacement of the liner is independent on the condition of drainage at the liner-rock mass contact. This recovers the case of isotropic rock.

The present work focused also on the transient hydro-mechanical problem. To take into account the distribution of the pore pressure over time, the transient solution can be computed as successive steady-state snapshots using a time dependent radius of influence. Hence, one can expand the solution of steady-state problem for transient one. It should be noted that, with this solution, only effects of hydraulics on the mechanics were considered which is known as one way coupling model.

Once the transient solution obtained, the relative errors in comparison with numerical solution were evaluated with the time and the radius of the tunnel. Applying the analytical solution for a tunnel without the liner, a phenomenon is observed with appearing of a tensile zone of effective radial stress at early instants and in the vicinity of tunnel wall. This could result in a nucleation zone of cracks or zone of plastic deformation. This is because the larger pore pressure whereas the total radial stress is small at the early instants and in the vicinity of the tunnel wall. For the one-way coupling model, this value of pore pressure is closed to the initial one.

The excess pore pressure is usually encountered in the case of low permeability or/and the high excavation velocity. The pore pressure increases due to volumetric deformation could not diffuse over time. This occurs only when one considers the mechanism of mechanical impact on the hydraulics. Thus, the analysis based on a fully-coupled model have been conducted which is considered as complete solution for analytical one. These numerical analysis confirmed that, with the very low permeability rock, the zone of excess pore pressure occurs always at the early instants and result in the tensile effective radial stress in the vicinity of the tunnel wall. Particularly, for the anisotropic rock, the excess pore pressure distribution is more important in the direction which has the higher stiffness. Several parameters have been also evaluated on the influence on the excess pore pressure.

An extension of the closed-form solution based on the approach of convergence-confinement method was also addressed for the purpose of application in tunnel design. Following that, this solution took into account the influence of the distance from the section of support installation to the tunnel face on the work of the support as well as the massif.

The analytical solutions on tunnel excavation on anisotropic porous rocks in steady and transient flow conditions could be used as a design tool for tunneling engineers. In fact, by combining these solutions with a convergence-confining approach it is possible to obtain quick decisions about the design of liner considering the rate of excavation.

As a first perspective an extension of the obtained solutions for the direction of the axis of the tunnel seems useful and necessary. The two-dimensional problem in plane strain is resolved by analytical solutions which assumes that the tunnel axis is parallel to the isotropic plane. An extension of these solutions can be proposed for the case of a tunnel with the axis in any direction from the isotropic plane.

Likewise, the analytical solutions developed for a circular tunnel can be extended to non-circular tunnel such as semi-circular, double-arc or rectangular cross-sections which are often used in practice. This can be conducted by using the conformal mapping technique.

In a longer time the extension of the approach for instantaneous and time-dependent non-linear behavior of rock masses is a perspective that could significantly improve the prediction capacities of analytic solution tool. As a first approach, the case of fractured rock masses with visco-elastic/visco-plastic fractures could be considered. In fact, it should be recalled that, the distribution of excess pore pressure field in the vicinity of the tunnel wall is more important in the direction where the rock has greater stiffness. This could be related to characteristic of EDZ on anisotropic rocks (for example, with observed features of EDZ around the tunnels in Bure URL in context of nuclear storage, where the convergence of the tunnel wall and the development of EDZ are more important in the direction where the rock has larger stiffness). A possible explanation is that, the tensile effective radial stress zone induced by the over pore pressure results in a plastic deformation/fracture zone in the vicinity of the tunnel wall preferentially in the stiffer direction. This leads at developing under a certain mechanism to an anisotropic EDZ. This kind of behavior could be described by the proposed approach including a time-dependent viscoelastic crack behavior. This requires to be proved by a numerical simulation based on visco-plastic/fracture model as mentioned above.

CONCLUSIONS ET PERSPECTIVES

Ce travail de recherche a été consacré à la modélisation du comportement d'un tunnel profond dans un milieu poreux saturé, élastique anisotrope avec une attention particulière sur le couplage entre les phénomènes hydrauliques et mécaniques.

Les concepts de base des milieux poreux élastiques ont été initialement décrits ainsi que les équations consécutives sous leurs formes isotropes et anisotropes. L'anisotropie inhérente de roches, hôte des ouvrages souterrains, est mise en relation avec la structure de la roche et les applications de la mécanique des roches. La solution analytique des champs de déplacements et de contraintes autour d'un tunnel dans un milieu élastique anisotrope, développée par Lekhnitskii, en utilisant l'approche du potentiel complexe a été présentée. Selon cette approche, le problème est divisé en plusieurs problèmes plus simples avec des solutions connues ou qui peuvent être facilement obtenues. Le problème mécanique est résolu en adoptant la technique de « conformal mapping » qui permet la projection du domaine à l'extérieur du tunnel du plan à celui à l'extérieur du cercle unité dans le plan transformé. Les fonctions potentielles complexes sont déterminées dans le plan transformé en utilisant la solution du problème aux valeurs limites avec des conditions aux limites spécifiques. Ensuite, la solution réelle du problème mécanique est obtenue par une transformation inverse. Le problème hydraulique dans le régime permanent est résolu en cherchant la répartition de la pression interstitielle, exprimée en termes du potentiel complexe hydraulique. L'impact de la répartition de pression sur les réponses mécaniques est considéré par les potentiels hydro-mécaniques.

L'interaction entre le massif rocheux et le revêtement est traitée par un problème d'interaction. Des contraintes interactives entre eux sont développées en forme de séries de Fourier. Les constantes de ces séries sont déterminées en imposant la condition de compatibilité de déplacement au niveau de l'interface entre le massif et le revêtement. Il faut noter que, la condition de contact parfait entre le massif et le revêtement est appliquée dans ce travail (alors que d'autres choix sont possibles). Une fois les contraintes d'interaction sont déterminées, il est possible de calculer les contraintes les déformations et les déplacements du revêtement en adoptant la théorie élastique des coques minces.

Les résultats obtenus par la solution analytique ont été comparés avec ceux obtenus par le code d'éléments finis ASTER.

Prenant l'avantage de la solution analytique, un ensemble d'études paramétriques a été réalisé sur tous les paramètres du modèle anisotrope hydro-mécanique. Les résultats de cette étude montré que le comportement anisotrope du tunnel dépend fortement du degré d'anisotropie du milieu. Contrairement aux idées répandues, la convergence en la paroi du tunnel ainsi que l'état de contrainte-déformation autour du tunnel dépendent non seulement de l'degré d'anisotropie des modules de Young et des perméabilités, mais également (et parfois autant que sur ceux-ci) du coefficient de Poisson, du module de cisaillement dans le plan isotrope, et du degré d'anisotropie du coefficient de Biot. Par ailleurs, les résultats montrent que la rigidité et de l'épaisseur du revêtement peut modifier fortement la réponse du tunnel. Dans les études paramétriques, l'effet de la condition de drainage au niveau de l'interface des massif-revêtement a été évalué. Les résultats démontrent que, lorsque la condition de drainage complète est appliquée au niveau du contact, un comportement anisotrope plus important est observé en comparaison avec le cas sans drainage. En particulier, lorsque l'hydraulique est isotrope, les contraintes et le déplacement radial du revêtement est indépendante de l'état de drainage au niveau du contact des massif-revêtement, similaire au cas d'une roche isotrope mécaniquement et hydrauliquement.

La réponse d'un tunnel dans un milieu anisotrope au cours de la transitoire hydraulique a été considérée dans la deuxième partie de cette thèse. La solution transitoire hydraulique donnant la distribution de la pression interstitielle en fonction de temps, a été calculée comme une succession d'état d'équilibre en utilisant un rayon de l'influence en fonction de temps. Au-delà de ce rayon d'influence l'état hydrique est non perturbé. Par conséquent, le problème peut être traité par les mêmes outils que celles développés pour le cas permanent. Soulignons le fait que, de par l'approche choisie seuls les effets de l'hydraulique sur la mécanique ont été considérés (et pas l'inverse) ce qui est connu comme un couplage unilatéral.

La solution analytique transitoire obtenue pour un tunnel sans revêtement fait apparaitre une zone de contrainte radiale effective en traction aux premiers instants de calcul, et au voisinage de la paroi du tunnel. L'intensité de cette contrainte effective peut souvent dépasser la résistance en traction des roches et provoquer une zone de fissures initiales ou une zone de déformations plastiques (selon l'approche de modélisation choisie). Ce phénomène, non observable pour un milieu élastique isotrope, est dû au fait que la pression de pore devient plus grande que la contrainte radiale totale (qui devient faible après creusement et proche de la paroi). Pour le modèle de couplage à sens unique, cette valeur de la pression interstitielle est approximativement égale à sa valeur initiale.

La surpression interstitielle est habituellement rencontré dans le cas d'un massif rocheux avec une faible perméabilité et / ou une grande vitesse de creusement. Dans le cas des milieux anisotropes, contrairement au cas isotrope, le creusement ne se fait pas à déformation volumique nulle. Dans le cas d'un couplage unilatéral ce fait n'est pas pris en compte car dans le cadre de ce couplage il n'y a pas d'impact de la mécanique sur l'hydraulique. Par conséquence, une étude numérique à couplage complet a été effectuée. Les analyses numériques ont confirmé que, pour un massif rocheux à très faible perméabilité, la zone de surpression de pores qui apparait dans les premiers instants de creusement provoque une contrainte radiale effective en traction au voisinage de la paroi du tunnel. En particulier, pour les milieux poreux anisotropes, la répartition de la surpression interstitielle est toujours plus importante dans la direction à plus grande rigidité. Certains paramètres ont été également évalués pour étudier leur influence sur la pression des pores.

Une extension de la solution analytique obtenue basant sur l'approche de la méthode convergence-confinement a également été abordée pour des applications dans la conception des tunnels. D'après cela, cette solution a tenu compte de l'influence de la distance de la section d'installation de soutènement au front de taille du tunnel sur le travail du soutènement ainsi que sur le massif.

Les solutions analytiques obtenues dans le cadre de cette thèse pourraient être utilisées comme des outils de conception et de dimensionnement par les ingénieurs. En effet, en combinant ces solutions avec la méthode de convergence-confinement, il est possible d'obtenir rapidement une décision sur la conception du revêtement en considérant le taux de déconfinement.

Comme la première perspective de ce travail, une extension des solutions obtenues pour tenir compte une orientation arbitraire de l'axe de creusement semblerait utile et nécessaire. En fait le cas de déformations planes traité dans ce travail englobe une grande partie des cas rencontrés en pratique où l'axe du tunnel est dans le plan d'isotrope. Dans plusieurs cas, n néanmoins cette direction est arbitraire et l'extension de ces solutions pourrait s'avérer important et utile.

De même, les solutions analytiques développés pour un tunnel de section circulaire peuvent être étendues pour des tunnels de sections non circulaires (semi-circulaire, double arc ou rectangulaires) qui sont encore utilisés dans la pratique. Cela peut être réalisé à l'aide de la technique de « conformal mapping ».

Dans une perspective plus lointaine, l'extension de l'approche pour le comportement non-linéaire instantané et différé des massifs rocheux est une voie qui pourrait améliorer considérablement les capacités de prédiction de l'outil développé ici. Comme une première approche, le cas des massifs rocheux fracturés avec des fractures viscoélastiques/visco-plastique pourrait être envisagé. Ces fractures/discontinuités pourrait être soit structurelles (schistosité, stratification) soit induites par l'excavation elle-même. Nous avons vu l'apparition des zones à surpression et contrainte effective de traction surtout dans la direction de la rigidité maximale. Cela peut expliquer dans une certaine mesure, certains caractéristiques EDZ observées autour des tunnels (par exemple, les observations de l'EDZ autour des tunnels à Bure dans le contexte de stockage déchets radioactifs, montre une convergence de la paroi du tunnel et un développement d'EDZ plus importante dans la direction où la roche a une plus grande rigidité). Le développement d'une zone de surpression et d'une fissuration initiée par une contrainte effective de traction peut être une explication possible. La description de cette fracturation induite pourrait être réalisée par l'approche proposée, comprenant un comportement viscoélastique des fissures en fonction du temps. La mise en place de cette approche demanderait un développement préalable d'un modèle visoplastique du massif/fractures validé par des essais de laboratoire et des observations in situ.

REFERENCES

Abousleiman, Y., Cheng, A.H-D., Gui, L., Detoumay, E., & Roegiers. J.-C., (1996). Mandel's problem revisited. Géotechnique 46 (2), 187-195.

Abousleiman A., & Cui L. (1998). Poroelastic solutions in transversely isotropic media for wellbore and cylinder. *Int. Jour. Sol. Struct., 35*, 4905-4929.

Abousleiman, Y., and Cui, L., (2000). The theory of anisotropic poroelasticity with applications, Modeling and Applications in Geomechanics, Eds. M. Zaman, J. Booker & G. Gioda, John Wiley & Sons.

Abousleiman, Y., and Ekbote, S., (2005). Solutions for the Inclined Borehole in a Porothermoelastic Transversely Isotropic Medium, Journal of Applied Mechanics.

Amadei, B. and Goodman, R.E. (198la). A 3-D constitutive relation for fractured rock masses. Proc. International Symposium on the Mechanical Behavior of Structured Media, Ottawa. Selvadurai, A.P.S. (Editor). Part B, 249-268.

Amadei, B. and Goodman, R.E. (198lb). Formulation of complete plane strain for regularly jointed rocks. Proc. 22nd Symposium on Rock Mechanics (M.I.T.), 245-251.

Amadei, B.. (1983). Rock anisotropy and the theory of stress measurement. Springer Verlag.

Amadei, B. and Savage, W.Z. (1993). Effect of joints on rock mass strength and deformability, in J. A. Hudson. E. T. Brown, C. Fairhurst and E. Hoek (eds), Comprehensive Rock Engineering Principles, Practice and Project, Volume I: Fundamentals, Pergamon Press, Oxford, 331-365.

Amadei, B. (1996). Importance of anisotropy when estimating and measuring in situ stresses in rock, Int. J. Rock Mech.,33, 293–325.

Armand G., Noireta A., Zghondi J., Seyedi D.M. (2013). Short- and long-term behaviors of drifts in the Callovo-Oxfordian claystone at the Meuse/Haute-Marne Underground Research Laboratory. Journal of Rock Mechanics and Geotechnical Engineering; 5: 221-230.

Armand G., F. Leveau, C. Nussbaum, R. de La Vaissiere, A. Noiret, D. Jaeggi, P. Landrein, C. Righini. (2014). Geometry and Properties of the Excavation-Induced Fractures at the Meuse/Haute-Marne URL Drifts. Rock Mech Rock Eng; 47:21–41.

Bear, J., and G. Dagan. (1965). The relationship between solutions of flow problems in isotropic and anisotropic soils. Journal of Hydrology 3, no. 2: 88–96.

Bear, J. (1972). Dynamics of fluids in porous media, 3rd ed., American Elsevier, USA.

Biot, M.A.. General theory of three-dimensional consolidation,' J. .Appl. Phys., 12, 155-164, 1941.

Biot. M. A.. Theory of Elasticity and consolidation of a porous anisotropic solid, J. Appl. Phys.. 26. 182-185, 1955.

Bobet A (2001). Analytical solutions for shallow tunnels in saturated ground. ASCE J. Eng. Mech. 127(12):1258–1266

Bobet A (2003). Effect of pore water pressure on tunnel support during static and seismic loading. Tunn Undergr Space Technol 18:377–393

Bobet A (2007a). Ground and liner stresses due to drainage conditions in deep tunnels. Felsbau 25(4):42–47.

Bobet A, Nam S. (2007b). Stresses around pressure tunnels with semipermeable liners. Rock Mech Rock Eng. 40 (3):287–315.

Bobet A (2009a) Characteristic curves for deep circular tunnels in poro-plastic rock. Rock Mech Rock Eng (in press).

Bobet A (2009b) Drained and undrained response of deep tunnels subjected to far-field shear loading. Tunn Undergr Sp Technol (in press).

Bobet A. (2011). Lined circular tunnels in elastic transversely anisotropic rock at depth. *Roc. Mec. Roc. Eng.*, *44,* 149–167.

Bobet A., & Yu H. (2015). Stress field near the tip of a crack in a poroelastic transversely anisotropic saturated rock. *Engineering Fracture Mechanics, 14*, 1–18.

Boresi, A.P., Chong K.P., Lee J.D., Elasticity in Engineering Mechanics, 3rd ed. John Wiley & Sons, Inc., New Jersey, 2011.

Bourbie T. et Zinszner B. (1985). Hydraulic and acoustic properties as a function of porosity in Fontainebleau sandstone. Journal of Geophysical Research. Vol. 90, N°. B13, PP 11524-11532.

Carranza-Torres C., Fairhurst C. (2000). Application of the convergence-confinement method design to rock masses that satisfy the Hoek-Brown failure criterion. Tunn Undergr Space Technol 15(2):187–213

Carranza-Torres C. (2004). Elasto-plastic solution of tunnel problems using the generalized form of the Hoek-Brown failure criterion. Int J Rock Mech Min Sci 34(3–4):075

Carranza-Torres C., & Zhao J. (2009). Analytical and numerical study of the effect of water pore pressure on the mechanical response of cylindrical lined tunnels in elastic and elasto-plastic porous media. *Int. Jour. Rock Mech. Min. Sci.*, *46*, 531–547.

Carter JP, Booker JR. (1982). Elastic consolidation around a deep circular tunnel. Int J Solids Struct. 18:1059–74.

Carter JP, Booker JR. (1984). Elastic consolidation around a lined circular tunnel. Int J Solids Struct. 20:589–608.

Charlier R., Collin F., Pardoen B, Talandier J., Radu JP., Gerard P. (2013). An unsaturated hydro-mechanical modelling of two in-situ experiments in Callovo–Oxfordian argillite. Eng Geol. 165:46–63.

Chen G., &Yu L. (2015). Consolidation around a tunnel in a general poroelastic medium under anisotropic initial stress conditions. *Computers and Geotechnics*, *66*, 39–52.

Chenevert (1964) The deformation failure Chatateristics of laminated sedimentary rock, PhD Thesis, The University of Texas at Austin.

Cheng, A.H-D. (1997). Material coefficients of anisotropic poroelasticity. Int. J. Rock Mech. Min. Sci., 34, 183-193.

Cheng AH-D. (1998). On generalized plan strain poroelasticity. Int. J. Rock Mech Min Sci 35(2):183–193.

Cheng AH-D. (2016). Poroelasticity. Theory and Applications of Transport in Porous Media. Springer.

Chern, J.C., F.Y. Shiao, and C.W. Yu (1998). An empirical safety criterion for tunnel construction. In Proc.Regional Symposium on Sedimentary Rock Engineering, Taipei, Taiwan, 222-227.

Chu, S.T. (1994). Transient Radius of Influence Model. ASCE J. Irrig. and Drainage Eng. 120 (5), 964-969.

Churchill, R.V., (1960). Complex Variables and Applications, second ed. McGraw-Hill Book Company, New York.

Cihan, A., Zhou, Q., Birkholzer, J.T., Kraemer, S.R., (2014). Flow in horizontallyanisotropic multilayered aquifer systems with leaky wells and aquitards. WaterResour. Res. 50 (1), 741-747.

Cleary, M.P., (1977). Fundamental solutions for a fluid-saturated porous solid, Int. J. Solids Structures, 13, 785-806.

Coussy, O., (1991). Mécanique des milieux poreux, Editions Technip.

Coussy, O., (1995). Mechanics of Porous Continua, John Wiley &: Sons, New York. 1995.

Coussy, O., (2004). Poromechanis, John Wiley &: Sons, New York.

De Groot, S.R., (1952). Thermodynamics of Irreversible Processes. North-Holland, Amsterdam.

Dao N. H., Vu M. N. (2016). Load sequence effects on the fatigue crack growth in a cylinder subjected to combined rotary bending moment and axial force loads. Theoretical and Applied Fracture Mechanics 82, 117-124.

Detournay E., & Cheng A. H. D. (1988). Poroelastic response of a borehole in a non-hydrostatic stress field. *Int. J. Rock Mech. Min. Sci. & Geomech.*, *25,* 171-182.

Detournay E, Cheng AH-D (1993). Fundamentals of poroelasticity. In: Hudson JA (ed.) Comprehensive rock engineering: principles, practice and projects. Pergamon Press, Oxford, UK, vol 2, pp 113–171.

Duncan, J.M. and Goodman, R.E. (1968). Finite element analysis of slopes in jointed rocks. Contract report S-68-3, U.S. Army Engineer Waterways Experiment Station, Corps of Engineers, Vicksburg, Mississippi.

Duncan C.Wyllie, (2005). Foundations on Rock. Taylor & Francis.

Einstein H.H., Schwartz C.W., (1979). Simplified analysis for tunnel supports. J. Geotech. Engng. Div. ASCE, pp. 499-517.

Exadaktylos G.E., Stavropoulou M.C. A closed-form elastic solution for stresses and displacements around tunnels. Int Jour. Rock Mech. Min Sci. 2002; 39:905–916.

Fitts, C. R. (2006). Exact solution for two-dimensional flow to a well in an anisotropic domain, Ground Water, 44(1), 99–101.

Flugge W. (1966). Stresses in Shells. Springer, New York.

Gill D.E., Leite M.H., (1995). Designing tunnel supports with the convergence-confinement method when the far stress field is anisotropic. Proc. 8th ISRM Cong., Tokyo, pp. 563-568.

Green, A.E. and Zerna W. (1968). Theoretical Elasticity. Dover Publications, Inc.

Green, A. E. (1940). General Bi-Harmonic Analysis for a Plate Containing Circular Holes. Proceedings of the Royal Society A: Mathematical, Physical and Engineering Sciences, 176(964), 121–139.

Green, D. H. & Wang, H. F. (1990). Specific storage as a poroelastic coefficient. Water Resour. Res. 26, 1631-1637.

Guayacan-Carrillo, L.M., Sulem, J., Seyedi, D.M., Ghabezloo, S., Noiret, A., Armand, G., 2015. Analysis of long-term anisotropic convergence in drifts excavated in callovo-oxfordian claystone. Rock Mech. Rock Eng.

Hefny A. M., & Lo K. Y. (1999). Analytical solutions for stresses and displacements around tunnels driven in cross-anisotropic rocks. *Int. Jour. Num. Ana. Methods Geomech*., *23,* 161–177.

Hoek, E. (1999). Personal communication.

Hoxha, D., Giraud, A., Blaisonneau, A., Homand, F., Chavant, C., (2004). Poroplastic modelling of the excavation and ventilation of a deep cavity. Int. J. Numer. Anal. Meth. Geomech. 28, 339-364.

Hwu, C., (2010). Anisotropic Elastic Plates. Springer.

Jaeger JC., Cook NGW., (2007). Fundamentals of rock mechanics, New York.

Jacob C.E, Lohman S.W., (1952). Nonsteady flow to a well of constant drawdown in an extensive aquifer. Trans AGU 33(4):559–569.

Kirsch EG (1898). The theory of elasticity and its application to the strength of materials. Zeitschrift des Vereines deutscher Ingenieure 42:797–807.

Kolymbas D., Wagner P., & Blioumi A. (2012). Cavity expansion in cross-anisotropic rock. *Int J Numer Anal Methods Geomech. 36*, 128–139.

Kucuk, F., and W. E. Birgham (1979). Transient flow in elliptical systems, Soc. Pet. Eng. J., 19, 401–410.

Kreyszig E. (1999). Advanced Engineering Mathematics, John Wiley, New York.

Lama, R. D. and Vutukuri, V.S (1978) Handbook on mechanical properties of rocks, Vol I and II of Series on Soil and Rock Mechacnis, Trans Tech Publication, Ohio.

Lekhnitskii S. G. (1963). Theory of elasticity of an anisotropic elastic body. San Francisco: Holden-Day, Inc.

Lekhnitskii S. G. (1963). Anisotropic Plate. Gordon and Breach Science Publishers. New York.

Lisjak A, Tatone B, Grasselli G, Vietor T. (2012). Numerical modelling of the anisotropic mechanical behaviour of Opalinus Clay at the laboratory-scale using FEM/DEM. Rock Mech Rock Eng.

Mathias, S. A., and A. P. Butler (2007), Flow to a finite diameter well in a horizontally anisotropic aquifer with wellbore storage, Water Resour. Res., 43, W07501.

François FRANÇOIS (2012). Mécanique des Roches et Travaux Souterrains. Cours et exercices corrigés. Huitième édition. ENS Cachan.

Millard A., Bond A.E., Nakama S., Zhang C., Barnichon J.D., Garitte B., (2013). Accounting for anisotropic effects in the prediction of the hydro-mechanical response of a ventilated tunnel in an argillaceous rock. Journal of Rock Mechanics and Geotechnical Engineering, 5 (2), 97–109.

Milne-Thomson LM (1960). Plane Elastic Systems, Springer Verlag, Berlin.

Muskhelishvili NJ., (1953). Singular Integral Equations, trans. JRM Radok and P Noordhoff, Groningen, The Netherlands.

Muskhelishvili NJ., (1963.). Some Basic Problems of the Theory of Elasticity, trans. JRM Radok and P Noordhoff, Groningen, The Netherlands.

Nam S., Bobet A. (2006). Liner stresses in deep tunnels below the water table. Tunn Undergr Space Technol. 21(6):626–635.

Nguyen S.T., Vu M. H., Vu M. N. (2015). Equivalent porous medium for modeling of elastic and sonic properties of sandstones. Journal of Applied Geophysics 120: 1-6.

Nguyen S.T., Vu M. H., Vu M. N. (2015). Extended analytical approach for electrical anisotropy of geomaterials. Journal of Applied Geophysics 123: 211-217.

Nguyen S.T., Vu M. H., Vu M. N., Nguyen T.N. (2015). Generalized Maxwell model for micro-cracked viscoelastic materials. International Journal of Damage Mechanics. Doi: 10.1177/1056789515608231.

Nguyen T. N., Nguyen S. T., Vu M. H., Vu M. N. (2015). Effective viscoelastic properties of micro-cracked heterogeneous materials. International Journal of Damage Mechanics. Doi: 10.1177/1056789515605557.

Nguyen S. T., Thai M. Q., Vu M. N., To Q. D. (2016). A homogenization approach for effective viscoelastic properties of porous media. Mechanics of Materials 100, 175-185.

Nguyen S. T., Pham D. C., Vu M. N., To Q. D. (2016). On the effective transport properties of heterogeneous materials. International Journal of Engineering Science 104, 75-86.

Nguyen S. T., Tran-Le A. D., Vu M. N., To Q. D., Douzane O., Langlet T. (2016). Modeling thermal conductivity of hemp insulation material: A multi-scale homogenization approach. Building and Environment 107, 127-134.

Panet, M., Guenot, A. (1982). Analysis of Convergence Behind The Face of a Tunnel, Proceedings, International Symposium Tunnelling'82, The Institution of Mining and Metallurgy. London, pp. 197-204.

Panet M. (1995). Le calcul des tunnels par la méthode convergence-confinement, Presses de l'EcoleNationale des Ponts et Chaussées.

Pardoen B, Seyedi DM, Collin F. (2015). Shear banding modelling in cross-anisotropic rocks. Int J Solids Struct. 2015;72:63–87.

Perrochet, P. (2005a). Confined flow into a tunnel during progressive drilling: an analytical solution. Ground Water 43, No. 6, 943-946.

Perrochet, P. (2005b). A simple solution to tunnel or well discharge under constant drawdown. Hydrology Journal 13, 886-888.

Pouya A., Vu M. N. (2012). Numerical modelling of steady-state flow in 2D cracked anisotropic porous media by singular integral equations method. Transport in Porous Media 93(3):475-493.

Pouya A., Vu M. N. (2012). Fluid Flow and Effective permeability of an infinite matrix containing disc-shaped cracks. Advance in Water Resources 42:37-46.

Pouya A., Vu M. N., Ghabezloo S., Bendjeddou Z. (2013). Flow around an unsaturated crack in a porous medium and related problems. International Journal of Solids and Structures 50(20-21): 3297-3307.

Rahn W. (1984). Stress Concentration Factors for the Interpretation of "Doorstopper" Stress Measurements in Anisotropic Rocks, Int. J. Rock Mech. Min. Sci. Geomech. Abstr. 21: 313-326.

Rice, J.R., and Cleary, M.P. (1976). Some basic stress diffusion solutions for fluid saturated elastic porous media with compressible constituents. Reviews of Geophysics and Space Physics 14(4), 227-241.

Sadd M.H., Elasticity: theory, applications, and numeric. Elsevier Inc.

Savin, G.N., (1961). Stress Concentration around Holes. Pergamon Press, London, UK.

Scheidegger, A.E., (1974). The Physics of Flow through Porous Media. 3rd edition. University of Toronto Press, Toronto.

Seyedi D., Vu M. N., Pouya A. (2015). A two-scale hydromechanical model for fault zone accounting for their heterogeneous structure. Computer and Geotechnics 68: 8-16.

Stroh, A.N., (1962). "Steady State Problems in Anisotropic Elasticity," Journal of Mathematical Physics, Vol. 41, pp. 77–103.

Tang A. M., Vu M. N., Cui Y-J. (2011): Effects of the maximum soil aggregates size and cyclic wetting-drying on the stiffness of a lime-treated clayey soil. Géotechnique 61(5):421-429.

Terzahghi. K. V. (1943). Theorical soil mechanics. John Wiley & Sons, Inc New York.

Thompson, M., and Willis, JJl., 'A reformulation of the equations of anisotropic poroelasticity,' J. Appl. Mech., ASME, 58, 612-616, 1991.

Timoshenko, S.P., Goodier, J.N., 1970. Theory of Elasticity. McGraw Hill Publishing Company, New York.

To Q. D., He Q. C., Nguyen S. T., Vu M. N. (2016). Periodic adhesive contact between an elastic anisotropic layer and a wavy rigid halfspace. International Journal of Solids and Structures 92, 54-63.

Tonon F., & Amadei B. (2002). Effect of elastic anisotropy on tunnel wall displacements behind a tunnel face. *Rock Mech. Rock Eng., 35*, 141–160.

Tran MH, (2014). Comportement des tunnels en terrain poussant. Thèse de doctorat. l'Université Paris Est.

Tran M. H., Sulem J., & Subrin D. (2015a). A closed-form solution for tunnels with arbitrary cross section excavated in elastic anisotropic ground. *Rock Mech. Rock Eng., 48,* 277–288.

Tran-M H., Sulem J., Subrin D., Billaux D. (2015b). Anisotropic time-dependent modeling of tunnel excavation in squeezing ground. Rock Mech Rock Eng.

Tran N.H., Do D.P, Hoxha D., (2016). A closed-form hydro-mechanical solution for deep tunnels in elastic anisotropic rock. Proceedings, 34th Conference of Civil Engineering University-AUGC, University of Liège, Belgium, 25 - 27 May 2016.

Verruijt A (1997) A complex variable solution for a deforming circular tunnel in an elastic half-plane. Int J Numer Anal Methods Geomech 21:77–89.

Verruijt A (1998) Deformations of an elastic half plane with a circular cavity. Int J Solids Struct 35(21):2795–2804.

Verruijt A, Booker JR (1996) Surface settlements due to deformation of a tunnel in an elastic half plane. Geotechnique 46:753–756.

Vu M. N., (2012). Modélisation des écoulements dans des milieux poreux fracturés par la méthode des équations aux intégrales singulières. Thèse de Doctorat, Université Paris Est.

Vu M. N., Pouya A., Seyedi D. (2013). Modelling of steady state fluid flow in 3D fractured isotropic porous media by singular integral equation method. International Journal for Numerical and Analytical Methods in Geomechanics 37(14): 2257-2277.

Vu M. N., Pouya A., Seyedi D. (2014). Theoretical and Numerical study on steady-state flow through finite fractured porous media. International Journal for Numerical and Analytical Methods in Geomechanics 38(3): 221-235.

Vu M. N., Geniaut S., Massin P., Marigo J.J. (2015). Numerical investigation on corner singularities in cracked plate using the G-theta method with an adapted theta field. Theoretical and Applied Fracture Mechanics 77: 59-68.

Vu M. N., Nguyen S.T., Vu M.H, Tang A.M, To V.T (2015). Heat conduction and thermal conductivity of 3D cracked media. International Journal of Heat and Mass Transfer 89: 1119-1126 11.

Vu M. N., Nguyen S. T., Vu M. H. (2015). Modeling of fluid flow through fractured porous media by a single boundary integral equation. Engineering Analysis with Boundary Elements 59: 166-171.

Walsh J. B. and Grosenbaugh M. A. (1979). A new model for analyzing the effect of fracture on compressibility. Journal of geophysical research, Vol. 84, N° B7, pp 3532-3536.

Walsh J.B and Brace W.F. (1984). The effect of pressure on porosity and the transport properties of rock. Journal of geophysical research, Vol. 89, N° B11, pp 9425-9431.

Wang Y (1996) Ground response of circular tunnel in poorly consolidated rock. J Geotech Eng 122(9):703–708.

Wang HF., (2000). Theory of linear poroelasticity with applications to geomechanics and hydrogeology. Princeton University Press, Princeton.

Wang M. B., & Wang G. (2013). A modified stress-displacement solutions for a pressure tunnel with a permeable liner in an elastic porous medium based on new model. *Rock Mech. Rock Eng., 46*, 259–268.

Wang, T.-T., & Huang, T.-H. (2013). Anisotropic Deformation of a Circular Tunnel Excavated in a RockMass Containing Sets of Ubiquitous Joints: Theory Analysis and Numerical Modeling. Rock Mechanics and Rock Engineering, 47(2), 643–657.

Wittke W., (2014). Rock Mechanics Based on an Anisotropic Jointed Rock Model. Wiley, Ernst and Sohn.

Zhang Z., & Sun Y., (2011). Analytical solution for a deep tunnel with arbitrary cross section in a transversely isotropic rock mass. *Int. Jour. Rock Mech. Min. Sci.*, *48,* 1359–1363.

Vu, T. M., Sulem, J., Subrin, D., & Monin, N. (2013a). Semi-Analytical Solution for Stresses and Displacements in a Tunnel Excavated in Transversely Isotropic Formation with Non-Linear Behavior. Rock Mechanics and Rock Engineering, 46(2), 213–229.

APPENDIX: DISPLACEMENTS IN ROCK MASS AND IN THE LINER AT THE ROCK MASS-LINER INTERFACE

In this appendix, we detail the expressions of displacements in rock mass as well as in the liner at the rock mass-liner interface ($r=r_0$).

- Displacements in rock mass obtained from the solution of the problem Ib:

$$U^{Ib}_{x,r_0} = \frac{r_0}{\mu_1 - u_2}\Big\{(\mu_1^2 s_{11} - s_{12})\big[(\sigma_h - \mu_2\sigma_v)cos\theta + (1+\mu_2)\tau_{vh}sin\theta\big]$$
$$-(\mu_2^2 s_{11} - s_{12})\big[\sigma_h - \mu_1\sigma_v)cos\theta + (1+\mu_1)\tau_{vh}sin\theta\big]\Big\};$$
$$U^{Ib}_{y,r_0} = \frac{r_0}{\mu_1 - u_2}\left\{(\frac{s_{22}}{\mu_2} - \mu_2 s_{12})\big[(\mu_1\sigma_v - \sigma_h)sin\theta + (1+\mu_1)\tau_{vh}cos\theta\big]\right. \tag{A.1}$$
$$\left.-\left(\frac{s_{22}}{\mu_1} - \mu_1 s_{12}\right)\big[\mu_2\sigma_v - \sigma_h)sin\theta + (1+\mu_2)\tau_{vh}cos\theta\big]\right\};$$

- Displacements in rock mass obtained from the solution of the problem Ic:

$$U^{Ic}_{x,r_0} = -\frac{1}{2}\frac{r_0}{\mu_1 - u_2}(\mu_1^2 s_{11} - s_{12})\Big\{[2(1-\mu_2)\sigma_0 + (1+\mu_2)(\sigma_2^a - \tau_2^a)]cos\theta$$
$$+(1+\mu_2)(\sigma_2^b + \tau_2^b)sin\theta + \sum_{n=3,5,7}^{\infty}\frac{1}{n}[(1-\mu_2)(\sigma_{n-1}^a + \tau_{n-1}^a) + (1+\mu_2)(\sigma_{n-1}^a - \tau_{n-1}^a)]cosn\theta$$
$$+\sum_{n=3,5,7}^{\infty}\frac{1}{n}[(1-\mu_2)(\sigma_{n-1}^b + \tau_{n-1}^b) + (1+\mu_2)(\sigma_{n-1}^b - \tau_{n-1}^b)]sinn\theta\Big\}$$
$$+\frac{1}{2}\frac{r_0}{\mu_1 - u_2}(\mu_2^2 s_{11} - s_{12})\Big\{[2(1-\mu_1)\sigma_0 + (1+\mu_1)(\sigma_2^a - \tau_2^a)]cos\theta \tag{A.2a}$$
$$+(1+\mu_2)(\sigma_2^b + \tau_2^b)sin\theta + \sum_{n=3,5,7}^{\infty}\frac{1}{n}[(1-\mu_1)(\sigma_{n-1}^a + \tau_{n-1}^a) + (1+\mu_1)(\sigma_{n-1}^a - \tau_{n-1}^a)]cosn\theta$$
$$+\sum_{n=3,5,7}^{\infty}\frac{1}{n}[(1-\mu_1)(\sigma_{n-1}^b + \tau_{n-1}^b) + (1+\mu_1)(\sigma_{n-1}^b - \tau_{n-1}^b)]sinn\theta\Big\};$$

$$U^{Ic}_{y,r_0} = -\frac{1}{2}\frac{r_0}{\mu_1 - u_2}(\frac{s_{22}}{\mu_1} - \mu_1^2 s_{11})\Big\{[2(i-\mu_2)\sigma_0 + (i+\mu_2)(\sigma_2^a - \tau_2^a)]sin\theta - (i+\mu_2)(\sigma_2^b + \tau_2^b)cos\theta$$
$$+\sum_{n=3,5,7}^{\infty}\frac{1}{n}[(i-\mu_2)(\sigma_{n-1}^a + \tau_{n-1}^a) + (i+\mu_2)(\sigma_{n-1}^a - \tau_{n-1}^a)]sinn\theta$$
$$-\sum_{n=3,5,7}^{\infty}\frac{1}{n}[(i-\mu_2)(\sigma_{n-1}^b - \tau_{n-1}^b) + (i+\mu_2)(\sigma_{n-1}^b + \tau_{n-1}^b)]cosn\theta\Big\}$$
$$+\frac{1}{2}\frac{r_0}{\mu_1 - u_2}(\frac{s_{22}}{\mu_2} - \mu_2^2 s_{11})\Big\{[2(i-\mu_1)\sigma_0 + (i+\mu_1)(\sigma_2^a - \tau_2^a)]sin\theta - (i+\mu_1)(\sigma_2^b + \tau_2^b)cos\theta \tag{A.2b}$$
$$+\sum_{n=3,5,7}^{\infty}\frac{1}{n}[(i-\mu_1)(\sigma_{n-1}^a + \tau_{n-1}^a) + (i+\mu_1)(\sigma_{n-1}^a - \tau_{n-1}^a)]sinn\theta$$
$$-\sum_{n=3,5,7}^{\infty}\frac{1}{n}[(i-\mu_1)(\sigma_{n-1}^b - \tau_{n-1}^b) + (i+\mu_1)(\sigma_{n-1}^b - \tau_{n-1}^b)]cosn\theta\Big\};$$

- Displacements in liner obtained from the solution of the problem Id:

$$U_{x,r_0}^{Id} = \frac{1-\nu_s^2}{E_s(I_s + r_0^2 A_s)} r_0^4 \sigma_0 cos\theta - Csin\theta + \frac{1}{2}\frac{1-\nu_s^2}{E_s I_s} r_0^2 \left\{ \frac{1}{12}[(2\sigma_2^a - \tau_2^a) r_0^2 - 3\frac{I_s}{A_s}\tau_2^a] cos\theta \right.$$

$$+ \frac{1}{12}[(2\sigma_2^b + \tau_2^b) r_0^2 + 3\frac{I_s}{A_s}\tau_2^b] sin\theta$$

$$+ \sum_{n=3,5,7}^{\infty} \left[\left(\frac{(n-1)\sigma_{n-1}^a - \tau_{n-1}^a}{n^2(n-1)^2(n-2)} + \frac{(n+1)\sigma_{n+1}^a - \tau_{n+1}^a}{n^2(n+1)^2(n+2)} \right) r_0^2 + \frac{I_s}{A_s} \left(\frac{\tau_{n-1}^a}{(n-1)^2} - \frac{\tau_{n+1}^a}{(n+1)^2} \right) \right] cosn\theta \tag{A.3a}$$

$$\left. + \sum_{n=3,5,7}^{\infty} \left[\left(\frac{(n-1)\sigma_{n-1}^b + \tau_{n-1}^b}{n^2(n-1)^2(n-2)} + \frac{(n+1)\sigma_{n+1}^b + \tau_{n+1}^b}{n^2(n+1)^2(n+2)} \right) r_0^2 - \frac{I_s}{A_s} \left(\frac{\tau_{n-1}^b}{(n-1)^2} - \frac{\tau_{n+1}^b}{(n+1)^2} \right) \right] sinn\theta \right\} ;$$

$$U_{y,r_0}^{Id} = \frac{1-\nu_s^2}{E_s(I_s + r_0^2 A_s)} r_0^4 \sigma_0 sin\theta + Ccos\theta + \frac{1}{2}\frac{1-\nu_s^2}{E_s I_s} r_0^2 \left\{ -\frac{1}{12}[(2\sigma_2^a - \tau_2^a) r_0^2 - 3\frac{I_s}{A_s}\tau_2^a] sin\theta \right.$$

$$+ \frac{1}{12}[(2\sigma_2^b + \tau_2^b) r_0^2 + 3\frac{I_s}{A_s}\tau_2^b] cos\theta$$

$$+ \sum_{n=3,5,7}^{\infty} \left[\left(\frac{(n-1)\sigma_{n-1}^a - \tau_{n-1}^a}{n^2(n-1)^2(n-2)} - \frac{(n+1)\sigma_{n+1}^a - \tau_{n+1}^a}{n^2(n+1)^2(n+2)} \right) r_0^2 + \frac{I_s}{A_s} \left(\frac{\tau_{n-1}^a}{(n-1)^2} + \frac{\tau_{n+1}^a}{(n+1)^2} \right) \right] sinn\theta \tag{A.3b}$$

$$\left. - \sum_{n=3,5,7}^{\infty} \left[\left(\frac{(n-1)\sigma_{n-1}^b + \tau_{n-1}^b}{n^2(n-1)^2(n-2)} + \frac{(n+1)\sigma_{n+1}^b + \tau_{n+1}^b}{n^2(n+1)^2(n+2)} \right) r_0^2 - \frac{I_s}{A_s} \left(\frac{\tau_{n-1}^b}{(n-1)^2} + \frac{\tau_{n+1}^b}{(n+1)^2} \right) \right] cosn\theta \right\}$$

- Expression of displacements in rock mass at the tunnel perimeter obtained from the solution of the problem IIa, chapter 2:

$$U_{x,r_0}^{IIa} = r_0(p_{ff} - p_0)\,\mathrm{Re}\left\{ \left[p_1 N_1 + p_2 N_2 + (p_w \eta - \beta_1) \right] \cos\theta + \right.$$

$$\left. \left[p_1 N_1 \mu_1 + p_2 N_2 \mu_2 + (p_w \eta - \beta_1)\mu_w \right] \sin\theta \right\}$$

$$- \frac{r_0}{\mu_1 - u_2} \left\{ (\mu_1^2 s_{11} + s_{12}) \left[i\Sigma_x - \mu_2 \Sigma_y) cos\theta + (i + \mu_2) \mathrm{T}_{xy} sin\theta \right] \right. \tag{A.4a}$$

$$\left. + (\mu_2^2 s_{11} + s_{12}) \left[i\Sigma_x - \mu_1 \Sigma_y) cos\theta + (i + \mu_1) \mathrm{T}_{xy} sin\theta \right] \right\};$$

$$U_{y,r_0}^{IIa} = r_0(p_{ff} - p_0)\,\mathrm{Re}\left\{ \left[q_1 N_1 + q_2 N_2 + q_w \eta - \frac{\beta_2}{\mu_w} \right] \cos\theta \right.$$

$$\left. + \left[q_1 N_1 \mu_1 + q_2 N_2 \mu_2 + (q_w \eta - \frac{\beta_2}{\mu_w})\mu_w \right] \sin\theta \right\}$$

$$- \frac{r_0}{\mu_1 - u_2} \left\{ (\frac{s_{22}}{\mu_2} + \mu_2 s_{12}) \left[(1 - i\mu_1) \mathrm{T}_{xy} cos\theta - (i\mu_1 \Sigma_y + \Sigma_x) sin\theta \right] \right. \tag{A.4b}$$

$$\left. + \left(\frac{s_{22}}{\mu_1} + \mu_1 s_{12} \right) \left[(1 - i\mu_2) \mathrm{T}_{xy} cos\theta - (i\mu_2 \Sigma_y + \Sigma_x) sin\theta \right] \right\};$$

- Expression for the displacements in rock mass and in the liner at the tunnel perimeter obtained from the solution of the problem IIb and IIc are the same forms of those of the problem Ic and Id respectively as presented previously by replacing the constants $\sigma_0, \sigma_n^a, \sigma_n^b, \tau_n^a, \tau_n^b$ by $\sigma_0^p, \sigma_n^{a,p}, \sigma_n^{b,p}, \tau_n^{a,p}, \tau_n^{b,p}$

- Expression of displacements in rock mass at the tunnel perimeter obtained from the solution of the problem IIa, chapter 3:

$$U^{IIa}_{x,r_0} = r_0(u_{ff} - u_0)\,\mathrm{Re}\Big\{\big[p_1N_1 + p_2N_2 + (p_w\eta - \beta_1)\big]\cos\theta +$$
$$\big[p_1N_1\mu_1 + p_2N_2\mu_2 + (p_w\eta - \beta_1)\mu_w\big]\sin\theta\Big\} + p_1P_1\frac{I_e(t_e)}{6}(\cos\theta + i\sin\theta)(i\mu_1 - 1)$$
$$-\frac{r_0}{\mu_1 - u_2}\Big\{(\mu_1^2 s_{11} + s_{12})\big[i\Sigma_x - \mu_2\Sigma_y)cos\theta + (i+\mu_2)\mathrm{T}_{xy}sin\theta\big]$$
$$+(\mu_2^2 s_{11} + s_{12})\big[i\Sigma_x - \mu_1\Sigma_y)cos\theta + (i+\mu_1)\mathrm{T}_{xy}sin\theta\big]\Big\};\tag{B.1}$$

$$U^{IIa}_{y,r_0} = r_0(p_{ff} - p_0)\,\mathrm{Re}\left\{\left[q_1N_1 + q_2N_2 + q_w\eta - \frac{\beta_2}{\mu_w}\right]\cos\theta\right.$$
$$\left. + \left[q_1N_1\mu_1 + q_2N_2\mu_2 + (q_w\eta - \frac{\beta_2}{\mu_w})\mu_w\right]\sin\theta\right\} + p_2P_2\frac{I_e(t_e)}{6}(\cos\theta + i\sin\theta)(i\mu_2 - 1)$$
$$-\frac{r_0}{\mu_1 - u_2}\left\{(\frac{s_{22}}{\mu_2} + \mu_2 s_{12})\big[(1 - i\mu_1)\mathrm{T}_{xy}cos\theta - (i\mu_1\Sigma_y + \Sigma_x)sin\theta\big]\right.$$
$$\left. + \left(\frac{s_{22}}{\mu_1} + \mu_1 s_{12}\right)\big[(1 - i\mu_2)\mathrm{T}_{xy}cos\theta - (i\mu_2\Sigma_y + \Sigma_x)sin\theta\big]\right\};\tag{B.2}$$

Nam Hung TRAN

COMPORTEMENT HYDRO-MECANIQUE DES TUNNELS PROFONDS DANS MILIEUX POREUX ANISOTROPE ELASTIQUE

Résumé:

Les tunnels profonds sont souvent construits dans les roches sédimentaires et métamorphiques stratifiées qui présentent habituellement des propriétés anisotropes en raison de leur structure et des propriétés des constituants. Le présent travail vise à étudier les tunnels profonds dans un massif rocheux anisotrope élastique en portant une attention particulière sur les effets des couplages hydromécaniques par des approches analytiques et numériques. Une solution analytique pour un tunnel creusé dans un massif rocheux anisotrope saturé est développée en tenant compte du couplage hydro-mécanique dans le régime permanent. Cette solution analytique est utilisée pour réaliser une série d'études paramétriques afin d'évaluer les effets des différents paramètres du matériau anisotrope sur le comportement du tunnel.

Dans un deuxième temps la solution analytique est élargie pour décrire le comportement du tunnel pendant la phase transitoire hydraulique. Afin de compléter ces études analytiques qui prennent en compte seulement un couplage unilatéral (dans le sens que seul le comportement hydraulique influence le comportement mécanique et pas l'inverse) de l'analyse numérique avec un couplage complet, ont été réalisés. Une application de la solution analytique sur la méthode de convergence-confinement est aussi bien abordée qui peut prendre en compte l'influence du front de taille du tunnel sur le travail du soutènement ainsi que sur le massif.

La solution obtenue peut servir comme un outil de dimensionnement rapide des tunnels en milieux poreux en le combinant avec des approches de dimensionnement comme celle de convergence-confinement.

Mots clés: tunnels profonds, comportement hydro-mécanique, roche anisotrope élastique, solution analytique, solution numérique, dimensionnement des tunnels.

HYDRO-MECHANICAL BEHAVIOR OF DEEP TUNNELS IN ANISOTROPIC PORO-ELASTIC MEDIUM

Summary:

Deep tunnels are often built in the sedimentary and metamorphic foliated rocks which exhibits usually the anisotropic properties due to the presence of the discontinuity. The analysis of rock and liner stresses due to tunnel construction with the assumption of homogeneous and isotropic rock would be incorrect. The present thesis aims to deal with the deep tunnel in anisotropic rock with a particular emphasis on the effects of hydraulic phenomenon on the mechanical responses or reciprocal effects of hydraulic and mechanical phenomena by combining analytical and numerical approach. On that point of view, a closed-formed solution for tunnel excavated in saturated anisotropic ground is developed taking into account the hydro-mechanical coupling in steady-state. Based on the analytical solution obtained, parametric studies are conducted to evaluate the effects of different parameters of the anisotropic material on the tunnel behavior. The thesis considers also to extend the analytical solution with a time-dependent behavior which takes into account the impact of the pore pressure distribution on mechanical response over time, i.e., one way coupling modeling. In addition, some numerical analysis based on fully-coupled modeling, i.e., two ways coupling, are conducted which are considered as the complete solution for the analytical solution. An application of the closed-form solution on convergence-confinement method is as well referred which can take into account the influence of the tunnel face on the work of the support as well as the massif.

The obtained solution could be used as a quick tool to calibrate tunnels in porous media by combining with design approaches such as convergence-confinement method.

Keywords: deep tunnels, hydro-mechanical behaviour, elastic anisotropic rock, analytical solution, numerical solution, calibrate tunnels.

Laboratoire PRISME
08 rue Leonard de Vinci, 45072 Orléans Cedex 2